Thèse n° 9185

Data-driven and Safe Networked Control with Applications to Microgrids

Présentée le 27 janvier 2022

Faculté des sciences et techniques de l'ingénieur
Groupe SCI STI GFT
Programme doctoral en robotique, contrôle et systèmes intelligents

pour l'obtention du grade de Docteur ès Sciences

par

Mustafa Sahin TURAN

Acceptée sur proposition du jury

Prof. C. N. Jones, président du jury
Prof. G. Ferrari Trecate, directeur de thèse
Prof. F. Pasqualetti, rapporteur
Prof. C. De Persis, rapporteur
Prof. A. Karimi, rapporteur

École
polytechnique
fédérale
de Lausanne

2022

I do not know, and it most probably depends...

To my *one and only*, Yekta...

Acknowledgements

Four years ago, I started my PhD not knowing. Now, as it comes to a bittersweet end, I still don't know, but can find out and learn better. This has been an incredibly enriching journey in many more aspects than I could have ever imagined. I feel indebted to a number of people for teaching me, at times even unknowingly, and bringing their unique colors to my life.

First, I would like to offer my sincere gratitude to Prof. Giancarlo Ferrari-Trecate for being a better PhD advisor than I could ever ask for. This thesis would not have been possible without his valuable guidance and encouragement. He has always been available to provide genuine support for research and personal matters alike. His enthusiasm and never-ending pursuit of scientific rigor have been profoundly inspiring. I would also like to thank Prof. Colin Jones, Prof. Alireza Karimi, Prof. Claudio De Persis, and Prof. Fabio Pasqualetti for taking part in my thesis jury and providing constructive feedback regarding my work. I would like to extend my thanks to Professors Josep Guerrero and Juan Vasquez for their help and support during my stay in Aalborg University. I am also grateful to my Bachelor's advisor Prof. Asif Šabanović who always pushed me out of my comfort zone and, thus, is the main reason I had the courage to start this academic journey at all.

Laboratoire d'Automatique (LA) is a fantastic place with a vibrant and friendly environment as well as a rich selection of marvellous people. I am thankful to all LA professors – Colin Jones, Giancarlo Ferrari-Trecate, Alireza Karimi, and Dominique Bonvin – for doing everything in their power to make LA a huge family. Special thanks to Christophe Salzmann for his admirable commitment to making this family function, be it technically or socially, to Ruth Benassi for having left a great impression of Swiss efficiency, and to Nicole Bouendin for our pre-covid cafeteria exchanges, often resulting in loud laughs thanks to her dark British *humour*.

I feel extremely privileged to have had a diverse collection of colleagues who turned into friends over the course of my doctoral studies. I would like to thank Michele, the gentleman from Piacenza, for his generous support at the beginning of these four years, his invaluable friendship ever since, and teaching me the correct name of "the other

football team of Milan". My heartfelt thanks go to Alex for being the loud Italian guy that I could always count on; to Emilio for philosophizing together, albeit to no avail whatsoever, and all the fun we had; to Harsh for being the dilemma that could both sing along with my pessimistic rants and lift spirits by his cheerful personality; to Pulkit for keeping books of my technological purchases and showing that it is possible to make the same group of people laugh with accent jokes for four consecutive years; to Peter for having a refined taste for offensive jokes; to Sohail for making me rediscover my mother tongue. Thanks to Clara, Baiwei, Andrea, Zak, Luca, Liang, Jean-Sébastien, and Mahrokh, for making DECODE the bright and fun research group it is. I would like to thank the other members of LA family, namely, Tomasz, Luca, Georgios, Ehsan, Yingzhao, Manuel, Philippe, Emanuele, Paul, Navid, Yuning, J1, and J2 for making this journey so enjoyable. I am also thankful to the people from *extended* LA: Olga, Vivi, Zarrin, Sofia, Echo, and Simon.

There are many other friends whom I will remember looking back at my PhD. A huge thanks goes to Ömer, Özge, Altuğ, Gözde, Bilal, Çağıl, Özgür, Soner, Fatma, Hüseyin abi, and Zhenishbek, who have made my stay in Lausanne much more meaningful. I also appreciate the friendship of *Ekmaanan* gang – Özhan, Hamdi, Talha – which will continue to have a special place for me. I would like to further thank the members of the infamous Call of Meka – Özhan, Doğacan, Can, Barbaros – for glorious gaming sessions, not triggering any rage attacks at all.

I am truly thankful to my extended family: to my father Ümit, my mother Elif, my grandmother Hatice, my mother-in-law İnci, my brother İsmail, my sisters-in-law Dilan and Esra, my brother-in-law Caner for their unconditional support and encouragement; to the *little ones*, namely, my niece Zeynep Irmak and my nephew Uzay, for bringing happiness.

My love Yekta, I am eternally grateful to you for sprinkling joy with your untamed rays of positivity. Your mere existence brightens my otherwise gloomy day. Without you, I would not have been the same. You gave me a *canvas*, so the people above could paint a colorful story for these four years. Thank you from the bottom of my heart for making me a better person.

Lausanne, October 25, 2021 Mustafa Şahin Turan

Abstract

Today, automatic control is integrated into a wide spectrum of real-world systems such as electrical grids and transportation networks. Many of these systems comprise numerous interconnected agents, perform safety-critical operations, or generate large amounts of data. Their automation, therefore, must address the challenges pertinent to these three characteristics. Specifically, in multi-agent systems (MASs), one common objective is that agents reach *consensus* on state or output variables for achieving a desired collective behavior. For consensus in large MASs, *distributed* controllers employing a communication network are required. When distributed architectures are used, the security of the closed-loop system can be compromised due to the vulnerability of the communication network to adversarial interferences called *cyber attacks*. Timely detection of attacks is vital for ensuring security of safety-critical systems. Finally, it is relevant in data-rich systems to develop control and state-estimation methods that provide guarantees by using a finite amount of data and bypassing the need of knowing system models.

Composed of three parts, this thesis contributes to address the abovementioned challenges of modern control systems. As an example, DC microgrids (DCmGs) are considered throughout the thesis for the development and validation of the proposed methods. The first part focuses on distributed consensus protocols. We first investigate the problem of state consensus in general linear interconnected MASs (LIMASs), for which we provide conditions based on the physical and communication graph properties as well as system matrices. Our results show that *weak* physical coupling and *well-connected* graphs are favorable features for consensus. We then focus on nonlinear DCmGs and propose a novel distributed controller to achieve voltage balancing and current sharing, which is a specific case of output consensus. By exploiting the structure of DCmG dynamics, we provide conditions on the attainment of these objectives and the stability of the closed-loop system.

In the second part, a distributed cyber-attack detection scheme is developed for LIMASs controlled in a distributed fashion. The detection architecture comprises local monitoring units collocated with each agent and checking the presence of cyber attacks in variables

communicated by neighboring agents. Each unit estimates the states of local and nearby agents, and detects an attack if a suitably defined error is *sufficiently* large. A thorough detectability analysis considering different types of attacks is also performed.

The final part of the thesis provides direct data-driven methods for control and state estimation based on finite data. First, we look at the worst-case optimal tracking problem in presence of measurement noises satisfying a quadratic bound. Control design is formulated as a semidefinite program (SDP), whose computational complexity is independent of the amount of data. Then, we turn our attention to state estimation in presence of unknown inputs, for which we present data-driven necessary and sufficient conditions. Under these conditions, a novel data-driven state estimation method with stability guarantees is provided.

Keywords: interconnected multi-agent systems, microgrids, distributed consensus, cyber-attack detection, unknown-input observers, data-driven control, data-driven state estimation.

Résumé

Aujourd'hui, l'automatisation est intégrée dans un large éventail de systèmes du monde réel, tels que les réseaux électriques et de transport. Beaucoup de ces systèmes comprennent de nombreux agents interconnectés, effectuent des opérations critiques en termes de sécurité ou génèrent de grandes quantités de données. Leur automatisation doit donc relever les défis liés à ces trois caractéristiques. Plus précisément, dans les systèmes multi-agents (MAS), un objectif commun est que les agents parviennent à un *consensus* sur les variables d'état ou de sortie pour obtenir un comportement collectif souhaité. Pour obtenir un consensus dans les grands MAS, des contrôleurs *distribués* utilisant un réseau de communication sont nécessaires. Lorsque des architectures distribuées sont utilisées, la sécurité du système en circuit fermé peut être compromise en raison de la vulnérabilité du réseau de communication aux interférences adverses appelées *attaque cybernétique*. La détection opportune des attaques est vitale pour assurer la sécurité des systèmes critiques de sécurité. Enfin, il est pertinent dans les systèmes riches en données de développer des méthodes de contrôle et d'estimation d'état qui fournissent des garanties en utilisant une quantité finie de données et en contournant la nécessité de connaître les modèles du système.

Composée de trois parties, cette thèse contribue à relever les défis susmentionnés des systèmes de contrôle modernes. A titre d'exemple, les microgrids DC (DCmG) sont considérés tout au long de la thèse pour le développement et la validation des méthodes proposées. La première partie se concentre sur les protocoles de consensus distribués. Nous étudions d'abord le problème du consensus d'état dans les MAS linéaires interconnectés (LIMAS) généraux, pour lequel nous fournissons des conditions basées sur les propriétés du graphe physique et de communication ainsi que sur les matrices du système. Nos résultats montrent que le couplage physique *faible* et les graphes *bien connectés* sont des caractéristiques favorables au consensus. Nous nous concentrons ensuite sur les DCmG non linéaires et proposons un nouveau contrôleur distribué pour réaliser l'équilibrage de la tension et le partage du courant, qui est un cas spécifique de consensus de sortie. En exploitant la structure de la dynamique des DCmG, nous fournis-

sons des conditions sur l'atteinte de ces objectifs et la stabilité du système en circuit fermé.

Dans la deuxième partie, un schéma distribué de détection d'attaque cybernétique est développé pour les LIMAS contrôlés de manière distribuée. L'architecture de détection comprend des unités de surveillance locales colocalisées avec chaque agent et vérifiant la présence d'attaque cybernétique dans les variables communiquées par les agents voisins. Chaque unité estime les états des agents locaux et proches, et détecte une attaque si une erreur définie de manière appropriée est *suffisamment* grande. Une analyse approfondie de la détectabilité, prenant en compte différents types d'attaques, est également réalisée.

La dernière partie de la thèse fournit des méthodes directes de contrôle et d'estimation d'état basées sur des données finies. Tout d'abord, nous examinons le problème du suivi optimal dans le pire des cas en présence de bruits de mesure satisfaisant une limite quadratique. La conception du contrôle est formulée comme un programme semi-défini (SDP), dont la complexité de calcul est indépendante de la quantité de données. Ensuite, nous nous intéressons à l'estimation d'état en présence d'entrées inconnues, pour laquelle nous présentons des conditions nécessaires et suffisantes basées sur les données. Sous ces conditions, une nouvelle méthode d'estimation d'état pilotée par les données avec des garanties de stabilité est fournie.

Mots-clés : Systèmes multi-agents interconnectés, micro-réseaux, consensus distribué, détection de cyber-attaques, observateurs à entrées inconnues, contrôle piloté par les données, estimation d'état pilotée par les données.

Contents

List of Figures

List of Tables

Acronyms

AC Alternating Current

CP Convex Programming

CPS Cyber-physical System

DC Direct Current

DCmG Direct-current Microgrid

DGU Distributed Generation Unit

FL Fundamental Lemma

LIMAS Linear Interconnected Multi-agent System

LMI Linear Matrix Inequality

LP Linear Program

LSS Large-scale System

LTI Linear Time-invariant

MARE Modified Algebraic Riccati Equation

MAS Multi-agent System

mG Microgrid

NCP Non-convex Programming

PCC Point of Common Coupling

PV Photovoltaic

RLC Resistive, Inductive, and Capacitive

SDP Semidefinite Program

UIO Unknown-input Observer

1 Introduction

1.1 Pervasive automation

The increasing availability of computational resources and the advancements in the fields of actuation and sensor technologies allow for automating an ever-growing variety of industrial processes. Moreover, the rise of embedded information technology in the past decades has accelerated the penetration of automatic control into a myriad of real-world systems. Examples of ubiquitous automation include urban infrastructure systems (e.g., electricity and transportation networks), vehicles, industrial processes, and consumer electronics [ÅM10]. Moreover, economics is a major field, where complex systems involving human agents can benefit from automation algorithms [LVLN92]. Recently, controllers have been proposed even for biological processes such as stimulation of brain networks [GPC+15, MPG+16] as well as cell growth and gene expression [MASSO+11, MARA+16].

More accurate sensors, better actuators, and more powerful computing platforms pave the way for the control of larger systems that can have a substantial number of variables and span vast geographical areas. Today's large-scale control systems include country-wide electrical grids, city-level traffic networks [GHR12], and swarms of robots consisting of thousands of agents [RCN14]. Control theory is also used to model, analyze, and act upon opinion dynamics [HK02, AO11] as well as the spread of epidemics [PSCVMV15, NKCdW+20] in human populations. It is noteworthy that most modern large-scale systems (LSSs) possess a distributed structure, i.e., they consist of smaller subsystems (also called *agents*) interconnected through a network enabling local interactions. For instance, the european power grid consists of more than 3000 generators and substations woven together via more than 200,000 kilometers of transmission lines [RCVS07], and opinions in a human society can be seen as millions of dynamical systems interacting through various norms of social circles [HK02], be it close relatives and friends, colleagues, or social network followers. This inherent structure has lead to the analysis and manipulation of modern LSSs through the lens of multi-agent systems

(MASs).

The abundance of digital elements in control loops also results in the generation of an unprecented and still increasing volume of data [LFK+14]. This inevitable rise calls for new paradigms of efficiently integrating data in the analysis and control of dynamical systems, which is evident from the rich array of data-driven methods recently proposed by the control community [DMM+20, MKK20, TMP20, MMWJ20, FGMFT21, BBP21, AKAJ21, DPT21].

In summary, inherent distributed structure with a large number of agents and vast quantities of available data can be identified as two prominent features of many modern systems. Next, we elaborate more on these characteristics and describe several associated control problems.

1.2 Challenges and existing work

In this section, we highlight three classes of modern control systems, identify some open questions in their automation, and provide a discussion of the existing body of work addressing these points (see Figure 1.1 for a visual summary). Note that a control system can belong to more than one of these classes, i.e., they are not mutually exclusive.

1.2.1 Interconnected multi-agent systems

The size of MASs raises several problems in terms of analysis and control. Indeed, it is very challenging to obtain accurate models and parameter estimates for the entire system when it has many variables and is possibly distributed over broad geographical areas. Moreover, various subsystems of today's MASs can be owned or operated by different entities (e.g., the european power grid [Web10]) that might not be interested in disclosing local parameters to a single control center. Even if an exact global model exists, it might still be infeasible to deploy centralized control structures, as they would require high transmission bandwidth and be susceptible to single-point failures [DD03]. This has motivated a large body of work on designing controllers ensuring *decentralized/distributed* operations [BPD02, DD03, SSS+03, Sil11]. Such architectures consist of several local units that require real-time information from a subset of nearby subsystems.

Consensus

In the context of MASs, a central problem is how to achieve coordinated behaviors among the subsystems. Examples include formation control in robotic MASs [BA98] and power sharing in microgrids [DPWD18]. Many desired coordination tasks in MASs can be formulated in the context of consensus [OPA15, OSFM07], which means that the subsystems come to an agreement on one or several output variables. Consensus protocols

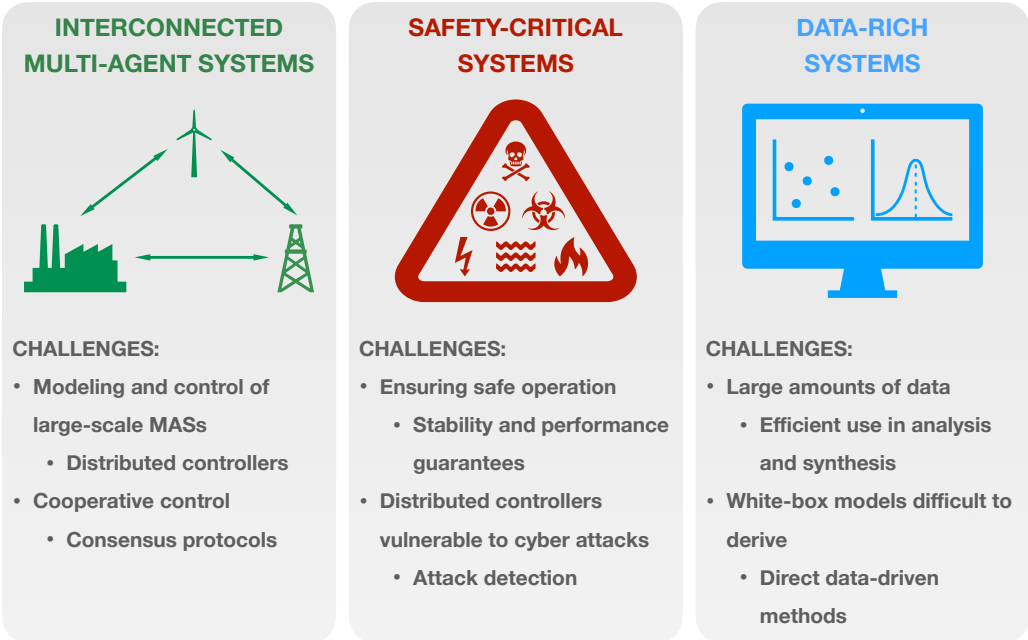

Figure 1.1: Three categories of modern control systems: interconnected MASs (left), safety-critical systems (middle), and data-rich systems (right).

often have a distributed structure, in which a communication network (equivalently called *cyber coupling network*) enables local information exchange among control modules of subsystems. The analysis and properties of the resulting control system depend heavily on the characteristics of the communication network and the subsystem dynamics [OSFM07, RB08].

There has been substantial research regarding the networked nature of distributed consensus protocols. For instance, the effects of quantization due to finite-bandwidth communication channels have been studied using hybrid systems theory in [CDPF11]. For output consensus in MASs with switching communication topologies, the authors of [WZF19] develop an approach based on the Lyapunov exponent of subsystem dynamics and a suitably defined synchronizability exponent for the switching topology. Their results reveal connections between consensus protocols, agent dynamics, and switching topology. Switching topologies and time delays in communication network have been considered in [OSM04], which shows the existence of a trade-off between the time to reach consensus and robustness to time delays. Moreover, the works [BFT08, LFZL18, ZXXY19, XZX19] consider communication delay among agents and derive upper bounds on the admissible delays to guarantee consensus. The authors of [ZTHK16] look at the sampled-data consensus problem for linear MASs under another communication nonideality: packet losses. They show that the asymptotic achievement of consensus heavily relies on the packet drop rate and the connectivity of the communication graph. The problem of finite-time consensus for linear MASs has been addressed in [ZLW+19], where a controller

is proposed for achieving consensus in a prespecified time.

It must be noted that most of the existing work on consensus in MASs assume that the subsystems have decoupled dynamics. This is not the case in interconnected MASs, in which the subsystems are physically coupled with nearby peers. Modern infrastructure (e.g., traffic, power, and water) networks are indeed interconnected MASs. The coexistence of both physical and cyber coupling impacts in a nontrivial way on the analysis and development of consensus protocols for interconnected MASs, which requires special attention.

1.2.2 Safety-critical systems

Systems whose failure can result in injury or death of humans, serious economical loss, or dire environmental consequences are termed *safety-critical*. Many large-scale MASs such as infrastructure networks have this feature; therefore, their safe and reliable operation is paramount [Kni02]. In particular, controllers must be designed to provide certificate guarantees for stability and performance, especially when using decentralized or distributed structures. Originally conceived for robotic systems, passivity-based control theory exploits energy-balancing properties of certain classes of systems to guarantee stability [OPNSR13]. This framework has been successfully used to ensure global stability of MASs regulated with decentralized controllers [NST+20, FGS+11, AML21]. Moreover, stability of distributed model-predictive controllers has been investigated for interconnected MASs in [SVR+10, CJMZ16, CJKT02]. The adoption of distributed control structures and the integration of a communication network renders the closed-loop system a cyber-physical system (CPS). There has been a huge academic interest in analyzing the stability and performance of CPSs in presence of network non-idealities [SSF+07, HNX07, LMT01, ZBP01].

Cyber security

The use of a communication network also exposes the system to adversarial interferences. Indeed, a malicious agent can tamper with the network to eavesdrop communication, change the operating point, or completely destabilize the system [TSSJ15b]. There has been numerous real-world examples to such attacks, one of which is the Maroochy water breach in Queensland, Australia. In March 2000, a disgruntled former employee hacked into the control network of the local wastewater system to control more than 100 pumping stations and release one million liters of sewage to local waterways [SM07]. This incident clearly demonstrated that, if security measures are not taken, cyber attacks can jeopardize the operation of many safety-critical CPSs. Differently from computer systems with communication protocols, CPSs also contain a physical component. As such, system- and control-theoretic approaches to cyber-security of CPSs have gained popularity in the recent years [CSS17, CPH+20]. In the context of secure control, as highlighted in [POM+18],

attack detection and resilience schemes can be often divided in *data-driven* [KP20] and *knowledge-based* approaches. In this thesis, we focus on the latter class. Among the numerous works in the field, some study *resilient* control systems maintaining closed-loop stability under certain classes of adversarial actions [RGM09, DPT15], while others tackle the problem of detecting these attacks [PDB13, MWS15, TSSJ15a, PDB15a]. For a comprehensive review of recent cyber-attack detection works, see [SRE+19, TGX+20].

Many of today's safety-critical systems are large-scale MASs, which hinders the use of centralized detection methods. Although the limitations to centralized architectures are well known, existing work on distributed detection methods is limited [NI14, PDB15b, DPA+18, AKP18, BRBP20, HRSJ21]. Note that most of these methods require the knowledge of the whole dynamics of the MAS for design and implementation. Therefore, their deployment in a large-scale MAS still poses modeling problems.

It is worth noting that attack-detection methods can be inspired by Fault Detection and Isolation (FDI) algorithms, for which distributed solutions have indeed been proposed [STSJ11, TSSJ14, BKLS16, DMK16, RBFTP16, BFK+17]. An analysis of the differences between fault and cyber-attack detection is provided in [PBB12].

1.2.3 Data-rich systems

All digital control systems embody sensors and actuators; therefore, data regarding control systems have long been available. A related challenge is to most efficiently and effectively exploit these data in control-related tasks. As such, the idea of using data in control system analysis and synthesis pipelines is hardly new. In fact, one of the earliest uses of data in control applications dates back to 1942, when Ziegler and Nichols provided an empirical method to tune the parameters of PID controllers [ZN42].

Shortly after the outset of state-space representation in the early 1960s, system identification was born in an effort to use data to infer system models instead of solely relying on first principles [Gev06]. Since then, several seminal works [HK66, ÅT65, ÅE71] and books [Lju98, Eyk74, SS89] have been published in the field. Consequently, system identification has quickly become one of the most vital instruments for incorporating data into control workflows. In the context of data-driven control, design approaches that first identify a model are referred to as *indirect* methods, while those that bypass system identification and construct controllers directly from data are termed *direct*. In this thesis, we focus on the latter class.

Direct data-driven control

Direct methods avoid building a model, which can be costly or require expertise when the underlying system has complex dynamics. As a result, the past three decades

have seen a surge of model-free control synthesis approaches including, but not limited to, iterative feedback tuning [HGGL98], correlation-based tuning [KMB04, MKBG07], virtual reference feedback tuning [GS00, CLS02], and model reference control [VHKB11]. We defer the reader to [HW13] for a comprehensive survey and classification of model-free control methods. Spurred by the rise of powerful machine learning algorithms, the control community started augmenting control synthesis with learning methods that were previously not feasible [PZ95, FL98]. More recently, learning-based direct data-driven controllers with stability guarantees have been proposed [NFM13, TFNM17].

Inspired by human psychology and banking on the idea of dynamic programming developed by Bellman [Bel57], a class of direct methods for solving optimal control problems emerged in late 1980s: reinforcement learning [SB18]. Originally formulated for Markov decision processes with discrete action and state spaces, they need effective function approximation methods to be applicable to most control tasks [BBDSE17]. Therefore, reinforcement learning has enjoyed a renewed interest in the last decade, owing to the increasing availability of powerful machine-learning algorithms for solving regression problems [VL10, MKS+15, SLA+15, LHP+15, SWD+17, HZAL18]. For an overview of modern reinforcement-learning algorithms as well as a discussion of the challenges in the field, see [ADBB17, HIB+18, DAMH19]. The review in [Rec19] focuses on continuous control problems and adopts a control-theory perspective. As highlighted in [DAMH19], most reinforcement-learning methods suffer from sample inefficiency and cannot ensure safety constraint satisfaction, making them not suitable for today's safety-critical control systems. In fact, it is a pertinent question in data-driven control to provide guarantees with a finite amount of data [Tu19, MPRT19, DMM+20].

The *behavioral theory* framework proposed by Jan Willems and his coworkers [WP97, MWVHDM06] has recently given rise to a new class of direct data-driven control methods. The behavioral approach provides a characterization of linear time-invariant (LTI) systems in terms of a collection of finite-length input-output trajectories (called *behavior*) instead of a model. The *Fundamental Lemma (FL)*, developed in the context of behavioral theory, allows one to express all input-output trajectories of an LTI system as a combination of its past data [WRMDM05], under the assumption that these data are persistently exciting [1]. The work in [MR08] provides algorithms and sufficient conditions for uniquely predicting output trajectories of a system. It was not until recently, however, that the behavioral theory caught the attention of the control community due to the works [CLD19b, DPT20]. The former builds on the method in [MR08] to introduce a direct data-enabled predictive control (DeePC) formulation for LTI systems, and show its equivalence to model-predictive control. This formulation has later been extended to robustly account for noise in data [CLD19a, BKMA20, CLD21, BKSA20], to capture nonlinear systems [BA20, LJ21, ABL+21, LWJ21], and to adapt to changes in system

[1] "Persistency of excitation" is a common concept in system identification and data-driven control, implying that the input sequence results in a *sufficient exploration* of the state space. See Section 5.2 for a precise definition.

dynamics [LSKJ21]. On the other hand, [DPT20] reformulates the FL for state-space representation and provides a completely data-driven parameterization of the open- and closed-loop dynamics of a system. This parameterization enables the authors to design robustly stabilizing state feedback controllers and linear quadratic regulators. The persistence of excitation requirement is relaxed in [vWETC20], where the authors provide necessary and sufficient conditions about the informativity of historical data for testing system properties and building stabilizing control laws. Similar parameterizations have been developed to tackle robust stabilization [BKSA20, vWCM20], robust linear quadratic regulation [DPT21], $\mathcal{H}_2$ and $\mathcal{H}_\infty$ control [vWCM20, BKSA20], system-level synthesis [XM21], model-reference control [BDPFT21], robust invariance [BDPT20a], and minimum-energy control [BP20]. Other applications of such parameterizations include addressing multiple datasets [vWDPCT20], verifying system properties [KBA20, RBKA19], and stabilizing nonlinear systems [BDPT20b, GDPT20, LDPT21].

In the next section, we provide a motivating real-world example of modern control systems, which has all three characteristics outlined in this section (see Figure 1.1). Moreover, this system will be used throughout the thesis for the development and validation of results.

1.3 Islanded DC microgrids

Thrust by the growing need to leverage the benefits of renewable energy sources, to rein in climate change and electricity costs, and to guarantee safe and reliable supply to areas lacking electric infrastructure, power generation is becoming increasingly distributed. A key component of this shift are microgrids (mGs), small-scale electric networks integrating distributed generation units (DGUs) (e.g., wind turbines, photovoltaic (PV) panels), storage devices, and loads. Microgrids, compatible with both alternating current (AC) and direct current (DC) operating standards, have been demonstrated to offer manifold advantages like enhanced power quality, reduced transmission losses, and capability to operate in grid-connected and islanded modes [BC12, PLMM06]. The latter proves pivotal in enabling autonomy in their operation and providing robustness in case of failure of connection to the main grid [SGV14]. In the islanded mode, an mG is an interconnected MAS, where DGUs, batteries, and loads are physically coupled via power lines (see Figure 1.2). Although practically smaller in size when compared to the conventional grid, islanded mGs can, in fact, be as large as entire islands [SCGGV14].

Nowadays, direct-current microgrids (DCmGs) are gaining ground. Their mounting popularity can be ascribed to technological improvements in power electronics devices and computational power of real-time controllers. Other contributing factors include the availability of inherently DC electronic loads (various appliances, LEDs, electric vehicles, computers, etc.) and presence of a natural interface with renewable energy sources (for instance PV modules) and batteries [MSFT+17]. As reviewed in [KAA19], DCmGs are now an economically viable solution for many types of residential and industrial

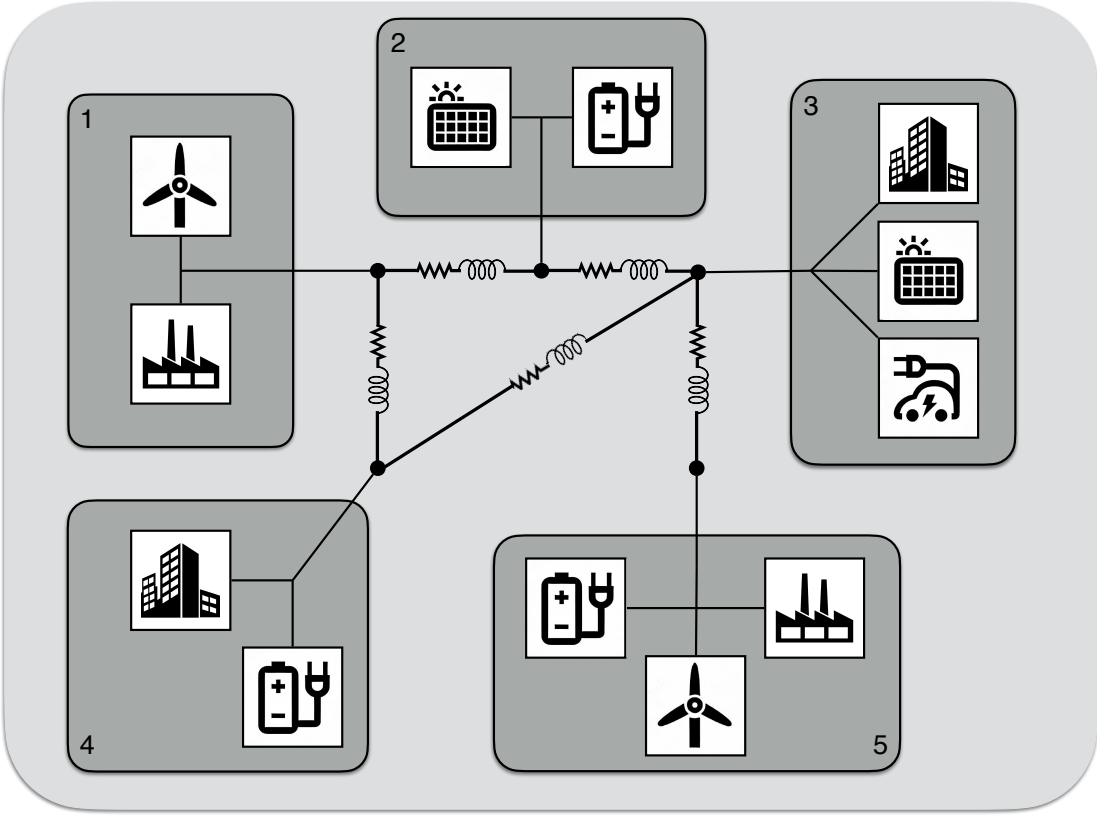

Figure 1.2: An islanded microgrid as an interconnected MAS. DGUs, batteries, and loads constitute the subsystems (numbered gray boxes), which are coupled through RL power lines.

applications such as data centers, telecom stations, fast electric vehicles (EVs), net-zero energy buildings, electric ships, and hybrid energy storage systems.

As islanded mGs are large-scale interconnected MASs, decentralized and distributed architectures have been very popular for their control [CIF17, NST+20, TFT20, SPM+20, KK17, SSK17, GCLL13]. Moreover, distributed consensus protocols are often used in mGs to achieve power or current sharing [DPWD18, CTDP+18, TCCS19, TMGFT18, ZD15]. All power networks, including islanded mGs, are safety-critical infrastructures. Thus, an area that has received specific attention has been the secure control and estimation of power networks, with specific focus on smart grids [MKB+12, MM09, KHLF10, ME10, SDB19], and mGs [ZYBV15, FIDSDB17, BNJD18, SMPD18]. Among the works addressing the security problem in mGs, [BNJD18, SMPD18] offer techniques to detect cyber attacks in DCmGs. In particular, the authors of [BNJD18] exploit *signal temporal logic* (STL) to detect whether an attack is present, by verifying whether given STL requirements are violated. In [SMPD18], on the other hand, the authors consider "balanced" attacks, and define a *cooperative vulnerability factor* for detection, exploiting secure knowledge of control inputs of neighboring DGUs. Thanks to the integration

of digital and smart elements [GCLL13], mGs also generate large quantities of data, which is already exploited for implementing data-driven control methods in recent works [ZZS+17, HNM17, MK19, DL19, MKK20]. In particular, model-free adaptive control has been used for stabilization [HNM17] and power sharing [ZZS+17]. The latter objective is also robustly achieved in [MK19, MKK20], where the data-driven control design is formulated as a convex program. Finally, an energy-management system based on reinforcement learning is proposed in [DL19]. This method allows for the operator of a distribution system composed of multiple mGs to determine electricity prices in order to maximize its profit.

1.4 Thesis contributions

This thesis contributes to the development of methods that address the challenges related to today's interconnected multi-agent, safety-critical, and data-rich control systems, as highlighted in Section 1.2. In particular, we *investigate distributed consensus in interconnected MASs, develop a distributed cyber-attack detection scheme for safety-critical interconnected MASs, and propose direct data-driven methods for general LTI systems.*

Correspondingly, the main body of the thesis is organized in three parts.

- Divided into two chapters, Part I concerns the study and development of distributed consensus protocols for interconnected multi-agent systems. In Chapter 2, we consider the problem of achieving consensus in general linear interconnected multi-agent systems (LIMASs) using linear protocols. Specifically, we give conditions that are either sufficient or necessary for the existence of control gains achieving consensus. Not taking advantage of the structure of subsystem dynamics, the results in this section are developed by adopting a worst-case analysis and, therefore, are conservative. In Chapter 3, we examine a modified consensus problem in a specific type of interconnected MASs, an islanded DCmG with nonlinear loads. By exploiting the inherent structure of subsystem dynamics, we propose a distributed control scheme to achieve sophisticated output consensus objectives.

- In Part II, which consists of Chapter 4, a distributed cyber-attack detection scheme for LIMASs is developed. The scheme comprises separate attack monitors collocated with each subsystem and combining two parallel modules that complement each other's performances. By means of a thorough detectability analysis, we provide theoretical guarantees on the detection characteristics of the proposed scheme.

- Part III is composed of two chapters, relating to direct data-driven control and state estimation methods, respectively. The results in this part are obtained for general LTI systems and based on behavioral theory. Chapter 5 presents a worst-case

optimal tracking control formulation based on semidefinite programs (SDPs). The proposed method provides robustness against measurement noise terms satisfying a quadratic bound. A novel direct approach for data-driven unknown-input state estimation is provided in Chapter 6. We give necessary and sufficient conditions based on data, under which the proposed estimator is shown to converge to the true system state.

Next, we include a brief summary of each chapter.

Chapter 2

In this chapter, we study the consensusability of LIMASs, which is a binary property certifying the existence of a distributed controller capable of driving the states of each subsystem to a consensus value. In particular, we consider LIMASs with scalar control inputs computed using linear consensus protocols. We show that consensusability is related to the simultaneous stabilizability of multiple LTI systems, and present a novel sufficient condition in form of a linear program (LP) for verifying this property. We also derive several necessary and sufficient consensusability conditions for LIMASs in terms of parameters of the subsystem matrices and the eigenvalues of the physical and communication graph Laplacians. The results show that weak physical couplings among subsystems and densely-connected physical and communication graphs are favorable for consensusability. We validate our results through simulations of real-world examples of LIMASs, namely, networks of supercapacitors and DCmGs.

The contents of this chapter are based on the following published articles.

[TXFT20] M. S. Turan, L. Xu, and G. Ferrari-Trecate, "Consensusability of linear interconnected multi-agent systems," *IFAC-PapersOnLine*, vol. 53, no. 2, pp. 2915–2920, 2020, 21th IFAC World Congress

[TXFT21] ——, "On consensusability of linear interconnected multi-agent systems and simultaneous stabilization," *IEEE Transactions on Control of Network Systems*, 2021, doi: 10.1109/TCNS.2021.3106446

Chapter 3

This chapter represents the study of a consensus problem specifically for DCmGs by exploiting the structure of the subsystem dynamics. In particular, we present a novel consensus-based secondary control scheme for current sharing and voltage balancing in DCmGs, composed of DGUs, dynamic resistive, inductive, and capacitive (RLC) lines, and nonlinear ZIE (constant impedance, constant current, and exponential) loads.

Note that current sharing is a modified output consensus condition. Situated atop a primary voltage control layer, our secondary controllers have a distributed structure, and utilize information exchanged over a communication network to compute necessary control actions. Besides showing that the desired objectives are always attained in steady state, we deduce conditions for the existence and uniqueness of an equilibrium point for constant power loads – exponential loads with zero exponent. Our control design hinges only on the local parameters of the DGUs, facilitating plug-and-play operations. This means that connecting or disconnecting a DGU does not necessitate the controllers of the neighboring DGUs to be modified. We provide a voltage stability analysis, and illustrate the performance and robustness of our designs via detailed computer simulations. All results hold for arbitrary, albeit connected, physical and communication network topologies.

The contents of this chapter are based on the following article, which has been accepted for publication on the IEEE Transactions on Control Systems Technology (TCST).

[NTFT20] P. Nahata, M. S. Turan, and G. Ferrari-Trecate, "Consensus-based current sharing and voltage balancing in DC microgrids with exponential loads," *arXiv preprint arXiv:2007.10134*, 2020

Chapter 4

Shifting our attention to cyber-attack detection in LIMASs, in this chapter, we present a residual-based distributed attack-monitoring scheme. The proposed architecture relies on a Luenberger observer together with a bank of unknown-input observers (UIOs) at each subsystem, providing attack detection capabilities. UIOs allow for estimation of the states of an LTI system without knowledge of all inputs. As such, they are used to estimate the states of the nearby subsystems. We analyze the monitoring architecture and derive conditions under which attacks are guaranteed to be detected, and, conversely, when they are *stealthy*. Our analysis shows that some classes of attacks cannot be detected using either module independently. Rather, by exploiting both modules simultaneously, we are able to improve the detection properties of the diagnostic tool as a whole. Theoretical results are backed up by simulations, where our method is applied to a realistic model of a DCmG under attack.

The contents of this chapter are based on the following published articles.

[GTB+20] A. J. Gallo, M. S. Turan, F. Boem, T. Parisini, and G. Ferrari-Trecate, "A distributed cyber-attack detection scheme with application to DC microgrids," *IEEE Transactions on Automatic Control*, vol. 65, no. 9, pp. 3800–3815, 2020

[GTN+18] A. J. Gallo, M. S. Turan, P. Nahata, F. Boem, T. Parisini, and G. Ferrari-Trecate, "Distributed cyber-attack detection in the secondary control of DC microgrids," in *2018 European Control Conference (ECC)*. Limassol, Cyprus: IEEE, 2018, pp. 344–349

A preliminary analysis and an extension of our detection scheme for a specific type of attack have been presented in the following paper; however, its contents are not included in this thesis.

[GTB+18] A. J. Gallo, M. S. Turan, F. Boem, G. Ferrari-Trecate, and T. Parisini, "Distributed watermarking for secure control of microgrids under replay attacks," in *7th IFAC Workshop on Distributed Estimation and Control in Networked Systems (NecSys'18)*, Groningen, The Netherlands, 2018, pp. 182–187

Chapter 5

This chapter focuses on direct data-driven control of discrete-time LTI systems using finite data. In particular, we study finite-horizon robust tracking control based on input-output data. Instead of using an explicit system model, we leverage behavioral theory to represent system trajectories through a set of noiseless *historical* data collected before the start of the control task. We consider that the *recent* output measurements, required for determining the initial conditions for the control horizon, are affected by noise terms verifying a quadratic bound. Then, we formulate an SDP for solving the robust tracking problem without any approximations. Our approach hinges on a parameterization of noise trajectories compatible with the data-dependent system representation and on a reformulation of the tracking cost, which enables the application of the S-lemma [PT07]. In addition, we propose a method for reducing the computational complexity and demonstrate that the size of the resulting SDP does not scale with the number of historical data. Finally, we show that the proposed formulation can easily incorporate actuator disturbances as well as constraints on inputs and outputs.

The contents of this chapter are based on the following articles.

[XTGFT21a] L. Xu, M. S. Turan, B. Guo, and G. Ferrari-Trecate, "A data-driven convex programming approach to worst-case robust tracking controller design," *arXiv preprint arXiv:2102.11918*, 2021

[XTGFT21b] ——, "Non-conservative design of robust tracking controllers based on input-output data," in *3rd Annual Learning for Dynamics and Control (L4DC) Conference*. Zurich, Switzerland: PMLR, 2021, pp. 138–149

Chapter 6

By combining the behavioral theory, which is also leveraged in Chapter 5, with the existing results on UIOs, this chapter provides a novel data-driven UIO. We give necessary and sufficient conditions on the data collected from the system for the existence of a UIO providing asymptotically converging state estimates, and propose a purely data-driven algorithm for their computation. Even though we focus on UIOs, our results also apply to the standard case of completely known inputs. As an example, we apply the proposed method to distributed state estimation in DCmGs and illustrate its potential for cyber-attack detection.

The contents of this chapter are taken from the following article.

[TFT22] M. S. Turan and G. Ferrari-Trecate, "Data-driven unknown-input observers and state estimation," *IEEE Control Systems Letters*, vol. 6, pp. 1424–1429, 2022

Finally, thesis conclusions as well as a discussion of future research directions are presented in Chapter 7. Appendix A contains the common notation and definitions used throughout the thesis.

Consensus in Interconnected Multi-agent Systems

Part I

2 Consensusability of linear interconnected multi-agent systems

2.1 Introduction

In this chapter, we discuss the problem of consensusability for interconnected MASs with linear dynamics, also called LIMASs for short. Consensusability refers to the existence of a distributed protocol from a predefined class such that agents can reach consensus on their states or outputs. As such, it is a binary property of the MAS. In the context of linear MASs, consensusability has been extensively studied in the past decades. For example, the authors in [MZ10] show that a continuous-time linear MAS can reach consensus if the dynamics of each agent is controllable and the communication topology is connected. The work [YX11] shows that, for discrete-time linear MASs, consensusability is guaranteed if the unstable eigenvalues of the agent state matrix verifies certain conditions related to the eigenvalues of the communication graph Laplacian. For consensus of MASs with switching topologies, [WZF19] shows that if the Lyapunov exponent of agent dynamics is less than a suitably defined synchronizability exponent of the switching topology, the MAS can achieve consensus. The authors of [XZXX18] and [XMX20] study consensus in presence of communication channels affected by fading and packet dropouts, and show that the consensusability condition is closely related to the statistics of the noisy communication channel, the eigenvalues of the communication graph Laplacian, and the instability degree of the agent dynamics.

The above research works assume that agents in MASs are coupled only through a cyber layer, i.e., a *communication* network. This is not the case in LIMASs, where the agents also interact through an additional physical layer, called a *physical* network. The presence of physical couplings necessitates the study of how they affect consensusability. This problem has been considered in [WWHL15, CU15, CLDA15]. The authors of [WWHL15] focus on consensus of multiple linear systems with uncertain subsystem interconnections for tracking a reference. They propose a distributed adaptive controller based on hierarchical decomposition and prove that the consensus error converges to a compact set if physical interconnections are sufficiently weak. Leader-follower tracking problems for LIMASs are

considered in [CU15]. Interactions between systems are treated as dynamic uncertainties and are described in terms of integral quadratic constraints. Two methods are proposed to design consensus-like tracking protocols. Sufficient conditions to guarantee that the system tracks the leader are obtained in terms of the feasibility of linear matrix inequalities (LMIs). The authors of [CLDA15] investigate the state consensus problem of a general LIMAS. They propose a linear consensus protocol and derive a sufficient and necessary criterion to guarantee convergence to consensus, which is expressed in terms of the Hurwitz stability of a matrix constructed from the parameters of the agents and the protocols. However, the aforementioned works lack a quantitative analysis of the relations of consensusability with physical interconnection and communication graphs.

2.1.1 Contributions

In this chapter, we study the consensusability of LIMASs equipped with linear distributed controllers, while providing analytic characterizations on how the physical and cyber couplings impact on it. In particular, we consider *homogeneous* LIMASs, whose subsystems have identical dynamics and control gains (see Section 2.2). Moreover, we direct our attention to LIMASs consisting of single-input subsystems interconnected via physical coupling with a Laplacian structure.

Our contributions to the existing literature are as follows. First, we show that the consensusability problem for LIMASs is related to a simultaneous stabilizability problem. Second, we present a sufficient condition, based on an LP, for verifying the simultaneous stabilizability of multiple LTI systems, which provides a simple alternative to existing methods relying on convex programming (CP). Third, we present several sufficient conditions, as well as a necessary condition, for the consensusability of LIMASs. Our results illustrate how consensusability is influenced by physical and communication coupling among subsystems.

This chapter is organized as follows. In Section 2.2, we introduce LIMASs and provide the problem formulation. Section 2.3 discusses the simultaneous stabilization problem of multiple LTI systems. Consensusability analysis of LIMASs is presented in Section 2.4. Simulation results are given in Section 2.5 and concluding remarks are presented in Section 2.6.

2.2 Problem formulation

The interaction among agents in a LIMAS equipped with distributed controllers is described by two undirected graphs with a common set of nodes $\mathcal{V} = \{1, \ldots, N\}$ associated with subsystems. A *physical* graph $\mathcal{G}_p = (\mathcal{V}, \mathcal{W}_p, \mathcal{E}_p)$ represents the physical interconnection among subsystems and a *cyber* graph $\mathcal{G}_c = (\mathcal{V}, \mathcal{W}_c, \mathcal{E}_c)$ represents the communication

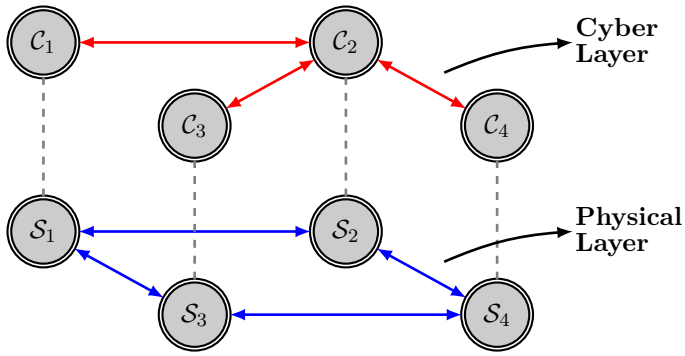

Figure 2.1: Illustration of a LIMAS. Blue arrows represent physical couplings among subsystems $\mathcal{S}_i$, dashed gray lines indicate connections between each subsystem and its corresponding controller, and red arrows represent communication channels among controllers $\mathcal{C}_i$.

network enabling information exchange among distributed control modules. Figure 2.1 shows an example LIMAS. Throughout the thesis, we assume that $\mathcal{G}_c$ is connected. In this chapter, the physical graph $\mathcal{G}_p$ is allowed to be disconnected. For a subsystem i, the sets of its neighbors in $\mathcal{G}_p$ and $\mathcal{G}_c$ are denoted by $\mathcal{N}_i^p$ and $\mathcal{N}_i^c$, respectively.

We consider a homogeneous LIMAS with subsystem dynamics described by

$$x_i^+ = Ax_i + A_p \sum_{j \in \mathcal{N}_i^p} a_{ij}(x_j - x_i) + Bu_i, \quad i = 1, \dots, N, \tag{2.1}$$

where $x_i \in \mathbb{R}^n$ are the states, $u_i \in \mathbb{R}$ are the scalar control inputs, $a_{ij} = a_{ji} \in \mathbb{R}_{>0}$ are the symmetric physical interconnection weights, and $A_p \in \mathbb{R}^{n \times n}$ is a matrix determining the physical coupling. We are interested in linear distributed controllers given by

$$u_i = K \sum_{j \in \mathcal{N}_i^c} b_{ij} \left(x_i - x_j\right), \quad i = 1, \dots, N, \tag{2.2}$$

where $K \in \mathbb{R}^{1 \times n}$ is the control gain common to all subsystems and $b_{ij} = b_{ji} \in \mathbb{R}_{>0}$ denote the symmetric communication weights in the cyber graph $\mathcal{G}_c$. The control gain K is a design parameter while b_{ij}, $\mathcal{G}_c$ are assumed to be given.

Remark 2.2.1. *Typical examples of LIMASs that can be modeled by* (2.1), (2.2) *are DCmGs, where distributed generation units are physically coupled through electric lines and communication networks are used for obtaining global coordinated behaviors, such as current sharing and voltage balancing [TMGFT18]. A detailed example is provided in Section 2.5. We note that, in the field of consensus for MASs, it is common to assume identical subsystem dynamics as in* (2.1)*. Such an assumption is reasonable in several application scenarios, where the hardware of subsystems is standardized for efficient serial production. For instance, individual converters in a DCmG can be chosen as identical, resulting in a homogeneous LIMAS. The simplifying assumption that each subsystem is assigned the same feedback gain K is required to facilitate the following analysis.*

Moreover, this assumption alleviates the burden of designing different consensus gains for each subsystem, which is critical in deploying control architectures for large-scale MASs.

By combining (2.1) and (2.2), the overall dynamics of the LIMAS can be compactly written as:

$$x^+ = (\mathbf{I}_N \otimes A - \mathcal{L}_p \otimes A_p + \mathcal{L}_c \otimes BK)\, x, \tag{2.3}$$

where $x = \left[x_1^\top, \ldots, x_N^\top\right]^\top \in \mathbb{R}^{Nn}$ is the cumulative state whereas $\mathcal{L}_p$ and $\mathcal{L}_c$ are the Laplacian matrices of $\mathcal{G}_p$ and $\mathcal{G}_c$, respectively. Note that the structure of physical interconnections in (2.1) gives the term $\mathcal{L}_p \otimes A_p$ in (2.3) involving the Laplacian matrix $\mathcal{L}_p$. For this reason, the coupling is termed *Laplacian*. Physical interconnections hamper the use of existing methods for analyzing consensusability of MASs. We define the consensusability problem in LIMASs as follows.

Problem 1: *Given the LIMAS* (2.3)*, provide conditions for the existence of a static feedback gain* $K \in \mathbb{R}^{1\times n}$ *such that the states of all subsystems converge to a global consensus vector, i.e.,*

$$\lim_{t\to\infty} |x_i(t) - \bar{v}| = \mathbf{0}_n, \quad \forall i \in \mathcal{V}, \tag{2.4}$$

for some $\bar{v} \in \mathbb{R}^n$*.*

To study this problem, we define the average state

$$\bar{x} \triangleq \frac{1}{N}\sum_{i=1}^{N} x_i = \frac{1}{N}\left(\mathbf{1}_N^\top \otimes \mathbf{I}_n\right) x,$$

and the deviation from $\bar{x}$

$$\delta \triangleq \left[x_1^\top - \bar{x}^\top, \ldots, x_N^\top - \bar{x}^\top\right]^\top = x - \mathbf{1}_N \otimes \bar{x} = \left(\left(\mathbf{I}_N - \frac{1}{N}\mathbf{1}_N\mathbf{1}_N^\top\right) \otimes \mathbf{I}_n\right) x. \tag{2.5}$$

The dynamics of δ can be derived from (2.3) and (2.5) as

$$\delta^+ = (\mathbf{I}_N \otimes A - \mathcal{L}_p \otimes A_p + \mathcal{L}_c \otimes BK)\, \delta. \tag{2.6}$$

The consensusability of the LIMAS is, therefore, equivalent to the stabilizability of (2.6).

Consider the following facts regarding the subspaces $\mathbb{H}^1$ and $\mathbb{H}^1_\perp$ (defined in Appendix A.2):

1. the columns of $\mathbf{1}_N \otimes \mathbf{I}_n/\sqrt{N}$ span the subspace $\mathbb{H}^1_\perp \otimes \mathbb{R}^n$
2. $(\mathbb{H}^1 \otimes \mathbb{R}^n) \perp (\mathbb{H}^1_\perp \otimes \mathbb{R}^n)$
3. $(\mathbb{H}^1 \otimes \mathbb{R}^n) \oplus (\mathbb{H}^1_\perp \otimes \mathbb{R}^n) = \mathbb{R}^{Nn}$

Together, they imply that there exists a unitary matrix $\Phi = \left[\mathbf{1}_N/\sqrt{N}, \phi_2, \ldots, \phi_N\right]$ where $\{\phi_2, \ldots, \phi_N\}$ form a basis for $\mathbb{H}^1$, such that, by defining $\tilde{\delta} = \left[\tilde{\delta}_1^\top, \ldots, \tilde{\delta}_N^\top\right]^\top \triangleq \left(\Phi^\top \otimes \mathbf{I}_n\right)\delta$, we have

$$\tilde{\delta}^+ = \left(\mathbf{I}_N \otimes A - \begin{bmatrix} \mathbf{0}_{n\times n} & \mathbf{0}_{n\times(N-1)n} \\ \mathbf{0}_{(N-1)n\times n} & \tilde{\mathcal{L}}_p \end{bmatrix} \otimes A_p + \begin{bmatrix} \mathbf{0}_{n\times n} & \mathbf{0}_{n\times(N-1)n} \\ \mathbf{0}_{(N-1)n\times n} & \tilde{\mathcal{L}}_c \end{bmatrix} \otimes BK\right)\tilde{\delta}. \tag{2.7}$$

$\tilde{\mathcal{L}}_p$ is a positive semidefinite matrix with eigenvalues $\{\lambda_{p,2}, \ldots, \lambda_{p,N}\}$. Similarly, the positive definite matrix $\tilde{\mathcal{L}}_c$ has eigenvalues $\{\lambda_{c,2}, \ldots, \lambda_{c,N}\}$. The transformation in (2.7) decomposes the dynamics of δ into two noninteracting parts: $\tilde{\delta}_1$ and $[\tilde{\delta}_2^\top, \ldots, \tilde{\delta}_N^\top]^\top$ representing the evolution of δ in $\mathbb{H}_\perp^1 \otimes \mathbb{R}^n$ and in $\mathbb{H}^1 \otimes \mathbb{R}^n$, respectively. Furthermore, we can show that $\tilde{\delta}_1 = \mathbf{0}_n$ by definition. Therefore, $\delta(t)$ asymptotically converges to zero if and only if the dynamics of $[\tilde{\delta}_2^\top, \ldots, \tilde{\delta}_N^\top]^\top$ is stable, i.e., the matrix

$$\mathbf{I}_{N-1} \otimes A - \tilde{\mathcal{L}}_p \otimes A_p + \tilde{\mathcal{L}}_c \otimes BK \tag{2.8}$$

is Schur stable. As will be shown in Section 2.4, the stability of (2.8) is related to the problem of simultaneous stabilization of a group of low-dimensional systems. Therefore, in the next section, we make a detour and provide novel conditions for simultaneous stabilization that, besides being useful for analyzing consensusability, also have an independent value.

2.3 A simultaneous stabilization test based on linear programming

The simultaneous stabilization problem has attracted the interest of several researchers, especially in the area of robust control [CS98]. Despite a number of results for linear systems [KY91, VV82, Blo94], prior work has shown that providing algebraic conditions for simultaneous stabilization of more than three systems is a difficult problem [BG93]. Extensive effort, therefore, has been put in developing numerical tests [CS98], mainly relying on CP and non-convex programming (NCP) [HTŠ99, BBFE93, HL91, Ack80]. In this section, we study the simultaneous stabilization of multiple LTI systems via linear static feedback. Existing criteria include sufficient and necessary conditions in terms of NCP [HL91, Ack80] and LMI-based sufficient conditions [BBFE93]. Here, we present a sufficient condition in terms of a LP, which requires less computational resources than its CP- and NCP-based counterparts [BV04].

We consider M single-input LTI systems described by

$$\check{x}_l^+ = A_l\check{x}_l + B_l\check{u}_l, \quad l = 1, \ldots, M, \tag{2.9}$$

where $\check{x}_l \in \mathbb{R}^m$ are system states and $\check{u}_l \in \mathbb{R}$ are control inputs. In the sequel, we assume

that all pairs (A_l, B_l) are reachable. A first result is stated in Lemma 2.3.1, which relies on a conservative parameterization of stabilizing controllers based on Ackermann's formula [Shi98]. Note that controller parameterization using Ackermann's formula has been exploited for simultaneous stabilization also in [Ack80, HL91]; however, these works provide necessary and sufficient conditions in terms of NCP, which can not be efficiently checked for very large m and M. Before presenting the lemma, we introduce the following definitions.

For $l = 1, \dots, M$, $\mathcal{M}_l = [B_l, A_l B_l, \dots, A_l^{m-1} B_l]$ is the reachability matrix of the pair (A_l, B_l), and the last row of its inverse is denoted as $r_{l,m} = [0 \ \dots \ 0 \ 1]\mathcal{M}_l^{-1}$. Accordingly, we define

$$\begin{aligned} V_l &= \mathrm{col}(-r_{l,m}\mathbf{I}_m, -r_{l,m}A_l, \dots, -r_{l,m}A_l^{m-1}), \\ v_l &= -r_{l,m}A_l^m. \end{aligned} \tag{2.10}$$

Finally, let $\Gamma = \mathrm{col}(\Gamma_{r,1}, \Gamma_{r,2}, \dots, \Gamma_{r,2^m}) \in \mathbb{R}^{2^m \times m}$, where $\Gamma_{r,j}$ are the different vectors in the set $\{-1, 1\}^{1\times m}$.

Lemma 2.3.1. *For the group of reachable systems (A_l, B_l), $l = 1, \dots, M$, there exists K such that $A_l + B_l K$ is Schur stable for every l if there exists a vector $c = [c_1^\top \ \dots \ c_M^\top]^\top \in \mathbb{R}^{Mm}$ satisfying*

$$Vc = v, \quad Hc \le h, \tag{2.11}$$

where

$$\begin{gathered} V = \begin{bmatrix} V_1^\top & -V_2^\top & \mathbf{0}_{m\times m} & \dots & \mathbf{0}_{m\times m} \\ \mathbf{0}_{m\times m} & V_2^\top & -V_3^\top & \ddots & \mathbf{0}_{m\times m} \\ \vdots & \ddots & \ddots & \ddots & \vdots \\ \mathbf{0}_{m\times m} & \dots & \mathbf{0}_{m\times m} & V_{M-1}^\top & -V_M^\top \end{bmatrix}, \\ v = [v_2 - v_1, \dots, v_M - v_{M-1}]^\top, \\ H = \mathbf{I}_M \otimes \Gamma, \qquad h = \mathbf{1}_{M2^m}. \end{gathered} \tag{2.12}$$

Moreover, if such a c exists, the vectors $c_l^\top V_l + v_l$ are identical and any of them provides a simultaneously stabilizing gain K.

Proof. We first describe the controller parametrization for the pair (A_l, B_l) and later show how to design a simultaneously stabilizing controller for all pairs (A_l, B_l) based on this parameterization.

In view of Ackermann's formula, we know that, for the reachable pair (A_l, B_l) and a vector collecting desired closed-loop eigenvalues $\lambda_l^D \triangleq [\lambda_{l,1}^D, \dots, \lambda_{l,m}^D]^\top \in \mathbb{C}^m$, the state-feedback controller $K_l = -r_{l,m} p_l^D(A_l) \in \mathbb{R}^{1\times m}$ assigns the eigenvalues of $A_l + B_l K_l$ to the elements

of λ_l^D, where the desired characteristic polynomial $p_l^D(A_l)$ is written as

$$\begin{aligned} p_l^D(A_l) &= \left(A_l - \lambda_{l,1}^D \mathbf{I}_m\right) \dots \left(A_l - \lambda_{l,m}^D \mathbf{I}_m\right) \\ &\triangleq A_l^m + c_{l,m-1} A_l^{m-1} + \dots + c_{l,1} A_l + c_{l,0} \mathbf{I}_m. \end{aligned} \tag{2.13}$$

Defining $c_l \triangleq [c_{l,0} \ \dots \ c_{l,m-1}]^\top$, one sees that $c_l = g(\lambda_l^D)$ is a polynomial function of order m. Therefore, a set $\mathbb{K}_l$ of stabilizing controllers K_l for (A_l, B_l) can be parameterized by λ_l^D as $\mathbb{K}_l = \{K_l = -r_{l,m} p_l^D(A_l) | \lambda_l^D \in \Lambda^D\}$, where

$$\Lambda^D = \{\lambda^D \in \mathbb{C}^m | \lambda_j^D \in \mathcal{B}_1 \ \ \forall j \in \{1, \dots, m\} \text{ and } \lambda_j^D \text{ are real or in conjugate pairs}\}.$$

Since the set Λ^D has a complex geometry, the computation of the set $\mathbb{K}_l$ is convoluted. To circumvent this problem, we leverage a classic result on Schur stable polynomials [Jur64]: $\lambda_l^D \in \Lambda^D$ if

$$\sum_{j=0}^{m-1} |c_{l,j}| < 1, \tag{2.14}$$

which can equivalently be written as $\Gamma c_l \leq \mathbf{1}_{2^m}$. Further noting that the polynomial $p_l^D(A_l)$ is an affine function of c_l and $K_l \in \mathbb{K}_l$ is a linear function of $p_l^D(A_l)$, we can define a new set $\mathbb{K}_l^s \subseteq \mathbb{K}_l$ of stabilizing controllers for system l in terms of c_l as $\mathbb{K}_l^s = \{K_l = c_l^\top V_l + v_l | \Gamma c_l \leq \mathbf{1}_{2^m}\}$, where V_l and v_l are defined in (2.10).

Based on the above results, we know that if $\bigcap_{l=1}^M \mathbb{K}_l^s \neq \emptyset$, there exists $K \in \bigcap_{l=1}^M \mathbb{K}_l^s$ simultaneously stabilizing all (A_l, B_l) pairs. The above condition is equivalent to the existence of vectors $c_l \in \mathbb{R}^m$ for $l \in \{1, \dots, M\}$ such that $c_l^\top V_l + v_l = c_{l+1}^\top V_{l+1} + v_{l+1}, \ \forall l \in \{1, \dots, M-1\}$, which yields the feasibility condition given by (2.11). The proof of the second part is straightforward as the feasibility of (2.11) means that stabilizing control gains $K_l = C_l^\top V_l + v_l$, $l = 1, \dots, M$ are identical. Therefore, it suffices to pick one. ■

Remark 2.3.1. *In Lemma 2.3.1, the only source of conservativity is the use of the condition in* (2.14) *for Schur stability of polynomials, which is only sufficient for $m > 1$, and gets more and more conservative as the system order m increases. Indeed,* (2.14) *is the main novelty of the proposed method, compared with the necessary and sufficient conditions in [Ack80, HL91]. Therefore, for scalar systems, i.e., $m = 1$, the results in Lemma 2.3.1 are necessary and sufficient. The conservativity of this lemma, however, does not increase with the number of systems M.*

We observe that the structure of the equality constraints in (2.11) can be further exploited to simplify the redundancies in the proposed LP. Therefore, in the following, we show that the result in Lemma 2.3.1 can be equivalently cast into a simpler LP with a smaller number of decision variables.

Theorem 2.3.1. *For the group of reachable systems (A_l, B_l), $l = 1, \dots, M$, the following hold:*

1. *The matrices V_l in* (2.10) *are invertible*

2. *The matrix V in* (2.12) *has full row rank and its right inverse $V^\dagger$ is given by*

$$V^\dagger = \begin{bmatrix} \left(V_1^\top\right)^{-1} & \left(V_1^\top\right)^{-1} & \dots & \left(V_1^\top\right)^{-1} \\ \mathbf{0}_{m\times m} & \left(V_2^\top\right)^{-1} & \dots & \left(V_2^\top\right)^{-1} \\ \vdots & \ddots & \ddots & \vdots \\ \mathbf{0}_{m\times m} & \dots & \mathbf{0}_{m\times m} & \left(V_{M-1}^\top\right)^{-1} \\ \mathbf{0}_{m\times m} & \mathbf{0}_{m\times m} & \mathbf{0}_{m\times m} & \mathbf{0}_{m\times m} \end{bmatrix}. \tag{2.15}$$

   Moreover, the null space of V is spanned by columns of the matrix

$$\Psi = \begin{bmatrix} V_1^{-1} & V_2^{-1} & \dots & V_M^{-1} \end{bmatrix}^\top. \tag{2.16}$$

3. *Pairs (A_l, B_l) are simultaneously stabilizable by a common gain K if there exists a vector $w \in \mathbb{R}^m$ such that*

$$H\Psi w \leq h - HV^\dagger v. \tag{2.17}$$

   Furthermore, if such a w exists, the feedback gain

$$K = v_M + w^\top \tag{2.18}$$

   stabilizes (A_l, B_l) for every $l \in \{1, \dots, M\}$.

Proof. 1. We prove that the matrix V_l is invertible if the pair (A_l, B_l) is reachable, by showing that the rows of V_l are linearly independent. For $m = 1$ it is trivial. For $m > 1$, we denote the inverse of $\mathcal{M}_l$ as

$$\mathcal{M}_l^{-1} = \begin{bmatrix} r_{l,1}^\top & \dots & r_{l,m}^\top \end{bmatrix}^\top.$$

From the last row of the equality $\mathcal{M}_l^{-1}\mathcal{M}_l = \mathbf{I}_m$, one has that $r_{l,m}B_l = r_{l,m}A_lB_l = \dots = r_{l,m}A_l^{m-2}B_l = 0$ and $r_{l,m}A_l^{m-1}B_l = 1$.

Considering the definition of V_l in (2.10), we show by contradiction that the vectors $\{-r_{l,m}A_l^j\}_{j\in\{0,\dots,m-1\}}$ are linearly independent. First, assume that they are linearly dependent. Then, there exists a nonzero vector $\beta = [\beta_0, \dots, \beta_{m-1}]^\top \neq \mathbf{0}_m$ such that

$$-\beta^\top V_l = \sum_{j=0}^{m-1} \beta_j r_{l,m} A_l^j = \mathbf{0}_{1\times m}. \tag{2.19}$$

Multiplying (2.19) from the right by B_l yields that

$$\sum_{j=0}^{m-2} \beta_j \underbrace{r_{l,m} A_l^j B_l}_{=0} + \beta_{m-1} \underbrace{r_{l,m} A_l^{m-1} B_l}_{=1} = 0.$$

Thus, $\beta_{m-1} = 0$ is implied by (2.19). Then, one can rewrite (2.19) by removing the last term:

$$-\beta^\top V_l = \sum_{j=0}^{m-2} \beta_j r_{l,m} A_l^j = \mathbf{0}_{1\times m}. \tag{2.20}$$

Again, one can multiply (2.20) from the right with $A_l B_l$ to obtain

$$\sum_{j=1}^{m-1} \beta_{j-1} r_{l,m} A_l^j B_l = \sum_{j=1}^{m-2} \beta_{j-1} \underbrace{r_{l,m} A_l^j B_l}_{=0} + \beta_{m-2} \underbrace{r_{l,m} A_l^{m-1} B_l}_{=1} = \beta_{m-2} = 0.$$

By iterating the same procedure, one has that (2.19) implies $\beta = \mathbf{0}_m$, which is a contradiction. Therefore, the matrix V_l is invertible.

2. Given that the matrices V_l are invertible, it is straightforward to see that the matrix V has full row rank, i.e., $\text{rank}(V) = (M-1)m$. Therefore, it is possible to find a right inverse for it. Given the definition of $V^\dagger$ in (2.15), we can verify that $VV^\dagger = \mathbf{I}_{(M-1)m}$. Moreover, from the rank-nullity theorem, $\dim(\ker(V)) = Mm - \text{rank}(V) = m$. As the full-rank matrix $\Psi \in \mathbb{R}^{Mm\times m}$ given in (2.16) satisfies $V\Psi = \mathbf{0}_{(M-1)m\times m}$, we conclude that its columns form a basis for $\ker(V)$.

3. Lemma 2.3.1 shows that the pairs (A_l, B_l) are simultaneously stabilizable if the LP (2.11) is feasible. Next, we will prove that the LP in (2.11) is equivalent to the LP in (2.17), which has a smaller number of decision variables and constraints. Considering point 2) of this theorem, all solutions c to the equality constraint in (2.11) can be written as

$$c = V^\dagger v + \Psi w \tag{2.21}$$

for a free vector $w \in \mathbb{R}^m$, i.e., w parametrizes all c solving $Vc = v$. On replacing c in the inequality constraint in (2.11) and removing the equality constraint, one obtains the equivalent reduced-order LP in (2.17). Furthermore, in view of Lemma 2.3.1, for a given solution c to (2.11), $K = c_1^\top V_1 + v_1$ is a simultaneously stabilizing control gain. From the parameterization of c in (2.21), we have $c_1 = (V_1^{-1})^\top (v_M^\top - v_1^\top + w)$. Therefore, the common control gain can be calculated as $K = c_1^\top V_1 + v_1 = v_M + w^\top$, concluding the proof.

■

Remark 2.3.2. *The LPs* (2.17) *and* (2.11) *are equivalent in spite of the reduction of the number of decision variables from Mm to m and the elimination of equality constraints. As such, the LP in* (2.17) *can be used to check the simultaneous stabilizability of a larger number of systems compared to* (2.11).

Table 2.1: Summary of Consensusability Results

Result	**Type**	**Feature**	**Assumptions**
Theorem 2.4.1	Sufficient	Algebraic Test	Scalar Subsystems
Corollary 2.4.1.1	Sufficient	Linear Program	Assumptions 2.4.1, 2.4.2
Theorem 2.4.2	Sufficient	Algebraic Test	Assumptions 2.4.1, 2.4.2, 2.4.3
Theorem 2.4.3	Necessary	Algebraic Test	Assumptions 2.4.1, 2.4.2

Remark 2.3.3. *The modified LP formulation* (2.17)*, compared to* (2.11)*, utilizes matrices* $V^\dagger$ *and* Ψ *which, according to* (2.15) *and* (2.16)*, can be computed by inverting the* $m \times m$ *matrices* V_l *associated to individual agents.*

Remark 2.3.4. *As expected,* (2.17) *is always feasible if* $(A_l, B_l) = (A, B)$ *for every* l*, as this condition implies* $v = \mathbf{0}_{(M-1)m}$*. Therefore,* $h - HV^\dagger v = \mathbf{1}_{M2^m}$ *and* $w = \mathbf{0}_m$ *is a feasible solution to* (2.17)*. Moreover,* $V^\dagger v$ *changes continuously with the matrices* A_l *and* B_l *if all pairs* (A_l, B_l) *are reachable. As such, the right-hand side of* (2.17) *is still nonnegative if the differences between the pairs* (A_l, B_l) *are sufficiently small, and* $w = \mathbf{0}_m$ *is still a feasible solution to* (2.17)*. Therefore, a group of reachable systems is always simultaneously stabilizable if the pairs* (A_l, B_l) *are sufficiently similar.*

Having presented our results on simultaneous stabilization, we resume our discussion of consensusability.

2.4 Conditions for consensusability of LIMASs

In this section, we analyze the consensusability of LIMASs with subsystems of order $n = 1$ and $n \geq 1$ separately. Indeed, the former case can be studied without restrictive assumptions while still giving important insight into the consensusability problem. Instead, the latter case is more difficult to analyze and requires additional assumptions. Table 2.1 summarizes the results presented in this section along with their applicability conditions. After presenting our results for these two cases in Sections 2.4.1 and 2.4.2, respectively, we discuss their implications in Section 2.4.3.

Our consensusability conditions are given in terms of the following quantities.

$$\lambda_{p,\max} \triangleq \max_{i\in\{2,\dots,N\}} \lambda_{p,i}, \quad \lambda_{p,\min} \triangleq \min_{i\in\{2,\dots,N\}} \lambda_{p,i}, \quad \Delta_p \triangleq \lambda_{p,\max} - \lambda_{p,\min},$$

$$\lambda_{c,\max} \triangleq \max_{i\in\{2,\dots,N\}} \lambda_{c,i}, \quad \lambda_{c,\min} \triangleq \min_{i\in\{2,\dots,N\}} \lambda_{c,i}, \quad \gamma_c \triangleq \frac{\lambda_{c,\max}}{\lambda_{c,\min}}.$$

We call the scalar $\gamma_c \geq 1$ the *eigenratio* of $\mathcal{L}_c$, where $\gamma_c = 1$ if and only if the graph is complete [YX11]. A low eigenratio means the graph is close to a complete graph. Furthermore, the eigenratio can be decreased by adding edges to the graph, meaning

that a γ_c close to 1 generally implies a *densely-connected* graph [BP02]. Δ_p denotes the difference between the largest and second smallest eigenvalues of $\mathcal{L}_p$. A low Δ_p value indicates that the eigenvalues of $\mathcal{L}_p$ are close to each other, which holds when the eigenratio of the physical interconnection graph is low, i.e., $\mathcal{G}_p$ is densely-connected [YX11, BP02]. A low Δ_p value is also achieved if eigenvalues of $\mathcal{L}_p$ are small, and consequently, the physical coupling between subsystems is weak.

2.4.1 Scalar subsystems

In this subsection, we present results for scalar subsystems. Without loss of generality, we assume $B = 1$ and denote matrices A and K as a and k, respectively. To simplify the analysis, the matrix A_p is omitted, as it can be lumped into the weights a_{ij}. Then, (2.8) simplifies to

$$a\mathbf{I}_{N-1} - \tilde{\mathcal{L}}_p + k\tilde{\mathcal{L}}_c. \tag{2.22}$$

Next, we present analytical sufficient conditions, which are based on results on the eigenvalues of the sum of two Hermitian matrices.

Theorem 2.4.1. *The LIMAS* (2.1) *with scalar subsystems is consensusable if either of the following conditions holds*

S1. $\lambda_{p,\min} > a - 1$ *and* $(\gamma_c - 1)(1 - a + \lambda_{p,\min}) < \gamma_c(2 - \Delta_p)$,

S2. $\lambda_{p,\max} < 1 + a$ *and* $(\gamma_c - 1)(1 + a - \lambda_{p,\max}) < \gamma_c(2 - \Delta_p)$.

Moreover, the control gain k *can be selected as* $k \in \mathbb{K}^+ \cap \mathbb{R}_{\geq 0}$ *if S1 is satisfied and* $k \in \mathbb{K}^- \cap \mathbb{R}_{<0}$ *if S2 is satisfied, where*

$$\begin{aligned} \mathbb{K}^+ &= \left(\frac{-1 - a + \lambda_{p,\max}}{\lambda_{c,\min}}, \frac{1 - a + \lambda_{p,\min}}{\lambda_{c,\max}} \right), \\ \mathbb{K}^- &= \left(\frac{-1 - a + \lambda_{p,\max}}{\lambda_{c,\max}}, \frac{1 - a + \lambda_{p,\min}}{\lambda_{c,\min}} \right). \end{aligned} \tag{2.23}$$

Proof. Since $a\mathbf{I}_{N-1} - \tilde{\mathcal{L}}_p$ and $k\tilde{\mathcal{L}}_c$ are symmetric matrices, upper and lower bounds on the eigenvalues of their summation can be found as a direct consequence of Weyl's inequalities [HJ12, Theorem 4.3.7]:

$$\begin{aligned} \lambda_{\max}\left(a\mathbf{I}_{N-1} - \tilde{\mathcal{L}}_p + k\tilde{\mathcal{L}}_c\right) &\leq \lambda_{\max}\left(a\mathbf{I}_{N-1} - \tilde{\mathcal{L}}_p\right) + \lambda_{\max}\left(k\tilde{\mathcal{L}}_c\right), \\ \lambda_{\min}\left(a\mathbf{I}_{N-1} - \tilde{\mathcal{L}}_p + k\tilde{\mathcal{L}}_c\right) &\geq \lambda_{\min}\left(a\mathbf{I}_{N-1} - \tilde{\mathcal{L}}_p\right) + \lambda_{\min}\left(k\tilde{\mathcal{L}}_c\right). \end{aligned} \tag{2.24}$$

Therefore, (2.22) is Schur stable if $k \in \mathbb{R}$ satisfies

$$a - \lambda_{p,\min} + \lambda_{\max}\left(k\tilde{\mathcal{L}}_c\right) < 1 \quad \text{and} \quad a - \lambda_{p,\max} + \lambda_{\min}\left(k\tilde{\mathcal{L}}_c\right) > -1. \tag{2.25}$$

Since the sign of k changes the expression of $\lambda_{\min}(k\tilde{\mathcal{L}}_c)$ and $\lambda_{\max}(k\tilde{\mathcal{L}}_c)$, we inspect the two possibilities $k \geq 0$ and $k < 0$ separately. For $k \geq 0$, we have $\lambda_{\min}(k\tilde{\mathcal{L}}_c) = k\lambda_{c,\min}$ and $\lambda_{\max}(k\tilde{\mathcal{L}}_c) = k\lambda_{c,\max}$, and the conditions (2.25) simplify to $k \in \mathbb{K}^+ \cap \mathbb{R}_{\geq 0}$, where $\mathbb{K}^+$ is as given in (2.23). This is possible if $\mathbb{K}^+ \neq \emptyset$ and $\mathbb{K}^+ \cap \mathbb{R}_{\geq 0} \neq \emptyset$, which directly translate into the conditions in S1. The result for $k < 0$ can be proved similarly, completing the proof. ■

Remark 2.4.1. *The only sources of conservativity in Theorem 2.4.1 are the upper and lower bounds used in* (2.24)*. From the proof of Weyl's inequalities [HJ12, Theorem 4.3.7], it can be seen that the equalities in* (2.24) *hold when the eigenpairs of matrices* $a\mathbf{I}_{N-1} - \tilde{\mathcal{L}}_p$ *and* $k\tilde{\mathcal{L}}_c$ *coincide. This is satisfied when* $\tilde{\mathcal{L}}_p = \mathbf{0}_{(N-1)\times(N-1)}$*, i.e., there is no physical coupling, and when* $\mathcal{L}_p$ *and* $\mathcal{L}_c$ *commute. The latter means that the matrix* Φ *can be selected such that* $\tilde{\mathcal{L}}_p$ *and* $\tilde{\mathcal{L}}_c$ *are both diagonal [HJ12]. Therefore, the conditions S1 and S2 are necessary and sufficient when there is no physical coupling or* $\mathcal{L}_p$ *and* $\mathcal{L}_c$ *commute. Indeed, in the former case, it is straightforward to see that Theorem 2.4.1 recovers the necessary and sufficient condition for consensusability of MASs in [YX11]. Furthermore, from the proof of [HJ12, Theorem 4.3.7], it can be seen that the inequalities* (2.24) *are tighter when the eigenpairs of* $a\mathbf{I}_{N-1} - \tilde{\mathcal{L}}_p$ *and* $k\tilde{\mathcal{L}}_c$ *(consequently, of* $\mathcal{L}_p$ *and* $\mathcal{L}_c$*) are closer to each other.*

As discussed later in Section 2.4.3, conditions S1 and S2 help understanding the roles of the physical interconnection and communication graphs in consensusability. We next analyze the consensusability problem for general subsystems.

2.4.2 General subsystems

From (2.8), the consensusability problem can be seen as the problem of designing a control gain $\tilde{K} = (\mathbf{I}_{N-1} \otimes K) \in \mathbb{R}^{(N-1)\times(N-1)n}$ with structural constraints to make the matrix

$$\mathbf{I}_{N-1} \otimes A - \tilde{\mathcal{L}}_p \otimes A_p + \left(\tilde{\mathcal{L}}_c \otimes B\right) \tilde{K}$$

Schur stable. Prior work shows that this problem is difficult to tackle without focusing on special system structures [RL05]. Therefore, to facilitate the analysis, we introduce the following technical assumption.

Assumption 2.4.1. *The Laplacian matrices* $\mathcal{L}_p$ *and* $\mathcal{L}_c$ *commute.*

Remark 2.4.2. *Assumption 2.4.1 is fulfilled when the two Laplacians are equal to each other up to scaling with a constant, i.e.,* $\mathcal{L}_p = \beta\mathcal{L}_c$*,* $\beta \in \mathbb{R}_{\geq 0}$*. Moreover, two Laplacians commute also when one of them is the Laplacian of a complete graph with uniform edge weights. Nevertheless, a necessary and sufficient condition for two generic Laplacians to commute is not yet available in the literature.*

Under Assumption 2.4.1, one can simultaneously diagonalize the two Laplacians $\mathcal{L}_p$ and $\mathcal{L}_c$ [HJ12], i.e., a unitary transformation matrix Φ can be chosen such that $\Phi^\top \mathcal{L}_p \Phi =$

$\Lambda_p = \operatorname{diag}(0, \lambda_{p,2}, \ldots, \lambda_{p,N})$ and $\Phi^\top \mathcal{L}_c \Phi = \Lambda_c = \operatorname{diag}(0, \lambda_{c,2}, \ldots, \lambda_{c,N})$. Note that, for each $i \in \{2, \ldots, N\}$, $\lambda_{p,i}$ and $\lambda_{c,i}$ have the same eigenspace. As such, the diagonal entries of Λ_p and Λ_c, hence $\lambda_{p,i}$ and $\lambda_{c,i}$, are not necessarily ordered by their magnitude. Assumption 2.4.1 thus allows one to decouple the dynamics of $\tilde{\delta}_i$, $i \in \{2, \ldots, N\}$ from each other:

$$\tilde{\delta}_i^+ = (A - \lambda_{p,i} A_p + \lambda_{c,i} BK)\, \tilde{\delta}_i, \quad \forall i \in \{2, \ldots, N\}. \tag{2.26}$$

Consequently, the consensusability of (2.3) is equivalent to the simultaneous stabilizability of (2.26). The following assumption is required before further derivations.

Assumption 2.4.2. *The pairs $(A - \lambda_{p,i} A_p, B)$ are reachable for all $i \in \{2, \ldots, N\}$.*

Remark 2.4.3. *Assumption 2.4.2 is necessary as the reachability of the pair $(A - \lambda_{p,i} A_p, B)$ is not implied by that of the pair (A, B) in general. We also stress that the reachability of $(A - \lambda_{p,i} A_p, B)$ implies that of $(A - \lambda_{p,i} A_p, \lambda_{c,i} B)$, as $\lambda_{c,i} > 0$, $\forall i \in \{2, \ldots, N\}$.*

Defining $A_i \triangleq A - \lambda_{p,i} A_p$ and $B_i \triangleq \lambda_{c,i} B$, $i \in \{2, \ldots, N\}$, consensusability of LIMAS (2.3) is equivalent to the simultaneous stabilizability of pairs (A_i, B_i), which is the problem addressed in Section 2.3. As mentioned in that section, this problem is difficult to analytically solve in general and we separate our discussion in two parts. Firstly, a numerical sufficient condition for consensusability is proposed based on Theorem 2.3.1. Secondly, for special LIMASs with $A_p = \alpha A$ for some scalar α, we give an algebraic sufficient condition for consensusability in Theorem 2.4.2. Finally, in Theorem 2.4.3, we present a necessary condition for the consensusability of (2.3).

Sufficient conditions

The following corollary presents an LP-based test for consensusability with generic system matrices A, A_p, and B. The result directly follows from Theorem 2.3.1; therefore, the proof is omitted.

Corollary 2.4.1.1. *Suppose that Assumptions 2.4.1 and 2.4.2 hold. The LIMAS* (2.3) *is consensusable if there exists a vector $w \in \mathbb{R}^n$ satisfying* (2.17)*, where the matrices V, v, H, h, $V^\dagger$, and Ψ are computed as in* (2.11)-(2.12),(2.15)-(2.16)*, by replacing (A_l, B_l) with $(A - \lambda_{p,i} A_p, \lambda_{c,i} B)$. Moreover, if such a w exists, a control gain achieving consensus is given by $K = v_N + w^\top$.*

In view of Remark 2.3.1, we point out that Corollary 2.4.1.1 can be applied to very large LIMASs. We also highlight that the above result relies on the knowledge of the eigenvalue pairs $(\lambda_{p,i}, \lambda_{c,i})$ having the same eigenspace. As such, the Laplacian matrices $\mathcal{L}_p$ and $\mathcal{L}_c$ need to be known.

Next, we seek an analytical sufficient condition for consensusability of LIMASs. As discussed in Section 2.3, it is difficult to provide analytical conditions on simultaneous

stabilizability of more than three systems [BG93]. For this reason, we limit our analysis to LIMASs verifying the following condition.

Assumption 2.4.3. *The physical interconnection matrix A_p satisfies $A_p = \alpha A$ for a scalar $\alpha \in \mathbb{R}$.*

Remark 2.4.4. *Assumption 2.4.3 is satisfied when the states x_i and x_j impact on the dynamics of x_i in the same way. In particular, consider a LIMAS where the subsystem dynamics is as follows:*

$$x_i^+ = \check{A}x_i + \check{A}\sum_{j\in\mathcal{N}_i^p} a_{ij}x_j + Bu_i.$$

In this case, the effect of x_j on x_i^+ is the same as that of x_i, up to a scalar multiplication. Indeed, one can rewrite this dynamics in the form of (2.1) with $A = (1+\sum_{j\in\mathcal{N}_i^p} a_{ij})\check{A}$ and $A_p = \check{A}$, which verifies Assumption 2.4.3. Although restrictive, this assumption enables us to develop sufficient conditions that provide insights into the effects that various components of a LIMAS have on consensusability.

Under Assumption 2.4.3, consensusability is equivalent to the simultaneous stabilizability of pairs $((1-\alpha\lambda_{p,i})A, \lambda_{c,i}B)$, i.e., A_i and B_i are now only characterized by scalar multiplications of common matrices A and B, respectively. This allows for easier analysis of Schur stability of matrices $A_i + B_iK$, for a given control gain K. For this purpose, we first define $\alpha_i \triangleq 1-\alpha\lambda_{p,i}$, $\alpha_{\max} \triangleq \max_i |\alpha_i|$, $\alpha_{\min} \triangleq \min_i |\alpha_i|$, $\bar{A} \triangleq \alpha_{\max}A$, and

$$\sigma_c \triangleq 1 - \frac{1}{\prod_k \left|\lambda_k^u\left(\bar{A}\right)\right|^2}, \tag{2.27}$$

where $\lambda_1^u(\bar{A})$, $\lambda_2^u(\bar{A})$, ... denote the unstable eigenvalues of $\bar{A}$. Moreover, in the sequel, we leverage the results in [SSF+07] stating that if $\sigma > \sigma_c$, there exists a matrix $P = P^\top \succ 0$ solving the modified algebraic Riccati equation (MARE)

$$\bar{A}^\top P\bar{A} - \sigma\bar{A}^\top PB\left(B^\top PB\right)^{-1}B^\top P\bar{A} - P \prec 0. \tag{2.28}$$

The following theorem presents an algebraic sufficient condition for consensusability under Assumption 2.4.3. Note that, unlike Corollary 2.4.1.1, following results do not require the knowledge of the specific eigenvalue pairs $(\lambda_{p,i}, \lambda_{c,i})$ associated to the same eigenspace.

Theorem 2.4.2. *Suppose that Assumptions 2.4.1, 2.4.2, and 2.4.3 hold. If $\bar{A}$ is Schur stable, the LIMAS in (2.3) is consensusable by using the control gain $K = \mathbf{0}_{1\times n}$. Besides, if $\bar{A}$ is not Schur stable and the following condition holds*

$$\left(\frac{\max_{i,j}\frac{\alpha_i}{\lambda_{c,j}} - \min_{i,j}\frac{\alpha_i}{\lambda_{c,j}}}{2}\right)^2 < \frac{\alpha_{\min}^2 - \alpha_{\max}^2\sigma_c}{\lambda_{c,\max}^2}, \tag{2.29}$$

the LIMAS in (2.3) *is consensusable by using the control gain* $K = -k^*(B^\top PB)^{-1}B^\top PA$ *where* $k^* = \frac{\min_{i,j}\frac{\alpha_i}{\lambda_{c,j}}+\max_{i,j}\frac{\alpha_i}{\lambda_{c,j}}}{2}$ *and* P *is the solution to the MARE* (2.28) *with* $\sigma = \min_{i,j}\frac{2\alpha_i\lambda_{c,j}k^*-\lambda_{c,j}^2(k^*)^2}{\alpha_{\max}^2}$.

Proof. Under Assumptions 2.4.1 and 2.4.3, consensusability of (2.3) is equivalent to the simultaneous stabilizability of

$$\tilde{\delta}_i^+ = (\alpha_i A + \lambda_{c,i}BK)\,\tilde{\delta}_i \quad \forall i \in \{2,\dots,N\}. \tag{2.30}$$

It is straightforward to see that, if $\bar{A}$ is Schur stable, so are $\alpha_i A$; therefore, the LIMAS (2.3) is consensusable with the control gain $K = \mathbf{0}_{1\times n}$.

Next, we will show that when $\bar{A}$ is not Schur stable, and if (2.29) holds, $\tilde{\delta}_i$ in (2.30) are simultaneously stabilized by the control gain designed in the theorem. For this purpose, we will first show in the sequel that if (2.29) holds, we have

$$\min_{i,j}\frac{2\alpha_i\lambda_{c,j}k^* - \lambda_{c,j}^2(k^*)^2}{\alpha_{\max}^2} > \sigma_c. \tag{2.31}$$

We start by realizing that $k^* = \frac{\min_{i,j}\frac{\alpha_i}{\lambda_{c,j}}+\max_{i,j}\frac{\alpha_i}{\lambda_{c,j}}}{2}$ is the minimizer of a function $f(k) \triangleq \max_{i,j}|k - \frac{\alpha_i}{\lambda_{c,j}}| \geq 0$. Moreover, one can show that

$$\arg\min_k \max_{i,j}\left(k - \frac{\alpha_i}{\lambda_{c,j}}\right)^2 = \arg\min_k f(k) = k^*;$$

therefore, it directly follows that

$$\min_k \max_{i,j}\left(k - \frac{\alpha_i}{\lambda_{c,j}}\right)^2 = \left(\frac{\max_{i,j}\frac{\alpha_i}{\lambda_{c,j}} - \min_{i,j}\frac{\alpha_i}{\lambda_{c,j}}}{2}\right)^2.$$

Thus, in view of (2.29), we have

$$\max_{i,j}\left(k^* - \frac{\alpha_i}{\lambda_{c,j}}\right)^2 < \frac{\alpha_{\min}^2 - \alpha_{\max}^2\sigma_c}{\lambda_{c,\max}^2}. \tag{2.32}$$

Noticing that

$$\lambda_{c,j}^2\left(k^* - \frac{\alpha_i}{\lambda_{c,j}}\right)^2 = -(2\alpha_i\lambda_{c,j}k^* - \lambda_{c,j}^2(k^*)^2) + \alpha_i^2,$$

we get

$$\max_{i,j}\lambda_{c,j}^2\left(k^* - \frac{\alpha_i}{\lambda_{c,j}}\right)^2 \geq -\min_{i,j}\left(2\alpha_i\lambda_{c,j}k^* - \lambda_{c,j}^2(k^*)^2\right) + \alpha_{\min}^2. \tag{2.33}$$

Furthermore, from the fact that

$$\lambda_{c,\max}^2 \max_{i,j} \left(k^* - \frac{\alpha_i}{\lambda_{c,j}}\right)^2 \geq \max_{i,j} \lambda_{c,j}^2 \left(k^* - \frac{\alpha_i}{\lambda_{c,j}}\right)^2,$$

and using (2.32), (2.33), we can obtain

$$-\min_{i,j} \left(2\alpha_i \lambda_{c,j} k^* - \lambda_{c,j}^2 (k^*)^2\right) + \alpha_{\min}^2 < \alpha_{\min}^2 - \alpha_{\max}^2 \sigma_c. \tag{2.34}$$

This inequality is equivalent to (2.31); therefore, a solution P to the MARE (2.28) exists with

$$\sigma = \min_{i,j} \frac{2\alpha_i \lambda_{c,j} k^* - \lambda_{c,j}^2 (k^*)^2}{\alpha_{\max}^2} > \sigma_c.$$

Further, defining $\sigma_i \triangleq \frac{2\alpha_i \lambda_{c,i} k^* - \lambda_{c,i}^2 (k^*)^2}{\alpha_{\max}^2}$, we see that $\sigma \leq \sigma_i$ holds by definition. Therefore, P also satisfies the following for each i,

$$\bar{A}^\top P \bar{A} - \sigma_i \bar{A}^\top P B \left(B^\top P B\right)^{-1} B^\top P \bar{A} - P \prec 0,$$

which further implies

$$\alpha_{\max}^2 A^\top P A + \left(\lambda_{c,i}^2 (k^*)^2 - 2\alpha_i \lambda_{c,i} k^*\right) A^\top P B \left(B^\top P B\right)^{-1} B^\top P A - P \prec 0. \tag{2.35}$$

This is equivalent to the existence of $P \succ 0$ and $K = -k^*(B^\top P B)^{-1} B^\top P A$ such that

$$\left(\alpha_i A + \lambda_{c,i} B K\right)^\top P \left(\alpha_i A + \lambda_{c,i} B K\right) - P \prec 0,$$

for all $i \in \{2, \ldots, N\}$. Therefore, the systems (2.30) are simultaneously stabilizable, which further shows that the LIMAS (2.3) is consensusable by the designed controller. ■

The algebraic conditions in Theorem 2.4.2 are easily verifiable and do not require to solve any optimization problem. Moreover, they provide important insights about the effects of physical interconnection and communication graphs on consensusability, as discussed in Section 2.4.3. We stress that the derivations (2.31)-(2.34) consider the worst-case scenario in terms of eigenvalue pairs $(\lambda_{p,i}, \lambda_{c,i})$, hence contributing to the conservativeness of the result. Furthermore, without physical couplings ($\alpha = 0$), the inequality (2.29) cannot recover the sufficient and necessary condition for consensusability of MASs proposed in [YX11].

Necessary conditions

We now provide algebraic necessary conditions for the consensusability of the LIMAS in (2.3), which will allow us to identify features of the LIMAS disfavoring consensusability. We note that the following theorem does not require Assumption 2.4.3.

Theorem 2.4.3. *Suppose that Assumptions 2.4.1 and 2.4.2 hold. If the LIMAS in* (2.3) *is consensusable, at least one of the following conditions N1-N3 holds:*

N1. $\max_i |\det(A_i)| < 1$,

N2. $\max_i |\det(A_i)| \geq 1$ *and* $\min_i |\det(A_i)| < 1$ *and* (2.36),

N3. $\min_i |\det(A_i)| \geq 1$ *and* (2.36) *and* (2.37),

where $A_i = A - \lambda_{p,i} A_p$ *and*

$$\max_i |\det(A_i)| - 1 < \gamma_c \min_i |\det(A_i)| + \gamma_c, \tag{2.36}$$

$$\gamma_c(\min_i |\det(A_i)| - 1) < \max_i |\det(A_i)| + 1. \tag{2.37}$$

Proof. The proof is a modification of the proof of Lemma 3.1 in [YX11]. Under Assumption 2.4.2, without loss of generality, each pair $(A - \lambda_{p,i} A_p, B)$ can be written in reachable canonical form

$$A - \lambda_{p,i} A_p = \begin{bmatrix} 0 & 1 & 0 & \dots \\ \vdots & \ddots & \ddots & \ddots \\ 0 & \dots & 0 & 1 \\ -a_{i,1} & -a_{i,2} & \dots & -a_{i,n} \end{bmatrix}, \quad B = \begin{bmatrix} 0 \\ \vdots \\ 0 \\ 1 \end{bmatrix},$$

where $|a_{i,1}| = |\det(A - \lambda_{p,i} A_p)|$. Given a simultaneously stabilizing feedback gain $K = [k_1, \dots, k_N]$, one can see that $|\det(A_{cl,i})| = |a_{i,1} - \lambda_{c,i} k_1|$ for the closed-loop matrix $A_{cl,i} = A - \lambda_{p,i} A_p + \lambda_{c,i} BK$. Since K is selected to stabilize $(A - \lambda_{p,i} A_p, \lambda_{c,i} B)$ for all $i \in \{2, \dots, N\}$, it holds that $\rho(A_{cl,i}) < 1$. Therefore, it holds that $|\det(A_{cl,i})| = \prod_j \lambda_j(A_{cl,i}) < 1$, yielding $|a_{i,1} - \lambda_{c,i} k_1| < 1$, which can be further manipulated to give

$$\frac{|a_{i,1}| - 1}{\lambda_{c,i}} < |k_1| < \frac{|a_{i,1}| + 1}{\lambda_{c,i}}.$$

This implies that $\bigcap_{i=2}^{N} \left(\frac{|a_{i,1}|-1}{\lambda_{c,i}}, \frac{|a_{i,1}|+1}{\lambda_{c,i}} \right) \neq \emptyset$; therefore,

$$\max_i \frac{|a_{i,1}| - 1}{\lambda_{c,i}} < \min_i \frac{|a_{i,1}| + 1}{\lambda_{c,i}}. \tag{2.38}$$

Below, we will show that the above inequality implies that at least one of the conditions N1-N3 holds. We start by noting that, the left-hand side of (2.38) can either be negative or nonnegative. In the former case, (2.38) is always satisfied and it holds that $\max_i |a_{i,1}| < 1$, yielding the condition N1. On the contrary, when the left-hand side of

(2.38) is nonnegative,

$$\max_i \frac{|a_{i,1}|-1}{\lambda_{c,i}} \geq \max_i \frac{|a_{i,1}|-1}{\max_j \lambda_{c,j}} = \frac{\max_i |a_{i,1}|-1}{\lambda_{c,\max}}$$

and

$$\min_i \frac{|a_{i,1}|+1}{\lambda_{c,i}} \leq \min_i \frac{|a_{i,1}|+1}{\min_j \lambda_{c,j}} = \frac{\min_i |a_{i,1}|+1}{\lambda_{c,\min}}$$

hold. Therefore, combining these inequalities with (2.38), one gets (2.36). In addition, we note that

$$\max_i \frac{|a_{i,1}|-1}{\lambda_{c,i}} \geq \max_i \frac{\min_j |a_{j,1}|-1}{\lambda_{c,i}},$$

which means that (2.38) implies

$$\max_i \frac{\min_j |a_{j,1}|-1}{\lambda_{c,i}} < \min_i \frac{|a_{i,1}|+1}{\lambda_{c,i}}. \tag{2.39}$$

We again make the distinction of two cases where $\min_j |a_{j,1}|-1$ is negative or nonnegative. When the former holds, (2.39) is always satisfied. Hence, combining $\min_j |a_{j,1}| < 1$ with $\max_i |a_{i,1}| \geq 1$ and (2.36), one forms the condition N2. Otherwise, when it is nonnegative, one can show that

$$\max_i \frac{\min_j |a_{j,1}|-1}{\lambda_{c,i}} = \frac{\min_j |a_{j,1}|-1}{\lambda_{c,\min}}.$$

We can also derive an upper bound to the term on the right-hand side of (2.39) as

$$\min_i \frac{|a_{i,1}|+1}{\lambda_{c,i}} \leq \min_i \frac{\max_j |a_{j,1}|+1}{\lambda_{c,i}} = \frac{\max_j |a_{j,1}|+1}{\lambda_{c,\max}}.$$

Incorporating the last two equations with (2.39), we get (2.37). Finally, condition N3 is obtained by combining (2.36) and (2.37) with $\min_j |a_{j,1}| \geq 1$. ■

Note that the conditions N1-N3 involve only the three quantities $\max_i |\det(A_i)|$, $\min_i |\det(A_i)|$, and γ_c, making them easy to verify. These conditions also provide an understanding of how these variables effect consensusability, as discussed in the next section. Finally, observe that N3 reduces to the necessary and sufficient condition for the consensusability of MASs provided in [YX11] when physical couplings are absent, i.e., when $A_p = \mathbf{0}_{n\times n}$.

We also highlight that, in addition to providing sufficient conditions for consensusability, Theorems 2.4.1 and 2.4.2 as well as Corollary 2.4.1.1 also show how to design the controller gain K for reaching consensus. Note that Corollary 2.4.1.1 and Theorem 2.4.2 each provide one such gain K, instead of a range as in Theorem 2.4.1. Our results hinge on the assumption that these gains are precisely computed and implemented in the control module of every subsystem $\mathcal{S}_i$. Analysis of our results when this assumption is not satisfied is deferred to future work. Nevertheless, a numerical study of this case is

presented at the end of Section 2.5.2.

2.4.3 Discussion of the consensusability results

Hereafter, we discuss implications of the results given in the previous section. Specific comments provided below point out that consensusability is easier to achieve in LIMASs with

1. *weak* physical coupling and
2. *densely-connected* physical and communication graphs.

Specifically, the conditions S1 and S2 in Theorem 2.4.1 can be satisfied only if $\Delta_p < 2$. This is possible if $\lambda_{p,\max}$ is close to $\lambda_{p,\min}$, or if the physical coupling is weak. We also note that, by assuming $\Delta_p < 2$ and that the first inequality of S1 is satisfied, γ_c values satisfying the second inequality can always be found in a neighborhood of $\gamma_c = 1$. Moreover, this also holds for condition S2, showing that communication graphs whose Laplacian have eigenvalues that are close to each other favor consensusability. These conditions imply that both graphs $\mathcal{G}_p$ and $\mathcal{G}_c$ are *densely connected*. Therefore, this feature favors consensusability.

The LP in (2.17) is *easier* to solve when the pairs (A_i, B_i) are *closer* to each other, as discussed in Remark 2.3.4. With the definition $A_i = A - \lambda_{p,i} A_p$, it is straightforward to see that these matrices are *close* to each other when $\|\lambda_{p,i} A_p\|$ is *small*, or $\lambda_{p,i}$ are similar. Analogously, $B_i = \lambda_{c,i} B$ are *close* to each other when $\lambda_{c,i}$ are similar. These observations point out once more that the LP in (2.17) is more likely to be feasible when the physical interconnection is weak and both physical and communication graphs are densely connected.

Considering Theorem 2.4.2, the condition (2.29) can be satisfied only if $\alpha_{\min}^2 > \alpha_{\max}^2 \sigma_c$. Taking into account that σ_c increases with $\alpha_{\max}$, the inequality is fulfilled only when $\alpha_{\max}$ is sufficiently small and close to $\alpha_{\min}$. Note that $\alpha_{\max}$ takes small values for small values of α, i.e., when the effect of physical coupling is weak. Moreover, $\alpha_{\min}$ and $\alpha_{\max}$ are close to each other when $\lambda_{p,\min}$ and $\lambda_{p,\max}$ are close. Also note that the left-hand side of the inequality (2.29) decreases as the ratio $\frac{\lambda_{c,\min}}{\lambda_{c,\max}}$ increases, i.e., as the eigenvalues of the communication graph get closer to each other. Therefore, the implications of the Theorem 2.4.2 match with the observations made for Theorem 2.4.1.

In order to show the role of physical coupling in Theorem 2.4.3, we look at the extreme case $A = \mathbf{0}_{n\times n}$, for which condition N1 is not satisfied for *strong* physical coupling characterized by large values of $|\det(A_p)|$ and $\lambda_{p,i}$. Similarly, the inequality (2.36) is more difficult to satisfy for *stronger* physical coupling for fixed γ_c, since $\max_i |\det(A_i)|$ will be much larger than $\min_i |\det(A_i)|$. One can also see that, for fixed A_i, the inequality (2.37) gets more difficult to satisfy as γ_c grows, which corresponds to a decrease in the

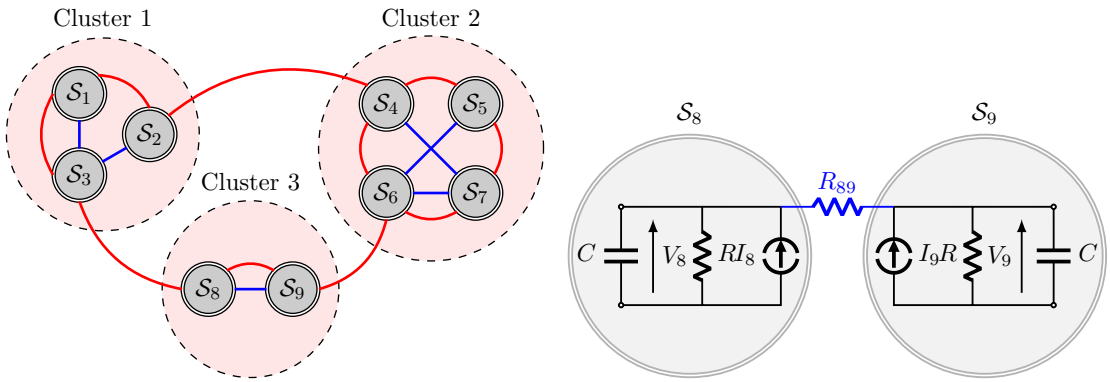

(a) Schematic of the network of identical supercapacitors arranged in multiple clusters. Lines in blue and red represent, respectively, the physical and communication interconnections.

(b) Electrical scheme of supercapacitors $\mathcal{S}_8$ and $\mathcal{S}_9$ in Cluster 3.

Figure 2.2: Network of identical supercapacitors considered for simulations in Section 2.5.1.

connectivity of the communication graph [BP02]. This, in turn, means that, it is more difficult to satisfy the condition N3 as the communication graph gets more *sparse*.

2.5 Simulation results

In this section, we present two different sets of simulations to validate the results in Sections 2.4.1 and 2.4.2, respectively.

2.5.1 Consensusability of a network of supercapacitors

In recent years, supercapacitors have been popularized as an alternative to batteries in application domains such as mGs, transportation systems, and automotive [IPQB13, FME15]. In some of these applications, a network of multiple supercapacitors can be utilized, making it a LIMAS. In the sequel, we consider a network of identical supercapacitors, which are arranged in clusters, as shown in Figure 2.2a. Such a system represents the scenario where groups of supercapacitors are far away from each other and no physical interconnection between them is possible.

As shown in Figure 2.2b, we model each subsystem i as a parallel RC circuit with $C = 10$ F, $R = 5$ $k\Omega$, and a current source supplying a time-varying current I_i. The resistance models the power *leak* from the capacitor. Subsystems are coupled through resistive electrical lines (see Figure 2.2b), whose resistance values R_{ij} are chosen randomly from the interval $[10, 50]$ Ω. We are interested in the problem of controlling the charging currents I_i such that the voltages across each supercapacitor reach consensus. In practical applications, this might be needed to ensure the same voltage level across all storage

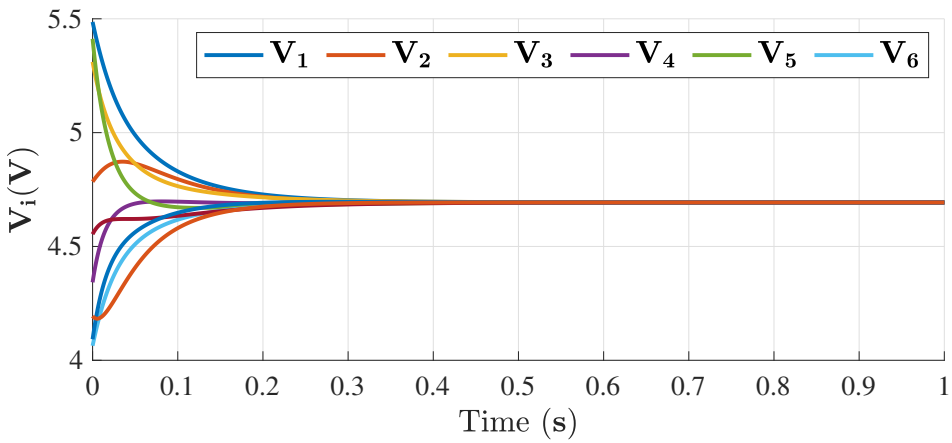

Figure 2.3: Voltages of the supercapacitors initialized with random initial voltages.

devices, as they might feed the same load during a *discharge* period (not considered here). We assume that, the input currents I_i are computed using the controller (2.2), utilizing the communication network represented in Figure 2.2a with unit edge weights. Applying Kirchoff's current and voltage laws, the voltage dynamics of the supercapacitor i is given by

$$C\dot{V}_i = -\frac{1}{R}V_i - \sum_{j\in\mathcal{N}_i^p}\frac{1}{R_{ij}}(V_i - V_j) + k\sum_{j\in\mathcal{N}_i^c}(V_i - V_j)\,. \tag{2.40}$$

In order to match the model (2.3), we discretize (2.40) in time by using the forward Euler method with a sampling period of $T_s = 0.1\ ms$. We obtain the dynamics

$$x^+ = (a\mathbf{I}_N - \mathcal{L}_p^m + k\mathcal{L}_c^m)x,$$

where $x = [V_1, \ldots, V_9]^\top$, $a = 1 - T_s\frac{1}{RC} \approx 1$, $\mathcal{L}_p^m \triangleq \frac{T_s}{C}\mathcal{L}_p$, and $\mathcal{L}_c^m \triangleq \frac{T_s}{C}\mathcal{L}_c$. Moreover, $\mathcal{L}_p$ and $\mathcal{L}_c$ are the Laplacian matrices of the physical and communication graphs, respectively. The *modified* Laplacian matrices $\mathcal{L}_p^m$ and $\mathcal{L}_c^m$ account for the effect of discretization, and are used in the analysis of consensusability.

On applying Theorem 2.4.1 to this system, we see that both conditions S1 and S2 are satisfied; therefore, any control gain k in the intervals $\mathbb{K}^+ \cap \mathbb{R}_{\geq 0} = [0, 4.071 \times 10^{-5})$ and $\mathbb{K}^- \cap \mathbb{R}_{<0} = (-4.071 \times 10^4, 0)$ guarantees the achievement of consensus. We choose $k = -200$ and initialize each supercapacitor with a random voltage value between $4V$ and $6V$ when running the continuous-time simulations of the LIMAS. As shown in Figure 2.3, all voltage levels converge to a common value, as guaranteed by Theorem 2.4.1. In order to see how tight the computed interval $\mathbb{K} = (-4.071 \times 10^4, 4.071 \times 10^{-5})$ of control gains is, we create a fine grid of k values strictly including $\mathbb{K}$ to check the values for which the matrix in (2.22) is Schur stable. We find that consensus is reached for k values in the interval $(-4.071 \times 10^4, 1.532 \times 10^{-4})$, which is very close to $\mathbb{K}$. This is expected since $\mathcal{L}_p^m$ is close to a zero matrix due to the small sampling time T_s (see Remark 2.4.1).

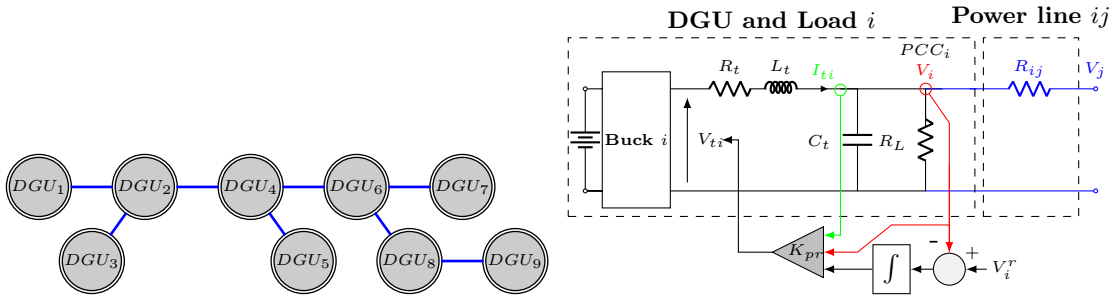

(a) Schematic of the DCmG. Blue lines represent the physical interconnection between DGUs, realized as resistive power lines.

(b) Electrical scheme of ith DGU along with load, connecting line(s), and local primary voltage regulator.

Figure 2.4: DCmG considered for simulations in Section 2.5.2.

Finally, because this LIMAS is consensusable and there exists a control gain k reaching consensus, Theorem 2.4.3 asserts that at least one of the conditions N1-N3 should hold. Upon setting $A_i = a - \lambda_i(\mathcal{L}_p^m)$, one sees that N1 is satisfied.

2.5.2 Consensusability of a DC microgrid

In this section, we consider a DCmG consisting of identical DGUs that are interconnected as shown in Figure 2.4a and study the consensusability problem. Each DGU is modeled as a Buck converter with an RLC filter, connecting a voltage source to a resistive load and neighboring DGUs, as shown in Figure 2.4b. We utilize the linear averaged state-space model [MS77] and assume that the voltage V_{ti} at the output of the Buck converter can be set to the desired value. Each DGU then includes a primary voltage controller to ensure voltage stability while steering the voltage value V_i at the PCC to the reference value V_i^r by manipulating V_{ti}. As depicted in Figure 2.4b, these primary controllers, developed in [NST+20], have a static state-feedback structure captured by the gain $K_{pr} = [k_{pr,1}, k_{pr,2}, k_{pr,3}]$ and integral action. On applying Kirchoff's voltage and current laws, the dynamics of the DGU i is written as

$$\begin{aligned} C_t\dot{V}_i &= -\frac{V_i}{R_L} + I_{ti} - \sum_{j\in\mathcal{N}_i^p} \frac{1}{R_{ij}}(V_i - V_j), \\ L_t\dot{I}_{ti} &= (k_{pr,1} - 1)V_i + (k_{pr,2} - R_t)I_{ti} + k_{pr,3}v_i, \\ \dot{v}_i &= -V_i + V_i^r, \end{aligned} \tag{2.41}$$

where I_{ti} is the filter current passing through the inductance and v_i is the integrator state of the primary controller. In this section, we seek to develop a secondary controller modifying the voltage references V_i^r of each DGU to achieve consensus on the states of all DGUs in the DCmG. Specifically, we consider a networked controller given by

$$V_i^r = V^r + K \sum_{j\in\mathcal{N}_i^c} b_{ij}(x_i - x_j), \tag{2.42}$$

where $x_i \triangleq [V_i, I_{ti}, v_i]^\top$ is the state of DGU i and $V^r = 48\ V$ is a common nominal voltage reference for all DGUs. We note that DGUs in the DCmG are physically coupled to each other and the secondary controller (2.42) is based on a communication network (inducing the set of neighbors $\mathcal{N}_i^c$). Therefore, after discretizing (2.41) with forward Euler method with a sampling period of $T_s = 0.1\ ms$, the overall dynamics of the DCmG can be written as

$$x^+ = (\mathbf{I}_N \otimes A - \mathcal{L}_p \otimes A_p + \mathcal{L}_c \otimes BK)\, x + (\mathbf{1}_N \otimes B)V^r,$$

where the system matrices are defined as $A = \mathbf{I}_3 - T_s A_{ct}$,

$$A_{ct} = \begin{bmatrix} -\frac{1}{R_L C_t} & \frac{1}{Ct} & 0 \\ \frac{k_{pr,1}-1}{L_t} & \frac{k_{pr,2}-R_t}{L_t} & \frac{k_{pr,3}}{L_t} \\ -1 & 0 & 0 \end{bmatrix},\ A_p = \begin{bmatrix} \frac{T_s}{C_t} & 0 & 0 \\ 0 & 0 & 0 \\ 0 & 0 & 0 \end{bmatrix},\ B = \begin{bmatrix} 0 \\ 0 \\ T_s \end{bmatrix}. \tag{2.43}$$

Note that the presence of the constant input $(\mathbf{1}_N \otimes B)V^r$ does not hinder the application of our results. Indeed, by undertaking the derivations in equations (2.3)-(2.5), it is straightforward to show that the deviation δ follows the dynamics (2.6). We use the parameter values $R_t = 0.2\ \Omega$, $C_t = 2.2\ mF$, $L_t = 1.8\ mH$, $R_L = 9\ \Omega$, and $K_{pr} = [-2.13, -0.16, 13.55]$ taken from [NST+20]. Moreover, $\mathcal{L}_p$ is derived from the physical interconnection topology in Figure 2.4a and edge weights $1/R_{ij}$, $\forall i \in \{1, \ldots, 9\}$, $j \in \mathcal{N}_i^p$, where power line resistances R_{ij} are selected randomly in the interval $[4, 8]\ \Omega$. In order to verify Assumption 2.4.1, we assume a complete communication graph with uniform edge weights. Therefore, $\mathcal{L}_c = \mathbf{I}_9 - \frac{1}{9}\mathbf{1}_9\mathbf{1}_9^\top$. With these definitions, it is easy to verify that Assumption 2.4.2 also holds. Hence, Corollary 2.4.1.1 can be utilized.

We construct the necessary matrices as shown in (2.11)-(2.12), (2.15)-(2.16) and verify that the LP in (2.17) is feasible. Hence, a consensus-enabling controller gain K can be designed. With this controller in place, we run a simulation from random initial conditions of DGUs, based on their continuous-time dynamics in (2.41). Figure 2.5 shows that consensus is quickly reached as Corollary 2.4.1.1 certifies, and the voltages are regulated, albeit relatively slowly, towards the nominal reference value of 48 V. Furthermore, condition N1 is satisfied, as Theorem 2.4.3 guarantees for this consensusable LIMAS.

In order to show the effect of physical coupling on consensusability, we gradually increase Δ_p by scaling down the line resistances, i.e., we use $\tilde{R}_{ij} \triangleq \xi R_{ij}$ in the definition of $\mathcal{L}_p$ for $\xi \in (0, 1)$. For $\xi = 0.072$, the LP in (2.17) becomes infeasible. Similarly, if a DCmG is not consensusable using the proposed results, weakening its physical coupling could make it consensusable.

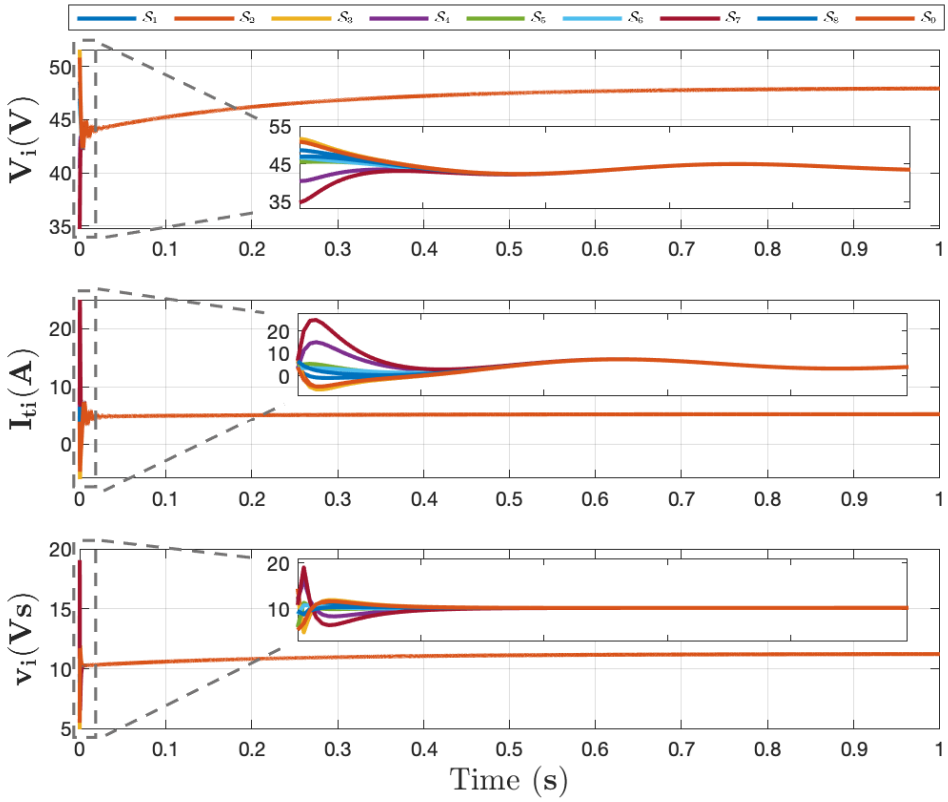

Figure 2.5: States of the DGUs in the DCmG equipped with consensus controllers. The zoomed-in figures show that consensus is achieved very quickly.

Violation of assumptions

We next investigate whether our consensusability test in Corollary 2.4.1.1 can be used even when Assumption 2.4.1 is not satisfied. We do this by changing the topology of $\mathcal{G}_c$. We see that the LP in (2.17) is infeasible for $\mathcal{G}_c$ with circle and star topologies and unit edge weights. Moreover, although (2.17) is feasible for a complete $\mathcal{G}_c$, it can become infeasible upon removal of 2 edges. By keeping the complete topology of $\mathcal{G}_c$ and selecting non-uniform edge weights between 0 and 1, we see that (2.17) becomes infeasible as well. This study reveals that our results depend critically on the satisfaction of Assumption 2.4.1.

We also discuss the effect of violating two implicit assumptions of our technical results, namely, that

A1. the control gain $K = v_N + w^\top$ is precisely computed by solving (2.17);
A2. every subsystem $\mathcal{S}_i$ uses the same control gain K.

For this purpose, we conduct new simulations where each DGU adopts a different control gain

$$K_i = K \circ (\mathbf{1} + \tilde{\Delta}_i),$$

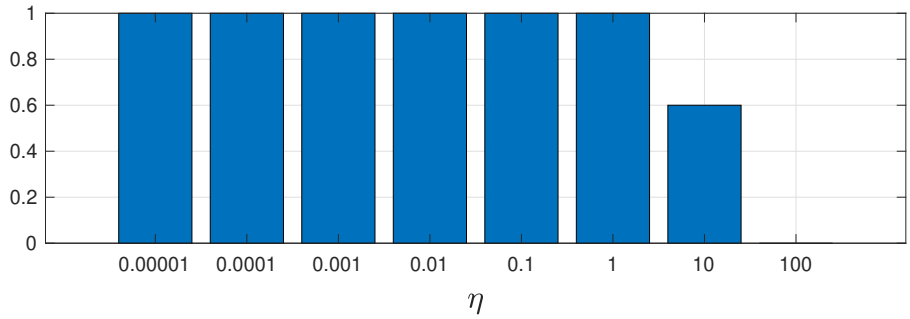

Figure 2.6: Proportion of simulation runs where consensus is reached.

where $\circ$ denotes element-wise matrix multiplication and $\tilde{\Delta}_i$ is a matrix whose elements are randomly chosen between $[-\eta,\ \eta]$. This definition captures the scenario in which the control gain is inaccurately known in each subsystem $\mathcal{S}_i$. Corollary 2.4.1.1 states that K ensures the achievement of consensus; however, the *perturbation* in gains K_i may hinder consensus. Indeed, the intensity of this perturbation increases with the parameter η, which takes values in $\{10^{-5},\ 10^{-4},\ 10^{-3},\ 10^{-2},\ 10^{-1},\ 10^{0},\ 10^{1},\ 10^{2}\}$ in our simulations. In particular, for each value of η, the continuous-time DCmG dynamics is simulated 10 times from random initial conditions. The proportion of simulation runs where the DCmG asymptotically reaches consensus are displayed in Figure 2.6 for different values of η. It is seen from this figure that the DGUs eventually reach consensus in most cases for $\eta \leq 10$.

Nevertheless, the perturbation in control gains results in large transient fluctuations of the DGU states. Recalling that the consensus state is denoted as $\bar{v}$, we define the maximum absolute fluctuation from $\bar{v}$ as

$$\widetilde{x}_{\max} = \begin{bmatrix} \widetilde{V}_{\max} \\ \widetilde{I}_{t,\max} \\ \widetilde{v}_{\max} \end{bmatrix} \triangleq \max_{t>0,\ i} |x_i(t) - \bar{v}|.$$

Figure 2.7 shows, for each value of η, the average $\widetilde{x}_{\max}$ among all simulations that reach consensus. It is seen in this figure that, despite the asymptotic attainment of consensus, high perturbations on gains K_i can lead to very large transient voltage and current values, thus limiting the applicability of the proposed controllers when A1 and A2 are violated.

2.6 Conclusions

In this chapter, we considered linear MASs with physical interconnections among subsystems (LIMASs) and studied their consensusability properties. We show that consensusability of LIMASs is related to a simultaneous stabilization problem and present an LP-based method for verifying simultaneous stabilization. Based on this result, we give a

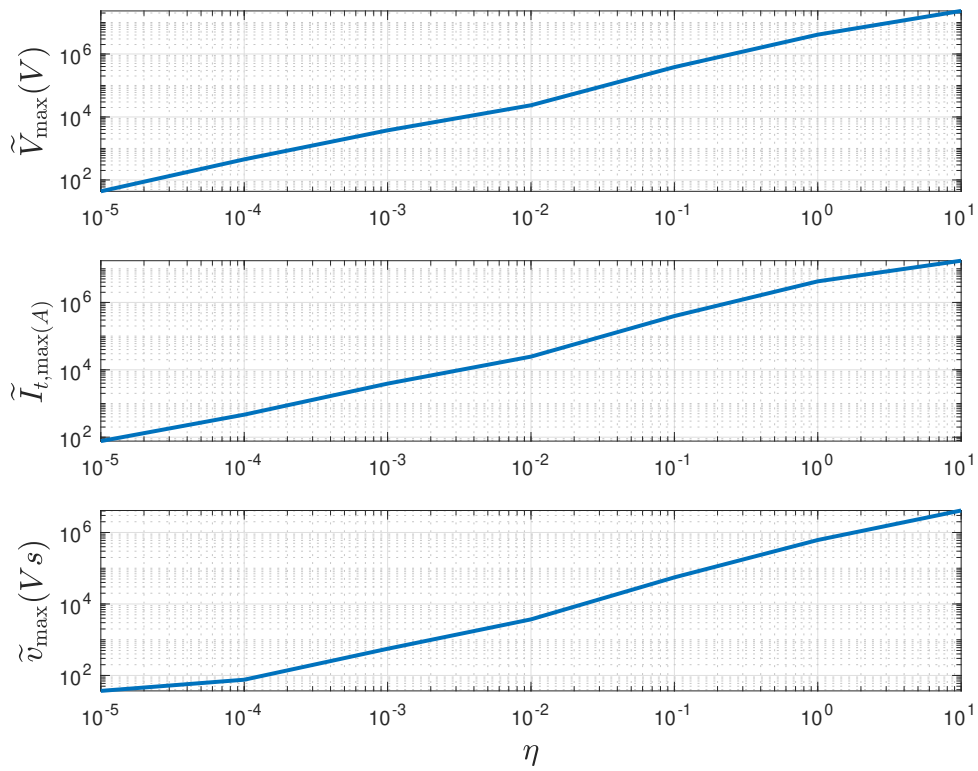

Figure 2.7: Average transient fluctuations $\widetilde{x}_{\max}$ among all simulations reaching consensus.

numerical sufficient condition for the consensusability of a LIMAS. Moreover, we propose several algebraic consensusability conditions that are either sufficient or necessary. The derived results show that *weak* physical coupling and *densely-connected* physical and communication graphs are favorable for consensusability. The results are verified in computer simulations of a network of supercapacitors and a DCmG.

We note that the results of this chapter apply for any LIMAS satisfying the assumptions. As such, they do not exploit the system structure that comes with a specific application example (see the sparsity patterns of the matrices in (2.43)). Indeed, in particular applications, it might be possible to achieve more sophisticated consensus objectives by exploiting these structures. In the next chapter, we show this by developing a consensus-based control scheme for current sharing and voltage balancing in DCmGs.

3 Consensus for current sharing in microgrids

3.1 Introduction

In control of islanded DCmGs, the main objective is voltage stability as it prevents voltages from either exceeding a critical level or dropping suddenly, consequently damaging connected loads [MSFT+17]. As discussed in Section 2.5.2, a primary voltage control layer is often employed for achieving voltage stability and tracking desired voltage references at the PCC [SGV14, MNF18, SPM+20, NST+20, TRFT18]. Besides stability, another desirable objective is current sharing, that is, DGUs share mG loads in accordance with their current ratings. Indeed, unregulated currents may otherwise overload generators and eventually lead to an mG failure. An additional goal of voltage balancing, requiring boundedness of weighted sum of PCC voltages, is often sought to complement current sharing [TMGFT18]. Being blind voltage reference emulators, primary controllers are unable to attain the aforementioned objectives all by themselves. Higher-level secondary control architectures [IRD+19, BNF19] are, therefore, necessary to coordinate the voltage references provided to the primary layers.

Distributed, consensus-based secondary regulators guaranteeing current sharing and voltage balancing have been the subject of many recent contributions. Centralized approaches to their synthesis are proposed in [NMDL15, SDA+14], but are prohibitive for large-scale mGs as they require knowledge of mG topology, lines, loads, and DGUs. Indeed, temporally varying DCmGs call for scalable design of decentralized controllers [NST+20, TRFT18], enabling the plug-in/-out of DGUs on the fly without spoiling the overall stability of the network. Scalable consensus-based secondary controllers discussed in [TMGFT18, ZD15] remedy the above limitations; but introduce a time-scale separation by abstracting primary-controlled DGUs as ideal voltage generators or first-order systems. Moreover, they assume static power lines. Efforts to incorporate DGU dynamics and RL lines have been made in [TCCS19, CTDP+18]. In [CTDP+18], a robust distributed control algorithm considering both objectives is studied; however, a suitable initialization of the controller is needed. The resistance of the DGU filter is neglected in [TCCS19] and

hence, voltage balancing cannot be guaranteed in steady state. Unlike [TMGFT18, ZD15, TCCS19, CTDP+18] limited to linear loads, [DPWD18] presents a power consensus algorithm intended for DCmGs feeding ZIP (constant impedance, constant current, and constant power) loads. However, this work assumes simplified DCmG dynamics and existence of a suitable steady state.

All the foregoing contributions exclude E (exponential) loads — generalized static loads which cover a wide variety of physical loads like industrial motors, fluorescent lighting, pumps, fans, etc. [Kun94, Rom02]. We highlight that, in DCmGs catering to E loads, steady-state current sharing and voltage balancing need to be backed by certificate guarantees. This is due to the fact that these nonlinear loads may jeopardize the stability of the DCmG by introducing a destabilizing negative impedance into the network (see Section 3.4).

3.1.1 Contributions

In this chapter, we introduce a distributed secondary control layer for proportional current sharing and weighted voltage balancing in DCmGs consisting of DGUs, loads, and interconnecting power lines. Compared to Section 2.5.2, in this chapter, we switch to a continuous-time setting, consider a more realistic DCmG model, and formulate a different consensus problem. In particular, the DCmG is allowed to have non-identical DGUs supporting ZIE (constant impedance, constant current, and exponential) loads instead of only resistive loads. Moreover, dynamic RLC power lines connect DGUs rather than static resistive ones. As it will be shown later, Assumption 2.4.1 is not needed in this chapter, as the communication graph can have any topology as long as it is connected. Consequently, the considered DCmG model corresponds to an interconnected MAS (see Figure 2.1). We stress that it is no longer a LIMAS due to the existence of non-linear ZIE loads. In this chapter, we do not consider a static feedback controller as in (2.2), but rather a dynamic one with a different structure. Finally, the objective in this chapter is not full state consensus, but current sharing, which is a specific example of output consensus in DCmGs.

The main novelties of this chapter when compared to the existing literature are four-fold. First, this work does away with the modeling limitations of several existing contributions. In addition to RLC lines, we consider DGU dynamics and filter resistances. Our Buck converter–interfaced DGUs are modeled after the linear, averaged state-space model [MS77]. On the load modeling front, we take into account nonlinear E loads, which are popularly referred to as generalized ZIP loads, and whose power consumption depends on the exponent of the PCC voltage. From what we know, this work is the very first treatise of E loads in the context of DCmGs. Second, we propose a new consensus-based secondary control scheme relying on the exchange of variables with the nearest neighbors over a connected communication network. To achieve current sharing and voltage balancing,

these secondary regulators operate at the same time scale as the primary controllers while appropriately modifying primary voltage references. In spite of their distributed structure, their control design is completely decentralized, allowing for plug-and-play operations. Third, we thoroughly investigate the steady-state behavior of the DCmG under secondary control, and show that the desired goals are always attained in steady state. In particular, the steady-state regime is governed by the physics of the DCmG, and our specific controller has no bearing on the existence of equilibria. Moreover, for the specific case of P loads — E loads with zero exponent, we deduce sufficient conditions on the existence and uniqueness of an equilibrium point meeting secondary goals. Such an analysis is not trivial due to the introduced nonlinearities, and entails finding solutions to DC power-flow equations constrained to a hyperplane. To the best of our knowledge, this has not been addressed in the literature before. Fourth, we present a voltage stability analysis of the closed-loop DCmG, which shows that stability is independent of the physical and communication topologies, and lays out conditions on the controller gains and power consumption of E loads. To substantiate the efficacy of our controllers, we also conduct realistic simulations accommodating non-ideal DGUs with nonlinear switching behavior, and abrupt load variations.

Section 3.2 recaps the DCmG model and primary voltage control. Section 3.3 sets forth our secondary control scheme, and details the steady-state behavior of the closed-loop DCmG in the presence of ZIE loads. Section 3.4 houses a stability analysis, which proves the convergence to an equilibrium point simultaneously fulfilling both current sharing and voltage balancing objectives. Simulations validating theoretical results are provided in Section 3.5. Finally, conclusions are drawn in Section 3.6.

3.2 DCmG model and primary voltage control

In this section, we start by reviewing the considered DCmG model [NST+20, TRFT18] comprising multiple DGUs interconnected with each other via power lines, and recall the concepts of primary voltage control.

DCmG Model: The DCmG is modeled as an interconnected MAS shown in Figure 2.1 consisting of two undirected and connected graphs: a physical coupling graph $\mathcal{G}_p = (\mathcal{V}, \mathcal{W}_p, \mathcal{E}_p)$ and a cyber coupling graph $\mathcal{G}_c = (\mathcal{V}, \mathcal{W}_c, \mathcal{E}_c)$. To each node, also referred to as PCC, is connected a DGU and a load. The interconnecting power lines are represented by the edges of $\mathcal{G}_p$. On assigning a number to each line, we equivalently express $\mathcal{E}_p = \{l_1, \ldots, l_M\}$ with M denoting the total number of lines. After defining B as the incidence matrix of $\mathcal{G}_p$, the *Kirchoff's Current Law* (KCL) can be represented as $x = B\xi$, where $x \in \mathbb{R}^{|\mathcal{V}|}$ and $\xi \in \mathbb{R}^{|\mathcal{E}|}$ respectively represent the nodal injections and edge flows. Assume that the edge $l \in \{1, ..., |\mathcal{E}|\}$ is oriented from i to j, then for any vector $V \in \mathbb{R}^{|\mathcal{V}|}$, $(B^\top V)_l = V_i - V_j$. Note that edge directions are arbitrarily assigned, and provide a reference system for positive currents.

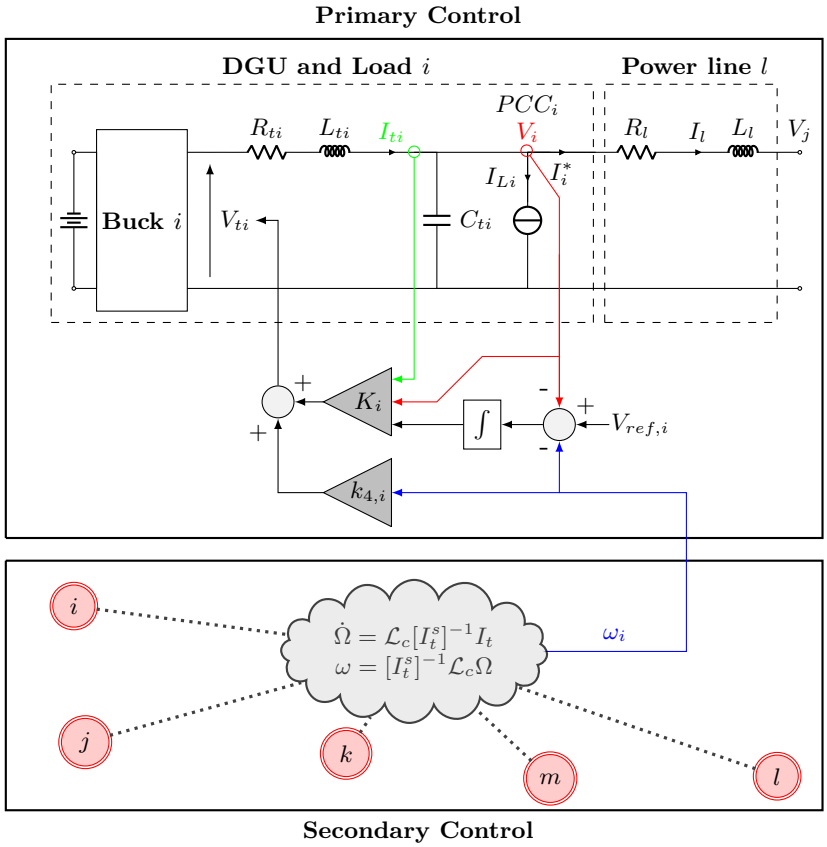

Figure 3.1: Schematic diagram showing primary and secondary control layers of the DCmG, as well as the electric scheme of ith DGU and load. Note that the topology of the communication network is not shown.

Dynamic model of a power line: Modeled after the π-equivalent model of transmission lines [Kun94], the dynamic behavior of lth power line is given by

$$\Sigma_{[l]}^{Line} : \left\{ \frac{dI_l}{dt} = -\frac{R_l}{L_l} I_l + \frac{1}{L_l} \sum_{i \in \mathcal{N}_l} B_{il} V_i \ , \right. \tag{3.1}$$

where $\mathcal{N}_l$ is the set of DGUs incident to the lth line, B_{il} represents the element in i^{th} row and l^{th} column of the incidence matrix B, and the variables V_i and I_l represent the voltage at PCC_i and the line current, respectively. Note that the line capacitances are assumed to be lumped with the DGU filter capacitance C_{ti}. Therefore, as shown in Figure 3.1, the RLC power line l is equivalently represented as an RL circuit with resistance $R_l > 0$ and inductance $L_l > 0$.

Dynamic model of a DGU: As in Section 2.5.2, the DGU comprises a DC voltage source (usually generated by a renewable resource), a Buck converter, and a series RLC filter. The ith DGU, feeding a local load at PCC_i, is connected to other DGUs via power lines.

A schematic electric diagram of the ith DGU along with load, connecting line(s), loads, and local PnP voltage controller is represented in Figure 3.1. Note the differences in this figure with respect to Figure 2.4b in terms of a ZIE load, RL power line, and different primary controller structure. Correspondingly, the electrical dynamics are written as

$$\Sigma_{[i]}^{DGU}: \begin{cases} C_{ti}\dfrac{dV_i}{dt} = I_{ti} - I_{Li}(V_i, r_i) - \displaystyle\sum_{l\in\mathcal{E}_p} B_{il}I_l \\ L_{ti}\dfrac{dI_{ti}}{dt} = -V_i - R_{ti}I_{ti} + V_{ti} \end{cases}, \quad i \in \mathcal{V}, \tag{3.2}$$

where $I_{Li}(V_i, r_i)$ is the current drawn by the nonlinear load and $\sum_{l\in\mathcal{E}_p} B_{il}I_l$ captures the total current injected into the DCmG by DGU i. The other terms and definitions are the same as in Section 2.5.2. Namely, $R_{ti} \in \mathbb{R}_{>0}$, $L_{ti} \in \mathbb{R}_{>0}$, and $C_{ti} \in \mathbb{R}_{>0}$ are the internal resistance, capacitance (lumped with the line capacitances), and inductance of the DGU converter, respectively.

Remark 3.2.1. ***(Modeling DC–DC converters).*** *We remind that we bank on the standard space averaging method [MS77] in developing the DCmG model, enabling us to disregard the switching behavior of V_{ti}. Consequently, we have $V_{ti} = d_iV_{si}$, where $d_i \in [0, 1]$ is the duty cycle of the Buck converter, and $V_{si} \in \mathbb{R}$ the voltage of its power source. Throughout, we suppose V_{si} is large enough to avoid saturation of d_i.*

Each DGU is equipped with a local voltage regulator, which along with other such regulators constitutes the *primary control layer*. The main objective of these controllers is to ensure that the voltage at each DGU's PCC tracks a reference voltage $V_{ref,i}$. For this purpose, we augment each DGU with a multivariable PI regulator (see Figure 3.1)

$$\begin{aligned} \dot{v}_i &= e_{[i]} = V_{ref,i} - V_i - \omega_i, \\ \mathbb{C}_{[i]}:\ V_{ti} &= K_{[i]}\hat{x}_{[i]} + k_{4,i}\omega_i, \end{aligned} \tag{3.3}$$

where $\hat{x}_{[i]} = [V_i\ I_{ti}\ v_i]^\top \in \mathbb{R}^3$ is the state of augmented DGU, $K_{[i]} = [k_{1,i}\ k_{2,i}\ k_{3,i}] \in \mathbb{R}^{1\times 3}$ and $k_{4,i} \in \mathbb{R}$ are feedback gains, and ω_i is an exogenous variable generated by the *secondary controller* (see Section 3.3 for more details). From (3.2)–(3.3), the closed-loop DGU model is similar to (2.41) except a few updated terms:

$$\hat{\Sigma}_{[i]}^{DGU}: \begin{cases} \dfrac{dV_i}{dt} = \dfrac{1}{C_{ti}}I_{ti} - \dfrac{1}{C_{ti}}I_{Li}(V_i, r_i) - \dfrac{1}{C_{ti}}I_i^* \\ \dfrac{dI_{ti}}{dt} = \alpha_iV_i + \beta_iI_{ti} + \gamma_iv_i + \delta_i\omega_i \\ \dfrac{dv_i}{dt} = -V_i + V_{ref,i} - \omega_i \end{cases}, \tag{3.4}$$

where

$$\alpha_i = \frac{(k_{1,i} - 1)}{L_{ti}},\ \beta_i = \frac{(k_{2,i} - R_{ti})}{L_{ti}},\ \gamma_i = \frac{k_{3,i}}{L_{ti}}, \tag{3.5}$$

and

$$\delta_i = \frac{k_{4,i}}{L_{ti}}. \tag{3.6}$$

We highlight that variable $\omega_i = 0$ when the secondary control layer is inactive or absent. The primary control architecture is hence decentralized as the computation of V_{ti} requires only the state of $\hat{\Sigma}_{[i]}^{DGU}$.

Load model: The ith load is the parallel combination of Z, I, and E loads. The total current $I_{Li}(V_i, r_i)$, a function of voltage at PCC_i, is given as

$$I_{Li}(V_i, r_i) = \underbrace{Y_{Li}V_i}_{Z} + \underbrace{\bar{I}_{Li}}_{I} + \underbrace{V_i^{r_i-1}P_{Li}^*}_{E}, \tag{3.7}$$

where Y_{Li} is the conductance of the Z load while $r_i \in \mathbb{R}$ the exponent of the E load. The constant $\bar{I}_{Li}$ is the current consumed by the I load, and P_{Li}^* is the power constant of the E load. Note that an E load corresponds to a constant-power load when $r_i = 0$, and covers wide range of physical loads depending upon the value of r_i. Some common examples are air conditioners ($r_i \in (0.50, 2.50)$), resistance space heaters ($r_i = 2$), and fluorescent lighting ($r_i \in (1, 3)$) [Kun94, Rom02].

Assumption 3.2.1. *The reference signals $V_{ref,i}$ and PCC voltages V_i are strictly positive for all $t \geq 0$.*

We remark that Assumption 3.2.1 is not a limitation, and rather reflects a common constraint in mG operation. Notice that, in Figure 3.1, one end of the load is connected to the PCC and the other to the ground, assumed be at zero potential by convention. Since the electric current and hence power flows from higher to lower potential, negative references and PCC voltages will reverse the role of loads and make them power generators. In order to ensure power balance in the network, the generators will have to absorb this surplus power. This, in effect, defeats the fundamental goal of the mG, that is, the satisfiability of the loads by virtue of the power generated by the DGUs. Furthermore, if $V_i, V_{ref,i} \in \mathbb{R}^N$, then a zero-crossing for the voltages may take place. As voltages tend to zero, the power consumed by the ZIE loads with exponents $r_i < 1$ approaches infinity.

3.3 Secondary control in DCmGs

3.3.1 Problem formulation

The primary control layer is designed to track a suitable reference voltage $V_{ref,i}$ at the PCC_i. As such, they do not ensure proportional current sharing and voltage balancing, defined as follows.

Definition 3.3.1. ***(Current sharing [TMGFT18, ZD15]).*** *The load is said to be*

shared proportionally among DGUs if

$$\frac{I_{ti}}{I_{ti}^s} = \frac{I_{tj}}{I_{tj}^s} \quad \textit{for all } i, j \in \mathcal{V}, \tag{3.8}$$

where the constant $I_{ti}^s > 0$ is the rated current of DGU i.

Current sharing ensures proportional sharing of loads amongst multiple DGUs, avoiding situations of DGU overloading, and preventing harm to the converter modules. As will be shown in the subsequent sections, the steady state voltages need not necessarily be equal to $V_{ref,i}$ when currents are shared proportionally. It is, however, desirable that PCC voltages remain close to the nominal reference voltages for normal operation of the DCmG. To this aim, we state the objective of weighted voltage balancing in the following definition.

Definition 3.3.2. ***(Weighted voltage balancing [CTDP+18]).*** *The voltages are said to be balanced in the steady state if*

$$\langle [I_t^s] V \rangle = \langle [I_t^s] V_{ref} \rangle, \tag{3.9}$$

with $V_{ref} \triangleq [V_{ref,1} \ \dots \ V_{ref,N}]^\top \in \mathbb{R}^N$ being the vector of reference voltages.

Voltage balancing implies that the weighted sum of PCC voltages is equal to the the weighted sum of voltage references, ensuring boundedness of DCmG voltages. As noticed in [ZD15], in its absence, the PCC voltages may experience drifts and increase monotonically despite the filter currents' being shared proportionally.

3.3.2 Consensus-based secondary control

To achieve the aforementioned objectives, we use a consensus-based secondary control layer. Consensus filters are commonly employed for achieving global information sharing or coordination through distributed computations [OSM04, Bul17]. In our case, we propose the following consensus scheme

$$\dot{\Omega}_i = \sum_{j=1, j\neq i}^{N} a_{ij} \left(\frac{I_{ti}}{I_{ti}^s} - \frac{I_{tj}}{I_{tj}^s} \right), \tag{3.10}$$

$$\omega_i = \frac{1}{I_{ti}^s} \sum_{j=1, j\neq i}^{N} a_{ij} \left(\Omega_i - \Omega_j \right), \tag{3.11}$$

where $a_{ij} > 0$ if DGUs i and j are connected by a communication link ($a_{ij} = 0$, otherwise). Information is exchanged according to the *cyber coupling graph* $\mathcal{G}_c$ defined in Section 3.2. We remind that $\mathcal{G}_c$ is assumed to be connected, but its topology can be completely

arbitrary. As shown in Figure 3.1, the consensus variable ω_i modifies the primary voltage controllers; see (3.3).

Remark 3.3.1. ***(Structure of secondary voltage regulators).*** *The proposed controllers have a distributed structure, and exchange Ω_i and I_{ti} with their communication neighbors. Utilizing the received information, the ith DGU simultaneously computes the variable ω_i used to adapt the voltage references $V_{ref,i}$ and the DGU command V_{ti}, with a view to attaining* (3.8)-(3.9)*. It is worth noting that the scheme discussed in this work is different from [TMGFT18], where only I_{ti} is communicated, and uniquely $V_{ref,i}$ is altered. In addition, this work does not reduce DGUs to ideal voltage generators or first-order systems, and eliminates assumptions on the topology of the communication network.*

The complete dynamics of the DCmG under primary and secondary control are given by (3.1)–(3.6) along with (3.10)–(3.11). These equations can be compactly rewritten as

$$\dot{X} = \mathcal{A}X + \mathcal{B}(V), \tag{3.12}$$

where $X = \begin{bmatrix} V^\top & I_t{}^\top & v^\top & I^\top & \Omega^\top \end{bmatrix}^\top \in \mathbb{R}^{4N+M}$,

$$\mathcal{A} = \underbrace{\begin{bmatrix} -C_t^{-1}Y_L & C_t^{-1} & \mathbf{0} & -C_t^{-1}B & \mathbf{0} \\ [\alpha] & [\beta] & [\gamma] & \mathbf{0} & [\delta][I_t^s]^{-1}\mathcal{L}_c \\ -\mathbf{I} & \mathbf{0} & \mathbf{0} & \mathbf{0} & -[I_t^s]^{-1}\mathcal{L}_c \\ L^{-1}B^\top & \mathbf{0} & \mathbf{0} & -L^{-1}R & \mathbf{0} \\ \mathbf{0} & \mathcal{L}_c[I_t^s]^{-1} & \mathbf{0} & \mathbf{0} & \mathbf{0} \end{bmatrix}}_{\mathcal{A}\in\mathbb{R}^{(4N+M)\times(4N+M)}},$$

and

$$\mathcal{B}(V) = \underbrace{\begin{bmatrix} -C_t^{-1}(\bar{I}_L + [V^{r-\mathbf{1}_N}]P_L^*) \\ \mathbf{0}_N \\ V_{ref} \\ \mathbf{0}_M \\ \mathbf{0}_N \end{bmatrix}}_{\mathcal{B}(V)\in\mathbb{R}^{(4N+M)}}.$$

Note that $V \in \mathbb{R}^N$, $I_t \in \mathbb{R}^N$, $v \in \mathbb{R}^N$, $I \in \mathbb{R}^M$, $P_L^* \in \mathbb{R}^N$, $\bar{I}_L \in \mathbb{R}^N$, $r \in \mathbb{R}^N$, $\alpha \in \mathbb{R}^N$, $\beta \in \mathbb{R}^N$, $\gamma \in \mathbb{R}^N$, $\delta \in \mathbb{R}^N$ are vectors of PCC voltages, filter currents, integrator states, line currents, load powers, load currents, E load exponents, and parameters α_i, β_i, γ_i, δ_i respectively. The matrices $R \in \mathbb{R}_{>0}^{M\times M}$, $L \in \mathbb{R}_{>0}^{M\times M}$, $Y_L \in \mathbb{R}_{>0}^{N\times N}$, and $C_t \in \mathbb{R}_{>0}^{N\times N}$ are diagonal matrices collecting electrical parameters R_l, L_l, Y_{Li}, and C_{ti}, respectively. $\mathcal{L}_c \in \mathbb{R}^{N\times N}$ is the Laplacian matrix of the communication network. Notice that the dynamics of the DCmG controlled only by the primary layer can be recuperated by

setting $\Omega = \mathbf{0}_N$ as

$$\dot{X}' = \underbrace{\begin{bmatrix} -C_t^{-1}Y_L & C_t^{-1} & \mathbf{0} & -C_t^{-1}B \\ [\alpha] & [\beta] & [\gamma] & \mathbf{0} \\ -\mathbf{I} & \mathbf{0} & \mathbf{0} & \mathbf{0} \\ L^{-1}B^\top & \mathbf{0} & \mathbf{0} & -L^{-1}R \end{bmatrix}}_{\mathcal{A}' \in \mathbb{R}^{(3N+M)\times(3N+M)}} \underbrace{\begin{bmatrix} V' \\ I_t' \\ v' \\ I' \end{bmatrix}}_{\dot{X}'} + \underbrace{\begin{bmatrix} -C_t^{-1}(\bar{I}_L + [(V')^{r-\mathbf{1}_N}]P_L^*) \\ \mathbf{0}_N \\ V_{ref} \\ \mathbf{0}_M \end{bmatrix}}_{\mathcal{B}'(V) \in \mathbb{R}^{(3N+M)}}, \tag{3.13}$$

We highlight that, for the sake of clarity, the superscript $'$ is introduced to denote DCmG states without secondary control.

The overall model of the DCmG (3.12) having been deduced, the next step is to show that the network is stable, and attains the control objectives (3.8) and (3.9) in the steady state. To this end, we first start by characterizing the equilibria of (3.12).

3.3.3 Analysis of equilibria

Before analyzing the stability of the closed-loop system (3.12), we study when an equilibrium exists such that (3.8) and (3.9) are jointly attained. We emphasize that, in a primary-controlled DCmG given by (3.13), a reference voltage $V_{ref,i}$ is directly enforced at the ith PCC. Thus, a unique equilibrium point

$$\bar{X}' = \begin{bmatrix} V_{ref} \\ B\bar{I} + Y_L V_{ref} + [V_{ref}]^{r-\mathbf{1}_N} P_L^* + \bar{I}_L \\ -[\gamma]^{-1}([\alpha]V_{ref} + [\beta]\bar{I}_t) \\ R^{-1}B^\top V_{ref} \end{bmatrix}, \tag{3.14}$$

always exists and can be found by setting $\dot{X}' = 0$ in (3.13) [NST+20]. On the contrary, once the secondary layer is activated, the voltage references are tweaked by ω_i (see (3.3)), which is governed by equations (3.10) and (3.11). Since the presence of exponential loads essentially renders the DCmG dynamics nonlinear, it may occur that an equilibrium point fails to exist (see Section 3.5 for a simulation example). Hence, in this section, we pursue whether the closed-loop system (3.12) possesses an equilibrium point, and if so, under what conditions on loads, topology of electrical and communication networks, and controller gains. We set off by presenting the following lemma.

Lemma 3.3.1. *Consider the DCmG dynamics* (3.12)*. The following statements hold:*

1. *In steady state, the objectives* (3.8) *and* (3.9) *are attained;*

2. *A steady state solution* $\bar{X} = [\bar{V}^\top, \bar{I}_t^\top, \bar{v}^\top, \bar{I}^\top, \bar{\Omega}^\top]^\top$ *exists only if there exists a* $\bar{V}$ *concurrently satisfying the following equations*

$$\mathcal{L}_p\bar{V} + \mathcal{L}_t[I_t^s]^{-1}([\bar{V}^{r-\mathbf{1}_N}]P_L^* + \bar{I}_L + Y_L\bar{V}) = 0, \tag{3.15a}$$

$$\mathbf{1}_N^\top[I_t^s]\bar{V} = \mathbf{1}_N^\top[I_t^s]V_{ref}, \tag{3.15b}$$

where $\mathcal{L}_t = [I_t^s] - (\mathbf{1}_N^\top[I_t^s]\mathbf{1}_N)^{-1}[I_t^s]\mathbf{1}_N\mathbf{1}_N^\top[I_t^s]$, *and* $\mathcal{L}_p = BR^{-1}B^\top$ *is the Laplacian matrix of the electrical network.*

Proof. Any steady state solution of (3.12) satisfies

$$-Y_L\bar{V} - \bar{I}_L - [\bar{V}^{r-\mathbf{1}_N}]P_L^* + \bar{I}_t - B\bar{I} = 0 \tag{3.16a}$$

$$[\alpha]\bar{V} + [\beta]\bar{I}_t + [\gamma]\bar{v} + [\delta][I_t^s]^{-1}\mathcal{L}_c\bar{\Omega} = 0 \tag{3.16b}$$

$$V_{ref} - \bar{V} - [I_t^s]^{-1}\mathcal{L}_c\bar{\Omega} = 0 \tag{3.16c}$$

$$B^\top\bar{V} - R\bar{I} = 0 \tag{3.16d}$$

$$\mathcal{L}_c[I_t^s]^{-1}\bar{I}_t = 0 \tag{3.16e}$$

One has from (3.16e) that $\bar{I}_t = \epsilon[I_t^s]\mathbf{1}_N$ for some $\epsilon \in \mathbb{R}$, warranting the attainment of (3.8). Since $\mathbf{1}_N^\top B = \mathbf{0}_M$, (3.16a) implies that $\mathbf{1}_N^\top\bar{I}_t = \mathbf{1}_N^\top(Y_L\bar{V} + \bar{I}_L + [\bar{V}^{r-\mathbf{1}_N}]P_L^*)$, then $\epsilon = (\mathbf{1}_N^\top[I_t^s]\mathbf{1}_N)^{-1}\mathbf{1}_N^\top(Y_L\bar{V} + \bar{I}_L + [\bar{V}^{r-\mathbf{1}_N}]P_L^*)$. We can equivalently represent

$$\bar{I}_t = (\mathbf{1}_N^\top[I_t^s]\mathbf{1}_N)^{-1}[I_t^s]\mathbf{1}_N\mathbf{1}_N^\top(Y_L\bar{V} + \bar{I}_L + [\bar{V}^{r-\mathbf{1}_N}]P_L^*). \tag{3.17}$$

Using (3.16d),

$$\bar{I} = R^{-1}B^\top\bar{V}. \tag{3.18}$$

On substituting (3.17) and (3.18) into (3.16a), one obtains (3.15a). Moreover, for an $\bar{\Omega}$ to exist such that (3.16c) holds, $[I_t^s](V_{ref} - \bar{V}) \in \mathbb{H}^1$, which yields (3.15b) and guarantees (3.9) in steady state. If there exists a $\bar{V}$ solving (3.15), $\bar{I}_t$ and $\bar{I}$ exist due to (3.17) and (3.18), respectively. As (3.15b) holds, from (3.16c), an equilibrium vector $\bar{\Omega} = \mathcal{L}_c^\dagger[I_t^s](V_{ref} - \bar{V}) + \eta\mathbf{1}_N, \eta \in \mathbb{R}$ exists. Finally, on substituting $\bar{V}, \bar{I}_t, \bar{I}$, and $\bar{\Omega}$ into (3.16b), one has $\bar{v} = [\gamma]^{-1}\Big(([\alpha] + [\delta])\bar{V} - [\delta]V_{ref} + [\beta]\bar{I}_t\Big)$. ■

Note that equations (3.15a)–(3.15b) represent the DC power-flow equations when DGU currents are shared proportionally and PCC voltages balanced. These equations are governed only by the electric network Laplacian $\mathcal{L}_p$, ZIE load parameters, DGU rated currents I_t^s, and voltage references V_{ref}. We conclude that the communication network Laplacian $\mathcal{L}_c$ and the controller (3.3) has no bearing on their solvability. In the ensuing discussion, we analyze the existence of a voltage solution to (3.15) when $r = \mathbf{0}_N$, that is,

the exponential loads behave as P loads. By setting $r = \mathbf{0}_N$, one can rewrite equation (3.15) as

$$\tilde{\mathcal{L}}V = \tilde{I} - \tilde{\mathcal{L}}_t[V^{-1}]P_L^*, \tag{3.19}$$

where $\tilde{\mathcal{L}} = \begin{bmatrix} \tilde{\mathcal{L}}_p \\ \mathbf{1}_N^\top[I_t^s] \end{bmatrix}$, $\tilde{\mathcal{L}}_p = \mathcal{L}_p + \mathcal{L}_t[I_t^s]^{-1}Y_L$, $\tilde{I} = \begin{bmatrix} -\mathcal{L}_t[I_t^s]^{-1}\bar{I}_L \\ \mathbf{1}_N^\top[I_t^s]V_{ref} \end{bmatrix}$, and $\tilde{\mathcal{L}}_t = \begin{bmatrix} \mathcal{L}_t[I_t^s]^{-1} \\ \mathbf{0} \end{bmatrix}$.

Remark 3.3.2. ***(Solvability of*** (3.19)***).*** *The existence and uniqueness of solutions of power-flow equations have been tackled in [SPDB16, BNF19]. As shown in what follows, the tools therein cannot be directly applied to ascertain the solvability of* (3.19) *as* (3.15b) *restricts the voltage solutions onto a hyperplane.*

Before presenting Theorem 3.3.1, the following assumption is needed.

Assumption 3.3.1. *The range space of $\tilde{\mathcal{L}}_p$ is $\mathbb{H}^1$.*

Remark 3.3.3. *Note that, by definition,* $\text{range}(\tilde{\mathcal{L}}_p) \subseteq \mathbb{H}^1$. *Considering* $\dim(\mathbb{H}^1) = N-1$ *and $\tilde{\mathcal{L}}_p \in \mathbb{R}^{N\times N}$, one only needs to check* $\dim(\ker(\tilde{\mathcal{L}}_p)) = 1$ *to verify Assumption 3.3.1. This is a centralized operation, i.e., it requires the knowledge of global variables $\mathcal{L}_p$, I_t^s, and Y_L about the whole DCmG.*

We are now in a position to state the main result.

Theorem 3.3.1. ***(Existence and uniqueness of a voltage solution).*** *Consider* (3.19) *along with the vector $V^* = \tilde{\mathcal{L}}^\dagger\tilde{I}$. Suppose that $[V^*]$ is invertible, Assumption 3.3.1 holds, and that the network parameters and loads satisfy*

$$\Delta = ||P_{cri}P_L^*||_\infty < 1. \tag{3.20}$$

Define the matrix $P_{cri} = 4[V^*]^{-1}\tilde{\mathcal{L}}^\dagger\tilde{\mathcal{L}}_t[V^*]^{-1}$ and the percentage deviations $\delta_- \in [0, \frac{1}{2})$ and $\delta_+ \in (\frac{1}{2}, 1]$ as the unique solutions of $\Delta = 4\delta_\pm(1-\delta_\pm)$. The following statements hold:

1) *The closed set $\mathcal{H}(\delta_-)$ contains a unique voltage solution V to* (3.19)*, where*

$$\mathcal{H}(\delta_-) := \{V \in \mathbb{R}^N | (1-\delta_-)V^* \leq V \leq (1+\delta_-)V^*\}. \tag{3.21}$$

Moreover, there exist no solutions of (3.19) *in the open set*

$$\mathcal{I} := \{V \in \mathbb{R}^N | (V > (1-\delta_+)V^* \text{ and } V \notin \mathcal{H}(\delta_-)\}; \tag{3.22}$$

2) *For $P_L^* = \mathbf{0}$, V^* is the unique solution of* (3.19)*;*

3) *If $(1-\delta_+)V^* < V_{ref}$, then, there exist no solutions of* (3.19) *in the closed set*

$$\mathcal{J} := \{V \in \mathbb{R}^N | (V \leq (1-\delta_+)V^*\}. \tag{3.23}$$

Proof. Any voltage solution to (3.19) must verify $\tilde{I}-\tilde{\mathcal{L}}_t[V]^{-1}P_L^* \in \text{range}(\tilde{\mathcal{L}})$. We therefore start by characterizing the column space of $\tilde{\mathcal{L}} \in \mathbb{R}^{(N+1)\times N}$. Let $\{l_1, l_2, \cdots, l_N\}, l_i \in \mathbb{R}^{N+1}$ be its column vectors. Therefore,

$$\text{range}(\tilde{\mathcal{L}}) = \left\{ \sum_{i=1}^{N} a_i l_i \mid a_i \in \mathbb{R} \right\} = \left\{ \underbrace{\begin{bmatrix} \tilde{\mathcal{L}}_p \\ \mathbf{0} \end{bmatrix}}_{c_1} a + (\sum_{i=1}^{N} I_{ti}^s a_i) \underbrace{\begin{bmatrix} \mathbf{0}_N \\ 1 \end{bmatrix}}_{c_2} \mid a \in \mathbb{R}^N, a_i \in \mathbb{R} \right\}.$$

The vectors c_1 and c_2 are orthogonal to each other. In view of Assumption 3.3.1, the vector c_1 can be equivalently written as

$$c_1 = \sum_{i=1}^{N-1} \tilde{a}_i \underbrace{\begin{bmatrix} h_i \\ 0 \end{bmatrix}}_{\tilde{h}_i}, \ \tilde{a}_i \in \mathbb{R},$$

where $\{h_1 \cdots h_{N-1}\}, \ h_i \in \mathbb{R}^{\mathbb{N}}$ is an orthogonal basis of $\mathbb{H}^1$. Hence,

$$\text{range}(\tilde{\mathcal{L}}) = \left\{ \sum_{i=1}^{N} \tilde{a}_i \tilde{h}_i \mid \tilde{a}_i \in \mathbb{R} \right\},$$

where $\tilde{h}_N = c_2$. Moreover, $\{\tilde{h}_1 \cdots \tilde{h}_N\}$ is an orthogonal basis of $\text{range}(\tilde{\mathcal{L}})$. Using the deduced basis, one can easily verify that $\tilde{I} \in \text{range}(\tilde{\mathcal{L}})$ and $\text{range}(\tilde{\mathcal{L}}_t) \subset \text{range}(\tilde{\mathcal{L}})$. It, therefore, holds that $\tilde{I} - \tilde{\mathcal{L}}_t[V]^{-1}P_L^* \in \text{range}(\tilde{\mathcal{L}}) \ \forall \ V \in \mathbb{R}^N$. Furthermore, we note that $\tilde{\mathcal{L}}$ is a matrix with full-column rank as $\dim(\text{range}(\tilde{\mathcal{L}})) = N$. By the fundamental theorem of linear algebra, [Str93], $\dim(\text{range}(\tilde{\mathcal{L}}^\top)) = \dim(\text{range}(\tilde{\mathcal{L}})) = N$, and thus $\text{range}(\tilde{\mathcal{L}}^\top) = \mathbb{R}^N$. Since the linear map $\tilde{\mathcal{L}}(\text{range}(\tilde{\mathcal{L}}^\top)|\text{range}(\tilde{\mathcal{L}}))$ is always invertible [Str93], and as $V \in \text{range}(\tilde{\mathcal{L}}^\top)$, $\tilde{I} - \tilde{\mathcal{L}}_t[V]^{-1}P_L^* \in \text{range}(\tilde{\mathcal{L}}) \ \forall \ V \in \mathbb{R}^N$, one can rewrite (3.19) as

$$\begin{aligned} V &= \tilde{\mathcal{L}}^\dagger \tilde{I} - \tilde{\mathcal{L}}^\dagger \tilde{\mathcal{L}}_t[V^{-1}]P_L^* \\ &= V^* - \tilde{\mathcal{L}}^\dagger \tilde{\mathcal{L}}_t[V^{-1}]P_L^* \end{aligned}, \tag{3.24}$$

where $\tilde{\mathcal{L}}^\dagger = (\tilde{\mathcal{L}}^\top \tilde{\mathcal{L}})^{-1}\tilde{\mathcal{L}}^\top$. We highlight that $\tilde{\mathcal{L}}^\top \tilde{\mathcal{L}}$ is always invertible for matrices with full-column rank [Str93]. On utilizing the change of variables $x := [V^*]^{-1}V - \mathbf{1}_N$, we obtain the equivalent representation of (3.24) as

$$x = f(x) := -[V^*]^{-1}\tilde{\mathcal{L}}^\dagger \tilde{\mathcal{L}}_t[V^*]^{-1}[P_L^*]r(x) \tag{3.25a}$$

$$= -\frac{1}{4}P_{cri}[P_L^*]r(x), \tag{3.25b}$$

where $r(x) = \left[\frac{1}{1+x_1}, \cdots, \frac{1}{1+x_N}\right]^\top$. Having transformed (3.24) into (3.25b), we can now apply the contraction mapping arguments presented in [SPDB16]. Statement 1) is a direct consequence of the Supplementary Theorem 1 of [SPDB16].

The proof of Statement 2) follows from (3.24) and the invertibility of $\tilde{\mathcal{L}}(\text{range}(\tilde{\mathcal{L}}^\top)|\text{range}(\tilde{\mathcal{L}}))$. With the objective of proving Statement 3), we consider a voltage solution $V \in \mathcal{J}$. Given that $(1-\delta_+)V^* < V_{ref}$, any voltage solution $V \in \mathcal{J}$ can be represented as $V = V_{ref} - b,\ b \in \mathbb{R}^N_{>0}$. It is evident that a voltage solution $V \in \mathcal{J}$ to (3.19) must satisfy (3.15b). Therefore,

$$\mathbf{1}_N^\top [I_t^s](V_{ref} - b) = \mathbf{1}_N^\top [I_t^s] V_{ref} \implies \mathbf{1}_N^\top [I_t^s] b = 0. \tag{3.26}$$

Since $I_t^s, b, \in \mathbb{R}^N_{>0}$, (3.26) never holds. This concludes the proof of Statement 3). ■

Remark 3.3.4. *Under the conditions provided in Theorem 3.3.1, the existence of an equilibrium point depends upon the critical power matrix P_{cri} and the power absorption P_L^*. As pointed out in [SPDB16], one can interpret P_{cri} as the sensitivity of PCC voltages to variations in power absorption by P loads. Consequently, the vector $P_{cri}P_L^*$ reflects the voltage variations in the network, caused by constant power loads. As such, for a DCmG,* (3.20) *means that these variations are sufficiently small. Note that P_{cri} is defined by the electrical topology of the DCmG network, the Z and I components of loads, and the voltage V^* appearing at PCCs when $P_L^* = 0$. Clearly, from* (3.19)*, the communication network topology $\mathcal{G}_c$ has no impact on P_{cri}. We also note that* (3.20) *is easier to satisfy for small values of P_{Li}^*.*

Remark 3.3.5. *The set $\mathcal{H}(\delta_-)$ in Statement 1, Theorem represents a set where a unique voltage solution V to* (3.19) *lies, whereas $\mathcal{I}$ is a set around $\mathcal{H}(\delta_-)$ where no solution exists. We note that the definitions and implications of these two sets resemble those of the secure solution and solutionless sets in [SPDB16]. Although, in our case, the variables V^* and P_{cri} defining these sets are different from [SPDB16]. Moreover, we point out that as $\Delta \to 0$, $\delta_- \to 0$ and $\delta_+ \to 1$, implying that $\mathcal{H}(\delta_-)$ converges to $\{V^*\}$ and $\mathcal{I}$ to the positive orthant of $\mathbb{R}^N$. On the contrary, as $\Delta \to 1$, $\delta_- \to \frac{1}{2}$ and $\delta_+ \to \frac{1}{2}$, meaning that the set $\mathcal{H}(\delta_-)$ expands and the set $\mathcal{I}$ shrinks. We finally note that the set $\mathcal{J}$ defines a low-voltage set with no solutions under the condition $(1-\delta_+)V^* < V_{ref}$.*

The previous theorem pertains to the existence of an equilibrium point for the closed-loop system (3.12), albeit feeding only ZIP loads. A detailed analysis of (3.15) with $r_i \in \mathbb{R}$ is deferred to future research, as it calls for a study on finding analytic solutions to polynomials of generic order. For E loads, we will rely on the following assumption.

Assumption 3.3.2. *The DCmG under primary and secondary control has an equilibrium point $\bar{X} = [\bar{V}^\top, \bar{I}_t^\top, \bar{v}^\top, \bar{I}^\top, \bar{\Omega}^\top]^\top$ with positive voltages $\bar{V} \in \mathbb{R}^N_{>0}$ satisfying equations* (3.15a)-(3.15b) *simultaneously.*

3.4 Stability of the DC microgrid network

In this section, we aim to study the stability of the closed-loop system (3.12), necessary in order for the DCmG to exhibit desired steady-state behavior investigated in Section

3.3.3. We start by introducing the following Lemma.

Lemma 3.4.1. *Consider a symmetric block matrix*

$$\mathcal{Z} = \begin{bmatrix} A & B \\ B & D \end{bmatrix} \in \mathbb{R}^{2n\times 2n},$$

where A, B and $D \in \mathbb{R}^{n\times n}$ are diagonal matrices. Assume that D is invertible and define the matrices

$$Z_i = \begin{bmatrix} A_i & B_i \\ B_i & D_i \end{bmatrix} \in \mathbb{R}^{2\times 2},$$

where A_i, B_i, and D_i represent the ith diagonal element of matrices A, B and C, respectively. The matrix $\mathcal{Z}$ is positive definite if and only if $Z_i \succ 0$ for all $i \in \{1, \ldots, n\}$. If at least one Z_i is positive semidefinite, then $\mathcal{Z}$ is positive semidefinite.

Proof. The matrix $\mathcal{Z}$ is positive definite if and only if $D \succ 0$, and its Schur's complement $A - BD^{-1}B \succ 0$. Considering that A, B, C, and D are diagonal matrices, the aforementioned conditions translate into $D_i > 0$, and $A_i - B_iD_i^{-1}B_i \succ 0$, $\forall i \in \{1, \ldots, n\}$. Note that $A_i - B_iD_i^{-1}B_i$ is the Schur's complement of Z_i. Therefore, if $Z_i \succ 0 \; \forall \; i \in \{1, \ldots, n\}$, $\mathcal{Z} \succ 0$. If the ith Z_i is positive semidefinite, then

$$\det(Z_i) = A_iD_i - B_iB_i = 0.$$

Since $D_{ii} \neq 0$, $A_i - B_iD_i^{-1}B_i = 0$. This implies that diagonal entry in the ith row of $A - BD^{-1}B$ is equal to zero, making the Schur's complement of $\mathcal{Z}$ positive semidefinite, and hence, $\mathcal{Z}$ positive semidefinte. ■

Theorem 3.4.1. ***(Stability of the closed-loop DCmG).*** *Consider the closed-loop system* (3.12)*, along with Assumption 3.3.2. Define the equilibrium power absorption of the ith exponential load as $\bar{P}^*_{Li} = P^*_{Li}\bar{V}_i^{r_i}$. For $i \in \mathcal{V}$, if the feedback gains $k_{1,i}$, $k_{2,i}$, and $k_{3,i}$ belong to the set*

$$\mathcal{Z}_{[i]} = \left\{ \begin{array}{l} k_{1,i} < 1, \\ k_{2,i} < R_{ti}, \\ 0 < k_{3,i} < \frac{1}{L_{ti}}(k_{1,i} - 1)(k_{2,i} - R_{ti}) \end{array} \right\}, \tag{3.27}$$

$k_{4,i} = k_{1,i} - 1$, and the Z and E components of the ZIE load (3.7) *with $r_i < 1$ verify*

$$(1 - r_i)\bar{P}^*_{Li} < Y_{Li}\bar{V}_i^2, \tag{3.28}$$

then the following statements hold:

1) *The equilibrium point $\bar{X}$ is locally asymptotically stable, and is globally asymptotically stable when $\bar{P}^*_L = 0$;*

2) In the absence of a communication network, the equilibrium point $\bar{X}'$ of the resulting closed-loop system (3.13) *is locally asymptotically stable.*

Proof. Statement 1): To study the behavior of trajectories resulting from (3.12), consider the following candidate Lyapunov function, attaining a minimum at $\bar{X}$

$$\mathcal{V}(\tilde{X}) = \frac{1}{2}\tilde{X}^\top \mathcal{P}\tilde{X}, \tag{3.29}$$

where $\tilde{X} = X - \bar{X}$. The matrix $\mathcal{P}$ is defined as

$$\mathcal{P} = \left[\begin{array}{c|c} \mathcal{P}_1 & \mathbf{0} \\ \hline \mathbf{0} & \mathcal{P}_2 \end{array}\right] = \left[\begin{array}{cccc|c} C_t & \mathbf{0} & \mathbf{0} & \mathbf{0} & \mathbf{0} \\ \mathbf{0} & [\beta][\omega]^{-1} & [\gamma][\omega]^{-1} & \mathbf{0} & \mathbf{0} \\ \mathbf{0} & [\gamma][\omega]^{-1} & [\alpha][\gamma][\omega]^{-1} & \mathbf{0} & \mathbf{0} \\ \mathbf{0} & \mathbf{0} & \mathbf{0} & L & \mathbf{0} \\ \hline \mathbf{0} & \mathbf{0} & \mathbf{0} & \mathbf{0} & \mathbf{I} \end{array}\right], \tag{3.30}$$

with $\mathcal{P}_1 \in \mathbb{R}^{(3N+M)\times(3N+M)}$, $\mathcal{P}_2 \in \mathbb{R}^{N\times N}$, and $[\omega] = [\gamma] - [\alpha][\beta] \in \mathbb{R}^{N\times N}$. To ensure (3.29) is a legitimate Lyapunov function, the matrix $\mathcal{P}$ must be positive definite. In fact, as $\mathcal{P}$ is a block diagonal matrix with $C_t \succ 0$, $L \succ 0$, and $I \succ 0$, its positive definiteness hinges on

$$\hat{\mathcal{P}} = \begin{bmatrix} [\beta][\omega]^{-1} & [\gamma][\omega]^{-1} \\ [\gamma][\omega]^{-1} & [\alpha][\gamma][\omega]^{-1} \end{bmatrix} \succ 0.$$

which, as a direct consequence of Lemma 3.4.1, translates into

$$\hat{\mathcal{P}}_i = \begin{bmatrix} \frac{\beta_i}{\omega_i} & \frac{\gamma_i}{\omega_i} \\ \frac{\gamma_i}{\omega_i} & \frac{\alpha_i\gamma_i}{\omega_i} \end{bmatrix} \succ 0, \forall i \in \mathcal{V}.$$

Using Sylvester's criterion [HJ12, Theorem 7.2.5] followed by some basic algebra, one can deduce that $\hat{\mathcal{P}}_i \succ 0$ if and only if $\beta_i, \gamma_i, \omega_i$ belong to the set

$$\mathcal{S}_i = \{(\beta_i, \gamma_i, \omega_i) : (\beta_i, \omega_i > 0, \gamma_i < 0) \text{ or } (\beta_i, \omega_i < 0, \gamma_i > 0)\}.$$

The time derivative of (3.29) along the solutions of (3.12) reads

$$\begin{aligned} \dot{\mathcal{V}}(\tilde{X}) &= \left(\frac{\partial \mathcal{V}}{\partial \tilde{X}}\right)^\top \dot{\tilde{X}} \\ &= \frac{1}{2}\left(X^\top \mathcal{A}^\top \mathcal{P}\tilde{X} + \tilde{X}^\top \mathcal{P}\mathcal{A}X\right) + \mathcal{B}(V)^\top \mathcal{P}\tilde{X} \\ &= \frac{1}{2}\left(\tilde{X}^\top \mathcal{A}^\top \mathcal{P}\tilde{X} + \tilde{X}^\top \mathcal{P}\mathcal{A}\tilde{X}\right) + \left(\mathcal{A}\bar{X} + \mathcal{B}(V)\right)^\top \mathcal{P}\tilde{X} \\ &= \tilde{X}^\top \mathcal{Q}(V)\tilde{X}, \end{aligned} \tag{3.31}$$

where

$$\mathcal{Q}(V) = -\frac{1}{2}\begin{bmatrix} 2(Y_L + Y_E(V)) & \begin{matrix} -\mathbf{I} + [\gamma][\omega]^{-1} \\ -[\alpha][\beta][\omega]^{-1} \end{matrix} & \mathbf{0} & \mathbf{0} & \mathbf{0} \\ \begin{matrix} -\mathbf{I} + [\gamma][\omega]^{-1} \\ -[\alpha][\beta][\omega]^{-1} \end{matrix} & -2[\beta]^2[\omega]^{-1} & -2[\beta][\gamma][\omega]^{-1} & \mathbf{0} & \begin{matrix} [I_t^s]^{-1}\left(-\mathbf{I} + [\gamma][\omega]^{-1}\right. \\ \left.-[\alpha][\beta][\omega]^{-1}\right)\mathcal{L}_c \end{matrix} \\ \mathbf{0} & -2[\beta][\gamma][\omega]^{-1} & -2[\gamma]^2[\omega]^{-1} & \mathbf{0} & \begin{matrix} [I_t^s]^{-1}\left([\alpha][\gamma][\omega]^{-1}\right. \\ \left.-[\delta][\gamma][\omega]^{-1}\right)\mathcal{L}_c \end{matrix} \\ \mathbf{0} & \mathbf{0} & \mathbf{0} & 2R & \mathbf{0} \\ \mathbf{0} & \begin{matrix} \mathcal{L}_c\left(-\mathbf{I} + [\gamma][\omega]^{-1}\right. \\ \left.-[\alpha][\beta][\omega]^{-1}\right)[I_t^s]^{-1} \end{matrix} & \begin{matrix} \mathcal{L}_c\left([\alpha][\gamma][\omega]^{-1}\right. \\ \left.-[\delta][\gamma][\omega]^{-1}\right)[I_t^s]^{-1} \end{matrix} & \mathbf{0} & \mathbf{0} \end{bmatrix}, \tag{3.32}$$

and $Y_E(V)$ is a diagonal matrix, whose i^{th} diagonal element is

$$Y_{Ei}(V_i) = \frac{\bar{P}^*_{Li}(V_i^{r_i-1} - \bar{V}_i^{r_i-1})}{\bar{V}_i^{r_i}(V_i - \bar{V}_i)}. \tag{3.33}$$

Using (3.5) and (3.6), one can simplify $\mathcal{Q}(V)$ as

$$\mathcal{Q}(V) = -\begin{bmatrix} Y_L + Y_E(V) & \mathbf{0} & \mathbf{0} & \mathbf{0} & \mathbf{0} \\ \mathbf{0} & -[\beta]^2[\omega]^{-1} & -[\beta][\gamma][\omega]^{-1} & \mathbf{0} & \mathbf{0} \\ \mathbf{0} & -[\beta][\gamma][\omega]^{-1} & -[\gamma]^2[\omega]^{-1} & \mathbf{0} & \mathbf{0} \\ \mathbf{0} & \mathbf{0} & \mathbf{0} & R & \mathbf{0} \\ \mathbf{0} & \mathbf{0} & \mathbf{0} & \mathbf{0} & \mathbf{0} \end{bmatrix},$$

To claim that $\dot{\mathcal{V}}(\tilde{X}) \leq 0$, and subsequently the stability of the equilibrium point $\bar{X}$, one needs

$$f_i(V_i) = Y_{Li} + Y_{Ei}(V_i) \geq 0, \ \forall i \in \mathcal{V} \tag{3.34}$$

and, from Lemma 3.4.1,

$$\hat{\mathcal{Q}}_i = \begin{bmatrix} -\frac{\beta_i^2}{\omega_i} & -\frac{\beta_i\gamma_i}{\omega_i} \\ -\frac{\beta_i\gamma_i}{\omega_i} & -\frac{\gamma_i^2}{\omega_i} \end{bmatrix} \succeq 0, \forall i \in \mathcal{V}.$$

Evidently, $\hat{\mathcal{Q}}_i \succeq 0$ if and only if ω_i belongs to

$$\mathcal{T}_i = \{\omega_i : \omega_i < 0\}.$$

Assume for the moment that (3.34) holds. For $\dot{\mathcal{V}}(\tilde{X}) \leq 0$ and $\mathcal{V}(\tilde{X}) > 0$ to be verified simultaneously, α_i, β_i, and γ_i should be such that $(\beta_i, \gamma_i, \omega_i) \in \mathcal{S}_i$, and $\omega_i \in \mathcal{T}_i$. Equivalently, $(\alpha_i, \beta_i, \gamma_i)$ must belong to

$$\mathcal{U}_i = \{(\alpha_i, \beta_i, \gamma_i) : \alpha_i < 0, \beta_i < 0, 0 < \gamma_i < \alpha_i\beta_i\}. \tag{3.35}$$

Using (3.5), one can rewrite set $\mathcal{U}_i$ in terms of $k_{1,i}$, $k_{2,i}$, and $k_{3,i}$ as (3.27). Now, as for (3.34), it is state dependent and should, at least, hold at $V_i = \bar{V}_i$. Note that $f_i(V_i)$ has a

finite limit for $V_i \to \bar{V}_i$, which one can show by employing Bernoulli-Hospital theorem as

$$\begin{aligned} f_i(\bar{V}_i) &= \lim_{V_i \to \bar{V}_i} f_i(V_i) \\ &= Y_{Li} + \lim_{V_i \to \bar{V}_i} \frac{\bar{P}^*_{Li}(V_i^{r_i-1} - \bar{V}_i^{r_i-1})}{\bar{V}_i^{r_i}(V_i - \bar{V}_i)}. \\ &= Y_{Li} - \frac{\bar{P}^*_{Li}}{\bar{V}_i^2}(1 - r_i) \end{aligned} \tag{3.36}$$

In view of (3.36), if (3.28) is verified by all the ZIE loads with $r_i < 1$, then the inequality (3.34) holds in a neighborhood of $X = \bar{X}$. Note that (3.28) is always satisfied when $r_i \geq 1$. We can now state that a compact level set $\mathcal{M}$ of $\mathcal{V}(\tilde{X})$ can be taken sufficiently small such that it is contained in the neighborhood within which (3.34) holds. As a result, if $X(0) - \bar{X} \in \mathcal{M}$, then $X - \bar{X} \in \mathcal{M}$ for all $t \geq 0$. To show local asymptotic stability, one can exploit the standard LaSalle's invariance principle and show that the largest invariant set $M \subset \mathcal{M}$ contains solely the equilibrium point $\bar{X}$. A detailed computation of M is skipped here and presented in Appendix 3.7.

We point out that when $P^*_L = 0$, one can call into use Theorem 3.3.1 and Lemma 3.3.1 to establish existence and uniqueness of $\bar{X}$. Moreover, (3.34) holds for all $X \in \mathbb{R}^{4N \times M}$. Hence, $\bar{X}$ is globally asymptotically stable.

Statement 2): This proof relies heavily on the preceding analysis. Consequently, instead of providing a detailed proof, we sketch the proof of Statement 2). In the absence of a communication network, the DCmG dynamics given by (3.13) admit a unique equilibrium; see (3.14). To show the asymptotic stability of $\bar{X}'$, consider the following Lyapunov function

$$\mathcal{V}(\tilde{X}') = \frac{1}{2}\tilde{X}'^T \mathcal{P}_1 \tilde{X}', \tag{3.37}$$

where $\tilde{X}' = X - \bar{X}'$. One can now trace the same steps as before to reach the conclusion. ■

Remark 3.4.1. ***(Power consumption of E loads and stability).*** *Based on Theorem 3.4.1, the permissible power drawn by E loads with $r_i < 1$ is restricted by* (3.28)*. To make plain sense out of* (3.28)*, one can state that, just like P loads [AKM13, WL14], E loads with $r_i < 1$ exhibit a negative incremental admittance ($dI/dV < 0$; see* (3.7)*) having a destabilizing impact. To preserve stability of the network, the DCmG operator needs to counter this negative damping with the positive damping of Z loads, constraining the power consumption of E loads with $r_i < 1$. Indeed, for E loads with $r_i < 1$, stability cannot be guaranteed in the absence of Z loads. Note that no upper limit exists for E loads with $r_i > 1$ as* (3.28) *is always fulfilled.*

Remark 3.4.2. ***(Compatibility with primary control and stability under a communication collapse).*** *Equations* (3.1) *and* (3.4) *represent the DCmG under primary control when the secondary layer is inactive. As shown in Theorem 3.4.1,* (3.27)

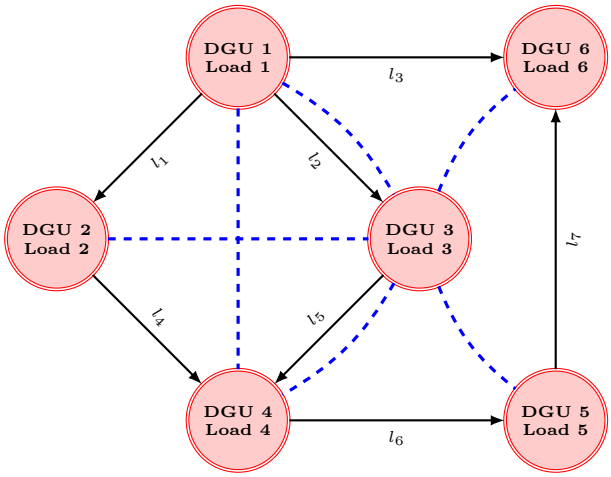

Figure 3.2: A representative diagram of the DCmG with the communication network appearing in dashed blue.

and (3.28) *also make possible the design of stabilizing primary controllers, allowing us to reach the following conclusions: (i) the proposed secondary controllers are design-wise fully compatible with the primary layer, and require only an additional control gain* $k_{4,i} = k_{1,i} - 1, k_{1,i} \in \mathcal{Z}_{[i]}$ *be set once activated; (ii) if the DCmG undergoes a communication collapse, the primary controllers maintain voltage stability without any human intervention, forcing each PCC to track* $V_{ref,i}$ *in steady state.*

Remark 3.4.3. ***(Plug-and-play operations).*** *To synthesize the proposed secondary regulators, one can use the feedback gains* (3.27)*, dependent on the DGU filter parameters* R_{ti} *and* L_{ti} *but not on* C_{ti} *— assumed to be lumped with line capacitances. Capable of taking into account the worst-case parameter variations around a nominal value, these explicit inequalities* (3.27) *cause the entire control design to be robust to uncertainties in filter parameters. Moreover, the secondary controllers, notwithstanding their distributed structure, can be designed in a completely decentralized fashion, enabling plug-and-play operations. For example, when a new DGU is plugged-in, its controller can be designed without the knowledge of any other parameter of the mG, and no other controller in the mG needs to be updated such that voltage stability is preserved. As a last comment, we note that if a power line with non-negligible capacitance is added or removed, no DGU controller needs to be updated as controller gains are independent of* C_{ti} *and, hence, the capacitance of lines.*

3.5 Simulation results

We assess the performance of the proposed consensus-based controller via realistic computer simulations using the *Specialized Power Systems Toolbox* of Simulink [HQ19]. The considered DCmG has 6 DGUs arranged in the topology given in Figure 3.2,

where electrical lines depicted in solid black arrows are assigned arbitrary directions[1], and bidirectional communication channels are shown in blue dashed lines. We further assume that power lines are equipped with switches so as to enable or interrupt power transfer. The DGUs consist of bidirectional Buck converters fed by source voltages of $V_{s,i} = 80V, \forall i \in \mathcal{N}$ as well as RLC filters and loads with non-identical parameter values. Bidirectional Buck converters are implemented as non-ideal insulated gate bipolar transistor (IGBT) switches which operate at 15 kHz and have snubber circuits as a safeguard against large transients that can damage electrical equipments. The parameters of filters and lines are adopted from [TRFT18], whereas those of the loads are selected so as to satisfy (3.28). Voltage reference values $V_{ref,i}$ are chosen to be between 45V and 50V, and the primary controller gains $k_{1,i}$, $k_{2,i}$, and $k_{3,i}$ are selected from the set $\mathcal{Z}_{[i]}$ in (3.27).

The simulations are divided into two parts. We first present a simulation scenario showing that the above DCmG with ZIP loads and proposed controller structure converges to the unique solution in $\mathcal{H}(\delta_-) \cup \mathcal{I}$; see (3.20), (3.21). We then change some ZIP loads to ZIE loads to show that stability and secondary control objectives are still achieved despite the results of Theorem 3.3.1 being no longer applicable. In the second part of simulations, we show that an equilibrium fails to exist when some parameters of the DCmG equipped with ZIP loads are modified such that conditions for Theorem 3.3.1 are not satisfied.

3.5.1 Convergence to an equilibrium

In this scenario, we show that the proposed controller achieves current sharing and voltage balancing while allowing plugging-in and unplugging of DGUs.

Initialization of the DCmG: First, the DCmG is initialized with all power lines and communication channels disconnected, i.e., there is no power transfer between the DGUs and the consensus-based controller is not activated. As such, the primary controllers of DGUs first regulate voltages at their PCCs to corresponding reference voltages $V_{ref,i}$, as seen in Figure 3.3a from 0s to 1.5s. At this stage, DGUs 1-5 supply ZIP loads, whereas DGU 6 has a ZIE load with exponent $r_6 = 0.65$.

Connection of DGUs: At $t = 1.5s$, the switches on the power lines l_1, l_2, l_4, l_5, and l_6 are closed, connecting the DGUs 1-5 to form a DCmG. Simultaneously, the consensus-based controller is activated with zero initial conditions for these DGUs. We would like to emphasize that, in this phase of the simulations, DGU 6 is still disconnected from the rest of the DCmG. Theorems 3.3.1 and 3.4.1 can be applied for this DCmG to conclude that there exists a unique voltage solution to (3.19) in $\mathcal{H}(\delta_-) = \{V \in \mathbb{R}^5 | (1-\delta_-)V^* \leq V \leq (1+\delta_-)V^*\}$, where $\delta_- = 3.94 \times 10^{-4}$ and $V^* = [47.15, 47.17, 47.18, 47.21, 47.26]^\top$. Moreover, this point is the unique solution in

[1] We recall that arrows define a reference frame for positive currents.

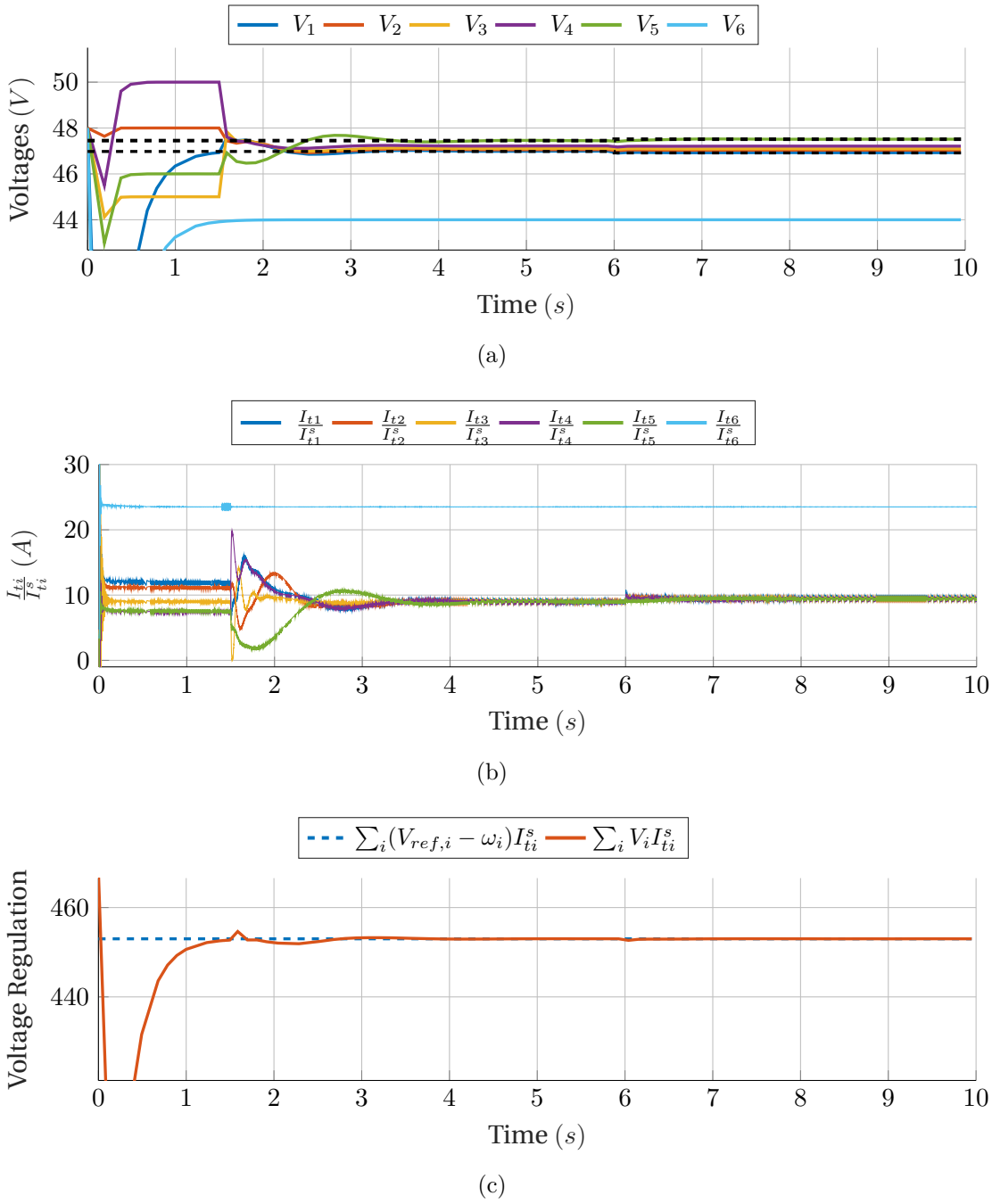

Figure 3.3: PCC voltages, weighted filter currents in *per unit*, and weighted voltage sum under secondary control with ZIP loads. In (a), the black dashed lines represent the highest and lowest voltage values in $\mathcal{H}(\delta_-)$, the set in which the unique equilibrium in $\mathcal{H}(\delta_-) \cup \mathcal{I}$ lies.

$\mathcal{H}(\delta_-) \cup \mathcal{I} = \{V \in \mathbb{R}^5 | V \geq (1 - \delta_+)V^*\}$ with $\delta_+ = 0.9996$, and is stable. Figure 3.3a shows that the PCC voltages indeed converge to this equilibrium point. Moreover, Figures 3.3b and 3.3c respectively present that current sharing is achieved and voltages

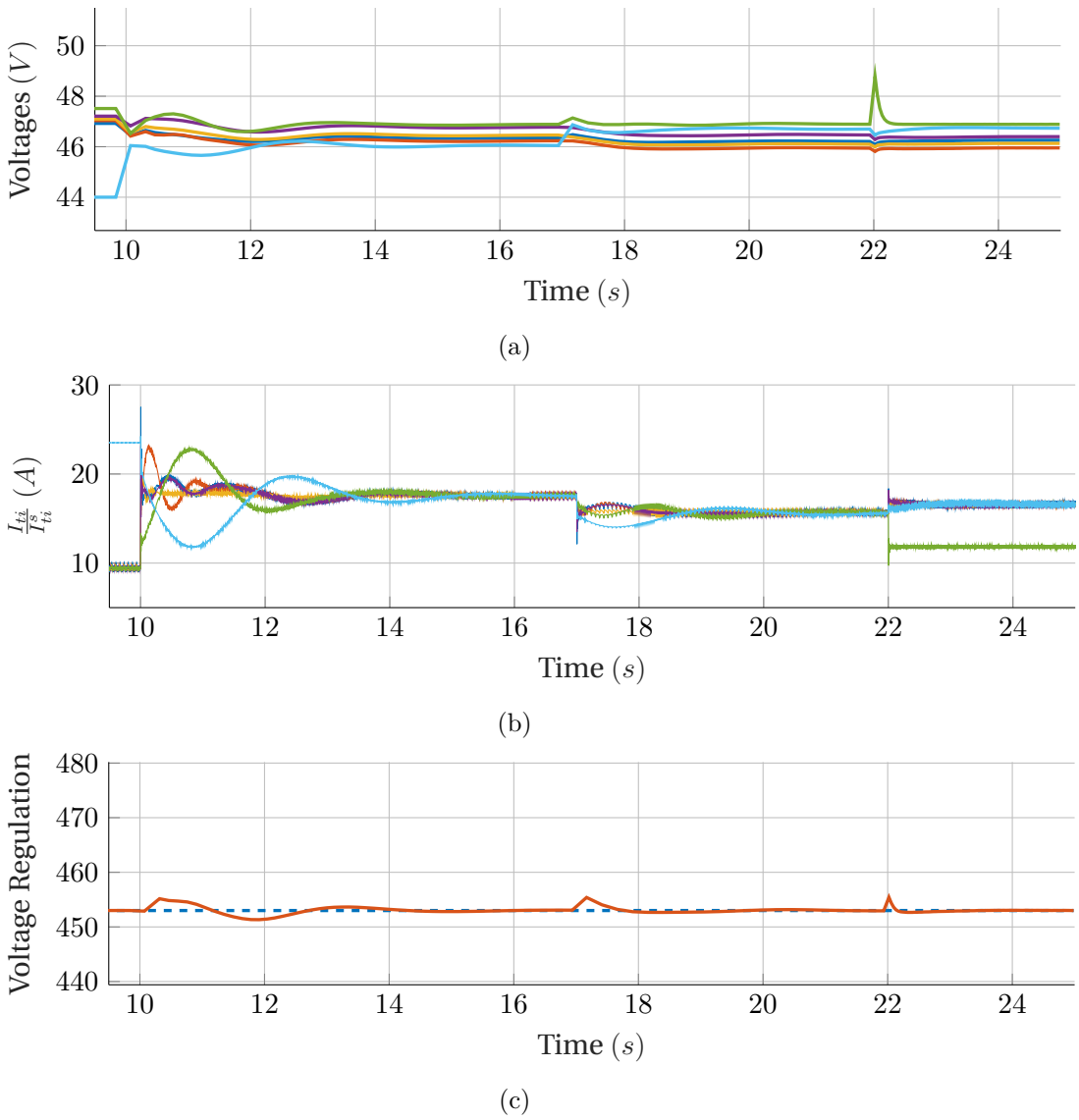

Figure 3.4: PCC voltages, weighted filter currents in *per unit*, and weighted voltage sum under secondary control with ZIE loads.

V_i are successfully regulated to the references $V_{ref,i} - \omega_i$.

Change of ZIP loads: At $t = 6s$, We modify the ZIP loads in DGUs 1 and 4 to increase their constant-impedance and constant-power loads, while ensuring that they still satisfy the conditions in Theorems 3.3.1 and 3.4.1. Consequently, it is guaranteed that a unique and stable voltage solution in $\mathcal{H}(\delta_-)$ exists with $\delta_- = 5.32 \times 10^{-4}$ and $V^* = [47.13, 47.16, 47.17, 47.20, 47.28]^\top$. Furthermore, this is the unique solution in $\mathcal{H}(\delta_-) \cup \mathcal{I}$ with $\delta_+ = 0.9995$. It can be seen in Figure 3.3 that voltages converge to this new equilibrium point with modified ZIP loads, as well as that current sharing and voltage regulation are achieved.

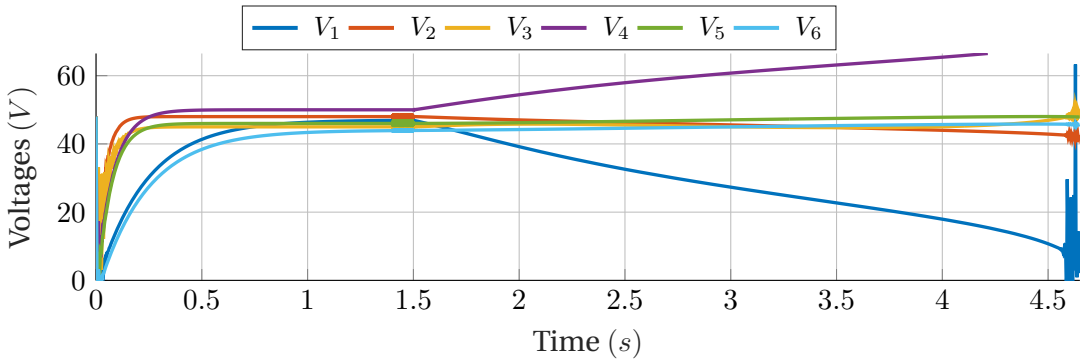

Figure 3.5: PCC voltages with ZIP loads, when (3.20) is not satisfied.

Plug-in of DGU 6***:*** At $t = 10s$, the physical lines l_3 and l_7 are attached so that DGU 6 is connected to the rest of the DCmG. At the same time, we activate the secondary controller of DGU 6, and update those of DGUs 3 and 5 to account for the communication from DGU 6. Simultaneously, the constant-power loads of DGUs 2, 3, and 5 are changed to exponential loads with exponents $r_2 = 0.6$, $r_3 = 0.55$, and $r_5 = 0.4$. Due to the existence of ZIE loads in the DCmG, Theorem 3.3.1 cannot be applied for this new DCmG; however, Theorem 3.4.1 can be applied to show that, if an equilibrium satisfying (3.28) exists, it is stable. Indeed, we see in Figures 3.4a and 3.4b that PCC voltages converge towards an equilibrium point in positive orthant of $\mathbb{R}^N$, which results in current sharing.

Change of ZIE loads: At $t = 17s$, exponents of the ZIE loads attached to DGUs 3 and 6 are changed to values greater than one, i.e., $r_3 = 1.45$ and $r_6 = 1.35$. This change of loads, in turn, change the dynamics of the DCmG, thus leading to a change of operation point. As can be seen in Figure 3.4, the primary and secondary control objectives are satisfied under this load change.

Unplugging of DGU 5***:*** At $t = 22s$, in order to show that the proposed controller works under unplugging of DGUs from the DCmG, the DGU 5 is isolated by opening the switches of lines l_6 and l_7. In doing so, its consensus-based controller is disabled, and those of its former neighbors, DGUs 4 and 6, are modified. Figure 3.4 shows that DGUs 1, 2, 3, 4, and 6 achieve current sharing and voltage balancing, whereas DGU 5 supplies its own load after unplugging from the DCmG.

3.5.2 Nonexistence of equilibria

Take into consideration the DCmG in Figure 3.2, where all DGUs have ZIP loads. In this scenario, we modify only the line resistances in the DCmG to show that a solution to (3.19) may fail to exist if necessary conditions are not satisfied. In particular, we increase the line resistances such that the condition in (3.20) is no longer satisfied. Consequently, Theorem 3.3.1 can not be applied, meaning that the current sharing may not be achieved.

To present this phenomenon through simulation, we initialize the DCmG with all the physical lines and communication channels disconnected, as in the first scenario above. Then, all electrical lines and communication channels are attached to connect all 6 DGUs together at $t = 1.5s$, also activating the secondary controllers. As can be seen in Figure 3.5, an equilibrium point does not exist. This results in a *voltage collapse* in a short period of time, i.e., one of the PCC voltages fall down to 0 V, which indicates an unsafe operating point where many electrical devices would either shut down or get damaged.

3.6 Conclusions

In this chapter, a novel secondary consensus-based control layer for current sharing and voltage balancing in DCmG was presented. We considered a DCmG composed of realistic DGUs, RLC lines, and ZIE loads. A rigorous steady-state analysis was conducted, and appropriate conditions ensuring the attainment of both objectives were derived. In addition, we provided a voltage stability analysis showing that the controllers can be synthesized in a decentralized fashion.

In the next part of the thesis, we turn to a relevant problem in LIMASs regulated via distributed control structures: detecting cyber attacks directed towards the cyber coupling graph.

3.7 Supplementary material: computation of the set M

On invoking LaSalle's invariance principle, one has that, if $\tilde{X}(0) \in \mathcal{M}$, then the state $\tilde{X}(t)$ asymptotically converges to the largest invariant set in

$$E = \{ \tilde{X} \in \mathcal{M} : \dot{\mathcal{V}}(\tilde{X}) = 0 \}. \tag{3.38}$$

Now by (3.31), $\dot{\mathcal{V}}(\tilde{X}) = 0$ if and only if $\tilde{X} \in \ker(\mathcal{Q})$. By direct computation, the set E can equivalently be represented in terms of the state $\tilde{X}$ as

$$E = \left\{ \tilde{X} \in \mathcal{M} \mid \tilde{X} = \begin{bmatrix} p \\ [\gamma]q \\ -[\beta]q \\ \mathbf{0}_M \\ s \end{bmatrix}, q, s \in \mathbb{R}^N \right\}, \tag{3.39}$$

where $p \in \mathbb{R}^N$ when $Y_L + Y_E(V) = \mathbf{0}$, otherwise $p = \mathbf{0}_N$. For evaluating the largest invariant set in E, we pick the general case, that is, $p \in \mathbb{R}^N$. In order to conclude the proof, we need to show that the largest invariant set $M \subseteq E \subseteq \mathcal{M}$ is uniquely the equilibrium point $\bar{X}$. To find the largest invariant set, we aim to deduce conditions on $\tilde{X} \in E$ such that $\dot{\tilde{X}} \in E$. Using (3.39) and (3.12) we obtain

$$\dot{\tilde{X}} = \dot{X} = \mathcal{A}\bar{X} + \mathcal{A} \begin{bmatrix} p \\ [\gamma]q \\ -[\beta]q \\ \mathbf{0}_M \\ s \end{bmatrix} + \mathcal{B}(V) = \begin{bmatrix} -C_t^{-1}(Y_L + Y_E(V))p + C_t^{-1}[\gamma]q \\ [\alpha]p + [\delta][I_t^s]^{-1}\mathcal{L}_c s \\ -p - [I_t^s]^{-1}\mathcal{L}_c s \\ L^{-1}B^\top p \\ \mathcal{L}_c[I_t^s]^{-1}[\gamma]q \end{bmatrix}.$$

Therefore, $\dot{\tilde{X}} \in E$, if and only if $L^{-1}B^\top p = \mathbf{0}_M$ and the following equations hold:

$$[\alpha]p + [\delta][I_t^s]^{-1}\mathcal{L}_c s = [\gamma]\tilde{q}, \tag{3.40a}$$

$$-p - [I_t^s]^{-1}\mathcal{L}_c s = -[\beta]\tilde{q}, \tag{3.40b}$$

where $\tilde{q} \in \mathbb{R}^N$. Left multiplying (3.40b) with $[\alpha]$, and then adding it with (3.40a) yields

$$[\alpha][\beta]q = [\gamma]q. \tag{3.41}$$

This necessitates

$$\alpha_i\beta_i = \gamma_i, \forall i \in \mathcal{V}. \tag{3.42}$$

Also, as the feedback gains $k_{1,i}, k_{2,i}$, and $k_{3,i}$ belong to the set $\mathcal{Z}_{[i]}$ in (3.27), then $\alpha_i < 0, \beta_i < 0$, and $0 < \gamma_i < \alpha_i\beta_i$. Thus, we conclude that (3.40a) and (3.40b) can be simultaneously satisfied only if $\tilde{q} = \mathbf{0}_N$. As for $L^{-1}B^\top p = \mathbf{0}_M$, one obtains that $p \in \ker(B^\top)$. Since the graph $\mathcal{G}_p$ is connected, $\ker(B^\top) = \mathbb{H}_\perp^1$ [Bul17]. Therefore, for $\dot{\tilde{X}}$

to remain in E, $\tilde{X}$ must stay in set $S \subset E$, where

$$S = \left\{ \tilde{X} \in \mathcal{M} \mid \tilde{X} = \begin{bmatrix} \kappa \mathbf{1}_N \\ \mathbf{0}_N \\ \mathbf{0}_N \\ \mathbf{0}_M \\ s \end{bmatrix}, s \in \mathbb{R}^N \right\}. \tag{3.43}$$

Furthermore, it must hold $M \subseteq S$. Then, in order to characterize M, we assume $\tilde{X} \in S$ and impose $\dot{\tilde{X}} \in S$. This translates into the following

$$\dot{\tilde{X}} = \dot{X} = \mathcal{A}\bar{X} + \mathcal{A} \begin{bmatrix} \kappa \mathbf{1}_N \\ \mathbf{0}_N \\ \mathbf{0}_N \\ \mathbf{0}_M \\ s \end{bmatrix} + \mathcal{B}(V) = \begin{bmatrix} -\kappa C_t^{-1}(Y_L + Y_E(V))\mathbf{1}_N \\ \kappa[\alpha]\mathbf{1}_N + [\delta][I_t^s]^{-1}\mathcal{L}_c s \\ -\kappa \mathbf{1}_N - [I_t^s]^{-1}\mathcal{L}_c s \\ \mathbf{0}_M \\ \mathbf{0}_N \end{bmatrix}.$$

Notice that, for $\dot{\tilde{X}} \in S$, it must hold that $[I_t^s]^{-1}\mathcal{L}_c s = -\kappa \mathbf{1}_N$. Since $\kappa \mathbf{1}_N \in \ker([I_t^s]^{-1}\mathcal{L}_c)$, it turns out that both $\kappa = 0$ and $s = \mathbf{0}_N$. This implies that the largest invariant set $M \subseteq E$ is $M = \{\tilde{X} \in \mathcal{M} \mid \tilde{X} = \mathbf{0}_{4N+M}\}$.

Cyber-attack Detection Part II

4 Distributed cyber-attack detection

4.1 Introduction

As discussed in Chapter 2, LIMASs contain both physical and cyber interconnections between subsystems. The presence of cyber coupling, usually realized through communication networks, is motivated by the goal of implementing distributed control structures, as LIMASs can grow significantly in size and complexity. Specific examples of such LIMASs are DCmGs controlled by using distributed architectures that achieve certain mG-wide objectives (see Chapter 3). The existence of a communication network between subsystems of a LIMAS makes it a CPS, which are known to be susceptible to cyber attacks. Therefore, in this chapter, we tackle the problem of distributed cyber-attack detection in LIMASs.

The design and analysis of monitoring schemes to detect cyber attacks for CPSs have attracted great interest in the literature, as demonstrated by the special issue [CSS17], as well as the surveys [SAJ15, UGC+16] and references cited therein. Specifically, we require that each subsystem is equipped with its own local diagnoser, and that the information needed for the design and operation of the monitor is limited to a subset of the LIMAS. In the literature, few works propose distributed methods, of which [NI14, DPA+18, AKP18, PDB15b, BRBP20, HRSJ21] are examples, but often requiring additional assumptions. For instance, [PDB15b, BRBP20] suppose secure communication between different monitoring units. In [AKP18] the differences between centralized and decentralized architectures in cyber-attack detection are analyzed in the context of stochastic interconnected systems. Finally, [NI14, DPA+18, HRSJ21] present *distributed* detection methods in which locally available information is exploited to estimate the global state of the system. These approaches share similarities with methods proposed for secure distributed state estimation, such as [MS16], where the global state of a LIMAS is reconstructed from partial measurements in the presence of cyber attacks. Note that, in this chapter, we use the term "distributed" differently. Indeed, our aim is to avoid using or estimating global variables of the LIMAS.

4.1.1 Contributions

In this chapter, we propose a novel distributed monitoring architecture devoted to the timely detection of attacks on the information network connecting subsystems of the LIMAS. Our method relies on two modules, employing a bank of UIOs and a distributed Luenberger observer, as will be further illustrated in Section 4.3. These two modules exploit different sets of relations and model knowledge to perform detection, thus compensating each other's vulnerabilities, and reducing the set of attacks that are not detected. In particular, while the Luenberger observer of the local state exploits analytical relations from the physical interconnection between subsystems to perform detection, the UIOs estimating the neighbors' states exploit knowledge of the model of the neighbors themselves. This difference proves critical in the analysis of the properties of each module, as it determines both the classes of attacks that are guaranteed to be detected and, more importantly, the classes of attacks that cannot be detected by each module independently. Indeed, the simultaneous use of both modules reduces the classes of attacks that are *stealthy* to the detection architecture, i.e., attacks that are guaranteed not to be detected. Finally, we verify the efficacy of our method through realistic computer simulations of a DCmG.

The main contributions of this chapter compared to the existing literature are:

1. to design a *local* monitoring unit $\mathcal{D}_i$ for the i-th subsystem, to detect attacks on the communication network;
2. to propose a distributed and scalable design technique in which the synthesis of $\mathcal{D}_i$ requires at most information from neighbors of subsystem i;
3. to provide theoretical results on detectability and stealthiness properties of the proposed attack detection scheme, given bounds on unknown noises influencing both subsystem dynamics and measurements;
4. to introduce a state augmentation technique to improve the detection capabilities of the UIO-based module;
5. to validate the monitoring scheme through analysis and simulations using a realistic model of a DCmG.

In Section 4.2 we provide the problem formulation. In Section 4.3, we illustrate the attack detection architecture, in which $\mathcal{D}_i$ utilizes two parallel modules. In Sections 4.4 and 4.5 we analyze the properties of the modules individually, in terms of *detectable* and *stealthy* attacks. In Section 4.6 we evaluate the detectability properties of $\mathcal{D}_i$ as a whole, thus showing the benefits of combining the two modules. In Section 4.7, extensive results from numerical simulations using realistic dynamics of a DCmG are given, and the effectiveness of the strategy demonstrated.

4.2 Problem formulation

4.2.1 LIMAS model

As in Chapter 2, we model a LIMAS as a network of N subsystems $\mathcal{S}_i$, each coupled with a set of *neighbors* $\mathcal{N}_i \subseteq \mathcal{V} \triangleq \{1, \ldots, N\}$, $N_i \triangleq |\mathcal{N}_i|$. The dynamics of each subsystem is written as

$$\mathcal{S}_i : \begin{cases} \dot{x}_{[i]} = A_{ii}x_{[i]} + B_i u_{[i]} + M_i d_{[i]} + \xi_{[i]} + w_{[i]} \\ y_{[i]} = C_i x_{[i]} + \rho_{[i]} \end{cases}, \tag{4.1}$$

where $x_{[i]} \in \mathbb{R}^{n_i}$, $u_{[i]} \in \mathbb{R}^{m_i}$, $d_{[i]} \in \mathbb{R}^{g_i}$, $y_{[i]} \in \mathbb{R}^{p_i}$ are respectively the subsystem state, control and exogenous input, and output; $\xi_{[i]} \in \mathbb{R}^{n_i}$ represents the physical interconnection between subsystems, defined as $\xi_{[i]} \triangleq \sum_{j \in \mathcal{N}_i} A_{ij} x_{[j]}$, while $w_{[i]} \in \mathbb{R}^{n_i}$ and $\rho_{[i]} \in \mathbb{R}^{p_i}$ model process and measurement noises. In this chapter, we assume that all pairs (C_i, A_{ii}) are observable. Note that (4.1) can be seen as a continuous-time generalization of the LIMAS model in (2.1), where the subsystems are allowed to have non-homogeneous dynamics and exogeneous inputs as well as process and measurement noises are considered.

Assumption 4.2.1. *Process and measurement noises $w_{[i]}(t)$ and $\rho_{[i]}(t)$ are unknown but bounded, i.e.*

$$|w_{[i]}(t)| \leq \bar{w}_{[i]}, \quad |\rho_{[i]}(t)| \leq \bar{\rho}_{[i]}, \tag{4.2}$$

for all $t \geq 0$, where $\bar{w}_{[i]}, \bar{\rho}_{[i]} > 0, \forall i \in \mathcal{V}$, are known.

Similarly to the previous chapters, we consider the control input $u_{[i]}$ to be the result of a distributed control architecture, utilizing a communication network based on a *cyber coupling graph*. Therefore, the control input $u_{[i]}$ depends directly on communicated variables $y^c_{[j,i]}$ that $\mathcal{S}_i$ *receives* from its neighbors. Here $y^c_{[j,i]}$ is used to differentiate the output $y_{[j]}$ *locally* available to $\mathcal{S}_j$ from the information that $\mathcal{S}_i$ receives. Throughout this chapter, we assume that the communication network shares the same topology as the physical coupling graph. We also consider that it is *ideal*, i.e. that it is not affected by non-idealities such as delays and packet drops, among others.

4.2.2 Model of cyber attack

The necessity of integrating a communication network in the control architecture of a LIMAS may expose the system to cyber-security threats [MKB+12]. The information received by $\mathcal{S}_i$ from $\mathcal{S}_j$ is written as

$$y^c_{[j,i]}(t) \triangleq y_{[j]}(t) + \beta_{j,i}(t - T_a^{j,i})\phi_{j,i}(t), \quad \forall t \geq 0 \tag{4.3}$$

where $\beta_{j,i}(t)$ is an activation function, $\phi_{j,i}(t)$ is an attack function, as defined by the attacker to achieve some unknown objective, and $T_a^{j,i} > 0$ is the unknown initial time of attack. The activation function can be any function of time satisfying $\beta_{j,i}(t) = 0$, $\forall t < 0$

and $\beta_{j,i}(t) \neq 0$, $\forall t \geq 0$. Readers are referred to [BGFTP17] for possible choices of this function. Note that, in nominal conditions (i.e. for $t < T_a^{i,j}$), the information received by $\mathcal{S}_i$ from $\mathcal{S}_j$ is the exact measurement vector, i.e. $y^c_{[j,i]}(t) = y_{[j]}(t)$.

Assumption 4.2.2. *Each edge $(i,j), \forall i,j \in \mathcal{V}$ is affected by at most one attack, and $T_a^{j,i} > 0, \forall i,j \in \mathcal{V}$.*

Remark 4.2.1. *Assumption 4.2.2 is not very restrictive, as it does not exclude the occurrence of complex attacks targeting multiple lines simultaneously.*

Through appropriate definition of $\phi_{j,i}(t)$ in (4.3), it is possible to model different types of attacks [TPSJ12], such as: *false data injection attacks*, where $\phi_{j,i} : \mathbb{R} \to \mathbb{R}^{n_i}$ is any attacker-defined function of time; *covert attacks*, where an attack of the form $\phi_{j,i}(t) \triangleq -y_{[j]}(t) + y^a_{[j]}(t)$ replaces the transmitted information with the output $y^a_{[j]}(t)$ of a *simulated system* with the same dynamics as $\mathcal{S}_j$; *replay attacks*, where transmitted information $y_{[j]}(t)$ is stored and then *replayed* periodically by the attacker, hiding any changes in operating condition of $\mathcal{S}_i$, and where $\phi_{j,i}(t) \triangleq -y_{[j]}(t) + y_{[j]}(t - nT)$, with $n \in \mathbb{N}$ modeling the periodicity of the attack.

Remark 4.2.2. *In the context of this chapter, we only consider attacks on the variables which are communicated between subsystems. Thus, both the local measurement $y_{[i]}$ and the control input $u_{[i]}$ are considered to be secure. This is motivated by the DCmG application, where controllers are colocated with the sensors and actuators interfacing the system.*

4.2.3 Attack detection

We now formulate the problem of *attack detection*. We define the activation time of the first attack on the incoming communication channels of a subsystem:

$$\check{T}_a^i \triangleq \min_{j \in \mathcal{N}_i} T_a^{j,i}.$$

Problem 1 (Attack Detection)**.** *Design, for each subsystem, an attack detector $\mathcal{D}_i$ to verify the null hypothesis*

$$\mathcal{H}_i^0(t) : \{y^c_{[j,i]}(t) = y_{[j]}(t), \forall j \in \mathcal{N}_i\} \tag{4.4}$$

at time t, i.e., the received communication is not under attack.

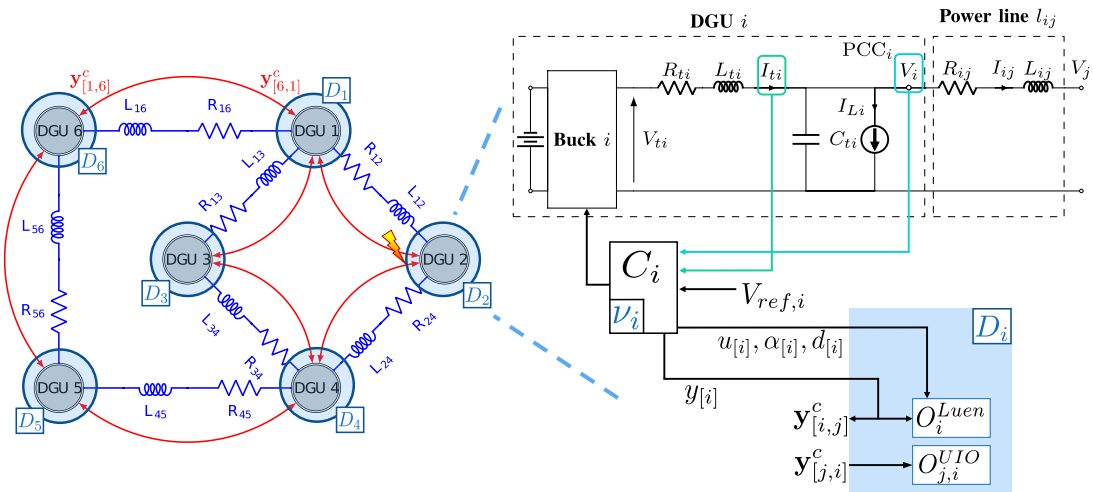

Figure 4.1: Diagram representation of the DCmG. On the left, the graph representing the DCmG; the physical interconnections are shown as the blue power lines, and the communication topology appears as the red arrows. Cyber attacks are directed at the communication lines. On the right, the circuit diagram of a DGU, together with the information structure of the detector D_i.

4.2.4 Islanded DCmGs

Model

As in the previous chapter, we represent an islanded DCmG as a network of N interconnected DGUs, each composed of a Buck converter, interfacing a variable DCmG source with the rest of the network through an RLC filter (see Figure 4.1). We assume that loads are connected to the DGU terminals[1], and DGUs are coupled through resistive lines. The interconnected dynamics of DGU i can be written as in (4.1), with state $x_{[i]} \triangleq [V_i, I_{ti}, \nu_i]^\top$ (where ν_i is an integrator state internal to the controller, used for reference voltage tracking), exogenous input $d_{[i]} \triangleq I_{Li}$, and input $u_{[i]} = [V_{ti}, \Delta V_i]^\top$, where ΔV_i is the result of a secondary control layer (e.g. a consensus protocol) used for current sharing across the network, and V_{ti} is the switching terminal voltage of the Buck converter. The specific definitions of the matrices in (4.1) can be found in Section 4.9.1, and the interested reader is referred to [TRFT18] for further details.

Remark 4.2.3. *In the literature, the design of controllers for DCmGs with DC-DC converters often relies on the so-called state-space averaging method, to disregard the switching behavior of the terminal input [MC76]. It is therefore possible to define an average control input $V_{ti}^{avg} \triangleq \delta_i V_{si}$, where $\delta_i \in [0, 1]$ is the duty cycle of the Buck converter and $V_{si} \in \mathbb{R}$ is the voltage of its power source.*

[1] If load buses appear elsewhere, they can be mapped to the output terminals of DGUs using Kron reduction [TRFT18].

Assumption 4.2.3. *For every DGU $i \in \mathcal{V}$, $C_i = \mathbf{I}$ and the measurement is affected by an unknown noise $\rho_{[i]}$.*

Assumption 4.2.3 is not restrictive as V_i and I_{ti} can be measured within the DGU, and ν_i is an internal state of the controller.

Controller architecture

The control strategies proposed for islanded DCmGs are often designed in the context of hierarchical architectures (see Chapter 3, the review [MSFT+17], and the references cited therein), where primary controllers within the DGUs guarantee global stability [TRFT18, ZD15, NST+20], while secondary and tertiary controllers achieve different operational objectives, such as current and power sharing, mG synchronization, and overall energy management [TMGFT18, ZD15, DPWD18, CBCZ16, NTFT20]. In this chapter, we consider that each DGU is controlled by primary and secondary controllers defined as in [NST+20] and [TMGFT18], respectively. Our choice is motivated by the fact that these controllers can be designed in a scalable fashion while providing stability of the whole DCmG. We note that this particular choice of controllers is very similar to the one in Chapter 3, and without loss of generality. Indeed, the results of this chapter hold for any distributed control scheme.

Specifically, the schemes presented in [NST+20, TMGFT18] define control laws to respectively compute the average terminal voltage V_{ti}^{avg} (and thus δ_i) to obtain global voltage stability, and the secondary control input ΔV_i, to achieve current sharing, by employing a consensus protocol reliant on neighbors' communicated outputs (4.3). To achieve coordination across the whole DCmG, reliable communication between DGUs is necessary. Thus, cyber attacks can easily alter the operating point of the DCmG as a whole.

Note that, here, we consider the case of *islanded* DCmGs. In the case of grid connection, DCmGs provide ancillary services to the main grid, typically through the use of an energy management system (EMS). In recent years, distributed optimization methods have been presented for distributed EMSs [WCWK16], which may be tackled with the distributed detection scheme here proposed.

Next, we provide a description of the proposed two-module detection scheme.

4.3 Attack detector $\mathcal{D}_i$ – Detection architecture

As previously mentioned, the proposed detection architecture, illustrated in Figure 4.1, relies on two modules simultaneously estimating the state of the local subsystem (through a Luenberger observer) and the states of the neighboring subsystems (with a bank of N_i

Table 4.1: Information required for design of $\mathcal{D}_i$ and attack detection

	UIO$(j,i), \forall j \in \mathcal{N}_i$	**Luenberger observer**
Offline Information	Matrices $\mathbf{A}_{jj}$,$\mathbf{E}_j$,$\mathbf{C}_j$, bounds $\bar{w}_{[j]}$ and $\bar{\rho}_{[j]}$	Model of $\mathcal{S}_i$, matrix $\mathbf{C}_j$, and bounds $\bar{w}_{[i]}$ and $\bar{\rho}_{[k]}$, for all $k \in \{i\} \cup \mathcal{N}_i$
Online Information	Communicated measurements $\mathbf{y}^c_{[j,i]}(t)$	Local measurements and inputs, and communicated measurements $\mathbf{y}^c_{[j,i]}(t)$

UIOs). The bank of UIOs compute an estimate $\hat{\mathbf{x}}_{[j,i]}(t)$ of a suitably defined augmented state $\mathbf{x}_{[j]}$ for each neighbor of $\mathcal{S}_i$, whilst the Luenberger observer generates an estimate $\hat{x}_{[i]}(t)$ of the state $x_{[i]}(t)$ of $\mathcal{S}_i$. The augmented state $\mathbf{x}_{[j]}$ and communicated output measurement $\mathbf{y}^c_{[j,i]}$ required for the design of the UIO-based modules in $\mathcal{D}_i$ are introduced in Section 4.4. The output estimates are compared respectively to $\mathbf{y}^c_{[j,i]}$ and $y_{[i]}$, and the resulting residual is then used to detect the presence of an attack, by evaluating the following inequalities:

$$\underbrace{\left|\mathbf{y}^c_{[j,i]}(t) - \mathbf{C}_j\hat{\mathbf{x}}_{[j,i]}(t)\right|}_{|r_{[j,i]}(t)|} \leq \bar{r}_{[j,i]}(t), \quad \forall j \in \mathcal{N}_i \tag{4.5a}$$

$$\underbrace{\left|y_{[i]}(t) - C_i\hat{x}_{[i]}(t)\right|}_{|r_{[i]}(t)|} \leq \bar{r}_{[i]}(t) \tag{4.5b}$$

where matrix $\mathbf{C}_j$ is defined in (4.11) and the thresholds $\bar{r}_{[j,i]}(t)$ and $\bar{r}_{[i]}(t)$ are defined appropriately to prevent false alarms, based on knowledge of the noise bounds in (4.2). This design choice, albeit guaranteeing that the process will not be interrupted without a certified threat, also implies that the thresholds are possibly conservative. If at any time $t > \check{T}^i_a$ either of the inequalities in (4.5) is violated, an attack is detected by $\mathcal{D}_i$. Moreover, if (4.5a) is violated, the attacked communication line is also isolated. The operation of the detection logic is summarized in Algorithm 1, while in Table 4.1 we highlight the information required by $\mathcal{D}_i$ at design time (*offline*), and during normal operations (*online*).

As shown in Table 4.1, the two modules exploit different model knowledge to detect the presence of cyber attacks. Specifically, each UIO exploits knowledge of augmented dynamics of $\mathcal{S}_j$ (i.e. matrices $\mathbf{A}_{jj}, \mathbf{E}_j, \mathbf{C}_j$) to estimate the state of each of its neighbors $\mathcal{S}_j, j \in \mathcal{N}_i$ from $\mathbf{y}^c_{[j,i]}$. This allows for detection of false data injection attacks, while being vulnerable to replay and covert attacks. On the other hand, the Luenberger-observer-based detection module uses knowledge of dynamics of $\mathcal{S}_i$ (4.1) to exploit the physical interconnections between subsystems, thus detecting attacks with analytical relations to the local dynamics.

Algorithm 1 Attack detection and isolation at time t

```
while S_i online ∀i ∈ V do
    Update estimates x̂_[j,i](t), ∀j ∈ N_i and x̂_[i](t);
    Update bounds r̄_[j,i](t), ∀j ∈ N_i and r̄_[i](t);
    Compute residuals r_[j,i](t), ∀j ∈ N_i and r_[i](t);
    Evaluate (4.5a) and (4.5b)
    if (4.5a) and (4.5b) hold then
        No attack is detected at time t
    else
        if |r_[j,i](t)| > r̄_[j,i](t) for any j ∈ N_i then
            Attack detected on link (j, i)
        else
            Attack detected, no link is isolated
        end if
    end if
end while
```

The detector $\mathcal{D}_i$, by combining the two modules in the same architecture and having them run simultaneously as illustrated in Algorithm 1, is capable of detecting attacks that would be stealthy to either of the modules independently as will be analytically presented in Section 4.6.

We now focus on the appropriate design of the two observer-based modules, the definition of thresholds $\bar{r}_{[j,i]}(t)$ and $\bar{r}_{[i]}(t)$, and analyze their individual properties.

Remark 4.3.1. *As can be seen from Algorithm 1 and Table 4.1, the design and operation of $\mathcal{D}_i$ rely at most on information from the set of neighbors $\mathcal{N}_i$ and are, therefore, distributed as well as scalable with the number of subsystems in the network.*

4.4 Bank of unknown-input observers

4.4.1 Design of the detection module

We first focus on the design and properties of $\mathcal{O}_{j,i}^{UIO}$, the UIO-based detection modules estimating the states of neighboring subsystems. UIOs are a class of observers designed to algebraically decouple the residual error from a vector of unknown inputs [CPZ96]. This proves fundamental for $\mathcal{D}_i$ to estimate the state $x_{[j]}$, $j \in \mathcal{N}_i$, as $\mathcal{S}_i$ does not have access to the inputs affecting the dynamics of its neighbors. To design the UIOs we rewrite the dynamics of $\mathcal{S}_j$ in (4.1) as

$$\begin{aligned} \dot{x}_{[j]} &= A_{jj}x_{[j]} + \bar{E}_j\bar{d}_{[j]} + w_{[j]}, \\ y_{[j]} &= C_j x_{[j]} + \rho_{[j]}, \end{aligned} \tag{4.6}$$

where $\bar{E}_j\bar{d}_j = \xi_{[j]} + B_j u_{[j]} + M_j d_{[j]}$ represents the effect of the unknown inputs on $x_{[j]}$. The matrix $\bar{E}_j \in \mathbb{R}^{n_j \times q_j}, q_j \leq n_j$ links the unknown inputs to the dynamics of $\mathcal{S}_j$, its columns constituting a basis for the range of matrix $E_j \triangleq \left[A_{jk_1}, \ldots, A_{jk_{N_j}}, B_j, M_j\right]$, where $\{k_1, \ldots, k_{N_j}\} = \mathcal{N}_j$ are the indices of the neighbors of $\mathcal{S}_j$. This definition ensures that $\bar{E}_j$ is full column rank, as required by [CPZ96]. The term $\bar{d}_{[j]}(t) \triangleq \hat{E}_j\hat{d}_{[j]}$ captures the combined effect of unknown inputs collected in $\hat{d}_{[j]}$, which is defined as

$$\hat{d}_{[j]} \triangleq \left[x_{[k_1]}^\top, \ldots, x_{[k_{N_j}]}^\top, u_{[j]}^\top, d_{[j]}^\top\right]^\top, \tag{4.7}$$

i.e., the vector containing all inputs to $\mathcal{S}_j$ unknown to $\mathcal{D}_i$. Matrix $\hat{E}_j$ is derived, following the choice of $\bar{E}_j$, such that $\bar{E}_j\hat{E}_j = E_j$. We omit its derivation since it is not relevant to the design of the UIOs. Indeed, for designing the UIO, determining a suitable matrix $\bar{E}_j$ is sufficient.

The full-order UIO state and state estimate of $\mathcal{S}_j$ can be defined as follows [CPZ96]:

$$\begin{aligned}
\dot{z}_{[j,i]}(t) &= F_j z_{[j,i]}(t) + \widehat{K}_j y^c_{[j,i]}(t),\\
\hat{x}_{[j,i]}(t) &= z_{[j,i]}(t) + H_j y^c_{[j,i]}(t),\\
\hat{y}_{[j,i]}(t) &= C_j \hat{x}_{[j,i]}(t),
\end{aligned} \tag{4.8}$$

whose matrices are defined as in [CPZ96] and are such that

$$(H_jC_j - \mathbf{I})\bar{E}_j = \mathbf{0}, \tag{4.9a}$$
$$S_j = \mathbf{I} - H_jC_j, \tag{4.9b}$$
$$F_j = S_jA_{jj} - \widetilde{K}_jC_j, \tag{4.9c}$$
$$\bar{K}_j = F_jH_j, \tag{4.9d}$$
$$\widehat{K}_j = \widetilde{K}_j + \bar{K}_j. \tag{4.9e}$$

The definition of S_j through design of H_j (4.9a)-(4.9b) decouples the residual error $r_{[j,i]}(t) \triangleq y^c_{[j,i]}(t) - \hat{y}_{[j,i]}(t)$ from the unknown input vector $\bar{d}_{[j]}$, while matrix $\widetilde{K}_j$ is such that F_j in (4.9c) is Hurwitz stable. The following necessary and sufficient conditions are given in [CPZ96] to verify the possibility of designing the UIO (4.8):

$$\operatorname{rank}(C_j\bar{E}_j) = \operatorname{rank}(\bar{E}_j); \tag{C1}$$
$$\text{the pair } (C_j, S_jA_{jj}) \text{ is detectable.} \tag{C2}$$

These two conditions need to be satisfied for a generic system of the form (4.6) in order to employ the proposed detection methodology. The following guarantees that these conditions are met in the special case of mGs:

Remark 4.4.1. *Given Assumption 4.2.3, $C_j = \mathbf{I}$, and thus conditions* (C1) *and* (C2) *are satisfied.*

This remark points out that, for DCmGs, a UIO can always be designed. However, notice that, in the case of DCmGs, $\text{rank}(\bar{E}_j) = \text{rank}(C_j) = n_j$. In the next lemma, we show that this condition prevents the use of the designed UIO for detecting attacks.

Lemma 4.4.1. *Consider a subsystem with dynamics in* (4.6) *such that* (C1) *and* (C2) *hold, and a UIO with dynamics as in* (4.8)*. If* $\text{rank}(C_j) = \text{rank}(\bar{E}_j) = q_j$ *the residual* $r_{[j,i]} = y^c_{[j,i]} - \hat{y}_{[j,i]}$ *is independent of the attack function* $\phi_{[j,i]} \neq \mathbf{0}$ *at all times.*

Proof. The proof is provided in Section 4.9.2 ■

Given the results stated in Lemma 4.4.1, in order to design an attack detection architecture, it is necessary either to reduce the number of unknown inputs (which may not be feasible), or increase the output information transmitted. To address the latter, additional sensors providing independent measurements could be added, although this may not be possible depending on the application. Indeed, in the case of DCmGs, all states are already measured and transmitted. Rather, here we augment the transmitted information such that the original output $y_{[j]}$ can be reconstructed – as it is necessary for control purposes – and it represents the output of a dynamical system known to $\mathcal{O}^{UIO}_{i,j}$.

Let us hence introduce the augmented state variable $\mathbf{x}_{[j]} = \left[x^{art}_{[j]}, e^{art}_{[j]}\right]$ with $x^{art}_{[j]}$ some *artificial* state the dynamics of which is known to $\mathcal{O}^{UIO}_{i,j}$, $\forall i \in \mathcal{N}_j$ and simulated by $\mathcal{S}_j$, and $e^{art}_{[j]} \triangleq x_{[j]} - x^{art}_{[j]}$. By construction,

$$\begin{aligned} x_{[j]} &= \begin{bmatrix} \mathbf{I} & \mathbf{I} \end{bmatrix} \mathbf{x}_{[j]}, \\ y_{[j]} &= \begin{bmatrix} C_j & C_j \end{bmatrix} \mathbf{x}_{[j]} + \rho_{[j]}, \end{aligned} \tag{4.10}$$

allowing for reconstruction of $y_{[j]}$. Let us define the dynamics of $\mathbf{x}_{[j]}$, and hence $x^{art}_{[j]}$, as

$$\begin{aligned} \dot{\mathbf{x}}_{[j]} &= \begin{bmatrix} A^{art}_{jj} & \mathbf{0} \\ A_{jj} - A^{art}_{jj} & A_{jj} \end{bmatrix} \mathbf{x}_{[j]} + \begin{bmatrix} \mathbf{E}_{j,1} & \mathbf{0} \\ \mathbf{0} & \mathbf{E}_{j,2} \end{bmatrix} \begin{bmatrix} \mathbf{d}_{[j,1]} \\ \mathbf{d}_{[j,2]} \end{bmatrix} + \begin{bmatrix} \mathbf{0} \\ \mathbf{I} \end{bmatrix} w_{[j]} \\ &= \mathbf{A}_{jj}\mathbf{x}_{[j]} + \mathbf{E}_j \mathbf{d}_{[j]} + \tilde{\mathbf{w}}_{[j]}, \\ \mathbf{y}_{[j]} &= \begin{bmatrix} \mathbf{I} & \mathbf{0} \\ C_j & C_j \end{bmatrix} \mathbf{x}_{[j]} + \begin{bmatrix} \mathbf{0} \\ \mathbf{I} \end{bmatrix} \rho_{[j]} = \mathbf{C}_j \mathbf{x}_{[j]} + \boldsymbol{\rho}_{[j]} = \begin{bmatrix} x^{art}_{[j]} \\ y_{[j]} \end{bmatrix}. \end{aligned} \tag{4.11}$$

where $A^{art}_{jj} \in \mathbb{R}^{n_j \times n_j}$ is any Hurwitz stable matrix. Nonzero matrices $\mathbf{E}_{j,1}$ and $\mathbf{E}_{j,2}$ are constructed such that $[\mathbf{E}_{j,1}, \mathbf{E}_{j,2}] = \bar{E}_j$, up to column permutations, and unknown input vectors $\mathbf{d}_{[j,1]}$ and $\mathbf{d}_{[j,2]}$ satisfy $[\mathbf{E}_{j,1}, \mathbf{E}_{j,2}]\,[\mathbf{d}^\top_{[j,1]}, \mathbf{d}^\top_{[j,2]}]^\top = \bar{E}_j \bar{d}_j$. Additionally, the following hold by construction: $\text{rank}(\mathbf{E}_{j,1}) < n_j$, $\text{rank}(\mathbf{E}_{j,2}) < q_j$, and $\text{range}(\mathbf{E}_{j,1}) \subset \text{range}(\bar{E}_j)$, $\text{range}(\mathbf{E}_{j,2}) \subset \text{range}(\bar{E}_j)$. Finally note that, as $x^{art}_{[j]}$ is *simulated* by $\mathcal{S}_j$, it is fully available and therefore appears in $\mathbf{y}_{[j]}$. We then redefine the communicated measurement in (4.3)

as

$$\mathbf{y}^c_{[j,i]}(t) \triangleq \mathbf{y}_{[j]}(t) + \beta_{j,i}(t - T_a^{j,i})\boldsymbol{\phi}_{j,i}(t) \tag{4.12}$$

with $\boldsymbol{\phi}_{j,i}(t) \triangleq [\varphi_{j,i}^\top(t), \phi_{j,i}^\top(t)]^\top \in \mathbb{R}^{n_j+p_j}$, where $\varphi_{j,i}(t)$ is the attack influencing the communicated artificial state. We note that the transmitted information, as seen in (4.12), is redefined to include both the output measurements, and the artificial state. In the following, we show how through state and output augmentation (4.11) necessary condition in Lemma 4.4.1 is satisfied.

Lemma 4.4.2. *If* (C1) *and* (C2) *hold for* $(A_{jj}, C_j, \bar{E}_j)$*, then they are also satisfied for* $(\mathbf{A}_{jj}, \mathbf{C}_j, \mathbf{E}_j)$*. If, additionally,* $\text{rank}(C_j) = \text{rank}(\bar{E}_j)$*, then* $\text{rank}(\mathbf{C}_j) > \text{rank}(\mathbf{E}_j)$*.*

Proof. Condition (C1) holds given definitions of $\mathbf{C}_j$ and $\mathbf{E}_j$:

$$\mathbf{C}_j\mathbf{E}_j = \begin{bmatrix} \mathbf{E}_{j,1} & \mathbf{0} \\ C_j\mathbf{E}_{j,1} & C_j\mathbf{E}_{j,2} \end{bmatrix}, \tag{4.13}$$

the rank of which, being block lower triangular, is such that

$$\text{rank}(\mathbf{C}_j\mathbf{E}_j) \geq \text{rank}(\mathbf{E}_{j,1}) + \text{rank}(C_j\mathbf{E}_{j,2}) = \text{rank}(\mathbf{E}_{j,1}) + \text{rank}(\mathbf{E}_{j,2}) = \text{rank}(\mathbf{E}_j). \tag{4.14}$$

Hence, noting that $\text{rank}(\mathbf{C}_j\mathbf{E}_j) \leq \min(\text{rank}(\mathbf{C}_j), \text{rank}(\mathbf{E}_j))$, it follows that $\text{rank}(\mathbf{C}_j\mathbf{E}_j) = \text{rank}(\mathbf{E}_j)$, thus satisfying (C1).

To show that (C2) is satisfied for the augmented system matrices, first note that a block-diagonal matrix $\mathbf{S}_j$ composed of blocks $S_{j,1}$ and $S_{j,2}$ can be found such that $\mathbf{S}_j\mathbf{E}_j = \mathbf{0}$. This is due to existence of solutions to $S_{j,1}\mathbf{E}_{j,1} = \mathbf{0}$ and $S_{j,2}\mathbf{E}_{j,2} = \mathbf{0}$, from $\text{rank}(\mathbf{E}_{j,1}) < n_j$, $\text{rank}(\mathbf{E}_{j,2}) < q_j \leq n_j$ by construction. Therefore $\mathbf{S}_j\mathbf{A}_{jj} = \begin{bmatrix} S_{j,1}A_{jj}^{art} & \mathbf{0} \\ \star & S_{j,2}A_{jj} \end{bmatrix}$, where $\star$ represents the additional term. Hence, the pair $(\mathbf{C}_j, \mathbf{S}_j\mathbf{A}_{jj})$ is detectable:

$$\begin{aligned} \text{rank}\left(\begin{bmatrix} s\mathbf{I} - \mathbf{S}_j\mathbf{A}_{jj} \\ \mathbf{C}_j \end{bmatrix}\right) &= \text{rank}\left(\begin{bmatrix} s\mathbf{I} - S_{j,1}A_{jj}^{art} & \mathbf{0} \\ \star & s\mathbf{I} - S_{j,2}A_{jj} \\ \mathbf{I} & \mathbf{0} \\ C_j & C_j \end{bmatrix}\right) \\ &= n_j + \text{rank}\left(\begin{bmatrix} s\mathbf{I} - S_{j,2}A_{jj} \\ C_j \end{bmatrix}\right), \end{aligned}$$

which, given detectability of the pair (C_j, S_jA_{jj}) by hypothesis, is equal to $2n_j, \forall s \in \mathbb{C}^+$, with $S_{j,2} = S_j$.
The second part of the proposition holds, as $\text{rank}(\mathbf{C}_j) = n_j + \text{rank}(C_j) > \text{rank}(\mathbf{E}_{j,1}) + \text{rank}(\mathbf{E}_{j,2})$, given $\text{rank}(\mathbf{E}_{j,1}) + \text{rank}(\mathbf{E}_{j,2}) = \text{rank}(\bar{E}_j)$ by construction and $\text{rank}(C_j) = \text{rank}(\bar{E}_j)$ by hypothesis. ■

Remark 4.4.2. *In the case of DCmGs, as can be seen from the definition of the system*

matrices in Section 4.9.1, $\text{rank}(\bar{E}_j) = \text{rank}(C_j) = n_j$*. As such it is not possible to design a UIO capable of detecting attacks and it is necessary to introduce the augmented state described above. Moreover, a good choice for the artificial state would be* $x^{art}_{[j]} \triangleq x^{avg}_{[j]}$ *(i.e. the state* $x_{[i]}$ *in* (4.1) *obtained by setting* $u_{[i]} = u^{avg}_{[i]} \triangleq [V^{avg}_{ti}, \Delta V_i]$*).*

In the remainder of this chapter, we will consider that the observers in $\mathcal{O}^{UIO}_{i,j}$ are defined as in (4.8)-(4.9), with system matrices taken from augmented dynamics in (4.11). Furthermore, to stress the use of the augmented measurements $\mathbf{y}^c_{[j,i]}$, bold symbols $\mathbf{z}_{[j,i]}$, $\hat{\mathbf{x}}_{[j,i]}$ and $\hat{\mathbf{y}}_{[j,i]}$ will be used to denote the observer's state, the augmented state, and output estimates, respectively.

Lemma 4.4.3. *If matrix* $A \in \mathbb{R}^{n\times n}$ *is Hurwitz stable, there exists a positive scalar* $\lambda > 0$*, and a matrix* $\Lambda \geq \mathbf{I}$ *such that*

$$\left|e^{At}\right| \leq e^{-\lambda t}\Lambda \tag{4.15}$$

holds for all $t \geq 0$*.*

Proof. The proof can be found in Section 4.9.3. ■

Given the appropriate design of filter matrices (4.9), the estimation error $\epsilon_{[j,i]} \triangleq \mathbf{x}_{[j]} - \hat{\mathbf{x}}_{[j,i]}$ is stable, and it is therefore possible to design a time-varying threshold $\bar{r}_{[j,i]}$ capable of bounding the UIO's residual error defined as output estimation error $r_{[j,i]} \triangleq \mathbf{y}^c_{[j,i]} - \hat{\mathbf{y}}_{[j,i]}$:

$$\begin{aligned}\bar{r}_{[j,i]}(t) \triangleq &\mathbf{C}_j e^{-\sigma_j t}\Sigma_j \left[\bar{\epsilon}_{[j,i]}(0) + |H_j|\,\bar{\boldsymbol{\rho}}_{[j]}\right] + |Z_j|\,\bar{\boldsymbol{\rho}}_{[j]} \\ &+ \mathbf{C}_j \int_0^t e^{-\sigma_j(t-\tau)}\Sigma_j \left[|S_j|\,\bar{\tilde{\mathbf{w}}}_{[j]} + \left|\widehat{K}_j\right|\bar{\boldsymbol{\rho}}_{[j]}\right] d\tau,\end{aligned} \tag{4.16}$$

where $Z_j \triangleq (\mathbf{I} - \mathbf{C}_j H_j)$ and $\mathbf{C}_j \geq \mathbf{0}$ is supposed without loss of generality. As F_j is Hurwitz stable, a scalar $\sigma_j > 0$ and a matrix $\Sigma_j \geq \mathbf{I}$ can be found as in Lemma 4.4.3 for $|e^{F_j t}|$. The following proposition guarantees that $\bar{r}_{[j,i]}$ in (4.16) is indeed an upper bound to the corresponding residual.

Proposition 4.4.1. *In the absence of an attack, given* F_j *Hurwitz stable by design and Assumption 4.2.1,* $\bar{r}_{[j,i]}(t)$ *in* (4.16) *is such that the inequality*

$$|r_{[j,i]}(t)| \leq \bar{r}_{[j,i]}(t) \tag{4.17}$$

holds for all $t < T^{j,i}_a$*,* $\forall j \in \mathcal{N}_i$*.*

Proof. Given the definition of the UIO matrices, it is possible to derive the dynamics of the estimation error $\epsilon_{[j,i]}(t)$ as

$$\dot{\epsilon}_{[j,i]}(t) = \dot{\mathbf{x}}_{[j]}(t) - \dot{\hat{\mathbf{x}}}_{[j,i]}(t) = F_j\epsilon_{[j,i]}(t) + S_j\tilde{\mathbf{w}}_{[j]}(t) - H_j\dot{\boldsymbol{\rho}}_{[j]}(t) - \widetilde{K}_j\boldsymbol{\rho}_{[j]}(t), \tag{4.18}$$

the solution of which, exploiting integration by parts, is

$$\begin{aligned}\epsilon_{[j,i]}(t) =& e^{F_j t}\left[\epsilon_{[j,i]}(0) + H_j \boldsymbol{\rho}_{[j]}(0)\right] - H_j \boldsymbol{\rho}_{[j]}(t) \\ &+ \int_0^t e^{F_j(t-\tau)}\left[S_j \tilde{\mathbf{w}}_{[j]}(\tau) - \widehat{K}_j \boldsymbol{\rho}_{[j]}(\tau)\right] d\tau.\end{aligned} \tag{4.19}$$

Given that $r_{[j,i]}(t) = \mathbf{C}_j \epsilon_{[j,i]}(t) + \boldsymbol{\rho}_{[j]}(t)$ in nominal conditions, the solution of residual $r_{[j,i]}(t)$ is

$$\begin{aligned}r_{[j,i]}(t) =& \mathbf{C}_j e^{F_j t}\left[\epsilon_{[j,i]}(0) + H_j \boldsymbol{\rho}_{[j]}(0)\right] + Z_j \boldsymbol{\rho}_{[j]}(t) \\ &+ \mathbf{C}_j \int_0^t e^{F_j(t-\tau)}\left[S_j \tilde{\mathbf{w}}_{[j]}(\tau) - \widehat{K}_j \boldsymbol{\rho}_{[j]}(\tau)\right] d\tau.\end{aligned} \tag{4.20}$$

By use of triangle inequality, bounds in Assumption 4.2.1, and Lemma 4.4.3, it is possible to bound the estimation error with

$$\begin{aligned}\bar{\epsilon}_{[j,i]}(t) \triangleq& e^{-\sigma_j t}\Sigma_j\left[\bar{\epsilon}_{[j,i]}(0) + |H_j|\,\bar{\boldsymbol{\rho}}_{[j]}\right] + |H_j|\,\bar{\boldsymbol{\rho}}_{[j]} \\ &+ \int_0^t e^{-\sigma_j(t-\tau)}\Sigma_j\left[|S_j|\,\bar{\tilde{\mathbf{w}}}_{[j]} + \left|\widehat{K}_j\right|\bar{\boldsymbol{\rho}}_{[j]}\right] d\tau,\end{aligned} \tag{4.21}$$

which will converge to a constant for $t \to \infty$, as F_j is Hurtwitz stable. Similarly, the threshold $\bar{r}_{[j,i]}(t)$ in (4.16) is such that inequality (4.17) is guaranteed to hold when the communication link between DGUs j and i is not under attack, i.e. $t < T_a^{j,i}$, thus proving the proposition. ■

Whenever inequality (4.5a) is violated, the monitoring module $\mathcal{D}_i$ detects the presence of an attack on the communication link between $\mathcal{S}_j$ and $\mathcal{S}_i$, thus isolating it. In order to perform detection using the UIO-based layer, $\mathcal{D}_i$ requires information *offline* to design the bank of UIOs, and information *online* to perform the updates to the estimate and to compute the residual. These requirements are found in Table 4.1.

4.4.2 Detectability properties of $\mathcal{O}_{j,i}^{UIO}$

We define a *detectable attack* as an attack function that is guaranteed to trigger the monitor $\mathcal{D}_i$ by some finite time $T_d \geq \check{T}_a^i$. In this and the following subsections, we will analyze the properties of the UIO-based detection module of $\mathcal{D}_i$ while under attack, i.e., for $t \geq \check{T}_a^i$. Note that, given that each UIO evaluates the security of a single communication line, we consider a single attack starting at $T_a^{j,i}$. Hence, let us define $T_a \triangleq T_a^{j,i}$ for clarity of exposition.

Once an attack is active on a communication link, i.e. for $t \geq T_a$, the residual error of

$\mathcal{O}_{j,i}^{UIO}$ can be expressed as

$$r_{[j,i]}(t) = r_{[j,i]}^{h}(t) + r_{[j,i]}^{a}(t) \tag{4.22}$$

where $r_{[j,i]}^{h}(t)$ is the same as the residual in nominal conditions defined in (4.20), and $r_{[j,i]}^{a}(t) \triangleq \mathbf{C}_j \epsilon_{[j,i]}^{a}(t) + \phi_{j,i}(t)$, with

$$\epsilon_{[j,i]}^{a}(t) \triangleq -H_j \boldsymbol{\phi}_{j,i}(t) + e^{F_j(t-T_a)} H_j \boldsymbol{\phi}_{j,i}(T_a) - \int_{T_a}^{t} e^{F_j(t-\tau)} \widehat{K}_j \boldsymbol{\phi}_{j,i}(\tau) d\tau. \tag{4.23}$$

The class of attacks that are guaranteed to be detected can therefore be expressed in the following proposition:

Proposition 4.4.2. *If attack function $\boldsymbol{\phi}_{j,i}(t)$ is such that, at any time $t \geq T_a$,*

$$\left| r_{[j,i]}^{a}(t) \right| > 2\bar{r}_{[j,i]}(t) \tag{4.24}$$

holds for any component, then detector $\mathcal{D}_i$ operating in accordance with Algorithm 1 will detect the attack, thanks to the UIO observer $\mathcal{O}_{j,i}^{UIO}$.

Proof. By using the triangle inequality, Proposition 4.4.1, and exploiting the decomposition in (4.22), one has

$$|r_{[j,i]}(t)| \geq \left| r_{[j,i]}^{a}(t) \right| - \left| r_{[j,i]}^{h}(t) \right| \geq \left| r_{[j,i]}^{a}(t) \right| - \bar{r}_{[j,i]}(t) \tag{4.25}$$

where we used the fact that $\left| r_{[j,i]}^{h}(t) \right|$ in (4.20) is upper bounded by $\bar{r}_{[j,i]}(t)$. For guaranteeing detection through violation of (4.5a), it is sufficient that the attack $\boldsymbol{\phi}_{j,i}(t)$ is such that

$$\left| r_{[j,i]}^{a}(t) \right| - \bar{r}_{[j,i]}(t) > \bar{r}_{[j,i]}(t) \tag{4.26}$$

is satisfied for some time $t > T_a$. As (4.24) is a sufficient condition for (4.26), this concludes the proof. ■

4.4.3 Classes of attacks stealthy to $\mathcal{O}_{j,i}^{UIO}$

Having evaluated the class of attacks which are guaranteed to be detected by $\mathcal{O}_{i}^{UIO}$ in $\mathcal{D}_i$, we now analyze the UIO-based module's *weakness*, i.e. those attacks which are *stealthy* to it.

Definition 4.4.1 (Stealthy Attacks)**.** *An attack is stealthy to $\mathcal{D}_i$ if it is guaranteed not to be detected at any time $t \geq T_a$.*

It is worth recalling that, as described in Remark 4.2.2, the attack only influences the output communicated between controllers, while not attacking any subsystem's dynamics

directly. Hence, the stealthiness properties differ with respect to those available in literature [TPSJ12, PDB13]. Again we exploit the decomposition of $r_{[j,i]}(t)$ into healthy and attacked components to analyze stealthiness. In order to give a complete overview of the stealthy attacks for this module, we will separately treat three classes of attacks defined in [TPSJ12]: false data injection attack; replay attack; covert attack.

False Data Injection Attacks: This class of attacks does not require any *disclosure* capabilities (i.e. the malicious agent does not need to eavesdrop the information sent through the communication link). By injecting an attack of this type, it is possible for the attacker to alter the equilibrium of the network as a whole. The influence of this type of attack on the residual $r_{[j,i]}(t)$ can be characterized as in (4.22).

Proposition 4.4.3. *If attacks $\boldsymbol{\phi}_{j,i}(t)$ are such that, for all $t \geq T_a$,*

$$\left| r^a_{[j,i]}(t) \right| = 0, \tag{4.27}$$

then they will be stealthy to the UIO-based module in $\mathcal{D}_i$.

Proof. Given that $\left| r^h_{[j,i]}(t) \right|$ is bounded by $\bar{r}_{[j,i]}(t)$ by construction, and exploiting the triangle inequality, it holds that:

$$\left| r_{[j,i]}(t) \right| = \left| r^h_{[j,i]}(t) + r^a_{[j,i]}(t) \right| \leq \bar{r}_{[j,i]}(t) + \left| r^a_{[j,i]}(t) \right|. \tag{4.28}$$

Given that, for the attack to be undetected, inequality (4.5a) must always hold, it is sufficient that $\boldsymbol{\phi}_{j,i}(t)$ is designed to satisfy $\left| r^a_{[j,i]}(t) \right| = 0, \forall t \geq T_a$ for it to be stealthy. ■

Remark 4.4.3. *Recalling that $r^a_{[j,i]} = \mathbf{C}_j \epsilon^a_{[j,i]} + \phi_{j,i}$, it is sufficient for attacks to be such that*

$$\boldsymbol{\phi}_{j,i}(T_a) = \mathbf{0}, \quad \boldsymbol{\phi}_{j,i}(t) \in \ker \left(\begin{bmatrix} \widehat{K}_j \\ Z_j \end{bmatrix} \right), \ t > T_a \tag{4.29}$$

for condition (4.27) *to be satisfied for all $t \geq T_a$.*

Replay Attacks: With an attacker capable of violating the integrity of the communication network (and thus of eavesdropping on the transmitted measurements) from some time $t = T_0$, a replay attack requires no knowledge of the system's model. Instead, it modifies the transmitted information by *replaying* stored old data, substituting it for the current data[2]. In particular, the attacker stores the output $\mathbf{y}_{[j]}(t)$ from time $T_a - T$ to T_a, where T is the replay buffer size. Then, at any time $t \geq T_a$ the attack is defined as

$$\boldsymbol{\phi}_{j,i}(t) = -\mathbf{y}_{[j]}(t) + \mathbf{y}_{[j]}(t - nT),$$

[2] A preliminary analysis of the stealthiness of replay attacks in $\mathcal{O}^{UIO}_{j,i}$ was presented in [GTB+18].

where the positive integer n is chosen such that $t-nT \in [T_a-T, T_a)$. Hence communicated information (4.12) will be

$$\mathbf{y}^c_{[j,i]}(t) = \mathbf{y}_{[j]}(t-nT).$$

It has been shown that replay attacks may be undetectable to attack monitoring schemes [MWS15], as the replayed data has both the same statistical properties of the non-attacked data, and it evolves following correct dynamics.

Note that, although a replay attack does not require any knowledge of the subsystem dynamics, it is possible for the attacker to disguise any changes to the operating conditions of a unit from its neighbors, thus altering the equilibrium of the LIMAS, or hiding faults.

Specifically, in our scenario, the following condition can be given:

Lemma 4.4.4. *If a replay attack is such that*

$$\Sigma_j \left|\epsilon^r_{[j,i]}(T_a) + H_j \boldsymbol{\rho}_{[j]}(T_a-T)\right| \leq \bar{\epsilon}_{[j,i]}(T_a) - |H_j|\, \bar{\boldsymbol{\rho}}_{[j]}, \tag{4.30}$$

then detection test (4.5a) *will hold for all* $t \in [T_a, T_a+T)$*, where*

$$\epsilon^r_{[j,i]}(t) \triangleq \mathbf{x}_{[j]}(t-T) - \hat{\mathbf{x}}_{[j,i]}(t).$$

Proof. Given T_a and T, for time $t \in [T_a, T_a+T)$, the UIO estimation error residual takes the form

$$r_{[j,i]}(t) = \mathbf{y}^c_{[j,i]}(t) - \hat{\mathbf{y}}_{[j,i]}(t) = \mathbf{C}_j \epsilon^r_{[j,i]}(t) + \boldsymbol{\rho}_{[j]}(t-T).$$

The dynamics of state estimation error $\epsilon^r_{[j,i]}(t)$ under replay attack can be derived from equations (4.11) and (4.8):

$$\dot{\epsilon}^r_{[j,i]}(t) = F_j \epsilon^r_{[j,i]}(t) + S_j \tilde{\mathbf{w}}_{[j]}(t-T) - \widetilde{K}_j \boldsymbol{\rho}_{[j]}(t-T) - H_j \dot{\boldsymbol{\rho}}_{[j]}(t-T) \tag{4.31}$$

the solution of which is

$$\begin{aligned}\epsilon^r_{[j,i]}(t) =& e^{F_j(t-T_a)}\left(\epsilon^r_{[j,i]}(T_a) + H_j \boldsymbol{\rho}_{[j]}(T_a-T)\right) \\ &- H_j \boldsymbol{\rho}_{[j]}(t-T) + \int_{T_a}^{t} e^{F_j(t-\tau)}\left[S_j \tilde{\mathbf{w}}_{[j]}(\tau-T) - \widehat{K}_j \boldsymbol{\rho}_{[j]}(\tau-T)\right] d\tau.\end{aligned} \tag{4.32}$$

Estimation error bound $\bar{\epsilon}_{[j,i]}(t)$ defined in (4.21) for time $t > T_a$ can be rewritten as

$$\begin{aligned}\bar{\epsilon}_{[j,i]}(t) =& e^{-\sigma_j(t-T_a)}\left[\bar{\epsilon}_{[j,i]}(T_a) - |H_j|\, \bar{\boldsymbol{\rho}}_{[j]}\right] + |H_j|\, \bar{\boldsymbol{\rho}}_{[j]} \\ &+ \int_{T_a}^{t} e^{-\sigma_j(t-\tau)} \Sigma_j \left[|S_j|\, \bar{\tilde{\mathbf{w}}}_{[j]} + \left|\widehat{K}_j\right| \bar{\boldsymbol{\rho}}_{[j]}\right] d\tau.\end{aligned} \tag{4.33}$$

In order to guarantee that $|r_{[j,i]}(t)| \leq \bar{r}_{[j,i]}(t)$, $\forall t \in [T_a, T_a+T)$, implying stealthiness, it

is sufficient that $|\epsilon^r_{[j,i]}(t)| \leq \bar{\epsilon}_{[j,i]}(t)$. By comparison, all terms in (4.32) except

$$e^{F_j(t-T_a)}\left(\epsilon^r_{[j,i]}(T_a) + H_j\boldsymbol{\rho}_{[j]}(T_a - T)\right)$$

are guaranteed to be bounded by their corresponding terms in (4.33), given the definition of the noise bounds in (4.2). Thus, as the following inequality holds:

$$\left|e^{F_j(t-T_a)}\left(\epsilon^r_{[j,i]}(T_a) + H_j\boldsymbol{\rho}_{[j]}(T_a - T)\right)\right| \leq e^{-\sigma_j(t-T_a)}\Sigma_j\left|\epsilon^r_{[j,i]}(T_a) + H_j\boldsymbol{\rho}_{[j]}(T_a - T)\right|,$$

it is sufficient for condition (4.30) to hold for stealthiness to be achieved, which proves the Lemma holds for $t \in (T_a, T_a + T)$.

To prove sufficiency of (4.30) for $|\epsilon^r_{[j,i]}(T_a)| \leq \bar{\epsilon}_{[j,i]}(T_a)$, we use the property of $\Sigma_j \geq \mathbf{I}$ and the inverse triangle inequality:

$$\Sigma_j|\epsilon^r_{[j,i]}(T_a)+H_j\boldsymbol{\rho}_{[j]}(T_a-T)| \geq |\epsilon^r_{[j,i]}(T_a)+H_j\boldsymbol{\rho}_{[j]}(T_a-T)| \geq \left|\epsilon^r_{[j,i]}(T_a)\right|-|H_j|\bar{\boldsymbol{\rho}}_{[j]}. \quad (4.34)$$

Hence, if (4.30) is satisfied, the following holds:

$$\left|\epsilon^r_{[j,i]}(T_a)\right| - |H_j|\bar{\boldsymbol{\rho}}_{[j]} \leq \bar{\epsilon}_{[j,i]}(T_a) - |H_j|\,\bar{\boldsymbol{\rho}}_{[j]}, \quad (4.35)$$

and therefore detection will not occur at time $t = T_a$.

Note finally that, given definition of $\bar{\epsilon}_{[j,i]}(t)$ in (4.21), the right hand side of (4.30) is guaranteed to be greater than zero. Hence, (4.30) is well defined. This completes the proof. ■

In the next result, we generalize Lemma 4.4.4 to find a condition on $\epsilon^r_{[j,i]}(T_a + kT)$, for any $k \in \mathbb{N}$ such that (4.5a) will hold for all $t \in [T_a + kT, T_a + (k+1)T)$.

Proposition 4.4.4. *If a replay attack is such that*

$$\Sigma_j\left|\epsilon^r_{[j,i]}(T_a) + M_{j,i}\right| \leq \bar{\epsilon}_{[j,i]}(T_a) - \Delta\bar{\epsilon}_{[j,i]}(T_a) - (\Sigma_j + \mathbf{I})|H_j|\bar{\boldsymbol{\rho}}_{[j]} \quad (4.36)$$

holds with $M_{j,i},\ \Delta\bar{\epsilon}_{[j,i]}(T_a) \geq \mathbf{0}$ *appropriately defined vectors, then detection test* (4.5a) *will hold for all* $t \geq T_a$.

Proof. The proof can be found in Section 4.9.4. ■

Remark 4.4.4. *Conditions in Lemma 4.4.4 and Proposition 4.4.4 depend on quantities unknown to the attacker, so it is not guaranteed that the attack will be able to satisfy them. However, as long as the attacker chooses* T_a *and* T *appropriately (i.e. such that* $\mathbf{y}_{[j]}(T_a) \approx \mathbf{y}_{[j]}(T_a - T)$*), it is likely (although not guaranteed) that* (4.5a) *will hold for all* $t \geq T_a$.

We note that a preliminary study of replay attacks on the UIO-based module has been presented and a novel *watermarking* scheme has been developed for their detection in [GTB+18]. This scheme consists of adding a small noise signal (called a *watermark*, named after a similar technique in the multimedia industry) on the communicated outputs $\mathbf{y}^c_{[j,i]}$, so as to increase the magnitude of the term $\epsilon^r_{[j,i]}(T_a)$ on the left-hand side of (4.36). This increase, in turn, causes the residuals to exceed the corresponding thresholds and enables detection. The contents of this paper are rather an extension to the detection scheme developed here, and are omitted in this thesis for clarity of exposition.

Covert Attacks: To perform a *covert attack*, the malicious agent must not only be able to disrupt the communication network, and be able to eavesdrop the information being transmitted, but must also have knowledge of the dynamics of $\mathcal{S}_j$. It is, therefore, capable of *simulating* the behavior of the subsystem and feeding this information to the control and monitoring architecture of $\mathcal{S}_i$. Specifically, a covert attack can be modeled as follows:

$$\boldsymbol{\phi}_{j,i}(t) = -\mathbf{y}_{[j]}(t) + \mathbf{y}^a_{[j]}(t), \tag{4.37}$$

where $\mathbf{y}^a_{[j]}(t)$ is the output of a simulated system with the following dynamics and initial condition:

$$\begin{aligned} \dot{\mathbf{x}}^a_{[j]}(t) &= \mathbf{A}_{jj}\mathbf{x}^a_{[j]}(t) + \mathbf{E}_j\mathbf{d}^a_{[j]}(t), \\ \mathbf{y}^a_{[j]}(t) &= \mathbf{C}_j\mathbf{x}^a_{[j]}, \\ \mathbf{x}^a_{[j]}(T_a) &= \mathbf{C}^\dagger_j\mathbf{y}_{[j]}(T_a), \end{aligned} \tag{4.38}$$

where $\mathbf{d}^a_{[j]}(t)$ is freely chosen by the attacker to substitute $\mathbf{d}_{[i]}$ in (4.11). Under this scenario, $\mathbf{y}^c_{[j,i]}(t) = \mathbf{y}^a_{[j]}(t)$.

Remark 4.4.5. *Note that, differently to the covert attack described in [TPSJ12, Smi15], we do not consider the case in which the attacker may alter the control input signals of $\mathcal{S}_j$, but only the information transmitted to $\mathcal{S}_i$, consistently with Remark 4.2.2. While this limits the scope of the attacker, through modification of the unknown input vector $\mathbf{d}^a_{[j]}(t) \neq \mathbf{d}_{[j]}(t)$, it is possible for it to change the operating condition of $\mathcal{S}_j$ as seen by $\mathcal{S}_i$, thus modifying the behavior of the LIMAS as a whole.*

Remark 4.4.6. *For* $\operatorname{rank}(\mathbf{C}_j) < 2n_j$*, it might not be possible to find a* $\mathbf{C}^\dagger_j$ *such that* $\mathbf{C}^\dagger_j\mathbf{C}_j = \mathbf{I}$*. This means that the attacker might not be able to choose an initial condition* $\mathbf{x}^a_{[j]}(T_a)$ *that is sufficiently close to* $\mathbf{x}_{[j]}(T_a)$*. Given observability of* $(\mathbf{C}_j, \mathbf{A}_{jj})$*, the effect of this error will be observable from* $\mathbf{y}^a_{[j]}(t)$*,* $t > T_a$*, and it may thus be possible for* $\mathcal{D}_i$ *to detect the attack. Here, we consider the worst-case scenario in which a* $\mathbf{C}^\dagger_j$ *verifying* $\mathbf{C}^\dagger_j\mathbf{C}_j = \mathbf{I}$ *exists. Then, the attacker's initial state* $\mathbf{x}^a_{[j]}(T_a)$ *is within a small neighborhood of the real state* $\mathbf{x}_{[j]}(T_a)$*, i.e.,* $\Delta\mathbf{x}^a_{[j]}(T_a) \triangleq \mathbf{x}_{[j]}(T_a) - \mathbf{x}^a_{[j]}(T_a) = \mathbf{C}^\dagger_j\boldsymbol{\rho}_{[j]}(T_a)$*.*

Proposition 4.4.5. *If an attack as in* (4.37) *is carried out, in which* $\mathbf{x}^a_{[j]}(t)$ *is the state*

of LTI system (4.38)*, and if* $\boldsymbol{\rho}_{[j]}$ *is such that*

$$\mathbf{C}_j \Sigma_j |(\mathbf{C}_j^\dagger - H_j)\boldsymbol{\rho}_{[j]}(T_a)| \leq |Z_j| \bar{\boldsymbol{\rho}}_{[j]}, \tag{4.39}$$

inequality (4.5a) *will hold for all* $t \geq T_a$*, and the attack will be stealthy.*

Proof. Start by noticing that for time $t = T_a$, the residual is

$$r_{[j,i]}(T_a) = \mathbf{C}_j \mathbf{x}^a_{[j]}(T_a) - \hat{\mathbf{y}}_{[j,i]}(T_a) = \mathbf{y}_{[j]}(T_a) - \hat{\mathbf{y}}_{[j,i]}(T_a), \tag{4.40}$$

and therefore condition (4.5a) will hold, given Proposition 4.4.1. For $t \geq T_a$, define $\varepsilon^a_{[j,i]}(t) \triangleq \mathbf{x}^a_{[j]}(t) - \hat{\mathbf{x}}_{[j,i]}(t)$ and note that $\varepsilon^a_{[j,i]}(T_a) = \epsilon_{[j,i]}(T_a) + \Delta\mathbf{x}^a_{[j]}(T_a) = \epsilon_{[j,i]}(T_a) + \mathbf{C}_j^\dagger \boldsymbol{\rho}_{[j]}(T_a)$. The dynamics of this error term can therefore be written as

$$\dot{\varepsilon}^a_{[j,i]}(t) = F_j \varepsilon^a_{[j,i]}(t) + S_j \mathbf{E}_j \mathbf{d}^a_{[j]}(t) = F_j \varepsilon^a_{[j,i]}(t),$$

as $S_j \mathbf{E}_j = \mathbf{0}$ by design (4.9a). Hence,

$$\begin{aligned} r_{[j,i]}(t) = \mathbf{C}_j e^{F_j(t-T_a)} \varepsilon^a_{[j,i]}(T_a) =& \mathbf{C}_j e^{F_j(t-T_a)} \left(\epsilon_{[j,i]}(T_a) + \mathbf{C}_j^\dagger \boldsymbol{\rho}_{[j]}(T_a)\right) \\ =& \mathbf{C}_j e^{F_j t} \left[\epsilon_{[j,i]}(0) + H_j \boldsymbol{\rho}_{[j]}(0)\right] \\ &+ \mathbf{C}_j e^{F_j(t-T_a)} \left(\mathbf{C}_j^\dagger - H_j\right) \boldsymbol{\rho}_{[j]}(T_a) \\ &+ \mathbf{C}_j \int_0^{T_a} e^{F_j(t-\tau)} \left[S_j \tilde{\mathbf{w}}_{[j]}(\tau) - \widehat{K}_j \boldsymbol{\rho}_{[j]}(\tau)\right] d\tau. \end{aligned} \tag{4.41}$$

Comparing (4.41) to the definition of the residual in healthy conditions (4.20), we see that the only term not guaranteed to be bounded by the corresponding terms in (4.16) is $\mathbf{C}_j e^{F_j(t-T_a)} \left(\mathbf{C}_j^\dagger - H_j\right) \boldsymbol{\rho}_{[j]}(T_a)$. Hence, to guarantee that (4.5a) holds, we must demonstrate that

$$\begin{aligned} \left|\mathbf{C}_j e^{F_j(t-T_a)} \left(\mathbf{C}_j^\dagger - H_j\right) \boldsymbol{\rho}_{[j]}(T_a)\right| \leq& |Z_j| \, \bar{\boldsymbol{\rho}}_{[j]} \\ &+ \mathbf{C}_j \int_{T_a}^t e^{-\sigma_j(t-\tau)} \Sigma_j \left[|S_j| \, \bar{\tilde{\mathbf{w}}}_{[j]} + \left|\widehat{K}_j\right| \bar{\boldsymbol{\rho}}_{[j]}\right]. \end{aligned} \tag{4.42}$$

Recalling that $|e^{F_j t}| \leq \Sigma_j e^{\sigma_j t}$, it is sufficient for condition (4.39) to hold for (4.42) to be satisfied, and therefore detection condition (4.5a) will hold for all $t \geq T_a$. ■

In this section, we have presented $\mathcal{O}^{UIO}_{j,i}$, as well as its detectability properties. It is worth noting that this detection module does not rely on the physical interconnections between subsystems, but only on the communicated values received from its neighbors $\mathcal{S}_j$.

4.5 Distributed estimation of local states

4.5.1 Design of the detection module

The second module of the attack detection monitor $\mathcal{D}_i$ is based on a distributed Luenberger observer $\mathcal{O}_i^{Luen}$. The following assumption is made in this section, motivated by the application to mGs (see Section 4.2.4):

Assumption 4.5.1. *Matrix C_i is invertible for all $\mathcal{S}_i$.*

We will give some indications as how this assumption could be removed in Remark 4.5.2. Note that, from Assumption 4.5.1, it follows that $\mathbf{C}_j$ is also non-singular. The dynamics of $\mathcal{O}_i^{Luen}$ can then be formulated as

$$\begin{aligned} \dot{\hat{x}}_{[i]} &= A_{ii}\hat{x}_{[i]} + \hat{\xi}_{[i]} + B_i u_{[i]} + M_i d_{[i]} - L_i \left(y_{[i]} - \hat{y}_{[i]} \right), \\ \hat{y}_{[i]} &= C_i \hat{x}_{[i]}, \end{aligned} \tag{4.43}$$

where L_i is designed such that $A_{Li} = (A_{ii} + L_i C_i)$ is Hurwitz stable, guaranteeing estimation error stability. The effect of the physical interconnection with neighbors in $\mathcal{N}_i$ is approximated as

$$\hat{\xi}_{[i]} \triangleq \sum_{j \in \mathcal{N}_i} A_{ij} \hat{x}_{[j,i]} = \sum_{j \in \mathcal{N}_i} A_{ij} \Gamma \mathbf{C}_j^{-1} \mathbf{y}_{[j,i]}^c,$$

where $\Gamma \mathbf{C}_j^{-1} \mathbf{y}_{[j,i]}^c$ is used as an estimate of $x_{[j]}$, with $\Gamma \triangleq \begin{bmatrix} \mathbf{I} & \mathbf{I} \end{bmatrix}$, recalling (4.10).

To verify whether hypothesis $\mathcal{H}_i^0(t)$ in Problem 1 is valid or not, $\mathcal{D}_i$ computes the residual error

$$r_{[i]}(t) \triangleq y_{[i]}(t) - \hat{y}_{[i]}(t), \tag{4.44}$$

and compares it with an appropriately defined time-varying threshold $\bar{r}_{[i]}(t)$ given by

$$\bar{r}_{[i]}(t) \triangleq C_i e^{-\lambda_i t} \Lambda_i \bar{\epsilon}_{[i]}(0) + C_i \int_0^t e^{-\lambda_i (t-\tau)} \Lambda_i \bar{\eta}_{[i]} d\tau + \bar{\rho}_{[i]}, \tag{4.45}$$

where $\lambda_i > 0$ and $\Lambda_i \geq \mathbf{I}$ are such that $|e^{A_{Li} t}| \leq e^{-\lambda_i t} \Lambda_i$ holds, thanks to Lemma 4.4.3; $\bar{\epsilon}_{[i]}(0)$ is an appropriately defined bound on the initial value of the estimation error $\epsilon_{[i]}(t) \triangleq x_{[i]}(t) - \hat{x}_{[i]}(t)$; and $\bar{\eta}_{[i]} \triangleq \bar{w}_{[i]} + |L_i| \bar{\rho}_{[i]} + \sum_{j \in \mathcal{N}_i} |A_{ij}| \Gamma \mathbf{C}_j^{-1} \bar{\boldsymbol{\rho}}_{[j]}$. The following proposition holds:

Proposition 4.5.1. *Given Assumption 4.2.1 and that A_{Li} is Hurwitz stable by design, the inequality*

$$|r_{[i]}(t)| \leq \bar{r}_{[i]}(t) \tag{4.46}$$

is guaranteed to be satisfied for all $t < \check{T}_a^i$, for residual $r_{[i]}$ in (4.44) and threshold $\bar{r}_{[i]}$ computed by $\mathcal{D}_i$ as in (4.45).

Proof. The residual error can be rewritten as $r_{[i]} = C_i\epsilon_{[i]} + \rho_{[i]}$. The dynamics of $\epsilon_{[i]}(t)$ can be derived from (4.1) and (4.43):

$$\dot{\epsilon}_{[i]}(t) = A_{Li}\epsilon_{[i]}(t) + \eta_{[i]}(t) \tag{4.47}$$

where $\eta_{[i]} = -\sum_{j\in\mathcal{N}_i} A_{ij}\Gamma\mathbf{C}_j^{-1}\boldsymbol{\rho}_{[j]} + w_{[i]} - L_i\rho_{[i]}$. The following explicit solution can be found:

$$\epsilon_{[i]}(t) = e^{A_{Li}t}\epsilon_{[i]}(0) + \int_0^t e^{A_{Li}(t-\tau)}\eta_{[i]}(\tau)d\tau. \tag{4.48}$$

Since A_{Li} is Hurwitz stable by design of L_i for all $i \in \mathcal{V}$, estimation error $\epsilon_{[i]}(t)$ is BIBO stable, and, given Assumption 4.2.1, it can be bounded by a time-varying quantity $\bar{\epsilon}_{[i]}(t)$. Using the triangle inequality and bounds defined in (4.2) as well as Lemma 4.4.3, a bound on the estimation error can be computed:

$$\bar{\epsilon}_{[i]}(t) \triangleq e^{-\lambda_i t}\Lambda_i\bar{\epsilon}_{[i]}(0) + \int_0^t e^{-\lambda_i(t-\tau)}\Lambda_i\bar{\eta}_{[i]}d\tau, \tag{4.49}$$

where $\lambda_i > 0$ and Λ_i are found following Lemma 4.4.3, and $\bar{\epsilon}_{[i]}(0)$ is appropriately defined. The threshold in (4.45) on the residual can similarly be computed by using the triangle inequality. ■

The information required by $\mathcal{D}_i$ to compute the estimate $\hat{x}_{[i]}(t)$ and threshold $\bar{r}_{[i]}(t)$ is provided in Table 4.1.

4.5.2 Detectability properties of $\mathcal{O}_i^{Luen}$

In this subsection, we will analyze the properties of the Luenberger-observer-based detection module of $\mathcal{D}_i$ while under attack, i.e. for $t \geq \check{T}_a^i$. Once an attack is active on a communication link, it will affect both the computation of the networked control $u_{[i]}(t)$ and of the variable $\hat{\xi}_{[i]}(t)$ in (4.43), which will become

$$\hat{\xi}_{[i]}(t) = \sum_{j\in\mathcal{N}_i} A_{ij}\Gamma\mathbf{C}_j^{-1}\left(\mathbf{C}_j\mathbf{x}_{[j]}(t) + \boldsymbol{\rho}_{[j]}(t)\right) + \sum_{j\in\widehat{\mathcal{N}}_i(t)} A_{ij}\Gamma\mathbf{C}_j^{-1}\boldsymbol{\phi}_{j,i}(t)\,,\ \forall t \geq \check{T}_a^i, \tag{4.50}$$

where $\widehat{\mathcal{N}}_i(t) \triangleq \{j \in \mathcal{N}_i : t \geq T_a^{j,i}\} \subseteq \mathcal{N}_i$ is the set of neighbors whose transmissions to $\mathcal{S}_i$ have been attacked at time t. As the attack is additive with respect to the dynamics (4.43), it is possible to write the residual as

$$r_{[i]}(t) = r_{[i]}^h(t) + r_{[i]}^a(t), \tag{4.51}$$

where

$$r_{[i]}^h(t) \triangleq C_i e^{A_{Li}t}\epsilon_{[i]}(0) + C_i\int_0^t e^{A_{Li}(t-\tau)}\eta_{[i]}(\tau)d\tau + \rho_{[i]}(t) \tag{4.52}$$

is the *healthy* part of the residual, and is independent of $\check{T}_a^i$. Hence $\left|r_{[i]}^h(t)\right| \leq \bar{r}_{[i]}(t)$ will hold for all $t \geq 0$. Moreover,

$$r_{[i]}^a(t) \triangleq C_i \int_{\check{T}_a^i}^t e^{A_{Li}(t-\tau)} \sum_{j \in \widehat{\mathcal{N}}_i(t)} A_{ij} \Gamma \mathbf{C}_j^{-1} \boldsymbol{\phi}_{j,i}(\tau) d\tau, \tag{4.53}$$

for all $t \geq \check{T}_a^i$, is the part of the residual affected by the attack.

Proposition 4.5.2. *If attack function $\boldsymbol{\phi}_{j,i}(t) \in \mathbb{R}^{n_j+p_j}$ is such that at any time $t > \check{T}_a^i$*

$$\left|r_{[i]}^a(t)\right| > 2\bar{r}_{[i]}(t) \tag{4.54}$$

holds for any of its components, then detector $\mathcal{D}_i$ operating in accordance with Algorithm 1 will detect the attack at some finite time $T_d > \check{T}_a^i$ thanks to $\mathcal{O}_i^{Luen}$.

Proof. The proof follows that of Proposition 4.4.2. ■

Having evaluated the class of attacks which are guaranteed to be detected by $\mathcal{O}_i^{Luen}$ in $\mathcal{D}_i$, we now analyze the Luenberger-observer-based module's *weakness*, i.e. the class of attacks which are *stealthy* to it.

We again exploit the decomposition of the residual $r_{[i]}(t)$ into healthy and attacked components to analyze stealthiness.

Proposition 4.5.3. *If attacks $\boldsymbol{\phi}_{j,i}(t)$ are such that for all $t \geq \check{T}_a^i$*

$$\left|r_{[i]}^a(t)\right| = 0, \tag{4.55}$$

holds, then they will be stealthy to the Luenberger-observer-based module in $\mathcal{D}_i$.

Proof. The proof follows that of Proposition 4.4.3. ■

Remark 4.5.1. *For Proposition 4.5.3 to hold for all $t \geq \check{T}_a^i$, it is sufficient that $\boldsymbol{\Phi}_{[i]}(t) \triangleq \mathrm{col}(\boldsymbol{\phi}_{j,i}(t))$, $\forall j \in \widehat{\mathcal{N}}_i(t)$ satisfy*

$$\boldsymbol{\Phi}_{[i]}(t) \in \ker(\mathbb{A}_{ij}(t)), \tag{4.56}$$
$$\mathbb{A}_{ij}(t) \triangleq \left[A_{ij_1}\Gamma\mathbf{C}_{j_1}^{-1}, \ldots, A_{ij_{\widehat{N}_i(t)}}\Gamma\mathbf{C}_{j_{\widehat{N}_i(t)}}^{-1}\right],$$

where $\mathbb{A}_{ij}(t)$ collects physical coupling matrices of the neighbors whose communication has been attacked, and as such may be time-varying, with $\widehat{N}_i(t) \triangleq |\widehat{\mathcal{N}}_i(t)|$. This is revealing, as it shows the dependency of the detectability of $\mathcal{O}_i^{Luen}$ on the physical interconnections of $\mathcal{S}_i$ and its neighbors. Specifically, (4.56) *implies that to design an attack stealthy to $\mathcal{O}_i^{Luen}$ an attacker could either leverage knowledge of the structure of the interconnection*

between subystems, and therefore of a subset of the state $x_{[j]}$ that does not influence (4.1)*, or compensate its effect on the residual through multiple channels, depending on whether matrices $A_{ij}, j \in \mathcal{N}_i$ are singular.*

Remark 4.5.2. *As previously mentioned, the analysis in this section was performed considering an invertible C_j. In the case when it is singular, it is possible to exploit the estimation of the neighbors' states $\hat{x}_{[j,i]} \triangleq \Gamma\hat{\mathbf{x}}_{[j,i]}$. Propositions 4.5.1-4.5.3 can then be shown to hold by making appropriate changes to $\bar{r}_{[i]}$, $\epsilon_{[i]}$, and $r^a_{[i]}$ in* (4.45)*,* (4.47)*, and* (4.53)*, respectively. Specifically, while recalling that the estimation error of $\mathcal{O}^{UIO}_{j,i}$ can be decomposed in its healthy and attacked components, we change $\mathbf{C}_j^{-1}\bar{\rho}_{[j]}$ in definition of $\bar{\eta}_{[i]}$ to $\bar{\epsilon}_{[j,i]}$, $\mathbf{C}_j^{-1}\rho_{[j]}$ in $\eta_{[i]}$ to $\epsilon^h_{[j,i]}$, and $\mathbf{C}_j^{-1}\boldsymbol{\phi}_{j,i}$ to $\epsilon^a_{[j,i]}$. Hence, proofs of Propositions 4.5.1-4.5.3 follow.*
A significant difference implied by this alteration of $\mathcal{O}^{Luen}_{j,i}$ is that the two modules in $\mathcal{D}_i$ are directly coupled, and that attack vector $\boldsymbol{\phi}_{[j,i]}$ no longer directly affects (4.53)*, but rather affects it through $\epsilon^a_{[j,i]}$.*
In such a scenario, the Luenberger-observer-based detector will require from the UIO-based module, at all times $t \geq 0$, the state estimate $\hat{\mathbf{x}}_{[j,i]}(t)$ and the bound on its estimation error $\bar{\epsilon}_{[j,i]}(t)$. Thus, for Proposition 4.5.3 to hold it is sufficient for the attack vector to satisfy a condition similar to that in (4.29) *with Z_j replaced by H_j. Furthermore, an attack would satisfy* (4.55) *also if it were such that $\epsilon^a_{[j,i]}(t)$ lie within* $\ker(\mathbb{A}_{ij})$ *with $\mathbf{C}_{j_k}^{-1} = \mathbf{I}$ for all $t \geq T_a$. Both these conditions rely on knowledge of parameters of $\mathcal{O}^{UIO}_{[j,i]}$.*

4.6 Detectability analysis of $\mathcal{D}_i$

We will show that the combined use of the two modules in $\mathcal{D}_i$ has advantages in terms of detectability. In fact, it is sufficient for either conditions in Proposition 4.4.2 or 4.5.2 to be satisfied for an attack to be guaranteed to be detected. In this section, we will therefore focus on two specific cases:

1. the class of bias injection attacks stealthy to $\mathcal{D}_i$;
2. the detectability of a replay or covert attack.

For the first of the two cases, it is clear to see that for invertible C_j, to be stealthy to $\mathcal{D}_i$, it is sufficient that

$$\mathbf{\Phi}_{[i]}(t) \in \ker\left(\begin{bmatrix} \mathbb{Z}_j(t) \\ \widehat{\mathbb{K}}_j(t) \end{bmatrix}\right) \cap \ker\left(\mathbb{A}_{ij}(t)\right), \tag{4.57}$$

while also satisfying $\boldsymbol{\phi}_{j,i}(T^a_{[j,i]}) = \mathbf{0}$, where $\widehat{\mathbb{K}}_j \triangleq \operatorname{diag}(\widehat{K}_{j_1}, \ldots, \widehat{K}_{j_{\widehat{N}_i(t)}})$ and $\mathbb{Z}_j \triangleq \operatorname{diag}\left(Z_{j_1}, \ldots, Z_{j_{\widehat{N}_i(t)}}\right)$. In fact, if (4.57) holds, then conditions for both Propositions 4.4.3 and 4.5.3 will hold. This, in turn, implies that neither of the modules of $\mathcal{D}_i$ will detect the attack, which will therefore be stealthy.

Table 4.2: Values for interpretation of replay and covert attacks

	Replay Attacks	**Covert Attacks**
$\mathbf{x}^a_{[j]}(T_a)$	$\mathbf{x}_{[j]}(T_a - T)$	$\mathbf{C}_j^\dagger \mathbf{y}_{[j]}(T_a)$
$\mathbf{d}^a_{[j]}(t)$	$\mathbf{d}_{[j]}(t - nT)$	$\mathbf{d}^a_{[j]}(t)$
$\tilde{\mathbf{w}}^a_{[j]}(t)$	$\tilde{\mathbf{w}}_{[j]}(t - nT)$	$\mathbf{0}$
$\boldsymbol{\rho}^a_{[j]}(t)$	$\boldsymbol{\rho}_{[j]}(t - nT)$	$\mathbf{0}$

Remark 4.6.1. *For the case of singular C_j, we refer to Remark 4.5.2 for derivation of equivalent conditions.*

In the second case, while replay and covert attacks are stealthy to the UIO-based module of $\mathcal{D}_i$, they may be detected by the Luenberger-based one. In order to simplify the analysis of this scenario, let us note that both replay and covert attacks can be interpreted as the following attack function:

$$\boldsymbol{\phi}_{j,i}(t) = -\mathbf{y}_{[j]}(t) + \mathbf{y}^a_{[j]}(t), \tag{4.58}$$

where $\mathbf{y}^a_{[j]}(t)$ is the output of the following LTI system:

$$\begin{aligned} \dot{\mathbf{x}}^a_{[j]}(t) &= \mathbf{A}_{jj}\mathbf{x}^a_{[j]}(t) + \mathbf{E}_j\mathbf{d}^a_{[j]}(t) + \tilde{\mathbf{w}}^a_{[j]}(t) \\ \mathbf{y}^a_{[j]}(t) &= \mathbf{C}_j\mathbf{x}^a_{[j]}(t) + \boldsymbol{\rho}^a_{[j]}(t), \end{aligned} \tag{4.59}$$

and the values of $\mathbf{d}^a_{[j]}(t), \tilde{\mathbf{w}}^a_{[j]}(t), \boldsymbol{\rho}^a_{[j]}(t)$, and initial condition $\mathbf{x}^a_{[j]}(T_a)$ can be defined as in Table 4.2. Note, furthermore, that, for replay attacks, $\mathbf{x}^a_{[j]}(t)$ is periodic, and may be discontinuous in time for $t \in \mathcal{T} \triangleq \{t \in \mathbb{R} | t = T_a + nT, \forall n \in \mathbb{N}^0\}$, as $\mathbf{x}^a_{[j]}(T_a + nT) = \mathbf{x}^a_{[j]}(T_a)$, $\forall n \in \mathbb{N}^0$. In this case we abuse notation by using (4.59), as it holds for $t \geq T_a, t \notin \mathcal{T}$.

For both covert and replay attacks it is possible to rewrite $\mathbf{d}^a_{[j]}(t) \triangleq \mathbf{d}_{[j]}(t) + \Delta\mathbf{d}_{[j]}(t)$, $\boldsymbol{\rho}^a_{[j]}(t) \triangleq \boldsymbol{\rho}_{[j]}(t) + \Delta\boldsymbol{\rho}_{[j]}(t)$, and $\tilde{\mathbf{w}}^a_{[j]}(t) \triangleq \tilde{\mathbf{w}}_{[j]}(t) + \Delta\tilde{\mathbf{w}}_{[j]}(t)$ as a nominal term, and a deviation term specific to the attack, derived from definitions in Table 4.2. Note that bounds $\bar{\tilde{\mathbf{w}}}_{[j]}$ and $\bar{\boldsymbol{\rho}}_{[j]}$ are always satisfied.

Note that it is possible to redefine the state of (4.59) as $\mathbf{x}^a_{[j,i]}(t) \triangleq \mathbf{x}_{[j]}(t) + \Delta\mathbf{x}_{[j,i]}(t)$, where $\Delta\mathbf{x}_{[j,i]}(t)$ includes the effect of the attack on the state. The solution of (4.59) can therefore be computed for both covert and replay attacks as

$$\begin{aligned} \mathbf{x}^a_{[j,i]}(t) = \mathbf{x}_{[j]}(t) &+ e^{\mathbf{A}_{jj}(t-T_a-nT)}\Delta\mathbf{x}_{[j,i]}(T_a + nT) \\ &+ \int_{T_a+nT}^{t} e^{\mathbf{A}_{jj}(t-\tau)} \left[\mathbf{E}_j\Delta\mathbf{d}_{[j]}(\tau) + \Delta\tilde{\mathbf{w}}_{[j]}(\tau)\right] d\tau, \end{aligned} \tag{4.60}$$

where, in the case of covert attacks, $nT \triangleq 0$. We stress that the terms on the right-hand side except $\mathbf{x}_{[j]}(t)$ represent $\Delta\mathbf{x}_{[j,i]}(t)$. From this, a (possibly discontinuous for replay attacks) solution of $\Delta\mathbf{x}_{[j,i]}(t)$ can be derived. The following holds for nonsingular $\mathbf{C}_j$:

Theorem 4.6.1. *If a replay or covert attack as in* (4.58)*, with dynamics as in* (4.59)*, and stealthy to the UIO-based detector in $\mathcal{D}_i$, is such that*

$$\left| C_i \int_{T_a}^{t} e^{A_{Li}(t-\tau)} \left[\sum_{j \in \widehat{\mathcal{N}}_i} A_{ij} \Gamma \Delta\mathbf{x}_{[j,i]}(\tau) \right] d\tau \right| > 2\bar{r}_{[i]}(t) \tag{4.61}$$

is satisfied for some $t \geq T_a$, then the attack will be detected by the Luenberger-observer-based detector in $\mathcal{D}_i$.

Proof. In order to prove that detection occurs, we must verify that either (4.5a) or (4.5b) must be violated, for some $t \geq T_a$. As it is assumed that attack function $\boldsymbol{\phi}_{j,i}(t)$ is defined as in (4.58), and is stealthy to $\mathcal{O}_{j,i}^{UIO}$ in $\mathcal{D}_i$, (4.5b) must not hold.

First, exploiting the formulation of the attack dynamics in (4.59), and the definition of $\Delta\mathbf{x}_{[j,i]}(t)$, one can see that $\mathbf{y}_{[j,i]}^c(t) = \mathbf{C}_j\mathbf{x}_{[j]}(t) + \boldsymbol{\rho}_{[j]}^a(t) + \mathbf{C}_j\Delta\mathbf{x}_{[j,i]}(t)$ and to detect the attack, $|r_{[i]}(t)| > \bar{r}_{[i]}(t)$ must be satisfied. Noting that, as seen from Table 4.2, $|\boldsymbol{\rho}_{[j]}^a(t)| \leq \bar{\boldsymbol{\rho}}_{[j]}$ is always satisfied, it is possible to divide the residual in healthy and attacked parts, as in Section 4.5, with

$$r_{[j]}^a(t) = -C_i \int_{T_a}^{t} e^{A_{Li}(t-\tau)} \left[\sum_{j \in \mathcal{N}_i} A_{ij} \Gamma \Delta\mathbf{x}_{[j,i]}(\tau) \right] d\tau.$$

The rest of the proof follows that of Proposition 4.5.1, through the use of the triangle inequality. ■

Remark 4.6.2. *In the case of singular C_j matrix, sufficient condition* (4.61) *changes to*

$$\left| C_i \int_{T_a}^{t} e^{A_{Li}(t-\tau)} \left[\sum_{j \in \widehat{\mathcal{N}}_i} A_{ij} \Gamma \epsilon_{[j,i]}^a(\tau) \right] d\tau \right| > 2\bar{r}_{[i]}(t),$$

where $\epsilon_{[j,i]}^a$ is as in (4.23) *with $\boldsymbol{\phi}_{[j,i]}(t) = \mathbf{C}_j\Delta x_{[j,i]}(t)$, i.e. the effect on $\mathcal{O}_i^{Luen}$ of the deviation provoked by $\Delta x_{[j,i]}$ on the UIO state estimate.*

Note that Theorem 4.6.1 provides bounds for *how much* an attacker implementing a covert or a replay attack may alter the behavior of the LIMAS, by establishing the maximum deviation of $\mathbf{x}_{[j,i]}^a$ from $\mathbf{x}_j$ before $\mathcal{O}_i^{Luen}$ is guaranteed to detect it. For replay attacks, this implies that if the operating condition of $\mathcal{S}_j$ changes significantly over time, then it will be detected by $\mathcal{O}_i^{Luen}$. On the other hand, for covert attacks, if the attacker's

input $\mathbf{d}^a_{[j]}(t)$ deviates significantly from the true $\mathbf{d}_{[j]}(t)$, it will be detected, limiting the malicious agent's impact on the LIMAS overall.

4.7 Simulation results

4.7.1 Simulation setup

The proposed scheme is verified through realistic simulations in Simulink, using the *Specialized Power Systems Toolbox* [HQ19]. The considered mG topology is that in Figure 4.1, having source voltages $V_{si} = 60\ V,\ \forall i \in \mathcal{V}$, and employing bidirectional Buck converters realized as non-ideal IGBT switches, operating at 10 kHz, with snubbers to suppress large transients and protect the equipment. Although power lines are considered to be purely resistive in the development of the results, RL power lines are employed for the physical connection of DGUs in the simulations.

The parameters of the electrical components and primary controllers are taken from [TMGFT16]. Voltages are measured in $[V]$ and currents are measured in $[A]$, whereas the unit of the integrator state is $[V \cdot s]$. The effect of model mismatch is modeled as bounded process noise $w_{[i]}$, $\forall i \in \mathcal{V}$. The process and measurement noises satisfy Assumption 4.2.1, with $\bar{w}_i = [0.05, 0.05, 0.01]^\top$ and $\bar{\rho}_i = [0.01, 0.01, 0]^\top$, $\forall i \in \mathcal{V}$.

The Luenberger observer gains L_i are calculated to assign the eigenvalues of A_{Li} to $\{-50, -100, -500\}$ for each DGU i. The UIO matrices $S_j = \mathbf{I} - H_j\mathbf{C}_j$ are selected to ensure $S_j\mathbf{E}_j = \mathbf{0}$. Matrices $\widetilde{K}_j$ are calculated to assign the eigenvalues of F_j to $\{-1, -1.5, -2, -2.5, -3, -3.5\}$. All other UIO matrices are computed as in (4.9). Two attack scenarios will be discussed in the following subsections. In the first, attacks on $\mathbf{y}^c_{[2,4]}$ and $\mathbf{y}^c_{[3,4]}$ will be designed to be stealthy to the Luenberger-observer-based module as per condition in Proposition 4.5.3. In the second scenario, a covert attack will be implemented on $\mathbf{y}^c_{[2,4]}$. These two scenarios have been specifically designed to demonstrate the interplay between the two modules of $\mathcal{D}_i$.

For both scenarios, the simulation proceeds as follows. At time $t = 0\ s$, all DGUs are started disconnected from each other, i.e., DGUs are running separately; therefore, power lines and communication links in Figure 4.1 are not in place. Consequently, at this phase of simulations, the secondary controllers of DGUs are not active and primary controllers track a constant voltage reference of $V_{ref} = 48\ V$. At time $t = 2\ s$, the DGUs are connected to each other through both RL power lines and communication links, and secondary controllers are activated. At this phase of the simulations, the communications are *healthy*, i.e., no attacks are active, and therefore, the secondary controllers will achieve current sharing and voltage balancing. Finally, at $t = 8\ s$, the attack is launched on the corresponding communication channels.

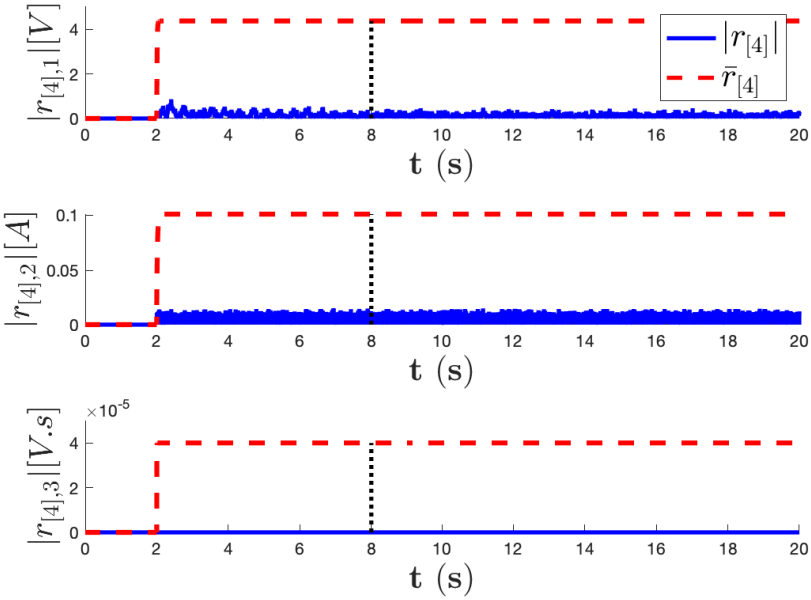

Figure 4.2: Residual and detection thresholds for $\mathcal{O}_4^{Luen}$ under Scenario I. The false data injection attacks $\boldsymbol{\phi}_{2,4}^{bi}$ and $\boldsymbol{\phi}_{3,4}^{bi}$ are not detected by $\mathcal{O}_4^{Luen}$, as Proposition 4.5.3 is satisfied.

4.7.2 Scenario I – False data injection stealthy to $\mathcal{O}_i^{Luen}$

In the first scenario, constant bias injection attacks are directed to communications $\mathbf{y}_{[2,4]}^c(t)$ and $\mathbf{y}_{[3,4]}^c(t)$, where the elements of the attack vector $\boldsymbol{\phi}_{2,4}^{bi}$ are selected randomly from a uniform distribution in the interval $[-0.02, 0.02]$. The fourth element of the attack vector $\boldsymbol{\phi}_{3,4}^{bi}$ is selected as $\boldsymbol{\phi}_{3,4_4}^{bi} = -\frac{R_{34}}{R_{24}}\boldsymbol{\phi}_{2,4_4}^{bi}$ making them stealthy to $\mathcal{O}_i^{Luen}$, as per condition (4.55). Remaining elements of the attack vector $\boldsymbol{\phi}_{3,4}^{bi}$ are again drawn from a uniform distribution in the interval specified above. Specifically, the constant attack vectors are:

$$\boldsymbol{\phi}_{2,4}^{bi} = [-0.0139, 0.0149, -0.0031, -0.0014, -0.0095, -0.0011]^\top,$$
$$\boldsymbol{\phi}_{3,4}^{bi} = [0.0037, 0.0185, 0.0174, 0.0021, 0.0178, 0.0180]^\top.$$

Figures 4.2, 4.3a, and 4.3b display the residuals and corresponding thresholds for the Luenberger-observer-based module for DGU 4, and UIO-based modules for communication $\mathbf{y}_{[j,4]}^c(t), j \in \{2, 3\}$, respectively. Moreover, in these figures, the vertical dashed lines in black indicate the time of the start of the attacks, i.e., $T_a^{2,4} = T_a^{3,4} = 8s$, whereas those in green indicate the time of detection for the corresponding module.

One can see that, through the proper selection of the attack vectors $\boldsymbol{\phi}_{2,4}^{bi}$ and $\boldsymbol{\phi}_{3,4}^{bi}$, the

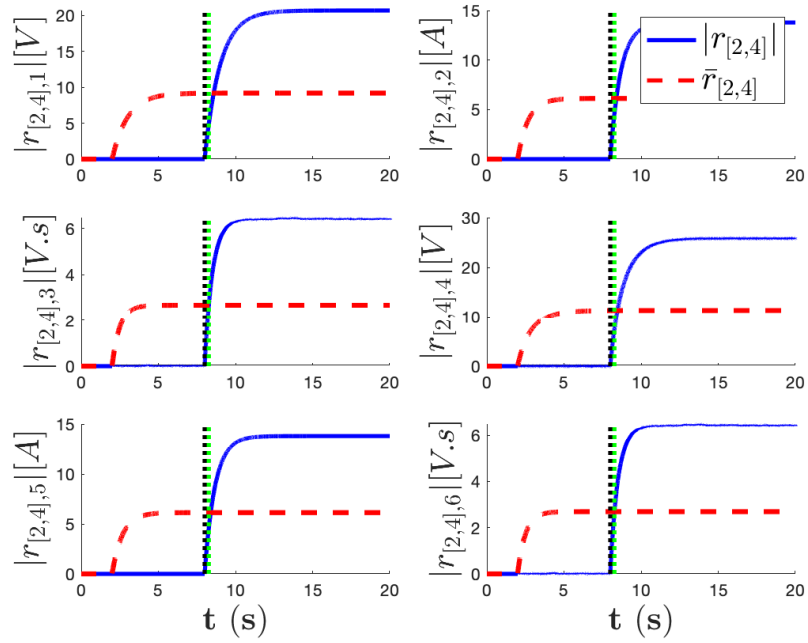

(a) Residuals and thresholds – $\mathcal{O}_{2,4}^{UIO}$

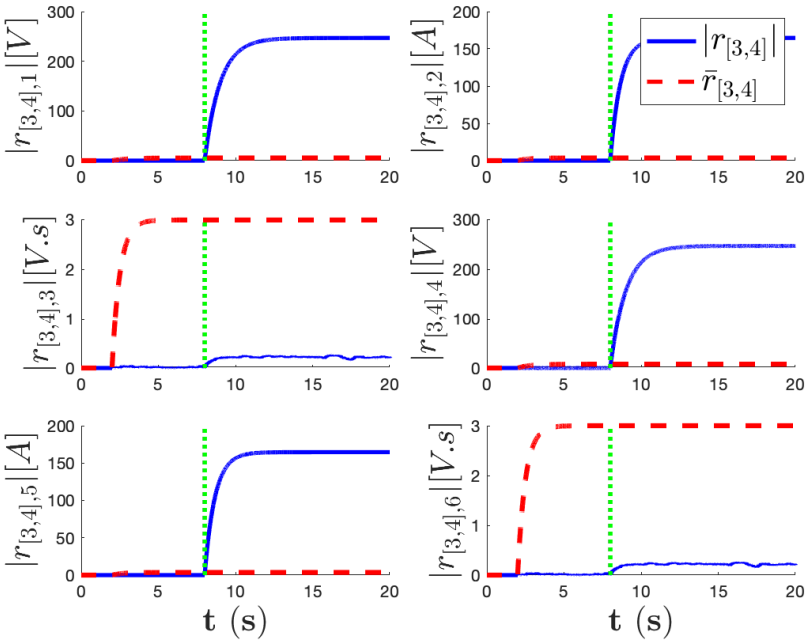

(b) Residuals and thresholds – $\mathcal{O}_{3,4}^{UIO}$

Figure 4.3: Residual and detection thresholds of the UIO modules in $\mathcal{D}_4$ under Scenario I. The false data injection attacks $\phi_{2,4}^{bi}$ and $\phi_{3,4}^{bi}$ are detected by the UIO modules $\mathcal{O}_{2,4}^{UIO}$ and $\mathcal{O}_{3,4}^{UIO}$.

attacker is able to achieve stealthiness condition (4.55) for $\mathcal{O}_i^{Luen}$. Hence, the residual of this module is unaffected by the attack, preventing detection, as shown in Figure 4.2. Nevertheless, the residuals of $\mathcal{O}_{j,i}^{UIO}$monitoring the two communication links are affected by the attack, leading to the violation of (4.17) for $(j,i) = (2,4)$ and $(j,i) = (3,4)$, in turn, triggering detection in both modules. The attacks are detected at times $T_d^{2,4} = 8.270$s and $T_d^{3,4} = 8.015$s, shortly after activation.

4.7.3 Scenario II – Covert attack

In the second scenario, a covert attack $\phi_{2,4}^c$ is launched on the communication $\mathbf{y}_{[2,4]}^c(t)$, with dynamics (4.38). The inputs $\mathbf{d}_{[2]}^a$ are such that the state dynamics of the attacked system act as if DGU 2 were disconnected from the rest of the mG, i.e. dynamics of $\mathbf{x}_{[2]}$ not influenced by its neighboring states nor by secondary control input. Furthermore, the attacker also specifies a difference in load current I_{L2}^a in $\mathbf{d}_{[2]}^a$, selected such that $\Delta I_{L2} = 2A$, to alter the operation point of $\mathbf{x}_{[2]}^a$ compared to $\mathbf{x}_{[2]}$.

Figures 4.4a-4.4b show the residuals and corresponding thresholds for the second attack scenario, for the Luenberger-observer-based module for DGU 4 and UIO-based module for communication $\mathbf{y}_{[2,4]}^c(t)$, respectively. Since this covert attack complies with the dynamics in (4.38), it is stealthy to the UIO-based detection module as proven in Proposition 4.4.5. Indeed, one can see from Figure 4.4b that the residual of the UIO-based module is unchanged by the onset of the attack and this module fails to detect the attack. On the other hand, residual of the Luenberger-observer-based module reflects the effect of the attack, and the covert attack is quickly detected at time $T_d^4 = 8.001s$.

4.8 Conclusions

In this chapter, we have presented a novel *distributed* attack detection technique for LIMASs inspired by and applied to islanded DCmGs. We have discussed the architecture and the properties of a two-module local detection unit $\mathcal{D}_i$, composed of a Luenberger-like observer and a bank of suitably designed UIOs estimating local and neighboring states, respectively. Details on the information necessary for the design of each module are given explicitly, requiring knowledge of dynamics of the local subsystem and of its neighbors. Thorough analysis has been provided as well as extensive simulation results on a realistic model of a DCmG showing the methodology's effectiveness.

The proposed methodology provides a safety component to the application of consensus-based networked controllers developed in Chapters 2 and 3. The results presented so far, both for control and cyber-attack detection, require model knowledge. In the next part of the thesis, we turn our attention to data-driven control and estimation, and change the setting from LIMASs, as the results presented in Chapters 5 and 6 are for general LTI systems. Nevertheless, the results in Chapter 6 have the potential of being used for distributed cyber-attack detection.

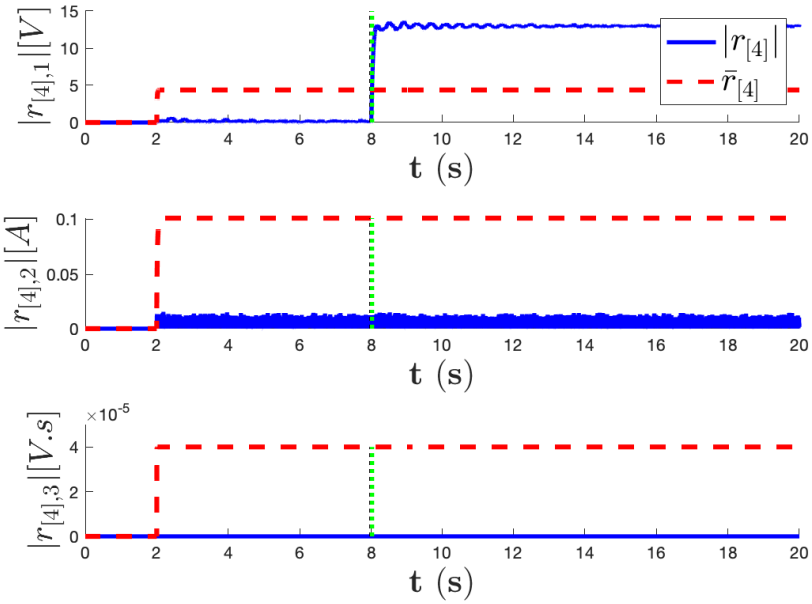

(a) Residuals and thresholds – $\mathcal{O}_4^{Luen}$

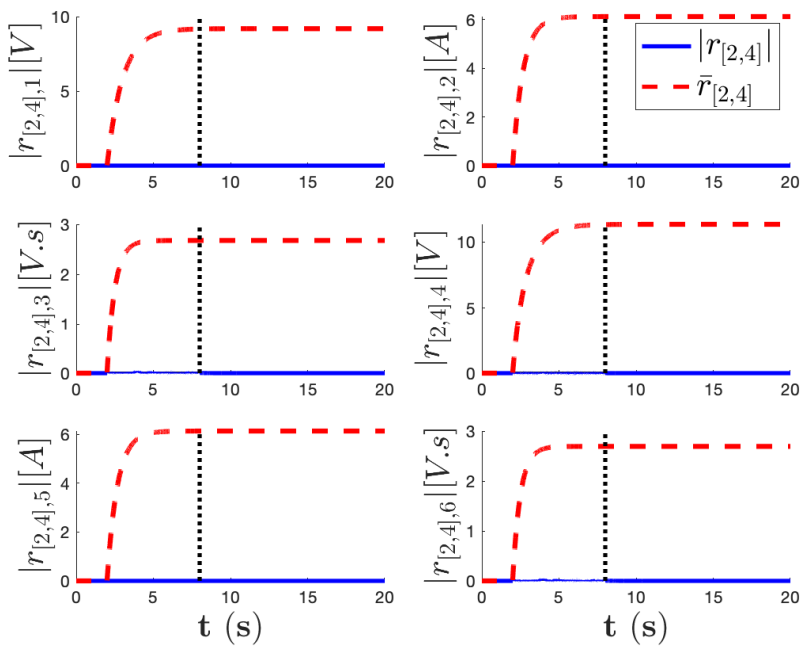

(b) Residuals and thresholds – $\mathcal{O}_{2,4}^{UIO}$

Figure 4.4: Residual and detection thresholds of the different modules in $\mathcal{D}_4$ under Scenario II. The covert attack $\phi_{2,4}^c$ is stealthy to the UIO modules, but is detected by $\mathcal{O}_4^{Luen}$.

4.9 Supplementary material

4.9.1 DGU matrices

Matrices A_{ii}, B_i, M_i, A_{ij}, K_i, and C_i are defined as in [TRFT18]:

$$A_{ii} = \begin{bmatrix} -\sum_{j\in\mathcal{N}_i} \frac{1}{R_{ij}C_{ti}} & \frac{1}{C_{ti}} & 0 \\ -\frac{1}{L_{ti}} & -\frac{R_{ti}}{L_{ti}} & 0 \\ -1 & 0 & 0 \end{bmatrix}, \quad B_i = \begin{bmatrix} 0 & 0 \\ \frac{1}{L_{ti}} & 0 \\ 0 & 1 \end{bmatrix}, \quad K_i = \begin{bmatrix} k_{i,1} & k_{i,2} & k_{i,3} \end{bmatrix},$$

$$M_i = \begin{bmatrix} -\frac{1}{C_{ti}} & 0 \\ 0 & 0 \\ 0 & 1 \end{bmatrix}, \quad A_{ij} = \begin{bmatrix} \frac{1}{R_{ij}C_{ti}} & 0 & 0 \\ 0 & 0 & 0 \\ 0 & 0 & 0 \end{bmatrix},$$

where $R_{ti}, L_{ti}, C_{ti}, R_{ij}$ are electrical parameters of the DGU as seen in Figure 4.1. For the design of the UIOs, the DGU dynamics are rearranged as in (4.11), with $\bar{E}_j = \mathbf{I}$ and $\hat{E}_j$ defined accordingly.

4.9.2 Proof of Lemma 4.4.1

We provide a sketch of the proof. To simplify notation, without risk of ambiguity, we remove all subscripts from variables in (4.6) and (4.9), and replace $\bar{E}$ with E:

$$\begin{aligned} \dot{x}(t) &= Ax(t) + Ed(t) + w(t) \\ y^c(t) &= Cx(t) + \rho(t) + \beta(t - T_a)\phi(t) \end{aligned}$$

Exploiting [CT98, Lemma 1], condition (C1) implies that there are nonsingular matrices P and Q such that

$$P^{-1}E = \begin{bmatrix} E_1 \\ \mathbf{0} \end{bmatrix} \quad Q^{-1}CP = \begin{bmatrix} C_1 & \mathbf{0} \end{bmatrix}, \tag{4.62}$$

where E_1 and C_1 have the same dimension and are both invertible. It is possible to construct a UIO for the transformed dynamics for state $\bar{x} = P^{-1}x$ and output $\bar{y}^c = Q^{-1}y^c$, noting that conditions (C1) and (C2) hold for the transformed dynamics, and defining $\bar{A} \triangleq P^{-1}AP$, $\bar{E} \triangleq P^{-1}E$, and $\bar{C} \triangleq Q^{-1}CP$, with $\bar{A}$ a 2-by-2 block matrix with entries $\bar{A}_{lk}, l, k \in \{1, 2\}$. From (4.9) one derives the following[3]:

$$\bar{H} = \begin{bmatrix} C_1^{-1} \\ \mathbf{0} \end{bmatrix}, \quad \bar{S} = \begin{bmatrix} \mathbf{0} & \mathbf{0} \\ \mathbf{0} & \mathbf{I}_{n-q} \end{bmatrix}, \quad \bar{\widetilde{K}} = \begin{bmatrix} \bar{\widetilde{K}}_1 \\ \bar{\widetilde{K}}_2 \end{bmatrix}$$

$$\bar{F} = \begin{bmatrix} -\bar{\widetilde{K}}_1 C_1 & \mathbf{0} \\ \bar{A}_{21} - \bar{\widetilde{K}}_2 C_1 & \bar{A}_{22} \end{bmatrix}, \quad \bar{\widehat{K}} = \begin{bmatrix} \mathbf{0} \\ \bar{A}_{21} C_1^{-1} \end{bmatrix}$$

[3] A bar $\bar{\cdot}$ has been added to the matrices to highlight their dependence on the transformed system.

where $\bar{F}$ is Hurwitz stable by design. Note that the pair $(\bar{F}, \bar{C})$ is not observable and thus the state $\bar{z}$ can be written as $\bar{z} = \left[\bar{z}_1^\top, \bar{z}_2^\top\right]^\top$, where $\bar{z}_1$ and $\bar{z}_2$ are respectively the observable and unobservable portions of the state. Furthermore, given the structure of transformed matrices above, it is evident that $\bar{y}^c$ does not influence the observable part of the state, $\bar{z}_1$, and $\hat{\bar{y}} = C_1\bar{z}_1 + \bar{y}^c$. Therefore, the residual defined as $r = Q\left(\bar{y}^c - \hat{\bar{y}}\right) = QC_1\bar{z}_1$ is independent of $\bar{y}^c(t)$ and $\phi(t), \forall t \geq T_a$.

4.9.3 Proof of Lemma 4.4.3

For any matrix A, it is possible to find its Jordan normal form $J = P^{-1}AP$. This implies that the equivalence $e^{At} = Pe^{Jt}P^{-1}$ holds. Note that e^{Jt} also has the same block-diagonal structure of J, where each block $e^{J_k t} \in \mathbb{R}^{n_k \times n_k}$ is upper-triangular. Following this, we define a block-diagonal matrix $\mathbf{P}$ such that each block $\mathbf{P}_k \in \mathbb{R}^{n_k \times n_k}$ is upper-triangular with all entries 1, and thus has the same non-zero structure as $e^{J_k t}$. We exploit the property that for any matrix M with element m_{ij} at i-th row and j-th column, it holds that $\max |m_{ij}| \leq \|M\|$ to show that $\left|Pe^{Jt}P^{-1}\right| \leq |P|\left|e^{Jt}\right||P^{-1}| \leq |P|\left\|e^{Jt}\right\|\mathbf{P}|P^{-1}|$ is satisfied elementwise. Hence, noting that if A is Hurwitz stable then J is also Hurwitz stable, it is possible to find scalars $\lambda > 0$ and $\mu \geq 1$ such that $\|e^{Jt}\| \leq \mu e^{-\lambda t}$, and to define $\Lambda \triangleq \mu|P|\mathbf{P}|P^{-1}|$. Finally, note that matrix Λ is such that $\Lambda \geq \mathbf{I}$ holds, as the following relationships can be derived: $|P|\mathbf{P}|P^{-1}| = |P|(\mathbf{I}+\Xi)|P^{-1}| = |P||P^{-1}|+|P|\Xi|P^{-1}| \geq \mathbf{I}+\mathbf{0}$, given that $\mathbf{P} = \mathbf{I} + \Xi$ with $\Xi \geq \mathbf{0}$, and that $|P||P^{-1}| \geq |PP^{-1}| = \mathbf{I}$, $|P|\Xi|P^{-1}| \geq \mathbf{0}$.

4.9.4 Proof of Proposition 4.4.4

Following the Proof of Lemma 4.4.4, if

$$\Sigma_j \left|\epsilon^r_{[j,i]}(T_a + kT) + H_j\boldsymbol{\rho}_{[j]}(T_a + (k-1)T)\right| \leq \bar{\epsilon}_{[j,i]}(T_a + kT) - |H_j|\bar{\boldsymbol{\rho}}_{[j]}, \tag{4.63}$$

then the replay attack will not be detected for $t \in [T_a + kT, T_a + (k+1)T)$. We therefore must characterize the solution of estimation error $\epsilon_{[j,i]}(T_a + kT)$ as $k \to \infty$. To do so, we note that the solution to the state estimate under replay attack for time $t \in \mathcal{T} \triangleq \{t | t = T_a + kT, \forall k \in \mathbb{N}\}$ is

$$\begin{aligned}
\hat{\mathbf{x}}_{[j,i]}(T_a + kT) &= e^{F_j kT}\mathbf{z}_{[j,i]}(T_a) + H_j\mathbf{y}^c_{[j,i]}(T_a + kT) \\
&\qquad + \int_{T_a}^{T_a+kT} e^{F_j(T_a+kT-\tau)}\widehat{K}_j\mathbf{y}^c_{[j,i]}(\tau)d\tau \\
&= e^{F_j kT}\mathbf{z}_{[j,i]}(T_a) + H_j\mathbf{y}_{[j]}(T_a - T) + \\
&\qquad + \sum_{s=0}^{k-1} e^{sTF_j}\int_{T_a-T}^{T_a} e^{F_j(T_a-\tau)}\widehat{K}_j\mathbf{y}_{[j]}(\tau)d\tau.
\end{aligned} \tag{4.64}$$

Given that F_j is Hurwitz by design, the series $\sum_{s=0}^{k-1} e^{sTF_j} \int_{T_a-T}^{T_a} e^{F_j(T_a-\tau)} \widehat{K}_j \mathbf{y}_{[j]}(\tau) d\tau$ converges. Hence $\epsilon^r_{[j,i]}(T_a + kT)$ can be expressed as

$$\begin{aligned}\epsilon^r_{[j,i]}(T_a + kT) &= \epsilon^r_{[j,i]}(T_a) + (\mathbf{I} - e^{F_j kT})\mathbf{z}_{[j,i]}(T_a) - \sum_{s=0}^{k-1} e^{sTF_j} \int_{T_a-T}^{T_a} e^{F_j(T_a-\tau)} \widehat{K}_j \mathbf{y}_{[j]}(\tau) d\tau \\ &= \epsilon^r_{[j,i]}(T_a) + \Delta\epsilon_{[j,i]}(k).\end{aligned}$$

Given the convergence of the series, it is possible to bound the estimation error under attack by

$$\left|\epsilon^r_{[j,i]}(T_a + kT)\right| \leq \left|\epsilon^r_{[j,i]}(T_a) + M_{j,i}\right| \tag{4.65}$$

where $M_{j,i} \geq \mathbf{0}$ is such that

$$\left|\Delta\epsilon_{[j,i]}(k)\right| \leq M_{j,i}\,,\ \forall k \in \mathbb{N}^0.$$

Hence, $M_{j,i}$ can be defined as $M_{j,i} \triangleq \sup_{k\in\mathbb{N}^0} \left|\Delta\epsilon_{[j,i]}(k)\right|$. Given the monotonicity of the LHS of the previous, $M_{j,i}$ is an upper bound on $\left|\Delta\epsilon_{[j,i]}(k)\right|$ for all $k \in \mathbb{N}$, implying

$$\begin{aligned}&|\epsilon^r_{[j,i]}(T_a + kT) + H_j \boldsymbol{\rho}_{[j]}(T_a + (k-1)T)| \\ &\qquad \leq \left|\epsilon^r_{[j,i]}(T_a) + M_{j,i} + H_j \boldsymbol{\rho}_{[j]}(T_a + (k-1)T)\right| \\ &\qquad \leq \left|\epsilon^r_{[j,i]}(T_a) + M_{j,i}\right| + |H_j| \bar{\boldsymbol{\rho}}_{[j]}.\end{aligned} \tag{4.66}$$

Finally, to complete the proof, note that $\bar{\epsilon}_{[j,i]}(t)$ is monotonic. We define a variable

$$\Delta\bar{\epsilon}_{[j,i]}(T_a) \triangleq \max\left(\mathbf{0}, \lim_{t\to\infty} \bar{\epsilon}_{[j,i]}(T_a) - \bar{\epsilon}_{[j,i]}(t)\right),$$

which is $\mathbf{0}$ if $\bar{\epsilon}_{[j,i]}(t)$ monotonically increasing, and greater than $\mathbf{0}$ otherwise. This definition allows us to state that $\bar{\epsilon}_{[j,i]}(T_a + kT) \geq \bar{\epsilon}_{[j,i]}(T_a) - \Delta\bar{\epsilon}_{[j,i]}(T_a), \forall k \in \mathbb{N}_0$.

Due to (4.66), (4.63) holds if

$$\Sigma_j \left|\epsilon^r_{[j,i]}(T_a) + M_{j,i}\right| + \Sigma_j |H_j| \bar{\boldsymbol{\rho}}_{[j]} \leq \bar{\epsilon}_{[j,i]}(T_a) - \Delta\bar{\epsilon}_{[j,i]}(T_a) - |H_j| \bar{\boldsymbol{\rho}}_{[j]},$$

which is equivalent to (4.36). Consequently, $|\epsilon^r_{[j,i]}(t)| \leq \bar{\epsilon}_{[j,i]}(t)$ will hold for all $t \geq T_a$.

Part III

Data-driven Control and State Estimation

5 Data-driven worst-case tracking control

5.1 Introduction

In this chapter, we turn our attention to the problem of designing robust optimal controllers for LTI systems using a finite amount of data. Recently, there has been a renewed interest in system analysis and control design methods relying on finite-length data sequences [DPT20, vWETC20, MPRT19, Tu19, BBP21]. Several works propose to use raw measurements for representing discrete-time systems and solving system analysis and control design problems [MMG20, KBA20, RBKA19, DPT20, vWETC20, vWM20, TvWC20, BKSA20, BDPT20a, vWCM20, DPT21, CLD19b, BKMA20, CLD21]. As mentioned in [DPT20], the main feature of these approaches is to bypass explicit system identification that is usually required in standard control design. Moreover, data-based system representations can be easier to update when new data are available, hence facilitating the deployment of adaptive control systems [ADL20, LSKJ21].

All above works assume the availability of *historical data*, i.e., finite-length trajectories produced by the open-loop system and measured offline. The works [DPT20, vWETC20, vWM20, TvWC20, BKSA20, BDPT20a, vWCM20, DPT21] consider system representations based on input-state historical data. In certain applications, the system state is not accessible and only input-output data can be collected. In this scenario, Willems' FL states that the whole set of input-output trajectories generated by a discrete-time linear system can be represented by finitely many historical data coming from sufficiently excited dynamics [WRMDM05]. In view of this result, [MR08] proposes to predict the system output from a given time t onwards by using a set of collected historical data and a finite amount of *recent past data*, i.e., an input-output trajectory measured right before time t. This approach is also used in the data-enabled predictive control (DeePC) scheme described in [CLD19b]. While originally developed for noiseless data, DeePC has been recently extended to noisy trajectories in [BKMA20, CLD21]. In [BKMA20], slack variables are introduced in the data-dependent system representation to account for noisy measurements. The modified control scheme is shown to be recursively feasible

and practically exponentially stable; however, the tracking performance is not analyzed. The authors of [CLD21] propose a distributionally robust variant of DeePC based on semi-infinite optimization. They then formulate a finite and convex program, whose optimal value is an upper bound to that of the original optimization problem. The work [KD20] considers using noiseless historical data and noisy recent output data to minimize the energy of the control input while robustly satisfying input/output constraints. The authors propose to separate the problems of estimation of the initial condition and control design, and show that the solution to the formulated problem is computed by consecutively solving two optimization problems.

5.1.1 Contributions

In this chapter, we provide a data-driven control design method for worst-case optimal reference tracking with explicit performance guarantees. In particular, we consider LTI systems for which no model knowledge is available.

We assume the historical data are noiseless while recent data are corrupted by noise terms satisfying a quadratic constraint similar to the one in [vWCM20]. This assumption corresponds to scenarios where historical data are generated through sophisticated offline experiments. For instance, very accurate (and, thus, expensive) sensors can be utilized to collect historical data; however, it might not be desirable to deploy these sensors in real-world use for the purpose of cutting costs. Moreover, offline experiments might exploit sensor fusion methods along with additional sensors (i.e. a motion capture system for a quadcopter) that are not available in online operations. Finally, historical data can be further *denoised* [YS20], which would be computationally restrictive for recent data. Nevertheless, in reality, noise cannot be completely eliminated. The technical consideration of noise in historical data is deferred to future work; however, Section 5.6.1 provides a numerical study thereof.

In safety-critical applications, such as power networks and industrial control systems, it is sometimes required to adopt a bounded-error perspective by enforcing robustness against all possible noise realizations and providing worst-case performance guarantees. This is the setting considered here and, for this purpose, we utilize the data-driven prediction method in [MR08]. We first characterize noises that are consistent with the input-output data, and then reformulate the tracking cost. This enables us to apply the S-lemma [PT07] to transform the worst-case robust control problem to an equivalent minimization problem with a linear cost and LMI constraints, i.e., an SDP. Moreover, we propose a method for reducing the size of LMI constraints, and also show that our formulation can easily incorporate input-output constraints as well as actuator disturbances. In contrast to [KD20], we consider to minimize quadratic cost on both inputs and outputs, while the method in [KD20] only deals with the minimization of the input energy.

The main features of our method are the following: (1) we consider the minimization of the worst-case tracking performance; (2) the proposed design procedure is non-conservative, meaning that we obtain the optimal tracking controllers without any approximations; (3) the complexity of the controller design procedure does not increase with the number of historical data instances.

This chapter is organized as follows. In Section 5.2, we provide preliminaries on data-driven prediction, which will also be used in Chapter 6. The problem formulation is given in Section 5.3. The data-based robust optimal tracking control problem is solved in Section 5.4. Extensions for considering input-output constraints as well as actuator disturbances are discussed in Section 5.5. Simulations are provided in Section 5.6, before giving the concluding remarks in Section 5.7.

5.2 Preliminaries on data-driven prediction

We consider a reachable and observable discrete-time LTI system $\mathcal{G}$ with state-space representation

$$\begin{aligned} x_{k+1} &= Ax_k + Bu_k, \\ y_k &= Cx_k + Du_k, \end{aligned} \tag{5.1}$$

where $x_k \in \mathbb{R}^n$, $u_k \in \mathbb{R}^m$, $y_k \in \mathbb{R}^p$ are the system state, input, and output, respectively. In this chapter, we assume that the system matrices (A, B, C, D) are unknown, the states x_k are not measurable, and only a finite set of input-output samples of $\mathcal{G}$ is available. In this section, we summarize how to form a data-based representation of $\mathcal{G}$ that allows for predicting the output given any input [WRMDM05, MR08].

We start by introducing the following definitions. The *lag* $\mathbf{l}(\mathcal{G})$ is the smallest integer l such that the l-step observability matrix $[C^\top, A^\top C^\top, \ldots, (A^{l-1})^\top C^\top]^\top$ has full column rank. Moreover, $\mathbf{l}(\mathcal{G}) \leq n$ since $\mathcal{G}$ is observable. A sequence $\{u_k, y_k\}_{k=l}^{l+T-1}$ is a *trajectory* of $\mathcal{G}$ if and only if there exists a state sequence $\{x_k\}_{k=l}^{l+T}$ such that (5.1) holds for $k = l, \ldots, l+T-1$. A sequence $\{v_k\}_{k=l}^{l+T-1}$ is *persistently exciting of order* L if the Hankel matrix $\mathcal{H}_L(v)$ is of full row rank.

In the following, we introduce the input-output data-based representation of linear systems in [WRMDM05] and the prediction method in [MR08]. Suppose a trajectory $\{\bar{u}_k, \bar{y}_k\}_{k=t_h}^{t_h+T_d-1}$ of $\mathcal{G}$ is collected, where $t_h \ll 0$. The trajectory is called *historical*, since it can be regarded as collected long before the start (indicated by time 0) of any control or prediction tasks. The FL proposed by Willems et al. [WRMDM05] shows how to use the historical trajectory to characterize all possible system trajectories of length T_f.

Lemma 5.2.1 (Fundamental Lemma [WRMDM05])**.** *Suppose that* $\{\bar{u}_k, \bar{y}_k\}_{k=t_h}^{t_h+T_d-1}$ *is a trajectory of* $\mathcal{G}$ *and that the input* $\bar{u}$ *is persistently exciting of order* $T_f + n$*. Then,*

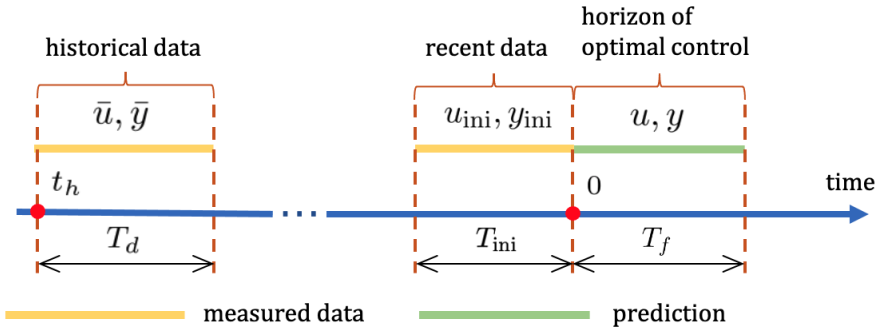

Figure 5.1: Chronological order of data used in data-driven prediction

$\{u_k, y_k\}_{k=0}^{T_f-1}$ *is a trajectory of* $\mathcal{G}$ *if and only if there exists* $g \in \mathbb{R}^{T_d-T_f+1}$ *such that*

$$\begin{bmatrix} \mathcal{H}_{T_f}(\bar{u}) \\ \mathcal{H}_{T_f}(\bar{y}) \end{bmatrix} g = \begin{bmatrix} u \\ y \end{bmatrix}. \tag{5.2}$$

For a given time $t \geq 0$, consider the problem of using (5.2) for computing predictions $y = \text{col}(\{y_k\}_{k=0}^{T_f-1})$ of the system output over a future horizon given the inputs $u = \text{col}(\{u_k\}_{k=0}^{T_f-1})$. There are infinitely many output trajectories y that satisfy (5.2), corresponding to different initial states x_0. The authors of [MR08] propose to implicitly fix the initial state by using recent input-output samples[1] $u_{\text{ini}} = \text{col}(\{u_k\}_{k=-T_{\text{ini}}}^{-1})$, $y_{\text{ini}} = \text{col}(\{y_k\}_{k=-T_{\text{ini}}}^{-1})$, which are available at time 0 (see Fig. 5.1). More precisely, let

$$U = \begin{bmatrix} U_p \\ U_f \end{bmatrix} \triangleq \mathcal{H}_{T_{\text{ini}}+T_f}(\bar{u}), \quad Y = \begin{bmatrix} Y_p \\ Y_f \end{bmatrix} \triangleq \mathcal{H}_{T_{\text{ini}}+T_f}(\bar{y}),$$

where U_p and Y_p consist of the first T_{ini} block rows of U and Y, respectively, while U_f and Y_f consist of the last T_f block rows of U and Y, respectively. The following lemma summarizes the prediction algorithm.

Lemma 5.2.2 ([MR08])**.** *Suppose that* $\bar{u}$ *is persistently exciting of order* $T_{\text{ini}} + T_f + n$, *and* $T_{\text{ini}} \geq \mathbf{l}(\mathcal{G})$. *Then, for a given recent system trajectory* $(u_{\text{ini}}, y_{\text{ini}})$ *and input sequence* u,

1. *there exists at least one vector* g *verifying*

$$\begin{bmatrix} U_p \\ Y_p \\ U_f \end{bmatrix} g = \begin{bmatrix} u_{\text{ini}} \\ y_{\text{ini}} \\ u \end{bmatrix}, \tag{5.3}$$

[1] We call $\{u_{\text{ini}}, y_{\text{ini}}\}$ *recent data.*

2. *the corresponding output trajectory y is unique and given by*

$$y = Y_f g, \tag{5.4}$$

for any g satisfying (5.3).

Note that, collectively, (5.3) and (5.4) are equivalent to (5.2), which can be rewritten as

$$\begin{bmatrix} U_p \\ Y_p \\ U_f \\ Y_f \end{bmatrix} g = \begin{bmatrix} u_{\text{ini}} \\ y_{\text{ini}} \\ u \\ y \end{bmatrix}.$$

Throughout the chapter, we assume that $\bar{u}$ and T_{ini} verify the conditions in Lemma 5.2.2, which implies that the matrices U, U_p, and U_f have full row rank.

5.3 Problem formulation

In view of the prediction algorithm described in Lemma 5.2.2, consider the following data-driven linear-quadratic tracking problem

$$\min_{u,y,g} \sum_{k=0}^{T_f-1} \left(\|y_k - r_k\|_Q^2 + \|u_k\|_R^2 \right) \text{ s.t. } (5.3), (5.4), \tag{5.5}$$

where $\{r_k\}_{k=0}^{T_f-1}$ is the tracking reference and $Q \succeq 0$, $R \succ 0$ are weight matrices. In this chapter, we assume that the recent outputs y_{ini} are noisy, verifying

$$y_{\text{ini}} = \check{y}_{\text{ini}} + w,$$

where $\check{y}_{\text{ini}}$ represents the noiseless output and w denotes the measurement noise. Besides, as in [DPT20, BKSA20, vWCM20], we assume that w satisfies the following quadratic constraint

$$\begin{bmatrix} 1 \\ w \end{bmatrix}^\top \underbrace{\begin{bmatrix} \Phi_{11} & \Phi_{12} \\ \Phi_{12}^\top & \Phi_{22} \end{bmatrix}}_{\Phi} \begin{bmatrix} 1 \\ w \end{bmatrix} \geq 0, \tag{5.6}$$

where $\Phi_{22} = \Phi_{22}^\top \prec 0$.

Remark 5.3.1. *The negative definiteness of Φ_{22} ensures that $\|w\|_2$ is bounded. In the special case that $\Phi_{12} = \mathbf{0}$ and $\Phi_{22} = -\mathbf{I}$,* (5.6) *reduces to*

$$w^\top w = \sum_k w_k^\top w_k \leq \Phi_{11},$$

which, as highlighted in [vWCM20], has the interpretation of bounded noise energy.

We are interested in designing a control input u that minimizes the worst-case quadratic tracking error among all feasible noise trajectories, which are defined as follows.

Definition 5.3.1. *For recent data* $(u_{\text{ini}}, y_{\text{ini}})$*, a noise trajectory* w *is called feasible if it verifies* (5.6) *and* $(u_{\text{ini}}, y_{\text{ini}} - w)$ *is a trajectory of* $\mathcal{G}$*.*

Next, we provide a robust formulation of the tracking problem (5.5) based on the linear quadratic tracking error

$$\text{LQTE}(u, y, w) \triangleq \sum_{k=0}^{T_f-1} \left(\|y_k - r_k\|_Q^2 + \|u_k\|_R^2 \right).$$

Problem P1: Find the input sequence u solving

$$\min_{u,y,g} \max_{w} \quad \text{LQTE}(u, y, w) \tag{5.7a}$$

$$\text{subject to} \quad \begin{bmatrix} U_p \\ Y_p \\ U_f \\ Y_f \end{bmatrix} g = \begin{bmatrix} u_{\text{ini}} \\ y_{\text{ini}} \\ u \\ y \end{bmatrix} - \begin{bmatrix} \mathbf{0} \\ w \\ \mathbf{0} \\ \mathbf{0} \end{bmatrix}, \tag{5.7b}$$

$$w \text{ is a feasible noise trajectory.} \tag{5.7c}$$

The constraint (5.7c) means that the min-max optimization problem is not straightforward to solve. However, as we show in the next section, this issue can be circumvented by using a suitable parameterization of feasible noise trajectories.

5.4 Robust controller design

Problem **P1** can be reformulated as follows

$$\begin{aligned} &\min_{u,\gamma,g,y} \quad \gamma \\ &\text{s.t.}, \text{LQTE}(u, y, w) \leq \gamma, \ \forall w \text{ satisfying } \ (5.7\text{c}). \end{aligned} \tag{5.8}$$

For notational simplicity, we have omitted the dependence of the problem on r. In the sequel, we will derive a convex reformulation of (5.8). We first show in Section 5.4.1 that any noise trajectory w fulfilling (5.7c) can be expressed as an affine function of a vector g_w satisfying a quadratic constraint. In Section 5.4.2, we show that the output y is completely determined by the input u and the vector g_w, which allows one to express the tracking error constraint as a quadratic constraint on g_w. In light of these results, in Section 5.4.3, we prove that (5.8) is equivalent to an SDP. Finally, in Section 5.4.4, we

show how to reduce the size of the LMI constraints and, consequently, the computational burden.

5.4.1 Feasible noise parameterization

Since $\bar{u}$ is persistently exciting of order $T_{\text{ini}} + T_f + n$, it is also persistently exciting of order $T_{\text{ini}} + n$. In view of Lemma 5.2.1, $(u_{\text{ini}}, y_{\text{ini}} - w)$ is a trajectory of $\mathcal{G}$ if and only if there exists $g_{\text{ini}} \in \mathbb{R}^{T_d - T_{\text{ini}} - T_f + 1}$ such that

$$\begin{bmatrix} u_{\text{ini}} \\ y_{\text{ini}} - w \end{bmatrix} = \begin{bmatrix} U_p \\ Y_p \end{bmatrix} g_{\text{ini}}. \tag{5.9}$$

Consider the solution $g_{\text{ini}}^* = U_p^\top \left(U_p U_p^\top\right)^{-1} u_{\text{ini}}$ to the first equation in (5.9), i.e., $U_p g_{\text{ini}}^* = u_{\text{ini}}$. Any other solution g_{ini} verifying $U_p g_{\text{ini}} = u_{\text{ini}}$ can be written as $g_{\text{ini}} = g_{\text{ini}}^* + M g_w$ for some $g_w \in \mathbb{R}^{T_d - (m+1)T_{\text{ini}} - T_f + 1}$, where $M = \mathcal{N}(U_p)$. Furthermore, from the second block row of (5.9), any w that makes $(u_{\text{ini}}, y_{\text{ini}} - w)$ a trajectory of $\mathcal{G}$ can be written as

$$w = -Y_p M g_w + \underbrace{(-Y_p g_{\text{ini}}^* + y_{\text{ini}})}_{w_0} \tag{5.10}$$

for some g_w.

In view of the above derivations, the feasible noise trajectories can be explicitly parameterized as follows.

Lemma 5.4.1. *The noise trajectory w is feasible if and only if there exists g_w satisfying* (5.10) *and*

$$\begin{bmatrix} 1 \\ g_w \end{bmatrix}^\top \underbrace{\begin{bmatrix} [A_w]_{11} & [A_w]_{12} \\ [A_w]_{12}^\top & [A_w]_{22} \end{bmatrix}}_{A_w} \begin{bmatrix} 1 \\ g_w \end{bmatrix} \geq 0, \tag{5.11}$$

where

$$\begin{aligned} [A_w]_{11} &= \Phi_{11} + w_0^\top \Phi_{12}^\top + \Phi_{12} w_0 + w_0^\top \Phi_{22} w_0, \\ [A_w]_{12} &= -\Phi_{12} Y_p M - w_0^\top \Phi_{22} Y_p M, \\ [A_w]_{22} &= M^\top Y_p^\top \Phi_{22} Y_p M. \end{aligned} \tag{5.12}$$

Proof. In addition to making $(u_{\text{ini}}, y_{\text{ini}} - w)$ a trajectory of $\mathcal{G}$, a feasible w should also satisfy the constraint (5.6). Substituting (5.10) into (5.6), we write the constraint on g_w as

$$\begin{aligned} \begin{bmatrix} 1 \\ w \end{bmatrix}^\top \Phi \begin{bmatrix} 1 \\ w \end{bmatrix} =& \Phi_{11} + (-Y_p M g_w + w_0)^\top \Phi_{12}^\top + \Phi_{12}(-Y_p M g_w + w_0) \\ &+ (-Y_p M g_w + w_0)^\top \Phi_{22} (-Y_p M g_w + w_0) \end{aligned}$$

$$= \begin{bmatrix} 1 \\ g_w \end{bmatrix}^\top A_w \begin{bmatrix} 1 \\ g_w \end{bmatrix},$$

with A_w defined in (5.11), (5.12). ■

Remark 5.4.1. *We note that, from* (5.10)*, for a given vector* g^*_{ini}*, there might be multiple* g_w *parameterizing the same noise trajectory* w*. In Section 5.4.4, we show that this redundancy increases the computational complexity of the proposed method, and provide a method to overcome this problem.*

5.4.2 Reformulation of the tracking error constraint

In this section, we show that, for a feasible noise trajectory w, the tracking error constraint $\text{LQTE}(u, y, w) \leq \gamma$ can be reformulated as a quadratic constraint on the parameter vector g_w. We achieve this goal by first writing the output y as an affine function of u and g_w, and then substituting the expression of y into the tracking error constraint.

To express y in terms of u and g_w, we compute g from the first three block rows of (5.7b), and substitute it into the last block row of (5.7b). First of all, we show how to construct a solution g from

$$\begin{bmatrix} U_p \\ Y_p \\ U_f \end{bmatrix} g = \begin{bmatrix} u_{\text{ini}} \\ y_{\text{ini}} - w \\ u \end{bmatrix}. \tag{5.13}$$

Since $(u_{\text{ini}}, y_{\text{ini}} - w)$ is a feasible system trajectory, in view of Lemma 5.2.2, for any given input u, there exists a (possibly nonunique) vector g verifying (5.13). Any solution g to (5.13) can be decomposed as $g \triangleq g_{\text{ini}} + g_u$, where g_{ini} verifies (5.9) and g_u solves

$$\begin{bmatrix} U_p \\ Y_p \\ U_f \end{bmatrix} g_u = \begin{bmatrix} \mathbf{0} \\ \mathbf{0} \\ u - U_f g_{\text{ini}} \end{bmatrix}. \tag{5.14}$$

Therefore, if we can find a solution g_u to (5.14), we can obtain a solution g to (5.13).

Before showing how to construct g_u in Lemma 5.4.2, the following results are needed. In view of Theorem 2 of [MDMVV89], the matrix $[U_p^\top, Y_p^\top, U_f^\top]^\top$ does not always have full row rank, even though $[U_p^\top, U_f^\top]^\top$ does. Therefore, there exists a row permutation matrix P_Y transforming Y_p as $P_Y Y_p = [Y_{p1}^\top, Y_{p2}^\top]^\top$ such that $\Lambda \triangleq [U_p^\top, Y_{p1}^\top, U_f^\top]^\top$ has full row rank and

$$\text{rank}\,(\Lambda) = \text{rank}\left(\begin{bmatrix} U_p \\ Y_p \\ U_f \end{bmatrix}\right).$$

Lemma 5.4.2. *A solution to* (5.14) *is given by*

$$g_u = \Lambda^\top(\Lambda\Lambda^\top)^{-1}\begin{bmatrix}\mathbf{0}\\ \mathbf{0}\\ u - U_f g_{\text{ini}}\end{bmatrix}. \tag{5.15}$$

Proof. Left multiply both sides of (5.14) with $\begin{bmatrix}\mathbf{I} & \mathbf{0} & \mathbf{0}\\ \mathbf{0} & P_Y & \mathbf{0}\\ \mathbf{0} & \mathbf{0} & \mathbf{I}\end{bmatrix}$ to obtain

$$\begin{bmatrix}U_p\\ Y_{p1}\\ Y_{p2}\\ U_f\end{bmatrix} g_u = \begin{bmatrix}\mathbf{0}\\ \mathbf{0}\\ \mathbf{0}\\ u - U_f g_{\text{ini}}\end{bmatrix}. \tag{5.16}$$

By definition, the rows of Y_{p2} can be written as linear combinations of the rows of $[U_p^\top, Y_{p1}^\top, U_f^\top]^\top$. Therefore there exists an ordered sequence of elementary row operations $\{E_k\}_{k=1}^{e}$ captured by the matrix $E \triangleq E_e E_{e-1} \dots E_1$ such that

$$E\begin{bmatrix}U_p\\ Y_{p1}\\ Y_{p2}\\ U_f\end{bmatrix} = \begin{bmatrix}U_p\\ Y_{p1}\\ \mathbf{0}\\ U_f\end{bmatrix}. \tag{5.17}$$

We next show by contradiction that the rows of Y_{p2} can also be written as linear combinations of the rows of $[U_p^\top, Y_{p1}^\top]^\top$. For this purpose, suppose that this is not the case. Then, necessarily, the matrix E also operates on the rows of U_f. Consequently, left multiplying E to both sides of (5.16), we obtain

$$\begin{bmatrix}U_p\\ Y_{p1}\\ \mathbf{0}\\ U_f\end{bmatrix} g_u = \begin{bmatrix}\mathbf{0}\\ \mathbf{0}\\ \text{linear combination of rows of } u - U_f g_{\text{ini}}\\ u - U_f g_{\text{ini}}\end{bmatrix}. \tag{5.18}$$

Since $[\mathbf{0}^\top, \mathbf{0}^\top]^\top$ is a feasible system trajectory for any LTI system, in view of Lemma 5.2.2, there always exists a g_u solving (5.14). Therefore, (5.14) and further (5.16), (5.18) should always be solvable for any $u - U_f g_{\text{ini}}$. However, it is clear from the third block row of (5.18) that, (5.18) is not always solvable for any $u - U_f g_{\text{ini}}$. This makes a contradiction. Therefore, the rows of Y_{p2} can be written as linear combinations of the rows of $[U_p^\top, Y_{p1}^\top]^\top$. As a result, the matrix E can be constructed such that

$$E\begin{bmatrix}\mathbf{0}\\ \mathbf{0}\\ \mathbf{0}\\ u - U_f g_{\text{ini}}\end{bmatrix} = \begin{bmatrix}\mathbf{0}\\ \mathbf{0}\\ \mathbf{0}\\ u - U_f g_{\text{ini}}\end{bmatrix}, \tag{5.19}$$

that is, the matrix E only applies elementary row operations on the first three block rows of $[\mathbf{0}^\top, \mathbf{0}^\top, \mathbf{0}^\top, (u - U_f g_{\text{ini}})^\top]^\top$.

The vector g_u in (5.15) satisfies

$$\begin{bmatrix} U_p \\ Y_{p1} \\ U_f \end{bmatrix} g_u = \begin{bmatrix} \mathbf{0} \\ \mathbf{0} \\ u - U_f g_{\text{ini}} \end{bmatrix}.$$

Then, we have

$$\begin{bmatrix} U_p \\ Y_{p1} \\ \mathbf{0} \\ U_f \end{bmatrix} g_u = \begin{bmatrix} \mathbf{0} \\ \mathbf{0} \\ \mathbf{0} \\ u - U_f g_{\text{ini}} \end{bmatrix}. \tag{5.20}$$

Left multiplying both sides of (5.20) by E^{-1}, in view of (5.17) and (5.19), one obtains

$$\begin{bmatrix} U_p \\ Y_{p1} \\ Y_{p2} \\ U_f \end{bmatrix} g_u = \begin{bmatrix} \mathbf{0} \\ \mathbf{0} \\ \mathbf{0} \\ u - U_f g_{\text{ini}} \end{bmatrix}.$$

Furthermore, from the definition of P_Y, we have

$$\begin{bmatrix} U_p \\ Y_p \\ U_f \end{bmatrix} = \begin{bmatrix} \mathbf{I} & \mathbf{0} & \mathbf{0} \\ \mathbf{0} & P_Y^{-1} & \mathbf{0} \\ \mathbf{0} & \mathbf{0} & \mathbf{I} \end{bmatrix} \begin{bmatrix} U_p \\ \begin{bmatrix} Y_{p1} \\ Y_{p2} \end{bmatrix} \\ U_f \end{bmatrix}.$$

Therefore, we conclude the proof by showing that

$$\begin{bmatrix} U_p \\ Y_p \\ U_f \end{bmatrix} g_u = \begin{bmatrix} \mathbf{I} & \mathbf{0} & \mathbf{0} \\ \mathbf{0} & P_Y^{-1} & \mathbf{0} \\ \mathbf{0} & \mathbf{0} & \mathbf{I} \end{bmatrix} \begin{bmatrix} \mathbf{0} \\ \begin{bmatrix} \mathbf{0} \\ \mathbf{0} \end{bmatrix} \\ u - U_f g_{\text{ini}} \end{bmatrix} = \begin{bmatrix} \mathbf{0} \\ \begin{bmatrix} \mathbf{0} \\ \mathbf{0} \end{bmatrix} \\ u - U_f g_{\text{ini}} \end{bmatrix}.$$

■

A solution $g = g_{\text{ini}} + g_u$ to (5.13) can be obtained from a g_{ini} verifying (5.9) and the g_u in Lemma 5.4.2. We next show that y can be expressed as an affine function of u and g_w, and further reformulate the tracking error constraint in terms of u and g_w.

Lemma 5.4.3. *Given a feasible noise trajectory w and a control sequence u, the unique output y satisfying* (5.7b) *is given by*

$$y = B_u u + B_w g_w + y_0, \tag{5.21}$$

where g_w *parameterizes* w *through* (5.10), $y_0 = B_{\text{ini}} g^*_{\text{ini}}$, $B_w = B_{\text{ini}} M$,

$$B_{\text{ini}} = Y_f \left(\mathbf{I} + \Lambda^\top (\Lambda\Lambda^\top)^{-1} \begin{bmatrix} \mathbf{0} \\ \mathbf{0} \\ -U_f \end{bmatrix} \right), \quad \textit{and} \quad B_u = Y_f \Lambda^\top (\Lambda\Lambda^\top)^{-1} \begin{bmatrix} \mathbf{0} \\ \mathbf{0} \\ \mathbf{I} \end{bmatrix}.$$

Moreover, the tracking error constraint $\text{LQTE}(u, y, w) \leq \gamma$ *can be equivalently expressed as*

$$\begin{bmatrix} 1 \\ g_w \end{bmatrix}^\top \underbrace{\begin{bmatrix} [Q_g]_{11} & [Q_g]_{12} \\ [Q_g]_{12}^\top & [Q_g]_{22} \end{bmatrix}}_{Q_g(u,\gamma)} \begin{bmatrix} 1 \\ g_w \end{bmatrix} \geq 0, \tag{5.22}$$

where

$$\begin{aligned} &\bar{R} = \mathbf{I} \otimes R, \quad \bar{Q} = \mathbf{I} \otimes Q, \\ &[Q_g]_{11} = \gamma - u^\top \bar{R} u - (B_u u + y_0 - r)^\top \bar{Q} (B_u u + y_0 - r), \\ &[Q_g]_{12} = -(B_u u + y_0 - r)^\top \bar{Q} B_w, \quad [Q_g]_{22} = -B_w^\top \bar{Q} B_w. \end{aligned}$$

Proof. As $g = g_{\text{ini}} + g_u$ solves (5.13), by substituting it into the fourth block row of (5.7b), one obtains

$$\begin{aligned} y &= Y_f g_{\text{ini}} + Y_f g_u \\ &= Y_f g_{\text{ini}} + Y_f \Lambda^\top (\Lambda\Lambda^\top)^{-1} \left(\begin{bmatrix} \mathbf{0} \\ \mathbf{0} \\ \mathbf{I} \end{bmatrix} u + \begin{bmatrix} \mathbf{0} \\ \mathbf{0} \\ -U_f \end{bmatrix} g_{\text{ini}} \right) \\ &= B_{\text{ini}} g_{\text{ini}} + B_u u = B_{\text{ini}} (g^*_{\text{ini}} + M g_w) + B_u u, \end{aligned}$$

which proves (5.21). We then have the following equivalent conditions

$$\begin{aligned} &\text{LQTE}(u, y, w) \leq \gamma \Leftrightarrow \gamma - u^\top \bar{R} u - (y - r)^\top \bar{Q} (y - r) \geq 0, \\ &\Leftrightarrow \gamma - u^\top \bar{R} u - (y_0 + B_w g_w + B_u u - r)^\top \bar{Q} (y_0 + B_w g_w + B_u u - r) \geq 0, \\ &\Leftrightarrow (5.22). \end{aligned}$$

■

5.4.3 Main result

The following theorem leverages the results obtained in Lemmas 5.4.1 and 5.4.3 to show that (5.8) and, hence, **P1**, are equivalent to an SDP.

Theorem 5.4.1. *The robust tracking control problem* ***P1*** *is equivalent to solving*

$$\min_{u,\gamma,\alpha \geq 0} \ \gamma \tag{5.23a}$$

$$\text{s.t.,} \begin{bmatrix} (\bar{R} + B_u^\top \bar{Q} B_u)^{-1} & \begin{bmatrix} u & \mathbf{0} \end{bmatrix} \\ \begin{bmatrix} u^\top \\ \mathbf{0} \end{bmatrix} & Q_g^a(u,\gamma) - \alpha A_w \end{bmatrix} \succeq 0, \tag{5.23b}$$

where

$$Q_g^a(u,\gamma) = Q_g(u,\gamma) + \begin{bmatrix} u^\top (R + B_u^\top \bar{Q} B_u) u & \mathbf{0} \\ \mathbf{0} & \mathbf{0} \end{bmatrix}, \tag{5.24}$$

A_w is defined in Lemma 5.4.1, and $\bar{Q}$, $\bar{R}$, Q_g, and B_u are defined in Lemma 5.4.3.

Proof. Based on Lemma 5.4.1 and Lemma 5.4.3, the minimization problem (5.8) is equivalent to

$$\begin{aligned} \min_{u,\gamma} \quad & \gamma \\ \text{s.t.,} \quad & (5.22) \text{ holds } \forall g_w \text{ satisfying } (5.11). \end{aligned}$$

In view of the S-lemma [PT07], the constraint of this minimization problem holds if and only if there exist u and $\alpha \geq 0$ such that

$$Q_g(u,\gamma) - \alpha A_w \succeq 0.$$

Using Schur complement [BEGFB94], the above matrix inequality can be transformed into the LMI in (5.23b). Note that the quadratic term $u^\top (R + B_u^\top \bar{Q} B_u) u$ in the right hand side of (5.24) cancels out with the quadratic term of u in $Q_g(u,\gamma)$, therefore making $Q_g^a(u,\gamma)$ a linear function of u and γ. Minimizing the performance index γ further gives the solution of (5.8) and hence **P1**. ■

5.4.4 Implementation aspects: Dimension reduction for computational efficiency

Recall from the analysis in Section 5.4.1 that the sequence w makes $(u_{\text{ini}}, y_{\text{ini}} - w)$ a trajectory of $\mathcal{G}$ if and only if there exists g_w, such that

$$w = -Y_p \mathcal{N}(U_p) g_w + w_0. \tag{5.25}$$

However, if g_w is mapped into w through (5.25), any $g_w + v$, where $v \in \ker(Y_p \mathcal{N}(U_p))$, is also mapped into the same w. This is especially true when the length T_d of historical data is large, i.e., $T_d \gg mT_{\text{ini}}$ and $T_d \gg pT_{\text{ini}}$, which makes $\ker(U_p) \cap \ker(Y_p)$ and, therefore, $\ker(Y_p \mathcal{N}(U_p))$ nonempty. As a result, any parameterization of a subspace through g_w is redundant. Redundancy affects also the constraint (5.23b). Indeed, if the length of the vector g_w is unnecessarily large, so are the sizes of the matrices A_w and $Q_g(u,\gamma)$ in (5.11), (5.22), as well as the LMI constraint in (5.23b), making the optimization problem (5.23) inefficient.

More formally, denote $\mathcal{W}$ as the set of noise trajectories w that make $(u_{\text{ini}}, y_{\text{ini}} - w)$ a trajectory of $\mathcal{G}$. We have, from (5.25), $\mathcal{W} = \text{range}(Y_p\mathcal{N}(U_p)) \oplus w_0$, where the vector space $\text{range}(Y_p\mathcal{N}(U_p))$ is represented as

$$\{Y_p\mathcal{N}(U_p)g_w | g_w \in \mathbb{R}^{T_d-(m+1)T_{\text{ini}}-T_f+1}\}. \tag{5.26}$$

The cause of redundancy is that the dimension of the free vector g_w in (5.26) can be much larger than the dimension of $\text{range}(Y_p\mathcal{N}(U_p))$. In the following theorem, we address this issue to present a non-redundant representation of $\mathcal{W}$.

Theorem 5.4.2. *The vector w belongs to $\mathcal{W}$ if and only if there exists $g_w \in \mathbb{R}^{\bar{n}_w}$ such that*

$$w = -Y_p\mathcal{N}(U_p)\mathcal{R}(\mathcal{N}(U_p)^\top Y_p^\top)g_w + w_0, \tag{5.27}$$

where $\bar{n}_w = \text{rank}(Y_p\mathcal{N}(U_p))$. Moreover, the above mapping from $\mathbb{R}^{\bar{n}_w}$ to $\mathcal{W}$ is bijective.

Proof. Note that two vector spaces are isomorphic if and only if they have the same dimension. As such, to eliminate the redundant representation problem, we introduce an isomorphism from $\mathbb{R}^{\bar{n}_w}$ to $\text{range}(Y_p\mathcal{N}(U_p))$ and represent $\text{range}(Y_p\mathcal{N}(U_p))$ in terms of this isomorphism. Notice that

$$\begin{aligned}
\text{range}(Y_p\mathcal{N}(U_p)) &= \{Y_p\mathcal{N}(U_p)g | g \in \mathbb{R}^{T_d-T_{\text{ini}}+1-T_{\text{ini}}m}\} \\
&\overset{(a)}{=} \{Y_p\mathcal{N}(U_p)(g_1+g_2) | g_1 \in \ker(Y_p\mathcal{N}(U_p)),\ g_2 \in \text{range}(\mathcal{N}(U_p)^\top Y_p^\top)\} \\
&= \{Y_p\mathcal{N}(U_p)g_2 | g_2 \in \text{range}(\mathcal{N}(U_p)^\top Y_p^\top)\} \\
&= \{Y_p\mathcal{N}(U_p)\mathcal{R}(\mathcal{N}(U_p)^\top Y_p^\top)g_w | g_w \in \mathbb{R}^{\bar{n}_w}\}
\end{aligned}$$

where (a) follows from the fact that

$$\ker(Y_p\mathcal{N}(U_p)) \perp \text{range}(\mathcal{N}(U_p)^\top Y_p^\top).$$

Therefore, an isomorphism from $\mathbb{R}^{\bar{n}_w}$ to $\text{range}(Y_p\mathcal{N}(U_p))$ is given by the matrix $Y_p\mathcal{N}(U_p)\mathcal{R}(\mathcal{N}(U_p)^\top Y_p^\top)$. Furthermore, since $\mathcal{W}$ is $\text{range}(Y_p\mathcal{N}(U_p))$ shifted by w_0, the mapping from $\mathbb{R}^{\bar{n}_w}$ to $\mathcal{W}$ given by (5.27) is bijective. ■

In view of the above theorem, the representation of $\mathcal{W}$ through (5.27) using $g_w \in \mathbb{R}^{\bar{n}_w}$ is non-redundant. To apply the above result in the implementation of (5.23), we only need to replace the matrix $M = \mathcal{N}(U_p)$ in the derivations of Section 5.4.1–5.4.3 with $M = \mathcal{N}(U_p)\mathcal{R}(\mathcal{N}(U_p)^\top Y_p^\top)$.

Remark 5.4.2. *Since*

$$\bar{n}_w = \text{rank}\left(\begin{bmatrix} U_p \\ Y_p \end{bmatrix}\right) - T_{\text{ini}}m \overset{(a)}{=} n,$$

where (a) follows from Theorem 2 of [MDMVV89], the length of the vector g_w in (5.27) *is equal to n. This guarantees that the size of the matrix in the LMI in* (5.23b) *scales*

with $n + T_f m$. On the contrary, the length of the vector g_w in (5.10) *scales with T_d. As T_d is usually significantly larger than n, the non-redundant parameterization shown in this section can reduce the size of the LMI constraint* (5.23b) *considerably.*

5.5 Generalizations

In this section, we provide several extensions to the robust control design method described in the previous section. First, in Section 5.5.1, we show how to add input and output constraints to the controller. In Section 5.5.2, we show how to take into account actuator disturbances, before presenting the overall LMI optimization problem incorporating both extensions in Section 5.5.3.

5.5.1 Input and output constraints

In this section, we show how to add quadratic input and output constraints to problem **P1**. Since constraints on the input can be directly incorporated into (5.23), hereafter we focus on constraints on the output y only and in the form

$$\theta(y) = \begin{bmatrix} 1 \\ y \end{bmatrix}^\top \underbrace{\begin{bmatrix} \Theta_{11} & \Theta_{12} \\ \Theta_{12}^\top & \Theta_{22} \end{bmatrix}}_{\Theta} \begin{bmatrix} 1 \\ y \end{bmatrix} \geq 0. \tag{5.28}$$

When $\Theta_{22} = \Theta_{22}^\top \prec 0$ and $\Theta_{12} = 0$, the above constraint imposes an upper bound on $\|y\|_2$.

Since the output is related to the input u and the noise trajectory w via (5.21), the output constraint (5.28) can be written as

$$\begin{aligned} &\Theta_{11} + \Theta_{12}\left(y_0 + B_u u + B_w g_w\right) + \left(y_0 + B_u u + B_w g_w\right)^\top \Theta_{12}^\top \\ &\quad + \left(y_0 + B_u u + B_w g_w\right)^\top \Theta_{22}\left(y_0 + B_u u + B_w g_w\right) \\ &\quad = \begin{bmatrix} 1 \\ g_w \end{bmatrix}^\top \underbrace{\begin{bmatrix} [\Theta_g]_{11} & [\Theta_g]_{12} \\ [\Theta_g]_{12}^\top & [\Theta_g]_{22} \end{bmatrix}}_{\Theta_g} \begin{bmatrix} 1 \\ g_w \end{bmatrix} \geq 0, \end{aligned}$$

where

$$\begin{aligned} [\Theta_g]_{22} &= B_w^\top \Theta_{22} B_w, \\ [\Theta_g]_{11} &= \Theta_{11} + \Theta_{12}\left(y_0 + B_u u\right) + \left(y_0 + B_u u\right)^\top \Theta_{12}^\top \\ &\quad + \left(y_0 + B_u u\right)^\top \Theta_{22}\left(y_0 + B_u u\right), \\ [\Theta_g]_{12} &= \Theta_{12} B_w + \left(y_0 + B_u u\right)^\top \Theta_{22} B_w. \end{aligned}$$

In principle, we want the constraint (5.28) to hold for all feasible noise trajectories. Similarly to the proof of Theorem 5.4.1, this requirement is equivalent to the existence of $\alpha_y \geq 0$ such that $\Theta_g - \alpha_y A_w \succeq 0$, which can be reformulated as an LMI constraint and added to the optimization problem (5.23).

5.5.2 Actuator disturbances

In this section, we show how to consider actuator disturbances. Suppose the actuation input $\check{u}_{\text{ini}}$ to the system $\mathcal{G}$ to generate the recent data is also noisy, i.e.,

$$\check{u}_{\text{ini}} = u_{\text{ini}} - d_{\text{ini}},$$

where u_{ini} is nominal control input and $-d_{\text{ini}}$ is the actuator disturbance[2]. Moreover, we also consider a disturbance $-d$ acting on the computed control input u, i.e., $\check{u} = u - d$. Therefore, the data-dependent relation (5.7b) becomes

$$\begin{bmatrix} U_p \\ Y_p \\ U_f \\ Y_f \end{bmatrix} g = \begin{bmatrix} u_{\text{ini}} \\ y_{\text{ini}} \\ u \\ y \end{bmatrix} - \begin{bmatrix} d_{\text{ini}} \\ w \\ d \\ \mathbf{0} \end{bmatrix}. \tag{5.29}$$

We assume that the actuator disturbance $\bar{d} \triangleq [d_{\text{ini}}^\top, d^\top]^\top$ satisfies the quadratic constraint

$$\begin{bmatrix} 1 \\ \bar{d} \end{bmatrix}^\top \underbrace{\begin{bmatrix} \Phi_{d,11} & \Phi_{d,12} \\ \Phi_{d,12}^\top & \Phi_{d,22} \end{bmatrix}}_{\Phi_d} \begin{bmatrix} 1 \\ \bar{d} \end{bmatrix} \geq 0, \tag{5.30}$$

where $\Phi_{d,22} \prec 0$.

Our goal is to solve a min-max robust control problem similar to **P1**. Due to the existence of actuator disturbances, we replace $\|u\|_R^2$ with the true system input $\|\check{u}\|_R^2$ in the cost (5.7a), replace (5.7b) with (5.29), and optimize over all feasible noise and disturbance trajectories $[d_{\text{ini}}^\top, w^\top, d^\top]^\top$. We first characterize feasible trajectories $[d_{\text{ini}}^\top, w^\top]^\top$ such that $(u_{\text{ini}} - d_{\text{ini}}, y_{\text{ini}} - w)$ is a trajectory of $\mathcal{G}$. Similarly to the argument in Section 5.4.1, $[d_{\text{ini}}^\top, w^\top]^\top$ satisfies the above requirement if and only if there exists g_{ini} such that

$$\begin{bmatrix} d_{\text{ini}} \\ w \end{bmatrix} = -\begin{bmatrix} U_p \\ Y_p \end{bmatrix} g_{\text{ini}} + \begin{bmatrix} u_{\text{ini}} \\ y_{\text{ini}} \end{bmatrix}. \tag{5.31}$$

Therefore, the set of noise and disturbance trajectories $[d_{\text{ini}}^\top, w^\top]^\top$ that make $(u_{\text{ini}} -$

[2]Note that the sign of the disturbance term is chosen for the clarity of the following derivations, and is without loss of generality.

$d_{\text{ini}}, y_{\text{ini}} - w)$ a trajectory of $\mathcal{G}$ is

$$\tilde{\mathcal{W}} = \text{range}\left(\begin{bmatrix} U_p \\ Y_p \end{bmatrix}\right) + \begin{bmatrix} u_{\text{ini}} \\ y_{\text{ini}} \end{bmatrix}.$$

Let $\bar{n}_d = \text{rank}\left(\left[\begin{smallmatrix} U_p \\ Y_p \end{smallmatrix}\right]\right) = \bar{n}_w + mT_{\text{ini}}$. Similarly to the analysis in Section 5.4.4, $[d_{\text{ini}}^\top, w^\top]^\top \in \tilde{\mathcal{W}}$ if and only if there exists $g_w \in \mathbb{R}^{\bar{n}_d}$ such that

$$\begin{bmatrix} d_{\text{ini}} \\ w \end{bmatrix} = -\begin{bmatrix} U_p \\ Y_p \end{bmatrix} \mathcal{R}\left(\begin{bmatrix} U_p \\ Y_p \end{bmatrix}^\top\right) g_w + \begin{bmatrix} u_{\text{ini}} \\ y_{\text{ini}} \end{bmatrix}. \tag{5.32}$$

Moreover, the above mapping from $\mathbb{R}^{\bar{n}_d}$ to $\tilde{\mathcal{W}}$ is bijective. Therefore, from (5.32), one gets

$$\begin{bmatrix} \begin{bmatrix} d_{\text{ini}} \\ w \end{bmatrix} \\ d \end{bmatrix} = \begin{bmatrix} -\begin{bmatrix} U_p \\ Y_p \end{bmatrix} \mathcal{R}\left(\begin{bmatrix} U_p \\ Y_p \end{bmatrix}^\top\right) & \mathbf{0} \\ \mathbf{0} & \mathbf{I} \end{bmatrix} \underbrace{\begin{bmatrix} g_w \\ d \end{bmatrix}}_{\bar{g}} + \begin{bmatrix} \begin{bmatrix} u_{\text{ini}} \\ y_{\text{ini}} \end{bmatrix} \\ \mathbf{0} \end{bmatrix}, \tag{5.33}$$

i.e., the vector $\bar{g} \in \mathbb{R}^{\bar{n}_d + mT_f}$ parameterizes all feasible noise and disturbance trajectories. By following the arguments used in the proof of Lemma 5.4.1, the quadratic constraints on w and $\bar{d}$ can be transformed into quadratic constraints on $\bar{g}$ as

$$\begin{bmatrix} 1 \\ w \end{bmatrix}^\top \Phi \begin{bmatrix} 1 \\ w \end{bmatrix} \geq 0 \iff \begin{bmatrix} 1 \\ \bar{g} \end{bmatrix}^\top \bar{\Phi}_w \begin{bmatrix} 1 \\ \bar{g} \end{bmatrix} \geq 0, \tag{5.34}$$

$$\begin{bmatrix} 1 \\ \bar{d} \end{bmatrix}^\top \Phi_d \begin{bmatrix} 1 \\ \bar{d} \end{bmatrix} \geq 0 \iff \begin{bmatrix} 1 \\ \bar{g} \end{bmatrix}^\top \bar{\Phi}_d \begin{bmatrix} 1 \\ \bar{g} \end{bmatrix} \geq 0, \tag{5.35}$$

where the matrices $\bar{\Phi}_w$ and $\bar{\Phi}_d$ directly follow from (5.6), (5.30), and (5.33), and their expressions are omitted for brevity.

Since every $[d_{\text{ini}}^\top, w^\top]^\top \in \tilde{\mathcal{W}}$ can be written as (5.32), by substituting this representation into (5.31), we obtain that for a given $[d_{\text{ini}}^\top, w^\top]^\top$, the solution g_{ini} to (5.31) is given by $g_{\text{ini}} = M_d g_w$, where $M_d = \mathcal{R}\left(\left[\begin{smallmatrix} U_p \\ Y_p \end{smallmatrix}\right]^\top\right)$. We can follow the procedure in Section 5.4.2 to derive the solution $g = g_{\text{ini}} + g_u$ to the first three equations in (5.29), where $g_u = \Lambda^\top(\Lambda\Lambda^\top)^{-1}\begin{bmatrix} \mathbf{0} & \mathbf{0} & (\check{u} - U_f g_{\text{ini}})^\top \end{bmatrix}^\top$ verifies (5.14) with the noisy control input $\check{u}$ instead of u. Then, since $y = Y_f g$, the following holds with the matrices B_{ini} and B_u defined in Lemma 5.4.3:

$$y = B_{\text{ini}} g_{\text{ini}} + B_u \check{u} = B_{\text{ini}} M_d g_w - B_u d + B_u u = \underbrace{\begin{bmatrix} B_{\text{ini}} M_d & -B_u \end{bmatrix}}_{\bar{B}_g} \bar{g} + B_u u.$$

Since $\check{u} = u - \Xi\bar{g}$, where $\Xi = [\mathbf{0}, \mathbf{I}]$, the performance constraint can be rewritten as

$$\begin{aligned}\gamma - \sum_{k=0}^{T_f-1} \left(\|y_k - r_{t+k}\|_Q^2 + \|\check{u}_k\|_R^2\right) =& \gamma - \check{u}^\top \bar{R}\check{u} - (y-r)^\top \bar{Q}(y-r) \\ =& \gamma - (u - \Xi\bar{g})^\top \bar{R}\,(u - \Xi\bar{g}) \\ &- (\bar{B}_g\bar{g} + B_u u - r)^\top \bar{Q}(\bar{B}_g\bar{g} + B_u u - r) \\ =& \begin{bmatrix}1\\ \bar{g}\end{bmatrix}^\top \underbrace{\begin{bmatrix}[\bar{Q}_g]_{11} & [\bar{Q}_g]_{12}\\ [\bar{Q}_g]_{12}^\top & [\bar{Q}_g]_{22}\end{bmatrix}}_{\bar{Q}_g(u,\gamma)} \begin{bmatrix}1\\ \bar{g}\end{bmatrix} \geq 0,\end{aligned}$$

where

$$\begin{aligned}[\bar{Q}_g]_{11} &= \gamma - u^\top \bar{R}u - (B_u u - r)^\top \bar{Q}\,(B_u u - r)\,,\\ [\bar{Q}_g]_{12} &= u^\top \bar{R}\Xi - (B_u u - r)^\top \bar{Q}\bar{B}_g,\\ [\bar{Q}_g]_{22} &= -\Xi^\top \bar{R}\Xi - \bar{B}_g^\top \bar{Q}\bar{B}_g.\end{aligned}$$

As such, the overall data-driven robust control objective is to find u and γ such that

$$\begin{bmatrix}1\\ \bar{g}\end{bmatrix}^\top \bar{Q}_g(u,\gamma) \begin{bmatrix}1\\ \bar{g}\end{bmatrix} \geq 0$$

holds for all feasible noise and disturbance trajectories parameterized by $\bar{g}$ satisfying quadratic constraints (5.34), (5.35). Using the S-lemma for multiple quadratic inequalities [PT07], this is true if there exist u, $\alpha_w \geq 0$, and $\alpha_d \geq 0$ such that

$$\bar{Q}_g(u,\gamma) - \alpha_w\bar{\Phi}_w - \alpha_d\bar{\Phi}_d \succeq 0. \tag{5.36}$$

We can further convert the above inequality into an LMI through the Schur complement. Therefore, the problem **P1** with input disturbances is solved if the following optimization problem is solved

$$\min_{u,\gamma,\alpha_w\geq 0,\alpha_d\geq 0} \gamma \quad \text{s.t., (5.36).}$$

5.5.3 Co-existence of constraints and actuator disturbances

In this section, we use the results in Sections 5.5.1 and 5.5.2 for dealing simultaneously with the quadratic input/output constraints and actuator disturbances. The overall robust control problem is given by

$$\min_{u} \max_{w,d_{\text{ini}},d} \quad \sum_{k=0}^{T_f-1} \left(\|y_k - r_k\|_Q^2 + \|u_k - d_k\|_R^2\right) \tag{5.37a}$$

$$\text{subject to} \quad \begin{bmatrix} U_p \\ Y_p \\ U_f \\ Y_f \end{bmatrix} g = \begin{bmatrix} u_{\text{ini}} \\ y_{\text{ini}} \\ u \\ y \end{bmatrix} - \begin{bmatrix} d_{\text{ini}} \\ w \\ d \\ \mathbf{0} \end{bmatrix}, \tag{5.37b}$$

$$\begin{bmatrix} 1 \\ u-d \end{bmatrix}^\top \underbrace{\begin{bmatrix} \Psi_{11} & \Psi_{12} \\ \Psi_{12}^\top & \Psi_{22} \end{bmatrix}}_{\Psi} \begin{bmatrix} 1 \\ u-d \end{bmatrix} \geq 0, \tag{5.37c}$$

$$\text{output constraint (5.28).} \tag{5.37d}$$

The following theorem provides an LMI-based representation of (5.37)[3].

Theorem 5.5.1. *Define* $\alpha \triangleq [\alpha_w, \alpha_d, \alpha_{u,w}, \alpha_{u,d}, \alpha_{y,w}, \alpha_{y,d}]^\top$. *The optimization problem* (5.37) *is solved when the following minimization problem is solved:*

$$\min_{u,\gamma,\alpha\geq 0} \gamma \quad s.t., \ (5.36), \ (5.41), \ (5.44), \tag{5.38}$$

where constraints (5.41) *and* (5.44) *are given in the proof.*

Proof. Similarly to the proof of Theorem 5.4.1, we aim to minimize γ, subject to the tracking error constraint and the constraint that the input/output constraints hold for all feasible noise and disturbance trajectories. The tracking error constraint can be shown to be given as (5.36). In the following, we show how to characterize the constraint that the input/output constraints hold for all feasible noise and disturbance trajectories.

In light of $\check{u} = u - \Xi\bar{g}$, one sees that the input constraint in (5.37c) is equivalent to

$$\bar{\psi}(\bar{g}) = \begin{bmatrix} 1 \\ \bar{g} \end{bmatrix}^\top \underbrace{\begin{bmatrix} [\bar{\Psi}]_{11} & [\bar{\Psi}]_{12} \\ [\bar{\Psi}]_{12}^\top & [\bar{\Psi}]_{22} \end{bmatrix}}_{\bar{\Psi}} \begin{bmatrix} 1 \\ \bar{g} \end{bmatrix} \geq 0, \tag{5.39}$$

where

$$\begin{aligned} [\bar{\Psi}]_{11} &= \Psi_{11} + u^\top \Psi_{22} u + \Psi_{12} u + u^\top \Psi_{12}^\top, \\ [\bar{\Psi}]_{12} &= -\Psi_{12}\Xi - u^\top \Psi_{22}\Xi, \qquad [\bar{\Psi}]_{22} = \Xi^\top \Psi_{22}\Xi. \end{aligned} \tag{5.40}$$

We need to ensure that (5.39) holds for all $\bar{g}$ satisfying the quadratic constraints (5.34), (5.35). In view of the S-lemma, this is possible if there exist u, $\alpha_{u,w} \geq 0$, and $\alpha_{u,d} \geq 0$

[3]Even though the matrix inequalities in the theorem and proof are not LMIs, they can be transformed to LMIs using Schur complement in a similar way to the proof of Theorem 5.4.1. To save space, the resulting LMIs are not displayed. Furthermore, we refer to these matrix inequalities as LMIs without ambiguity.

such that

$$\bar{\Psi} - \alpha_{u,w}\bar{\Phi}_w - \alpha_{u,d}\bar{\Phi}_d \succeq 0, \tag{5.41}$$

which can be converted to an LMI. Similarly, considering $y = \bar{B}_g\bar{g} + B_u u$, the output constraint in (5.28) is equivalent to

$$\bar{\theta}(\bar{g}) = \begin{bmatrix} 1 \\ \bar{g} \end{bmatrix}^\top \underbrace{\begin{bmatrix} [\bar{\Theta}]_{11} & [\bar{\Theta}]_{12} \\ [\bar{\Theta}]_{12}^\top & [\bar{\Theta}]_{22} \end{bmatrix}}_{\bar{\Theta}} \begin{bmatrix} 1 \\ \bar{g} \end{bmatrix} \geq 0, \tag{5.42}$$

where

$$\begin{aligned} [\bar{\Theta}]_{11} &= \Theta_{11} + u^\top B_u^\top \Theta_{22} B_u u + \Theta_{12} B_u u + u^\top B_u^\top \Theta_{12}^\top, \\ [\bar{\Theta}]_{12} &= \Psi_{12}\bar{B}_g + u^\top B_u^\top \Theta_{22}\bar{B}_g, \qquad [\bar{\Theta}]_{22} = \bar{B}_g^\top \Theta_{22}\bar{B}_g. \end{aligned} \tag{5.43}$$

Following the same procedure as for input constraint, it can be shown that (5.42) is satisfied if there exist u, $\alpha_{y,w} \geq 0$, and $\alpha_{y,d} \geq 0$ such that the following is satisfied:

$$\bar{\Theta} - \alpha_{y,w}\bar{\Phi}_w - \alpha_{y,d}\bar{\Phi}_d \succeq 0, \tag{5.44}$$

which can be converted to an LMI. Combining the above results, we get (5.38). ■

Remark 5.5.1. *The extensions presented in this section involve the use of the S-lemma with multiple quadratic constraints [PT07] and Schur complement with semidefinite matrices [BEGFB94], which are only sufficient. Therefore, the control design procedure in* (5.38) *is conservative, i.e., it may have no solution even though a control input u solving the min-max control problem* (5.37) *exists.*

Remark 5.5.2. *The proposed control design can be easily applied in a receding horizon fashion, in order to implement a data-driven predictive controller. In doing so, at each time instance, one needs to update the output reference r as well as recent input and output data u_{ini} and y_{ini} with the online data, solve* (5.38)*, and apply only the first control input from the computed optimal control sequence u. Moreover, it can be shown that the resulting controller is equivalent to a robust model predictive controller (MPC) with bounded uncertainty on the initial state. As such, the stability of the resulting closed-loop system can be studied using the existing results on robust MPC. Such a discussion is omitted so as to emphasize the robust data-driven nature of the proposed controller, which is the main contribution.*

5.6 Simulation results

We illustrate the performance of the proposed controller through numerical simulations, where we consider an unstable LTI system (5.1) with randomly selected system matrices

$$A = \begin{bmatrix} 0.6799 & -0.0331 & -0.8332 & 0.4924 \\ 0.9748 & 1.0060 & 0.3666 & 0.5863 \\ 0.7311 & 0.3693 & -1.0711 & 0.1603 \\ -0.7442 & 0.0330 & 0.0667 & 0.1961 \end{bmatrix}, \quad B = \begin{bmatrix} -0.7841 & -0.1798 & -0.0757 \\ 0.5204 & -0.5806 & -0.6510 \\ 0.1974 & 0.2140 & -0.4851 \\ -0.9378 & 0.7881 & -0.1826 \end{bmatrix},$$

$$C = \begin{bmatrix} 0.4458 & 0.4911 & 0.7394 & -0.1359 \\ 0.0733 & -0.1468 & -0.6357 & 0.7353 \end{bmatrix}, \quad D = \mathbf{0}.$$

By choosing a random initial condition, historical input-output data of length $T_d = 110$ are collected with inputs generated from a uniform distribution in the interval $[-1, 1]$. We assume that the exact order $n = 4$ of the system is unknown and only the upper bound $\bar{n} = 6$ is available. Consequently, *recent* input-output data of length $T_{\text{ini}} = \bar{n} = 6 \geq \mathbf{l}(\mathcal{G})$ are collected with inputs from the uniform distribution in $[-1, 1]$. Moreover, recent data is corrupted by input disturbances and output noises as in Section 5.5.3, where the trajectories w and $\bar{d}$ are selected to satisfy quadratic constraints (5.6) and (5.30), respectively, with

$$\begin{aligned} \Phi_{11} = T_{\text{ini}} p\epsilon, \;\; \Phi_{12} = \mathbf{0}, \;\; \Phi_{22} = -\mathbf{I}, \\ \Phi_{d,11} = (T_{\text{ini}} + T_f)\, m\epsilon, \;\; \Phi_{d,12} = \mathbf{0}, \;\; \Phi_{d,22} = -\mathbf{I}, \end{aligned} \tag{5.45}$$

and $\epsilon = 0.001$. We are interested in solving the min-max problem (5.37). We select $T_f = 20$, $r = \mathbf{0}$, $Q = \mathbf{I}$, and $R = \mathbf{I}$ to robustly regulate the output of the system to zero within a horizon of length 20. Moreover, we seek to do so while ensuring that $\check{u}$ and y satisfy quadratic constraints (5.37c), (5.28) with

$$\begin{aligned} \Psi_{11} = T_f \epsilon_u, \;\; \Psi_{12} = \mathbf{0}, \;\; \Psi_{22} = -\mathbf{I}, \\ \Theta_{11} = T_f \epsilon_y, \;\; \Theta_{12} = \mathbf{0}, \;\; \Theta_{22} = -\mathbf{I}, \end{aligned}$$

and $\epsilon_u = \epsilon_y = 0.5$.

As shown in Theorem 5.5.1, it is possible to convert this robust control input design problem into the minimization problem (5.38). This problem is then solved using Yalmip [Löf04] on Matlab with MOSEK [MOS20] specified as the solver, which returns the optimal control sequence u. This control sequence is tested with multiple compatible realizations of noise trajectories. In particular, we randomly select 100 vectors $\bar{g}$ that satisfy the quadratic constraints (5.34) and (5.35), which, in view of (5.33), parameterize 100 feasible sequences of w and $\bar{d}$. As shown in Figure 5.2, output trajectories are quickly brought around zero for all noise and disturbance realizations. Moreover, Figure 5.3 displays the robustness of the closed-loop system. Specifically, the first plot in Figure 5.3 shows that $\gamma \leq \gamma^*$ for all selected noise and disturbance realizations, where each blue circle corresponds to a specific realization and γ^* is the optimal value of (5.38). Moreover, the second and third plots show that the input and output constraints are satisfied for all selected noise and disturbance trajectories, i.e., $\psi(\check{u}) \geq 0$ and $\theta(y) \geq 0$, respectively.

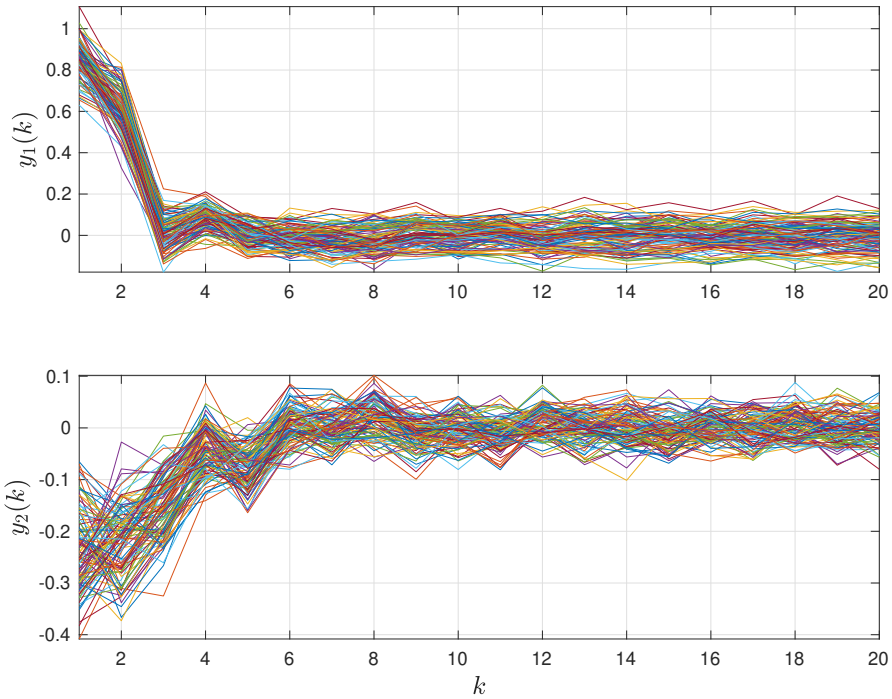

Figure 5.2: Output responses with the designed robust control under different feasible noise and disturbance trajectories.

When parameterizing the noise trajectories as in (5.33), the parameterization methods proposed in Sections 5.4.4 and 5.5.2 allow for a significant reduction in the sizes of the LMI conditions (5.36), (5.41), and (5.44). In particular, the size of each LMI condition is reduced from 291 to 143.

It is seen from Figure 5.3 that the obtained γ values are not as high as the optimal value γ^*. Moreover, the input and output constraints are not active in any of the different simulation scenarios, i.e., $\psi(\check{u}) \neq 0$ and $\theta(y) \neq 0$. These limitations are due to the fact that the version of S-lemma for multiple quadratic inequalities and the semidefinite version of Schur complement used in Section 5.5.3 are conservative. In order to demonstrate that they are the only sources of conservativity, we run another simulation with the same LTI system, in which we do not consider actuator disturbances and input/output constraints.

Specifically, the same *historical* data as in the previous simulation are used to construct the Hankel matrices U_p, U_f, Y_p, and Y_f. Moreover, the same input sequence u_{ini} is used to generate the *recent* trajectory. Differently to the previous case, only the recent output trajectory y_{ini} is affected by measurement noise w. This noise is chosen to satisfy (5.6) with the matrix Φ defined by (5.45). The T_f, r, Q, and R of the previous example are chosen to ensure robust regulation of system output to zero. By utilizing the results of Section 5.4, we solve the problem (5.23) with the matrix M defined in (5.27). Similarly

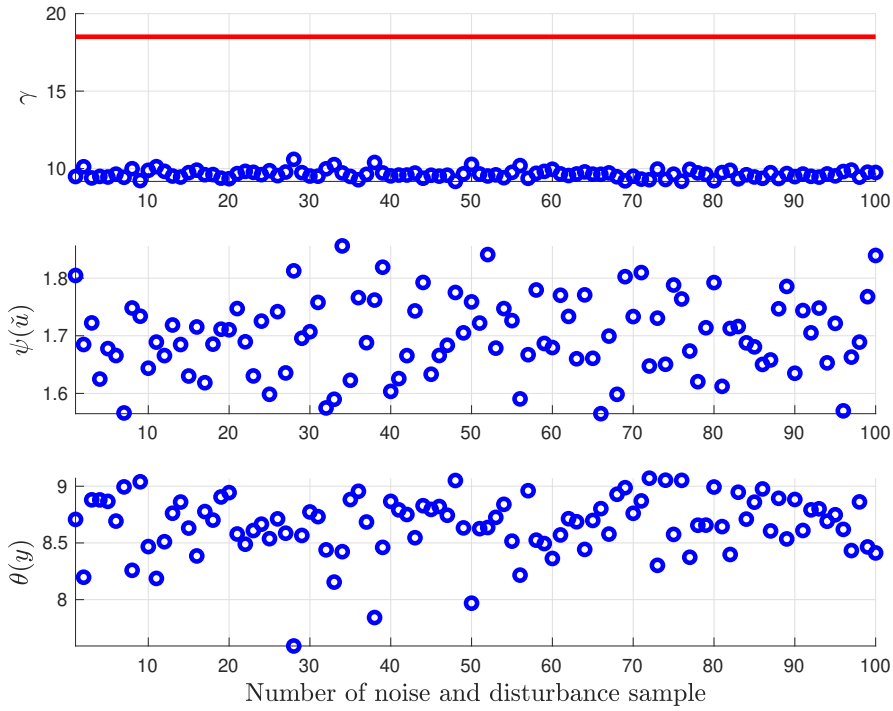

Figure 5.3: Robustness against different noise and disturbance trajectories. Top: Tracking errors $\gamma = y^\top Q y + \check{u}^\top R \check{u}$ (blue circles), and the optimal value γ^* (red line) computed from (5.38). Middle: Values of the input constraint $\psi(\check{u})$ computed as in (5.37c). Bottom: Values of the output constraint $\theta(y)$ computed as in (5.28).

to the previous simulation, the calculated control input u is used to control the system with 100 different realizations of the vector g_w parameterizing different feasible noise trajectories w. The results of this simulation are presented in Figure 5.4, where one sees that the tracking costs γ in blue circles are smaller than the robust optimal tracking cost γ^* computed from (5.23) for all feasible noise trajectories. It can also be seen from this figure that some γ values get quite close to γ^*, hence supporting the claim that Theorem 5.4.1 in Section 5.4 is not conservative.

5.6.1 Noise in historical data

In this section, we investigate the effect of noisy historical data on our control method. In particular, we consider the previous simulation, where we solve the SDP (5.23) to produce the results in Figure 5.4. Differently from that setting, historical data are now corrupted by noise, i.e., noisy outputs

$$\bar{y}_k = \bar{\check{y}}_k + \bar{w}_k$$

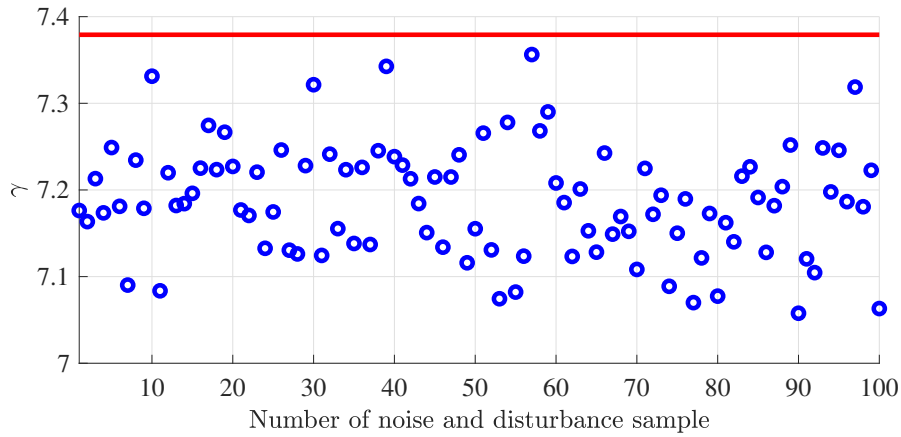

Figure 5.4: Tracking errors $\gamma = y^\top Q y + u^\top R u$ (blue circles), and the optimal value γ^* (red line) computed from (5.23).

are collected from the system, where the noise trajectory $\bar{w} \triangleq \mathrm{col}(\{\bar{w}_k\}_{k=t_h}^{t_h+T_d-1})$ satisfies the quadratic constraint (5.6) with

$$\Phi_{11} = T_d p \bar{\epsilon}, \;\; \Phi_{12} = \mathbf{0}, \;\; \Phi_{22} = -\mathbf{I}.$$

We consider 5 different values of $\bar{\epsilon}$, logarithmically spaced between 10^{-7} and 10^{-3}, to represent various noise levels. For each value, we conduct 10 offline experiments with random initial conditions and noise realizations to collect separate batches of historical data. Furthermore, for every one of these, (5.23) is solved to compute the optimal control sequence u and tracking cost γ^*. Similarly to the previous simulation setting, each u is tested in 50 test simulations with random realizations of the noise w on recent data. Figure 5.5 displays, for each value of $\bar{\epsilon}$, the proportion of test simulations where the tracking cost γ exceeds the optimal value γ^*. It can be seen in this figure that, due to the existence of noise in historical data, $\gamma < \gamma^*$ does not always hold and is more likely to be violated as $\bar{\epsilon}$ increases. Nevertheless, Figure 5.5 shows that our control method is reasonably robust against *sufficiently small* noise in the historical data.

5.7 Conclusions

Willems' FL shows that finite-length persistently exciting data can characterize the behaviors of linear systems, which enables data-driven simulation and control. In this chapter, we build on this data-dependent representation to consider the case that the recent output data are noisy and solve worst-case robust optimal tracking control problems in a data-driven fashion. The key ingredient of our approach is a suitable parameterization of the feasible noise trajectories and the performance specification, which allows one to express them as quadratic constraints. Then, by applying the S-lemma, we show that the

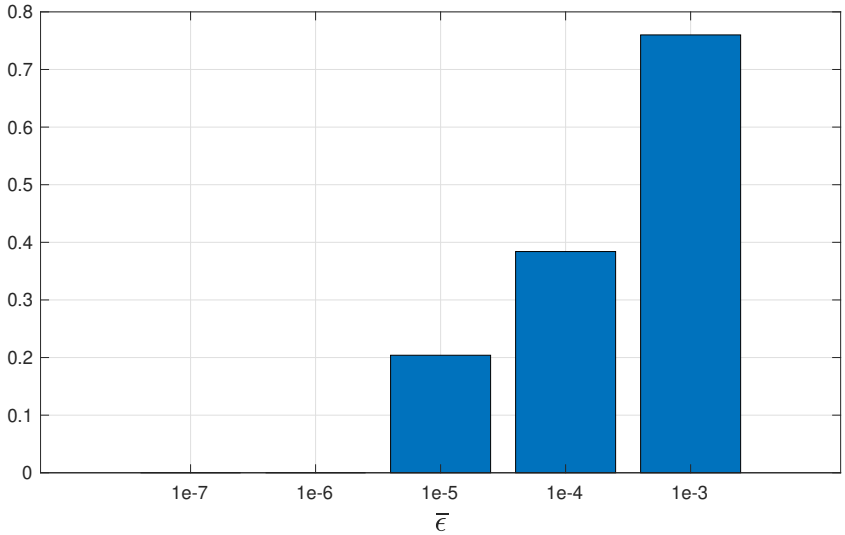

Figure 5.5: Proportion of simulations where $\gamma < \gamma^*$ is violated.

worst-case robust control problem is equivalent to an SDP. Moreover, by carefully selecting the noise parameterization, we can show that the dimension of the LMI optimization problem does not scale with the length of historical data. Our method can also easily incorporate input and output constraints, as well as actuator disturbances.

The methods proposed in this chapter can be used for a variety of control applications for generic LTI systems. In the next chapter, we provide a generic data-driven framework for state estimation in the presence of unknown inputs to the system.

6 Data-driven unknown-input observers and state estimation

6.1 Introduction

The problem of estimating the states of an LTI system when some inputs cannot be measured has been studied within the control community for almost half a century [MH73], and has been motivated by applications in control, robust estimation, and fault diagnosis. Among approaches available in the literature, some use *a priori* information about the unknown inputs d, whereas some others assume no such prior and develop *unknown-input decoupling* observers, i.e., state estimators whose estimation error is independent of d and asymptotically converges to zero [DZX94]. In this chapter, we focus on the latter class. Such observers, introduced as UIOs in Chapter 4, have been developed for continuous-time [DZX94] and discrete-time systems [Val99]. UIOs are often used for fault detection [CPZ96, GLC15] and, more recently, for cyber-attack detection (see Chapter 4). They are an attractive tool in *remote* and *distributed* settings, where state estimators are not collocated with the system, and therefore, do not have access to all its inputs.

The work [Val99] provides necessary and sufficient UIO existence conditions based on system matrices, which represent suitable observability and decoupling properties of the system. It also gives a model-based UIO design procedure under these conditions. Though for the discrete-time setting, these conditions and design procedure are very similar to those given in Section 4.4 for continuous-time setting. Nevertheless, the literature lacks end-to-end methodologies using data instead of a system model. In particular, no existing work provides a data-driven formulation of UIO existence conditions and design. An approach to achieve this goal is to follow a two-step procedure by first identifying the system from the collected data and then designing a UIO for the reconstructed model.

Among the techniques for identifying systems with fully- or partially-unknown inputs, subspace identification can be used when d is a zero-mean stationary white noise [VODM12]. Similarly, errors-in-variables (EIV) methods can be applied when the unknown inputs

can be modeled by additive stationary noise perturbing known input variables [Söd07]. In order to remove the above assumptions on the unknown inputs, the authors in [LE17] have proposed a novel system identification method called the *indirect framework*. The goal is achieved by introducing system-level assumptions ensuring that some inputs can be directly measured, and certain parts of the system dynamics are known. The element-level system identification method proposed in [WH94] does away with assumptions on the system or the unknown inputs, but restricts the focus on mechanical systems. Similarly, [YV16] proposes a *blind subspace identification* scheme under the assumption of persistently exciting unknown inputs.

We highlight that, except [LE17], none of the above methods guarantees the exact identification of the system with finite data, even without noise in the measured variables. Moreover, conditions for the existence of a UIO are rank-based (see [Val99] and conditions (C1)-(C2) in Section 4.4), and therefore extremely sensitive to errors in the identified system matrices. Identification errors may also result in poor estimation performance of UIOs as input-decoupling conditions are inherently sensitive to uncertainties in the system matrices. In addition, [LE17] does not identify the input channels corresponding to the unknown inputs, hampering the application of existing model-based UIO design methods.

6.1.1 Contributions

An alternative to the two-step approach would be to check the existence of a UIO and design the observer directly from data, without building a model of the system. In this chapter, we propose a method with these features by exploiting the behavioral methods summarized in Section 5.2. In particular, we exploit the results in [DPT20, MR08] to give necessary and sufficient conditions for the existence of a UIO and develop a design procedure.

Throughout this chapter, we consider the case of noiseless data, as the considered problem has not been previously solved even with this assumption. Unlike two-step approaches that rely on subspace identification, EIV methods, or the indirect framework, we do not assume any knowledge of the system dynamics or the process generating d. Moreover, we give guarantees on the convergence of estimates to the real state. We emphasize that our results can be directly extended to standard state estimation with no unknown inputs. In a simulation example, we use the proposed UIO for distributed state estimation in DCmGs, and show how it can be embedded into the cyber-attack detection scheme in Chapter 4.

This chapter is organized as follows. Section 6.2 formally presents the problem, while the UIO design is discussed in Section 6.3. The application example is given in Section 6.4, before concluding the chapter in Section 6.5.

6.2 Problem formulation

Consider a system $\mathcal{G}$ with the state-space representation

$$\begin{aligned} x_{t+1} &= Ax_t + Bu_t + Ed_t, \\ y_t &= Cx_t, \end{aligned} \tag{6.1}$$

where $x_t \in \mathbb{R}^n$ are the states, $u_t \in \mathbb{R}^m$ are the (known) inputs, $y_t \in \mathbb{R}^p$ are the outputs, and $d_t \in \mathbb{R}^{m_d}$ are the *unknown* inputs (e.g. disturbances) of the system, and hence unmeasured. We assume that the system is in minimal form, i.e., $(A, [B\ E])$ is reachable and (A, C) is observable.

We next provide a formal definition of a UIO in the discrete-time setting.

Definition 6.2.1 (UIO [Val99])**.** *An LTI system of the form*

$$\begin{aligned} z_{t+1} &= A_{\text{UIO}} z_t + B_{\text{UIO}} v_t, \\ \hat{x}_t &= z_t + D_{\text{UIO}} v_t, \end{aligned} \tag{6.2}$$

with inputs $v \triangleq [u^\top\ y^\top]^\top$ *and outputs* $\hat{x}$ *is a UIO for the system in* (6.1) *if* $\hat{x}_t - x_t \to \mathbf{0}$ *as* $t \to \infty$ *for any initial states* x_0 *and* z_0*, input* u*, and unknown input* d*.*

Remark 6.2.1. *When* $m_d = 0$*, the formulation in* (6.1) *and* (6.2)*, as well as the following analysis, capture standard state-estimation problems where all inputs are known.*

If the matrices A, C, and E of the system (6.1) satisfy certain unknown-input observability conditions, a UIO exists and can be designed through a straightforward procedure [Val99]. We emphasize that these conditions and design procedure, similar to their continuous-time counterparts in Section 4.4, are model-based. They are not relevant to the following developments and, therefore, are omitted.

Remark 6.2.2. *As shown in [Val99], if a UIO can be designed, the state-estimation error* $e_t \triangleq x_t - \hat{x}_t$ *follows the autonomous dynamics* $e_{t+1} = A_{\text{UIO}} e_t$*. By setting the initial condition of the UIO as* $z_0 = x_0 - D_{\text{UIO}} y_0$*, one gets* $\hat{x}_0 = x_0$ *and, consequently,* $\hat{x}_t = x_t\ \ \forall t$*. Therefore, for any input-output-state trajectory* (u, y, x) *of* $\mathcal{G}$*,* $([u^\top\ y^\top]^\top, x)$ *is an input-output trajectory of the UIO* (6.2)*.*

In the sequel, we assume that x_0 is not available and, thus, z_0 cannot be chosen as above. Regardless, the observation in Remark 6.2.2 is key in our approach as it enables us to *collect data* from the UIO without even constructing it.

In this chapter, we build on the same background on data-driven control and prediction as in Chapter 5; therefore, all definitions in Section 5.2 apply. Next, we provide the details of the data-driven setting specific to this chapter.

We assume that an *offline* experiment has been conducted with the system $\mathcal{G}$ before the start of any estimation task, and the corresponding *historical* input-output-state trajectories $\bar{u} \triangleq \mathrm{col}(\{\bar{u}_i\}_{i=t_h}^{t_h+T_d-1})$, $\bar{y} \triangleq \mathrm{col}(\{\bar{y}_i\}_{i=t_h}^{t_h+T_d-1})$, $\bar{x} \triangleq \mathrm{col}(\{\bar{x}_i\}_{i=t_h}^{t_h+T_d-1})$ have been collected, where $t_h \ll 0$. These data define the following matrices:

$$U \triangleq \mathcal{H}_L(\bar{u}), \;\; Y \triangleq \mathcal{H}_L(\bar{y}), \;\; X \triangleq \mathcal{H}_L(\bar{x}), \tag{6.3}$$

for some $L \leq T_d$. Similarly, define the Hankel matrix corresponding to $\bar{v} \triangleq \mathrm{col}(\{\bar{v}_i\}_{i=t_h}^{t_h+T_d-1})$ $= \mathrm{col}(\{[\bar{u}_i^\top \;\; \bar{y}_i^\top]^\top\}_{i=t_h}^{t_h+T_d-1})$ as $V \triangleq \mathcal{H}_L(\bar{v})$. Although d is not measured, we introduce the notations $\bar{d} \triangleq \mathrm{col}(\{\bar{d}_i\}_{i=t_h}^{t_h+T_d-1})$ for historical unknown input data, and $D \triangleq \mathcal{H}_L(\bar{d})$ for the corresponding Hankel matrix.

When a UIO (6.2) exists, Lemma 5.2.2 can be applied to predict its outputs, which is equivalent to computing state estimations. This methodology requires, at each time step t, to specify *recent* data $v_{t,\mathrm{ini}} \triangleq \mathrm{col}(\{v_i\}_{i=t-T_{\mathrm{ini}}}^{t-1})$, $\hat{x}_{t,\mathrm{ini}} \triangleq \mathrm{col}(\{\hat{x}_i\}_{i=t-T_{\mathrm{ini}}}^{t-1})$ consisting of T_{ini} samples. This data uniquely determines the the state z_{t-1} of the UIO if $T_{\mathrm{ini}} \geq l_{\mathrm{UIO}}$, where l_{UIO} is the observability index of the UIO. Lemma 5.2.2 can be used to compute UIO output predictions for a future horizon of T_f samples based on the recent data and *future* UIO inputs $v_{t,f} \triangleq \mathrm{col}(\{v_i\}_{i=t}^{t+T_f-1})$. For this purpose, Hankel matrices are split into *past* and *future* blocks denoted by subscripts p and f, respectively:

$$U = \begin{bmatrix} U_p \\ U_f \end{bmatrix}, \;\; Y = \begin{bmatrix} Y_p \\ Y_f \end{bmatrix}, \;\; X = \begin{bmatrix} X_p \\ X_f \end{bmatrix}, \;\; V = \begin{bmatrix} V_p \\ V_f \end{bmatrix}, \tag{6.4}$$

where the upper block matrices consist of T_{ini} block rows, and the lower block matrices consist of T_f block rows. In this chapter, we iteratively apply the abovementioned lemma with one-step-ahead predictions (see Section 6.3); therefore, we take $T_f = 1$. We also take $T_{\mathrm{ini}} = 1$, since the output matrix of the UIO (6.2) is the identity, which implies $l_{\mathrm{UIO}} = 1$.

In what follows, it is assumed that inputs and outputs of the system $\mathcal{G}$ are accessible. The states are considered to be measured in the offline experiment to collect the historical data, but not accessible in real-time operation.

Remark 6.2.3. *Our assumption on the availability of the states is often fulfilled in a remote estimation scenario, where the observer is not collocated with the system. As such, it might be impossible, unsafe, or unfeasible for the system to transmit the state measurements to the observer in real time over a communication network. Instead, the historical state data can be collected offline and transferred once and for all to the observer by using a different physical medium. Moreover, historical states can be measured once in dedicated lab experiments using sensors that can be costly to install in real-time applications. As cost reduction is a key driver in industry [MvD21], it might be desirable to estimate states in online operations instead of adding sensors, especially if several copies of the same system are created. Finally note that infinitely many state-space*

realizations of $\mathcal{G}$ exist [VODM12]. In order to estimate the states of $\mathcal{G}$ uniquely in the absence of model knowledge, it is required to fix their basis, which is implied by the availability of historical state measurements.

Definition 6.2.2. *A trajectory $(\{v_i\}_{i=0}^{N-1}, \{x_i\}_{i=0}^{N-1})$ is compatible with the historical data $(\bar{v}, \bar{x})$ if*

$$\begin{bmatrix} v_i \\ x_i \\ v_{i+1} \\ x_{i+1} \end{bmatrix} \in \text{range}\left(\begin{bmatrix} V_p \\ X_p \\ V_f \\ X_f \end{bmatrix}\right), \quad \forall i \in \{0, 1, \ldots, N-2\}. \tag{6.5}$$

Moreover, the set of all trajectories compatible with $(\bar{v}, \bar{x})$ is defined as

$$\mathbb{T}_c(\bar{v}, \bar{x}) \triangleq \{(\{v_i\}_{i=0}^{N-1}, \{x_i\}_{i=0}^{N-1}) | \text{ (6.5) holds}\}. \tag{6.6}$$

We further introduce the set of all trajectories $(\{v_i\}_{i=0}^{N-1}, \{x_i\}_{i=0}^{N-1})$ that can be generated by $\mathcal{G}$:

$$\mathbb{T}_{\mathcal{G}} \triangleq \{(\{[u_i^\top \ y_i^\top]^\top\}_{i=0}^{N-1}, \{x_i\}_{i=0}^{N-1}) | \ \exists \{d_i\}_{i=0}^{N-1} \text{ verifying (6.1)}, \ \forall i \in \{0, 1, \ldots, N-2\}\}. \tag{6.7}$$

Definition 6.2.2 and equation (6.7) are used for checking whether the historical data are *representative* of all input-output trajectories of $\mathcal{G}$. Note that this is achieved when all trajectories of $\mathcal{G}$ are compatible with the historical data, i.e., $\mathbb{T}_{\mathcal{G}} = \mathbb{T}_c(\bar{v}, \bar{x})$. Indeed, if historical trajectories are very short or poorly chosen, the range of $[V_p^\top \ X_p^\top \ V_f^\top \ X_f^\top]^\top$ might be very small and incompatible trajectories of $\mathcal{G}$ might exist.

In this chapter, we assume all data to be noiseless in order to provide the theory for data-driven UIO[1]. As discussed in Remark 6.2.3, in certain applications, historical data can be generated in dedicated experiments. In such cases, historical data can be assumed noiseless when sophisticated and accurate sensors are used. The presence of measurement noise in recent data is discussed later in Remark 6.3.3.

6.3 Data-driven UIO

In this section, we present the proposed data-driven UIO formulation. Our method is enabled by the observation in Remark 6.2.2 that the input-output-state trajectories of $\mathcal{G}$ also represent input-output trajectories of the UIO. Therefore, if a UIO exists, historical data collected from $\mathcal{G}$ can be used to provide a data-driven representation of the trajectories of the UIO, when $\mathbb{T}_{\mathcal{G}} = \mathbb{T}_c(\bar{v}, \bar{x})$ [DPT20].

[1]Noiseless historical data, which corresponds to perfect model knowledge, and noiseless recent (online) data are standard assumptions in the setting in which Luenberger observer and UIOs were originally developed.

The presentation of our results is structured in three steps. In Lemma 6.3.1, we give a sufficient condition for having $\mathbb{T}_{\mathcal{G}} = \mathbb{T}_c(\bar{v}, \bar{x})$. In Lemma 6.3.2, we present necessary and sufficient conditions for the existence of a system of the form (6.2) that generates all trajectories in $\mathbb{T}_c(\bar{v}, \bar{x})$. Finally, Theorem 6.3.1 characterizes the existence of a UIO and provides a data-driven UIO estimation scheme. The following assumption is required in the sequel.

Assumption 6.3.1. *The historical data* $\{[\bar{u}_i^\top \;\; \bar{d}_i^\top]^\top\}_{i=t_h}^{t_h+T_d-1}$ *are persistently exciting of order* $n+2$.

Lemma 6.3.1. *If Assumption 6.3.1 holds,* $\mathbb{T}_c(\bar{v}, \bar{x}) = \mathbb{T}_{\mathcal{G}}$.

Proof. Since $v_t = [u_t^\top \; y_t^\top]^\top$, there exists a row permutation matrix P_R such that

$$P_R \begin{bmatrix} v_t \\ x_t \\ v_{t+1} \\ x_{t+1} \end{bmatrix} = \begin{bmatrix} u_{[t:t+1]} \\ y_{[t:t+1]} \\ x_{[t:t+1]} \end{bmatrix},$$

for any vector $[v_t^\top \; x_t^\top \; v_{t+1}^\top \; x_{t+1}^\top]^\top$ corresponding to a trajectory of $\mathcal{G}$. From (6.1), the variables on the right-hand side of the above equation verify

$$\begin{bmatrix} u_{[t:t+1]} \\ y_{[t:t+1]} \\ x_{[t:t+1]} \end{bmatrix} = \underbrace{\begin{bmatrix} \mathbf{I} & \mathbf{0} & \mathbf{0} \\ \mathcal{T}_{uy,2} & \mathcal{T}_{dy,2} & \mathcal{O}_{y,2} \\ \mathcal{T}_{ux,2} & \mathcal{T}_{dx,2} & \mathcal{O}_{x,2} \end{bmatrix}}_{\triangleq \Theta} \begin{bmatrix} u_{[t:t+1]} \\ d_{[t:t+1]} \\ x_t \end{bmatrix}, \tag{6.8}$$

where

$$\mathcal{T}_{uy,2} = \begin{bmatrix} \mathbf{0} & \mathbf{0} \\ CB & \mathbf{0} \end{bmatrix}, \; \mathcal{T}_{dy,2} = \begin{bmatrix} \mathbf{0} & \mathbf{0} \\ CE & \mathbf{0} \end{bmatrix}, \; \mathcal{O}_{y,2} = \begin{bmatrix} C \\ CA \end{bmatrix},$$
$$\mathcal{T}_{ux,2} = \begin{bmatrix} \mathbf{0} & \mathbf{0} \\ B & \mathbf{0} \end{bmatrix}, \; \mathcal{T}_{dx,2} = \begin{bmatrix} \mathbf{0} & \mathbf{0} \\ E & \mathbf{0} \end{bmatrix}, \; \mathcal{O}_{x,2} = \begin{bmatrix} \mathbf{I} \\ A \end{bmatrix}.$$

Therefore, for any trajectory $(\{v_i\}_{i=0}^{N-1}, \{x_i\}_{i=0}^{N-1}, \{d_i\}_{i=0}^{N-1})$ of the system $\mathcal{G}$, it holds that, for all $t \in \{0, \ldots, N-2\}$,

$$\begin{bmatrix} v_t \\ x_t \\ v_{t+1} \\ x_{t+1} \end{bmatrix} = P_R^{-1} \Theta \begin{bmatrix} u_{[t:t+1]} \\ d_{[t:t+1]} \\ x_t \end{bmatrix}. \tag{6.9}$$

Moreover, given a sequence of inputs $(\{u_i\}_{i=0}^{N-1}, \{d_i\}_{i=0}^{N-1})$ and an initial state x_0, any sequence $(\{v_i\}_{i=0}^{N-1}, \{x_i\}_{i=0}^{N-1})$ obtained by iteratively solving for the left-hand side of (6.9) for $t \in \{0, \ldots, N-2\}$ is a trajectory of $\mathcal{G}$. For any set of historical data $(\bar{v}, \bar{x}, \bar{d})$ generated by $\mathcal{G}$, it holds that

$$\begin{bmatrix} V_p \\ X_p \\ V_f \\ X_f \end{bmatrix} = P_R^{-1}\Theta \begin{bmatrix} U \\ D \\ X_p \end{bmatrix} \tag{6.10}$$

because every column of the left-hand side of the above equation is a trajectory of $\mathcal{G}$. Therefore, $\mathbb{T}_c(\bar{v}, \bar{x}) \subseteq \mathbb{T}_{\mathcal{G}}$. We next show that $\mathbb{T}_{\mathcal{G}} \subseteq \mathbb{T}_c(\bar{v}, \bar{x})$. For this, it is sufficient to verify that for any trajectory $(\{v_i\}_{i=0}^{N-1}, \{x_i\}_{i=0}^{N-1})$ of $\mathcal{G}$, every vector $[v_t^\top \ x_t^\top \ v_{t+1}^\top \ x_{t+1}^\top]^\top$ is in the range of $[V_p^\top \ X_p^\top \ V_f^\top \ X_f^\top]^\top$. Under Assumption 6.3.1, Theorem 1 in [vWDPCT20] can directly be applied to show that $[U^\top \ D^\top \ X_p^\top]^\top$ has full row rank. As a direct consequence, given a vector $[u_{[t:t+1]}^\top \ d_{[t:t+1]}^\top \ x_t^\top]^\top$, there exists a vector g_{t+1} such that

$$\begin{bmatrix} U \\ D \\ X_p \end{bmatrix} g_{t+1} = \begin{bmatrix} u_{[t:t+1]} \\ d_{[t:t+1]} \\ x_t \end{bmatrix}.$$

Then, multiplying (6.10) from the right by g_{t+1} yields

$$\begin{bmatrix} V_p \\ X_p \\ V_f \\ X_f \end{bmatrix} g_{t+1} = \begin{bmatrix} v_t \\ x_t \\ v_{t+1} \\ x_{t+1} \end{bmatrix},$$

where the vector $[v_t^\top \ x_t^\top \ v_{t+1}^\top \ x_{t+1}^\top]^\top$ satisfies (6.9). Since any trajectory of $\mathcal{G}$ consists of v_t, x_t, v_{t+1}, x_{t+1} satisfying (6.9), one gets $\mathbb{T}_{\mathcal{G}} \subseteq \mathbb{T}_c(\bar{v}, \bar{x})$. ■

Remark 6.3.1. *Lemma 6.3.1 requires persistency of excitation of the unknown inputs $\bar{d}$, which is not verifiable using the available data. This assumption can be satisfied when the unknown inputs cannot be measured or modified, but change randomly. It is also satisfied if $\bar{d} = \bar{d}_0 + \delta\bar{d}$, where $\bar{d}_0$ is a (not necessarily exciting) deterministic component and $\delta\bar{d}$ is a small random component. For example, in DCmGs, unknown inputs include the current loads connected to generation units (see Section 6.4). Loads are dictated by current consumption which can be assumed to have a random component*[2]*. Persistency of excitation can also be satisfied when $\delta\bar{d}$ belongs to certain classes of deterministic signals such as pseudo-random binary sequences (PRBSs), and sums of sinusoids [SS89, Chapter 5].*

In the following, we make use of the vector g_{t+1} solving

$$\begin{bmatrix} V_p \\ X_p \\ V_f \end{bmatrix} g_{t+1} = \begin{bmatrix} v_t \\ x_t \\ v_{t+1} \end{bmatrix} \tag{6.11}$$

[2]Loads might include aggregated domestic consumption based on complex daily activity patterns of many consumers, which can be assumed stochastic. Load currents are also affected by noise terms that are induced by switches in power-electronics converters used for connecting loads.

for given V_p, X_p, V_f and a compatible recent trajectory $v_{[t:t+1]}$, x_t. All solutions to (6.11) can be written as

$$g_{t+1} = \Xi[v_t^\top \ x_t^\top \ v_{t+1}^\top]^\top + \nu, \tag{6.12}$$

for a vector $\nu \in \ker([V_p^\top \ X_p^\top \ V_f^\top]^\top)$ and a properly defined matrix Ξ. There are infinitely many such matrices and a particular choice is $([V_p^\top \ X_p^\top \ V_f^\top]^\top)^\dagger$. We partition this matrix as $\Xi = [\Xi_{V_p} \ \Xi_{X_p} \ \Xi_{V_f}]$, where Ξ_{V_p}, Ξ_{X_p}, and Ξ_{V_f} have $m+p$, n, and $m+p$ columns, respectively.

Lemma 6.3.2. *There exists an LTI system of the form* (6.2) *that can generate every compatible input-output trajectory* $(\{v_i\}_{i=0}^{N-1}, \{x_i\}_{i=0}^{N-1})$ *if and only if*

$$\ker\left(\begin{bmatrix} V_p \\ X_p \\ V_f \end{bmatrix}\right) \subseteq \ker(X_f). \tag{6.13}$$

Proof. ($\Longleftarrow$) We show the existence of a system (6.2) with matrices

$$A_{\text{UIO}} = X_f \Xi_{X_p}, \ B_{\text{UIO}} = X_f(\Xi_{V_p} + \Xi_{X_p} X_f \Xi_{V_f}), \ D_{\text{UIO}} = X_f \Xi_{V_f}. \tag{6.14}$$

Note that every compatible trajectory is a sequence of input-output data v_t and x_t, and verifies (6.5). If (6.13) holds, the vector x_{t+1} is uniquely determined by $X_f g_{t+1}$ for any vector g_{t+1} fulfilling (6.12). Therefore, for any compatible trajectory and t, x_{t+1} is given by

$$x_{t+1} = X_f \Xi_{V_p} v_t + X_f \Xi_{X_p} x_t + X_f \Xi_{V_f} v_{t+1}, \tag{6.15}$$

since $\nu \in \ker([V_p^\top \ X_p^\top \ V_f^\top]^\top) \subseteq \ker(X_f)$. On defining $z_{t+1} \triangleq X_f \Xi_{V_p} v_t + X_f \Xi_{X_p} x_t$ and replacing the time index $t+1$ with t, equation (6.15) reduces to $x_t = z_t + X_f \Xi_{V_f} v_t$ which is the output equation in (6.2) with D_{UIO} in (6.14). Replacing x_t with $z_t + X_f \Xi_{V_f} v_t$ in the definition of z_{t+1} yields the state update in (6.2) with A_{UIO} and B_{UIO} matrices in (6.14). As such, the relation (6.15) between the elements of the tuple $(v_t, x_t, v_{t+1}, x_{t+1})$ is equivalently represented as the relation between the inputs and outputs of the system in (6.2) with the matrices $(A_{\text{UIO}}, B_{\text{UIO}}, D_{\text{UIO}})$ in (6.14) and the initial state $z_0 = x_0 - D_{\text{UIO}} v_0$.

($\Longrightarrow$) Note that the system in (6.2) generates all trajectories compatible with the historical data; therefore, the columns of $[V_p^\top \ X_p^\top \ V_f^\top \ X_f^\top]^\top$ represent input-output trajectories of this system. Denote its corresponding historical state data by $\bar{z} \triangleq \text{col}(\{\bar{z}_i\}_{i=t_h}^{t_h+T_d-1})$, which define the matrices Z, Z_p, and Z_f as in (6.3), (6.4). Since it holds that $Z_f = A_{\text{UIO}} Z_p + B_{\text{UIO}} V_p$, $X_p = Z_p + D_{\text{UIO}} V_p$, and $X_f = Z_f + D_{\text{UIO}} V_f$, one gets

$$\begin{aligned} X_f =& (B_{\text{UIO}} - A_{\text{UIO}} D_{\text{UIO}}) V_p + A_{\text{UIO}} X_p + D_{\text{UIO}} V_f \\ =& \begin{bmatrix} B_{\text{UIO}} - A_{\text{UIO}} D_{\text{UIO}} & A_{\text{UIO}} & D_{\text{UIO}} \end{bmatrix} \begin{bmatrix} V_p \\ X_p \\ V_f \end{bmatrix}. \end{aligned}$$

This, in turn, implies (6.13), concluding the proof. ■

Next, we discuss the existence of a UIO and provide a data-driven unknown-input state-estimation scheme.

Theorem 6.3.1 (Data-driven UIO)**.** *Suppose that Assumption 6.3.1 holds. There exists a UIO of the form* (6.2) *with the matrices in* (6.14) *if and only if* (6.13) *holds and* $X_f \Xi_{X_p}$ *is Schur stable. Moreover, for any* $\hat{x}_0 \in \mathbb{R}^n$*, the state estimations* $\hat{x}_{t+1}$*,* $t = 0, 1, \ldots$ *computed through the iterative formula*

$$\hat{x}_{t+1} = X_f \Xi [u_t^\top \ y_t^\top \ \hat{x}_t^\top \ u_{t+1}^\top \ y_{t+1}^\top]^\top \tag{6.16}$$

asymptotically converge to the state x_{t+1} *of* $\mathcal{G}$*.*

Proof. ($\Longleftarrow$) When Assumption 6.3.1 and condition (6.13) are satisfied, Lemmas 6.3.1 and 6.3.2 guarantee that the system (6.2) with matrices given in (6.14) can generate any compatible trajectory, hence, any trajectory of $\mathcal{G}$. Next, we focus on the iterative process (6.16) of computing estimations $\hat{x}_t$ from an initial condition $\hat{x}_0$ for any input u and unknown input d. As described in the proof of Lemma 6.3.2, this process is equivalent to generating output trajectories of the system in (6.2) with the initial state $z_0 = \hat{x}_0 - D_{\text{UIO}}[u_0^\top \ y_0^\top]^\top$ and inputs $v_t = [u_t^\top \ y_t^\top]^\top$. That proof also shows that the actual state x_t of $\mathcal{G}$ corresponds to the output of the same system with the same inputs but a different initial state: $z_0' = x_0 - D_{\text{UIO}}[u_0^\top \ y_0^\top]^\top$. The state estimation error $e = x - \hat{x}$ is the difference between these two outputs of (6.2), which follows the autonomous dynamics $e_{t+1} = A_{\text{UIO}} e_t$. If A_{UIO} is Schur stable, this error converges to zero and the LTI system in (6.2) is a UIO by Definition 6.2.1.

($\Longrightarrow$) From Definition 6.2.1 and Remark 6.2.2, a UIO has Schur stable dynamics. Using Lemma 6.3.2, existence of a UIO of the form (6.2) implies (6.13). ■

Note that all Ξ matrices such that g_{t+1} in (6.12) verifies (6.11) can be characterized as $\Xi = \Xi_0 + \Delta$, where $\Xi_0 = ([V_p^\top \ X_p^\top \ V_f^\top]^\top)^\dagger$ and Δ is any matrix such that $\text{range}(\Delta) \subseteq \ker([V_p^\top \ X_p^\top \ V_f^\top]^\top)$. Under (6.13), it also holds that $\text{range}(\Delta) \subseteq \ker(X_f)$. This implies that whether a UIO exists and, if yes, its matrices in (6.14), are independent of the particular choice of Ξ.

Remark 6.3.2. *Unlike the proposed data-driven UIO, existing model-based design procedures provide a degree of freedom in choosing UIO matrices [Val99, CPZ96], which can be exploited to tune the estimation performance. Therefore, our UIO with matrices* (6.14) *corresponds to one specific choice among those that can be achieved using model-based design methods.*

Remark 6.3.3. *If recent data* $\{v_i\}_{i=0}^{N-1} = \{[u_i^\top \ y_i^\top]^\top\}_{i=0}^{N-1}$ *are affected by noise, the recursive algorithm* (6.16) *results in estimation errors. Note that* (6.16) *is equivalent to*

computing output trajectories of the UIO (6.2) *with matrices in* (6.14)*. Therefore, the noise in recent data acts as an input disturbance to* (6.2)*, i.e.,* $\tilde{v}_t = v_t + w_t$ *is applied as input instead of* v_t*, where* w_t *is the measurement noise. Standard LTI system theory can be used to analyze the estimation error, which is the perturbation on the output of* (6.2) *caused by* w_t*.*

We next provide an application example to demonstrate the use of the proposed method on DCmGs. We also show that it can be used for distributed cyber-attack detection.

6.4 Distributed state estimation in DCmGs

Recall the distributed cyber-attack detection scheme comprising attack monitors collocated with every DGU in Chapter 4. One of the key ingredients of local monitors are UIOs, used for estimating the state of neighboring DGUs. Hereafter, we use the proposed data-driven UIOs to replace the model-based ones and show their effectiveness. This would eliminate the need for constructing accurate models of DGUs, which can be costly or require expertise.

Through computer simulations, we briefly demonstrate the potential of the proposed UIO for cyber-attack detection, without the pretence of providing an end-to-end data-driven formulation of the whole detection scheme in Chapter 4. Indeed, when compared to the simulation study in Chapter 4, we consider a simplified setting for clarity of exposition and without loss of generality. In particular, we do not consider switching behavior of the Buck converters and, hence, omit the *augmented* state representation in (4.11). We focus on the problem of estimating the state of one neighboring DGU only, as the same design procedure can be easily replicated for all neighbors.

The considered electrical scheme of a DGU is the same as in Figure 4.1, which defines relevant electrical parameters and variables (we refer the reader to Chapters 3 and 4 for a comprehensive description of these quantities). When equipped with the primary and secondary controllers proposed in [NST+20, TMGFT18], the continuous-time dynamics of a DGU is $\dot{x} = A_c x + E_c d$, with $x \triangleq [V_i \; I_{ti} \; v_i]^\top$, $d = [I_{\text{net},i} + I_{Li} \;\; V_{\text{ref},i} + \Delta V_i]^\top$, and

$$A_c = \begin{bmatrix} 0 & \frac{1}{C_{ti}} & 0 \\ \frac{k_{i,1}-1}{L_{ti}} & \frac{k_{i,2}-R_{ti}}{L_{ti}} & \frac{k_{i,3}}{L_{ti}} \\ -1 & 0 & 0 \end{bmatrix}, \; E_c = \begin{bmatrix} -\frac{1}{C_{ti}} & 0 \\ 0 & 0 \\ 0 & 1 \end{bmatrix}. \tag{6.17}$$

$I_{\text{net},i} = \sum_{j \in \mathcal{N}_i} I_{ij}$ is the net current injected into the mG by DGU i. As in Chapter 4, we assume all states are measured and transmitted to the neighboring units. The unknown inputs can be measured; however, they are not sent to the neighboring units for security and privacy reasons. Indeed, transmitting these variables in real time would make them vulnerable to cyber attacks, thus compromising the purpose of attack detection. Moreover, sharing historical data $\bar{d}_i$ with neighboring units might cause privacy violations.

Indeed, the loads I_{Li} often correspond to consumption, which can reveal the occupancy and daily activities of the consumers [Har92]. Furthermore, the variables $I_{\text{net},i}$ and ΔV_i may contain sensitive information regarding the neighbors of DGU i, which might not be desirable to share.

By using exact discretization, the discrete-time model of a DGU is given by system (6.1) with[3]

$$A = e^{A_c T_s},\ B = \mathbf{0},\ E = \left(\int_{\tau=0}^{T_s} e^{A\tau} d\tau \right) E_c,\ C = \mathbf{I} \tag{6.18}$$

for a sampling period $T_s > 0$, which we assume to be 10 ms in our experiments. At each time step t, the neighboring DGU j receives the following communicated output from DGU i

$$y_t^c = y_t + \phi_t, \tag{6.19}$$

where ϕ_t is the additive cyber attack vector at time t. T_a denotes the start of the attack; therefore, ϕ_t is zero for all $t < T_a$, and non-zero for, at least, a time instant $t \geq T_a$.

As in Section 4.4, we are interested in building a monitor collocated with the neighbor j of DGU i, that estimates the states x of DGU i from the communicated outputs y^c by assuming *safe operation*. i.e., that there are no attacks and, therefore, $y_t^c = y_t$. This corresponds to the problem of designing a UIO for the system in (6.1) with the matrices in (6.18).

We collect historical data by initializing the DGU from a random state. These data are not affected by attacks, as they are collected and sent to the neighboring units offline (see Remark 6.2.3). As discussed in Remark 6.3.1, it is sufficient that $V_{\text{ref},i}$ and I_{Li} have stochastic components to verify Assumption 6.3.1. This can indeed be satisfied as $V_{\text{ref},i}$ is a free reference variable and I_{Li} is the load current, which can be assumed to have a stochastic element as discussed in Remark 6.3.1.

The historical data verifies the conditions in Theorem 6.3.1 for the existence of a UIO; therefore, (6.16) can be used to compute state estimates. This is expected, since a model-based UIO also exists for the same system (see [GTN+18] and Chapter 4). We initialize the DCmG from a random initial condition, and simulate it for $N = 10$ time steps with no attack and $d = d_0 + \delta d$, where d_0 is a nominal vector and δd is a small random component. As shown in Figure 6.1, the estimates quickly converge to the real states. In view of Remark 6.3.2, the same UIO estimates can also be obtained by a model-based design procedure when the DGU matrices in (6.17) are known.

As shown in Lemma 4.4.1, it is possible that a UIO cannot detect any attack. We next introduce an attack in y_t^c to illustrate that the data-driven UIO designed above can detect at least one attack and be used in the distributed cyber-attack detection

[3]Hereafter, we omit the subscript i as it is irrelevant for the UIO design.

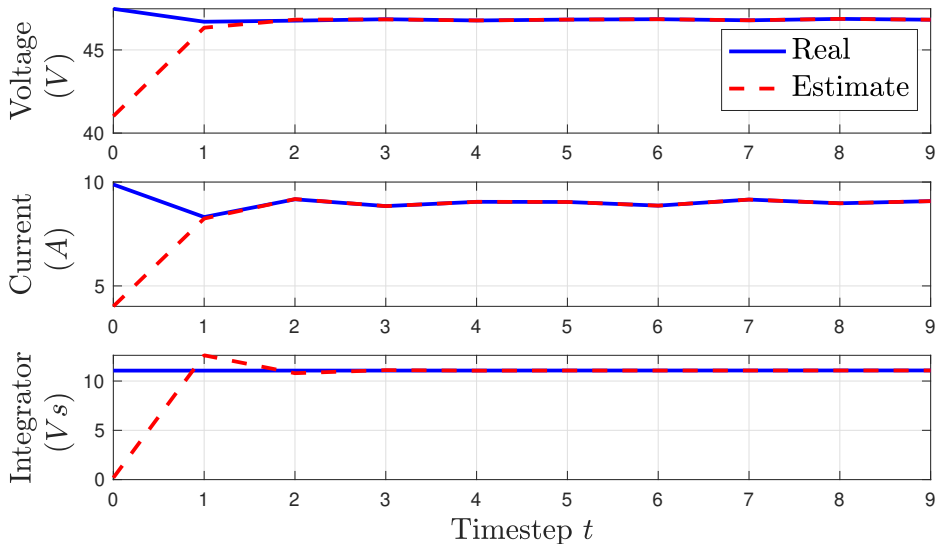

Figure 6.1: States and estimates in safe operation.

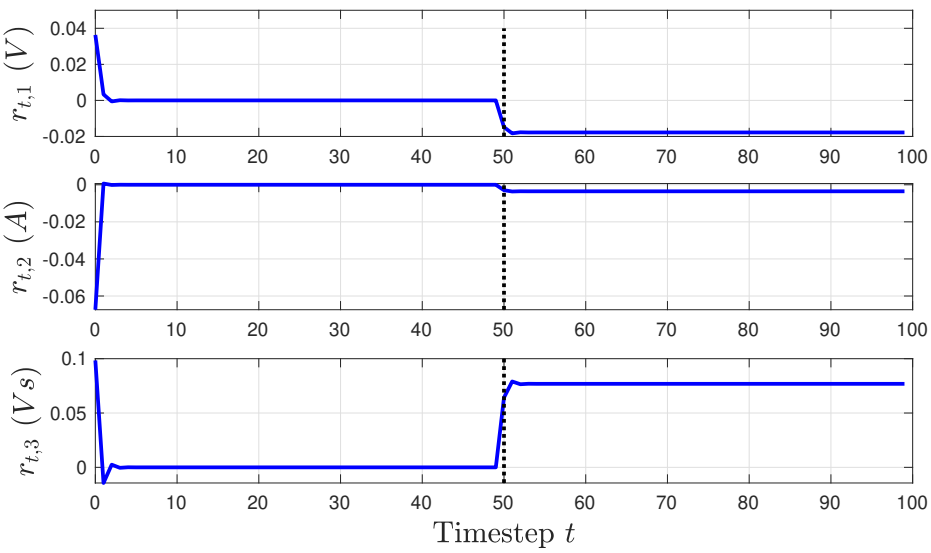

Figure 6.2: Residual signals in presence of attack. The vertical dotted line represents the start of the attack.

scheme in Chapter 4. Using the same historical data, we run another simulation of length $N = 100$ timesteps with random x_0 and d. Differently from the first case, a constant attack $\phi_t = [0.1\ 0.1\ 0.1]^\top$ is added on the communicated output variables in (6.19) after an attack start time of $T_a = 50$. In this case, the residual can be computed from the information available at the DGU j as $r_t = y_t^c - \hat{x} = [r_{t,1}\ r_{t,2}\ r_{t,3}]^\top$. Figure 6.2 demonstrates that the residuals are affected by the attack, showing the potential of the proposed method in distributed cyber-attack detection.

6.5 Conclusions

In this chapter, we provided data-driven necessary and sufficient conditions for the existence of a UIO for an LTI system and proposed a data-driven unknown-input state-estimation method. We also showed the effectiveness of the algorithm for distributed state estimation in DCmGs, and its potential for use in distributed cyber-attack detection. Indeed, the simulation results demonstrate that the proposed method is promising for a data-driven implementation of the scheme in Chapter 4.

7 Conclusions and future directions

7.1 Thesis conclusions

In this thesis, we proposed methods for addressing three relevant challenges for modern control systems: *distributed consensus*, *cyber-attack detection*, and *data-driven control and estimation*.

Many of today's control systems are composed of several smaller subsystems, possibly dispersed over large geographical areas. Cooperative control of these systems often hinges on the analysis and development of distributed consensus protocols. In turn, communication networks employed in distributed architectures are prone to cyber attacks, detection of which is vital for ensuring safe operation. Control of large-scale systems also raises the challenge of developing model-free solutions. The work presented in this thesis addresses these three points. Particularly, Part I is devoted to the study and design of distributed consensus protocols in interconnected MASs. First, an analysis on the existence of controllers achieving state consensus in general linear interconnected MASs is carried out. Focusing on a specific type of systems, namely islanded DCmGs, we then provide a distributed consensus-based scheme to achieve current sharing and voltage balancing.

Part II focuses on the security issues introduced by cyber coupling in LIMASs and develops a distributed cyber-attack detection scheme. The proposed method comprises local detectors associated to individual subsystems, monitoring the incoming communications from the neighbors. Each of these local units consists of two parallel modules that complement detection performances of one another by exploiting different pieces of information about the underlying subsystems. We also conduct extensive analyses regarding the detectability properties of the proposed scheme against different types of attacks.

Part III pertains to the development of direct data-driven control and state estimation

methods for LTI systems. We first develop a worst-case optimal tracking controller based on SDPs and using finite number of data points. Notably, the computational complexity of the design procedure is independent of the total number of data points. Extensions to input disturbances and input-output constraints are also provided. The last contribution of the thesis concerns state estimation. We give necessary and sufficient conditions, based on data, for the existence of a UIO for an LTI system. Moreover, we show how to iteratively compute state estimations of the data-driven UIO, which are proven to converge to the actual state.

7.2 Future perspectives

In this concluding section, we identify several research directions that might be of interest for advancing theoretical developments and improving the real-world applicability of the methods presented in the thesis. Below, we discuss these points separately for each part of the thesis.

Distributed consensus

The general consensusability results for LIMASs with vector subsystem dynamics rely on the assumption that the Laplacians of physical and communication graphs commute (see Section 2.4.2). Given a physical graph, this assumption imposes a restriction on the communication graph topology, which may not be verified for general LIMASs. Eliminating this assumption is, therefore, important for improving the applicability of our results, and will be considered in future works.

Also note that Chapter 2 considers state consensus. Another possible direction for follow-up research is to study output synchronization for LIMASs, which is a more general problem. Indeed, it captures a larger class of cooperative control tasks such as vehicle formations [FM04] and current sharing in DCmGs (see Chapter 3).

Finally, all works presented in the first part of the thesis assume ideal communication between subsystems of an interconnected MAS. This is, however, not the case in real communication networks. Future work can focus on studying the impact of network non-idealities (such as transmission delays, data quantization, and packet drops) on the stability and performance of the presented methods.

Together, the above improvements would enable the development of a framework for studying a broad range of relevant cooperation tasks in real-world LIMASs.

Beyond attack detection

In Chapter 4, we only looked into the detection of cyber attacks, which, by itself, does not ensure safe operation. For this purpose, it might be desirable to explore the possibility of tackling follow-up actions for attack mitigation. Specifically, an automatic reconfiguration strategy can be developed for the purpose of disabling attacked communication channels, all the while guaranteeing safe and reliable operation of the whole LIMAS. Another possibility is to enhance the detection scheme to *estimate* the attack vector, in order to grant the controllers resilience against attacks. Such extensions would eliminate the need of human intervention in case of an attack, by automatically guaranteeing the safety of the closed-loop system.

Moreover, the proposed detection scheme is model-based, which might pose a challenge in LIMASs with unknown, uncertain, or time-varying dynamics. In this case, model-based design methods in Sections 4.4 and 4.5 might not be applicable. To address this issue, a completely data-driven attack-detection scheme can be devised in the future by combining the results in Chapters 4 and 6. This scheme would have the potential of continuously adapting to changes in system dynamics by using newly available data.

The research directions highlighted above are critical for creating a truly autonomous attack-detection and mitigation scheme in LIMASs.

Advanced data-driven methods

At present, data-driven methods proposed in the third part of the thesis assume that historical data is noiseless. This assumption is not verified for systems equipped with inaccurate sensors. In order to improve the real-world applicability of the proposed results, future work may be devoted to robustly taking into account noise terms also in historical data. In particular, prior knowledge on the distribution of stochastic noise can be incorporated into the synthesis problem to provide high-probability guarantees [YIS20]. Another possibility is to develop methodologies to *denoise* the Hankel matrices constructed using noisy data [YS20].

Moreover, direct data-driven methods have the advantage of being completely model-free. This brings the possibility of considering systems with time-varying dynamics. In particular, the proposed methods can be modified to adapt in an online fashion to changing system behaviors, similarly to some existing works [LSKJ21]. Such a framework would be crucial for achieving full autonomy and adaptability in the closed-loop system.

A Notation

A.1 Symbol definitions

$\mathbb{R}$ (resp. $\mathbb{R}_{>0}$)	The set of real (resp. strictly positive real) numbers
$\mathbb{N}^0$	The set of natural numbers
$\ker(A)$	Null space (kernel) of matrix A
$\text{range}(A)$	Column space (range) of matrix A
$\mathcal{K}(A)$	A matrix whose columns form a basis for $\ker(A)$
$\mathcal{R}(A)$	A matrix whose columns form a basis for $\text{range}(A)$
$A \succ 0$ (resp. $A \succeq 0$)	Matrix A is positive definite (resp. semidefinite)
$A \prec 0$ (resp. $A \preceq 0$)	Matrix A is negative definite (resp. semidefinite)
$A^\top$ (resp. $v^\top$)	Transpose of matrix A (resp. of vector v)
$A^\dagger$	Right pseudo-inverse of matrix A
$\rho(A)$	Spectral radius of the matrix A
$\|A\|$	2-norm of matrix A
$\mathcal{B}_1$	Unit disk in the complex plane
$\mathbf{1}_n$	A column vector in $\mathbb{R}^n$ whose elemens are equal to 1
$\mathbf{0}_n$	A column vector in $\mathbb{R}^n$ whose elemens are equal to 0
$\mathbf{I}_n$ (resp. $\mathbf{I}$)	Identity matrix in $\mathbb{R}^{n\times n}$ (resp. of suitable dimension)
$\mathbf{0}_{N\times n}$ (resp. $\mathbf{0}$)	Zero matrix in $\mathbb{R}^{N\times n}$ (resp. of suitable dimension)
$\lceil a \rceil$	Ceiling function applied on the scalar a
$\lfloor a \rfloor$	Floor function applied on the scalar a
$\dim(V)$	Dimension of the vector space V
$\bigcup$	Set union
$\bigcap$	Set intersection
$\mathcal{X} \subseteq \mathcal{Y}$	Set $\mathcal{X}$ is a subset of set $\mathcal{Y}$
$\oplus$	Direct subspace sum
$\otimes$	Kronecker product
$\mathcal{H}_L(v)$	Hankel matrix of depth L associated to vector v

A.2 Sets and operators

When applied to a set, the operator $|\cdot|$ denotes its cardinality. With a slight abuse of notation, Kronecker product is also defined for subspaces, i.e., for two subspaces $\mathbb{X}$ and $\mathbb{Y}$, $\mathbb{X} \otimes \mathbb{Y} = \{x \otimes y | x \in \mathbb{X},\ y \in \mathbb{Y}\}$. $\mathbb{H}^1$ is the $(N-1)$-dimensional subspace of $\mathbb{R}^N$ comprising vectors with zero average, i.e., $\mathbb{H}^1 = \{v \in \mathbb{R}^N | \mathbf{1}_N^\top v = 0\}$. $\mathbb{H}^1_\perp$ is the 1-dimensional subspace orthogonal to $\mathbb{H}^1$, composed of N-dimensional vectors of identical elements, i.e., $\mathbb{H}^1_\perp \perp \mathbb{H}^1$ and $\mathbb{H}^1_\perp = \{a\mathbf{1}_N | a \in \mathbb{R}\}$. Then, it holds that $\mathbb{H}^1 \oplus \mathbb{H}^1_\perp = \mathbb{R}^N$. The set $\{-1, 1\}^{m\times n}$ with cardinality 2^{mn} consists of all the different $m \times n$ matrices comprising elements -1 and 1. For a matrix $A \in \mathbb{R}^{m\times n}$, $A(\mathbb{X}|\mathbb{Y})$ denotes the linear map $A : \mathbb{X} \to \mathbb{Y}$ where $\mathbb{X}$ and $\mathbb{Y}$ are subspaces of $\mathbb{R}^n$ and $\mathbb{R}^m$, respectively.

A.3 Algebraic graph theory

An undirected weighted graph of N nodes is defined as $\mathcal{G} = (\mathcal{V}, \mathcal{W}, \mathcal{E})$, where $\mathcal{V} = \{1, 2, \ldots, N\}$ is the set of nodes and $\mathcal{E} \subseteq \mathcal{V} \times \mathcal{V}$ is the set of edges. If a number $l \in \{1, ..., |\mathcal{E}|\}$ is assigned to each edge, the diagonal weight matrix $\mathcal{W}$ is collects the weights of the corresponding edges on its diagonals. Assigning arbitrary directions to edges, the only non-zero elements of the incidence matrix $B \in \mathbb{R}^{|\mathcal{V}|\times|\mathcal{E}|}$ are the following: $B_{il} = 1$ if node i is the source node of edge l, and $B_{il} = -1$ if node j is the sink node of edge l. The set of neighbors of node i is defined as $\mathcal{N}_i = \{j | (i, j) \in \mathcal{E}\}$. A path p_{ij} is an ordered sequence of consecutive edges such that every edge in the sequence is in $\mathcal{E}$, the first edge starts from node i, and the last edge ends in node j. The adjacency matrix of $\mathcal{G}$ is defined as $\mathcal{A} = [a_{ij}]_{N\times N}$, where $a_{ij} = 0$ if $(i, j) \notin \mathcal{E}$ or $i = j$ and $a_{ij} > 0$ is the positive weight of edge $(i, j) \in \mathcal{E}$. The degree of a node i is defined as $d_i = \sum_{j\in\mathcal{N}_i} a_{ij}$ along with the degree matrix $\mathcal{D} = \mathrm{diag}\,(d_1, d_2, \ldots, d_N)$. The Laplacian matrix of $\mathcal{G}$ is given by $\mathcal{L} = \mathcal{D} - \mathcal{A} = BWB^T$. An undirected graph is connected if there exists a path from every node i to every other node. In this case, it holds that $\ker(B^T) = \ker(\mathcal{L}) = \mathbb{H}^1_\perp$.

A.4 Matrices, vectors, and polynomials

When applied to matrices and vectors, the operator $|\cdot|$ denotes element-wise absolute value. For a matrix $Q \succeq 0$ and a vector x, $\|x\|_Q \triangleq \sqrt{x^\top Q x}$. When used with vectors and matrices, inequalities are taken component-wise. A polynomial is called Schur if all its roots are in $\mathcal{B}_1$. Given a vector $v \in \mathbb{R}^n$, $[v] \in \mathbb{R}^{n\times n}$ is a diagonal matrix collecting the elements of v on the main diagonal. The operator $\mathrm{diag}(M_1, \ldots, M_N)$ returns a block-diagonal matrix whose diagonal blocks comprise the matrices M_k, $k \in \{1, \ldots, N\}$. For vectors $x,\ y \in \mathbb{R}^n$, the term x^y represents a vector in $\mathbb{R}^n$ whose i^{th} element is $x_i^{y_i}$. We define the average of a vector $x \in \mathbb{R}^n$ as $\langle x\rangle = \frac{1}{n}\sum_{i=1}^n x_i = \frac{1}{n}\mathbf{1}^\top x$. The operator $\mathrm{col}(v_i, \ldots, v_j)$ represents the column concatenation of vectors v_k, $k = \{i, i+1, \ldots, j\}$. It is also compactly written as $\mathrm{col}(\{v_k\}_{k=i}^j)$. When v_k are column vectors, the vector

resulting from their column concatenation is denoted as $v_{[i:j]}$, or simply v when the indices i and j are clear from the context. The *Hankel matrix of depth* L associated to $v_{[i:j]}$, $j \geq i + L - 1$, is defined as

$$\mathcal{H}_L(v) \triangleq \begin{bmatrix} v_i & v_{i+1} & \cdots & v_{j-L+1} \\ v_{i+1} & v_{i+2} & \cdots & v_{j-L+2} \\ \vdots & \vdots & \ddots & \vdots \\ v_{i+L-1} & v_{i+L} & \cdots & v_j \end{bmatrix}. \tag{A.1}$$

Bibliography

[ABL+21] M. Alsalti, J. Berberich, V. G. Lopez, F. Allgöwer, and M. A. Müller, "Data-based system analysis and control of flat nonlinear systems," *arXiv preprint arXiv:2103.02892*, 2021.

[Ack80] J. Ackermann, "Parameter space design of robust control systems," *IEEE Transactions on Automatic Control*, vol. 25, no. 6, pp. 1058–1072, 1980.

[ADBB17] K. Arulkumaran, M. P. Deisenroth, M. Brundage, and A. A. Bharath, "Deep reinforcement learning: A brief survey," *IEEE Signal Processing Magazine*, vol. 34, no. 6, pp. 26–38, 2017.

[ADL20] D. Alpago, F. Dörfler, and J. Lygeros, "An extended Kalman filter for data-enabled predictive control," *IEEE Control Systems Letters*, vol. 4, no. 4, pp. 994–999, 2020.

[ÅE71] K. J. Åström and P. Eykhoff, "System identification — a survey," *Automatica*, vol. 7, no. 2, pp. 123–162, 1971.

[AKAJ21] A. Alanwar, A. Koch, F. Allgöwer, and K. H. Johansson, "Data-driven reachability analysis using matrix zonotopes," in *3rd Annual Learning for Dynamics and Control (L4DC) Conference*. Zurich, Switzerland: PMLR, 2021, pp. 163–175.

[AKM13] M. Ashourloo, A. Khorsandi, and H. Mokhtari, "Stabilization of DC microgrids with constant-power loads by an active damping method," in *4th Annual International Power Electronics, Drive Systems and Technologies Conference*, 2013, pp. 471–475.

[AKP18] R. Anguluri, V. Katewa, and F. Pasqualetti, "Attack detection in stochastic interconnected systems: Centralized vs decentralized detectors," in *57th IEEE Conference on Decision and Control (CDC)*, 2018, pp. 4541–4546.

[ÅM10] K. J. Åström and R. M. Murray, *Feedback systems*. Princeton, NJ, USA: Princeton University Press, 2010.

[AML21] A. Aboudonia, A. Martinelli, and J. Lygeros, "Passivity-based decentralized control for discrete-time large-scale systems," in *2021 American Control Conference (ACC)*. New Orleans, LA, USA: IEEE, 2021, pp. 2037–2042.

[AO11] D. Acemoglu and A. Ozdaglar, "Opinion dynamics and learning in social networks," *Dynamic Games and Applications*, vol. 1, no. 1, pp. 3–49, 2011.

[ÅT65] K.-J. Åström and B. Torsten, "Numerical identification of linear dynamic systems from normal operating records," *IFAC Proceedings Volumes*, vol. 2, no. 2, pp. 96–111, 1965.

[BA98] T. Balch and R. Arkin, "Behavior-based formation control for multirobot teams," *IEEE Transactions on Robotics and Automation*, vol. 14, no. 6, pp. 926–939, 1998.

[BA20] J. Berberich and F. Allgöwer, "A trajectory-based framework for data-driven system analysis and control," in *2020 European Control Conference (ECC)*. IEEE, 2020, pp. 1365–1370.

[BBDSE17] L. Buşoniu, R. Babuška, B. De Schutter, and D. Ernst, *Reinforcement learning and dynamic programming using function approximators*. CRC press, 2017.

[BBFE93] S. Boyd, V. Balakrishnan, E. Feron, and L. ElGhaoui, "Control system analysis and synthesis via linear matrix inequalities," in *Proceedings of the American Control Conference (ACC)*, San Francisco, CA, USA, 1993, pp. 2147–2154.

[BBP21] G. Baggio, D. S. Bassett, and F. Pasqualetti, "Data-driven control of complex networks," *Nature Communications*, vol. 12, no. 1, pp. 1–13, 2021.

[BC12] S. N. Bhaskara and B. H. Chowdhury, "Microgrids: A review of modeling, control, protection, simulation and future potential," in *2012 IEEE Power and Energy Society General Meeting*, 2012, pp. 1–7.

[BDPFT21] V. Breschi, C. De Persis, S. Formentin, and P. Tesi, "Direct data-driven model-reference control with Lyapunov stability guarantees," *arXiv preprint arXiv:2103.12663*, 2021.

[BDPT20a] A. Bisoffi, C. De Persis, and P. Tesi, "Controller design for robust invariance from noisy data," *arXiv preprint arXiv:2007.13181*, 2020.

[BDPT20b] ——, "Data-based stabilization of unknown bilinear systems with guaranteed basin of attraction," *Systems & Control Letters*, vol. 145, p. 104788, 2020.

[BEGFB94] S. Boyd, L. El Ghaoui, E. Feron, and V. Balakrishnan, *Linear matrix inequalities in system and control theory.* Philadelphia, PA, USA: SIAM, 1994.

[Bel57] R. Bellman, *Dynamic programming.* Princeton, NJ, USA: Princeton University Press, 1957.

[BFK+17] F. Boem, R. M. G. Ferrari, C. Keliris, T. Parisini, and M. M. Polycarpou, "A distributed networked approach for fault detection of large-scale systems," *IEEE Transactions on Automatic Control*, vol. 62, no. 1, pp. 18–33, 2017.

[BFT08] P.-A. Bliman and G. Ferrari-Trecate, "Average consensus problems in networks of agents with delayed communications," *Automatica*, vol. 44, no. 8, pp. 1985–1995, 2008.

[BG93] V. Blondel and M. Gevers, "Simultaneous stabilizability of three linear systems is rationally undecidable," *Mathematics of Control, Signals and Systems*, vol. 6, no. 2, pp. 135–145, 1993.

[BGFTP17] F. Boem, A. J. Gallo, G. Ferrari-Trecate, and T. Parisini, "A distributed attack detection method for multi-agent systems governed by consensus-based control," in *56th IEEE Annual Conference on Decision and Control (CDC)*, 2017, pp. 5961–5966.

[BKLS16] M. Blanke, M. Kinnaert, J. Lunze, and M. Staroswiecki, "Distributed fault diagnosis and fault-tolerant control," in *Diagnosis and Fault-Tolerant Control.* Springer, 2016, pp. 467–518.

[BKMA20] J. Berberich, J. Köhler, M. A. Muller, and F. Allgöwer, "Data-driven model predictive control with stability and robustness guarantees," *IEEE Transactions on Automatic Control*, vol. 66, no. 4, pp. 1702–1717, 2020.

[BKSA20] J. Berberich, A. Koch, C. W. Scherer, and F. Allgöwer, "Robust data-driven state-feedback design," in *Proceedings of the 2020 American Control Conference.* Denver, CO, USA: IEEE, 2020, pp. 1532–1538.

[Blo94] V. Blondel, *Simultaneous stabilization of linear systems.* Berlin, Germany: Springer-Verlag, 1994.

[BNF19] A. L. Bella, P. Nahata, and G. Ferrari-Trecate, "A supervisory control structure for voltage-controlled islanded DC microgrids," in *2019 IEEE 58th Conference on Decision and Control (CDC)*, 2019, pp. 6566–6571.

[BNJD18] O. A. Beg, L. V. Nguyen, T. T. Johnson, and A. Davoudi, "Signal temporal logic-based attack detection in DC microgrids," *IEEE Transactions on Smart Grid*, 2018.

[BP02] M. Barahona and L. M. Pecora, "Synchronization in small-world systems," *Physical Review Letters*, vol. 89, no. 5, pp. 1–4, 2002.

[BP20] G. Baggio and F. Pasqualetti, "Learning minimum-energy controls from heterogeneous data," in *2020 American Control Conference (ACC)*. IEEE, 2020, pp. 3991–3996.

[BPD02] B. Bamieh, F. Paganini, and M. Dahleh, "Distributed control of spatially invariant systems," *IEEE Transactions on Automatic Control*, vol. 47, no. 7, pp. 1091–1107, 2002.

[BRBP20] A. Barboni, H. Rezaee, F. Boem, and T. Parisini, "Detection of covert cyber-attacks in interconnected systems: A distributed model-based approach," *IEEE Transactions on Automatic Control*, vol. 65, no. 9, pp. 3728–3741, 2020.

[Bul17] F. Bullo, *Lectures on Network Systems*. Version 0.95, 2017, http://motion.me.ucsb.edu/book-lns.

[BV04] S. P. Boyd and L. Vandenberghe, *Convex optimization*. Cambridge, UK: Cambridge University Press, 2004.

[CBCZ16] G. Cavraro, S. Bolognani, R. Carli, and S. Zampieri, "The value of communication in the voltage regulation problem," in *55th IEEE Conference on Decision and Control (CDC)*. Las Vegas, NV, USA: IEEE, 2016, pp. 5781–5786.

[CDPF11] F. Ceragioli, C. De Persis, and P. Frasca, "Discontinuities and hysteresis in quantized average consensus," *Automatica*, vol. 47, no. 9, pp. 1916–1928, 2011.

[CIF17] M. Cucuzzella, G. P. Incremona, and A. Ferrara, "Decentralized sliding mode control of islanded AC microgrids with arbitrary topology," *IEEE Transactions on Industrial Electronics*, vol. 64, no. 8, pp. 6706–6713, 2017.

[CJKT02] E. Camponogara, D. Jia, B. Krogh, and S. Talukdar, "Distributed model predictive control," *IEEE Control Systems Magazine*, vol. 22, no. 1, pp. 44–52, 2002.

[CJMZ16] C. Conte, C. N. Jones, M. Morari, and M. Zeilinger, "Distributed synthesis and stability of cooperative distributed model predictive control for linear systems," *Automatica*, vol. 69, pp. 117–125, 2016.

[CLD19a] J. Coulson, J. Lygeros, and F. Dörfler, "Regularized and distributionally robust data-enabled predictive control," in *IEEE 58th Conference on Decision and Control (CDC)*. Nice, France: IEEE, 2019, pp. 2696–2701.

[CLD19b] J. Coulson, J. Lygeros, and F. Dörfler, "Data-enabled predictive control: In the shallows of the DeePC," in *Proceedings of the 18th European Control Conference*. Naples, Italy: IEEE, 2019, pp. 307–312.

[CLD21] J. Coulson, J. Lygeros, and F. Dorfler, "Distributionally robust chance constrained data-enabled predictive control," *IEEE Transactions on Automatic Control*, 2021, doi: 10.1109/TAC.2021.3097706.

[CLDA15] Y. Chen, W. Li, G. Dai, and A. Y. Aleksandrov, "Consensus analysis and design of linear interconnected multi-agent systems," *Acta Mathematica Scientia*, vol. 35, no. 6, pp. 1305–1317, 2015.

[CLS02] M. C. Campi, A. Lecchini, and S. M. Savaresi, "Virtual reference feedback tuning: A direct method for the design of feedback controllers," *Automatica*, vol. 38, no. 8, pp. 1337–1346, 2002.

[CPH+20] Z. Chen, F. Pasqualetti, J. He, P. Cheng, H. L. Trentelman, and F. Bullo, "Guest editorial: Special issue on security and privacy of distributed algorithms and network systems," *IEEE Transactions on Automatic Control*, vol. 65, no. 9, pp. 3725–3727, 2020.

[CPZ96] J. Chen, R. J. Patton, and H.-Y. Zhang, "Design of unknown input observers and robust fault detection filters," *International Journal of Control*, vol. 63, no. 1, pp. 85–105, 1996.

[CS98] Y.-Y. Cao and Y.-X. Sun, "Static output feedback simultaneous stabilization: ILMI approach," *International Journal of Control*, vol. 70, no. 5, pp. 803–814, 1998.

[CSS17] P. Cheng, L. Shi, and B. Sinopoli, "Guest editorial special issue on secure control of cyber-physical systems," *IEEE Transactions on Control of Network Systems*, vol. 4, no. 1, pp. 1–3, 2017.

[CT98] M. Corless and J. Tu, "State and input estimation for a class of uncertain systems," *Automatica*, vol. 34, no. 6, pp. 757–764, 1998.

[CTDP+18] M. Cucuzzella, S. Trip, C. De Persis, X. Cheng, A. Ferrara, and A. van der Schaft, "A robust consensus algorithm for current sharing and voltage regulation in DC microgrids," *IEEE Transactions on Control Systems Technology*, no. 99, pp. 1–13, 2018.

[CU15] Y. Cheng and V. Ugrinovskii, "Leader–follower tracking control with guaranteed consensus performance for interconnected systems with linear dynamic uncertain coupling," *International Journal of Control*, vol. 88, no. 8, pp. 1663–1677, 2015.

[DAMH19] G. Dulac-Arnold, D. Mankowitz, and T. Hester, "Challenges of real-world reinforcement learning," *arXiv preprint arXiv:1904.12901*, 2019.

[DD03] R. D'Andrea and G. Dullerud, "Distributed control design for spatially interconnected systems," *IEEE Transactions on Automatic Control*, vol. 48, no. 9, pp. 1478–1495, 2003.

[DL19] Y. Du and F. Li, "Intelligent multi-microgrid energy management based on deep neural network and model-free reinforcement learning," *IEEE Transactions on Smart Grid*, vol. 11, no. 2, pp. 1066–1076, 2019.

[DMK16] M. Davoodi, N. Meskin, and K. Khorasani, "Simultaneous fault detection and consensus control design for a network of multi-agent systems," *Automatica*, vol. 66, pp. 185–194, 2016.

[DMM+20] S. Dean, H. Mania, N. Matni, B. Recht, and S. Tu, "On the sample complexity of the linear quadratic regulator," *Foundations of Computational Mathematics*, vol. 20, no. 4, pp. 633–679, 2020.

[DPA+18] S. M. Dibaji, M. Pirani, A. M. Annaswamy, K. H. Johansson, and A. Chakrabortty, "Secure control of wide-area power systems: Confidentiality and integrity threats," in *57th IEEE Conference on Decision and Control (CDC)*. Miami Beach, FL, USA: IEEE, 2018, pp. 7269–7274.

[DPT15] C. De Persis and P. Tesi, "Input-to-state stabilizing control under denial-of-service," *IEEE Transactions on Automatic Control*, vol. 60, no. 11, pp. 2930–2944, 2015.

[DPT20] ——, "Formulas for data-driven control: Stabilization, optimality, and robustness," *IEEE Transactions on Automatic Control*, vol. 65, no. 3, pp. 909–924, 2020.

[DPT21] ——, "Low-complexity learning of linear quadratic regulators from noisy data," *Automatica*, vol. 128, p. 109548, 2021.

[DPWD18] C. De Persis, E. Weitenberg, and F. Dörfler, "A power consensus algorithm for DC microgrids," *Automatica*, vol. 89, pp. 364 – 375, 2018.

[DZX94] M. Darouach, M. Zasadzinski, and S. J. Xu, "Full-order observers for linear systems with unknown inputs," *IEEE Transactions on Automatic Control*, vol. 39, no. 3, pp. 606–609, 1994.

[Eyk74] P. Eykhoff, *System identification parameter and state estimation*. London, UK: Wiley-Interscience, 1974.

[FGMFT21] L. Furieri, B. Guo, A. Martin, and G. Ferrari-Trecate, "Near-optimal design of safe output feedback controllers from noisy data," *arXiv preprint arXiv:2105.10280*, 2021.

[FGS+11] A. Franchi, P. R. Giordano, C. Secchi, H. I. Son, and H. Bülthoff, "A passivity-based decentralized approach for the bilateral teleoperation of a group of UAVs with switching topology," in *IEEE International Conference on Robotics and Automation.* Shanghai, China: IEEE, 2011, pp. 898–905.

[FIDSDB17] G. Fiore, A. Iovine, E. De Santis, and M. D. Di Benedetto, "Secure state estimation for DC microgrids control," in *13th IEEE Conference on Automation Science and Engineering (CASE)*, Xi'an, China, 2017, pp. 1610–1615.

[FL98] R. Fierro and F. L. Lewis, "Control of a nonholonomic mobile robot using neural networks," *IEEE Transactions on Neural Networks*, vol. 9, no. 4, pp. 589–600, 1998.

[FM04] J. A. Fax and R. M. Murray, "Information flow and cooperative control of vehicle formations," *IEEE Transactions on Automatic Control*, vol. 49, no. 9, pp. 1465–1476, 2004.

[FME15] T. J. Freeborn, B. Maundy, and A. S. Elwakil, "Fractional-order models of supercapacitors, batteries and fuel cells: A survey," *Materials for Renewable and Sustainable Energy*, vol. 4, no. 9, pp. 1–7, 2015.

[GCLL13] J. M. Guerrero, M. Chandorkar, T. L. Lee, and P. C. Loh, "Advanced control architectures for intelligent microgrids - part I: Decentralized and hierarchical control," *IEEE Transactions on Industrial Electronics*, vol. 60, no. 4, pp. 1254–1262, 2013.

[GDPT20] M. Guo, C. De Persis, and P. Tesi, "Data-driven stabilization of nonlinear polynomial systems with noisy data," *arXiv preprint arXiv:2011.07833*, 2020.

[Gev06] M. Gevers, "A personal view of the development of system identification: A 30-year journey through an exciting field," *IEEE Control Systems Magazine*, vol. 26, no. 6, pp. 93–105, 2006.

[GHR12] N. Geroliminis, J. Haddad, and M. Ramezani, "Optimal perimeter control for two urban regions with macroscopic fundamental diagrams: A model predictive approach," *IEEE Transactions on Intelligent Transportation Systems*, vol. 14, no. 1, pp. 348–359, 2012.

[GLC15] Z. Gao, X. Liu, and M. Z. Chen, "Unknown input observer-based robust fault estimation for systems corrupted by partially decoupled disturbances," *IEEE Transactions on Industrial Electronics*, vol. 63, no. 4, pp. 2537–2547, 2015.

[GPC+15] S. Gu, F. Pasqualetti, M. Cieslak, Q. K. Telesford, B. Y. Alfred, A. E. Kahn, J. D. Medaglia, J. M. Vettel, M. B. Miller, S. T. Grafton, and D. S. Bassett, "Controllability of structural brain networks," *Nature Communications*, vol. 6, no. 1, pp. 1–10, 2015.

[GS00] G. O. Guardabassi and S. M. Savaresi, "Virtual reference direct design method: An off-line approach to data-based control system design," *IEEE Transactions on Automatic Control*, vol. 45, no. 5, pp. 954–959, 2000.

[GTB+18] A. J. Gallo, M. S. Turan, F. Boem, G. Ferrari-Trecate, and T. Parisini, "Distributed watermarking for secure control of microgrids under replay attacks," in *7th IFAC Workshop on Distributed Estimation and Control in Networked Systems (NecSys'18)*, Groningen, The Netherlands, 2018, pp. 182–187.

[GTB+20] A. J. Gallo, M. S. Turan, F. Boem, T. Parisini, and G. Ferrari-Trecate, "A distributed cyber-attack detection scheme with application to DC microgrids," *IEEE Transactions on Automatic Control*, vol. 65, no. 9, pp. 3800–3815, 2020.

[GTN+18] A. J. Gallo, M. S. Turan, P. Nahata, F. Boem, T. Parisini, and G. Ferrari-Trecate, "Distributed cyber-attack detection in the secondary control of DC microgrids," in *2018 European Control Conference (ECC)*. Limassol, Cyprus: IEEE, 2018, pp. 344–349.

[Har92] G. W. Hart, "Nonintrusive appliance load monitoring," *Proceedings of the IEEE*, vol. 80, no. 12, pp. 1870–1891, 1992.

[HGGL98] H. Hjalmarsson, M. Gevers, S. Gunnarsson, and O. Lequin, "Iterative feedback tuning: Theory and applications," *IEEE Control Systems Magazine*, vol. 18, no. 4, pp. 26–41, 1998.

[HIB+18] P. Henderson, R. Islam, P. Bachman, J. Pineau, D. Precup, and D. Meger, "Deep reinforcement learning that matters," in *Proceedings of the AAAI Conference on Artificial Intelligence*, vol. 32, no. 1, 2018.

[HJ12] R. A. Horn and C. R. Johnson, *Matrix Analysis*, 2nd ed. New York, NY, USA: Cambridge University Press, 2012.

[HK66] B. Ho and R. E. Kálmán, "Effective construction of linear state-variable models from input/output functions," *at-Automatisierungstechnik*, vol. 14, no. 1-12, pp. 545–548, 1966.

[HK02] R. Hegselmann and U. Krause, "Opinion dynamics and bounded confidence models, analysis, and simulation," *Journal of Artificial Societies and Social Simulation*, vol. 5, no. 3, pp. 1–33, 2002.

[HL91] G. D. Howitt and R. Luus, "Simultaneous stabilization of linear single-input systems by linear state feedback control," *International Journal of Control*, vol. 54, no. 4, pp. 1015–1030, 1991.

[HNM17] S. A. Hashjin and B. Nahid-Mobarakeh, "Active stabilization of a microgrid using model free adaptive control," in *2017 IEEE Industry Applications Society Annual Meeting*. Cincinnati, OH, USA: IEEE, 2017, pp. 1–8.

[HNX07] J. Hespanha, P. Naghshtabrizi, and Y. Xu, "A survey of recent results in networked control systems," *Proceedings of the IEEE*, vol. 95, no. 1, pp. 138–162, 2007.

[HQ19] Hydro-Québec. (2019) Simscape electrical: User's guide (specialized power systems). The MathWorks, Inc. (accessed: 12.02.2019).

[HRSJ21] X. He, X. Ren, H. Sandberg, and K. H. Johansson, "How to secure distributed filters under sensor attacks," *IEEE Transactions on Automatic Control*, 2021, doi: 10.1109/TAC.2021.3092603.

[HTŠ99] D. Henrion, S. Tarbouriech, and M. Šebek, "Rank-one LMI approach to simultaneous stabilization of linear systems," *Systems & Control Letters*, vol. 38, no. 2, pp. 79–89, 1999.

[HW13] Z.-S. Hou and Z. Wang, "From model-based control to data-driven control: Survey, classification and perspective," *Information Sciences*, vol. 235, pp. 3–35, 2013.

[HZAL18] T. Haarnoja, A. Zhou, P. Abbeel, and S. Levine, "Soft actor-critic: Off-policy maximum entropy deep reinforcement learning with a stochastic actor," in *International Conference on Machine Learning*. PMLR, 2018, pp. 1861–1870.

[IPQB13] F. A. Inthamoussou, J. Pegueroles-Queralt, and F. D. Bianchi, "Control of a supercapacitor energy storage system for microgrid applications," *IEEE Transactions on Energy Conversion*, vol. 28, no. 3, pp. 690–697, 2013.

[IRD+19] A. Iovine, T. Rigaut, G. Damm, E. De Santis, and M. D. Di Benedetto, "Power management for a DC microgrid integrating renewables and storages," *Control Engineering Practice*, vol. 85, pp. 59–79, 2019.

[Jur64] E. I. Jury, *Theory and Application of the z-Transform Method*. NY, USA: John Wiley & Sons, 1964.

[KAA19] J. Kumar, A. Agarwal, and V. Agarwal, "A review on overall control of DC microgrids," *Journal of Energy Storage*, vol. 21, pp. 113 – 138, 2019.

[KBA20] A. Koch, J. Berberich, and F. Allgöwer, "Verifying dissipativity properties from noise-corrupted input-state data," in *Proceedings of the 59th IEEE Conference on Decision and Control*, Jeju Island, Korea, 2020, pp. 616–621.

[KD20] D. Kastsiukevich and N. Dmitruk, "Data-driven optimal control of linear time-invariant systems," *IFAC-PapersOnLine*, vol. 53, no. 2, pp. 7191–7196, 2020.

[KHLF10] H. Khurana, M. Hadley, N. Lu, and D. A. Frincke, "Smart-grid security issues," *IEEE Security & Privacy*, vol. 8, no. 1, pp. 81–85, 2010.

[KK17] C. Kammer and A. Karimi, "Decentralized and distributed transient control for microgrids," *IEEE Transactions on Control Systems Technology*, vol. 27, no. 1, pp. 311–322, 2017.

[KMB04] A. Karimi, L. Mišković, and D. Bonvin, "Iterative correlation-based controller tuning," *International Journal of Adaptive Control and Signal Processing*, vol. 18, no. 8, pp. 645–664, 2004.

[Kni02] J. Knight, "Safety critical systems: challenges and directions," in *Proceedings of the 24th International Conference on Software Engineering*, Orlando, FL, USA, 2002, pp. 547–550.

[KP20] V. Krishnan and F. Pasqualetti, "Data-driven attack detection for linear systems," *IEEE Control Systems Letters*, vol. 5, no. 2, pp. 671–676, 2020.

[Kun94] P. Kundur, *Power System Stability and Control.* New York, NY, USA: McGraw-Hill, 1994.

[KY91] P. Kabamba and C. Yang, "Simultaneous controller design for linear time-invariant systems," *IEEE Transactions on Automatic Control*, vol. 36, no. 1, pp. 106–111, 1991.

[LDPT21] A. Luppi, C. De Persis, and P. Tesi, "On data-driven stabilization of systems with quadratic nonlinearities," *arXiv preprint arXiv:2103.15631*, 2021.

[LE17] J. Linder and M. Enqvist, "Identification of systems with unknown inputs using indirect input measurements," *International Journal of Control*, vol. 90, no. 4, pp. 729–745, 2017.

[LFK+14] H. Lasi, P. Fettke, H.-G. Kemper, T. Feld, and M. Hoffmann, "Industry 4.0," *Business & Information Systems Engineering*, vol. 6, no. 4, pp. 239–242, 2014.

[LFZL18] L. Li, M. Fu, H. Zhang, and R. Lu, "Consensus control for a network of high order continuous-time agents with communication delays," *Automatica*, vol. 89, pp. 144–150, 2018.

[LHP+15] T. P. Lillicrap, J. J. Hunt, A. Pritzel, N. Heess, T. Erez, Y. Tassa, D. Silver, and D. Wierstra, "Continuous control with deep reinforcement learning," *arXiv preprint arXiv:1509.02971*, 2015.

[LJ21] Y. Lian and C. N. Jones, "Nonlinear data-enabled prediction and control," in *3rd Annual Learning for Dynamics and Control (L4DC) Conference*. Zurich, Switzerland: PMLR, 2021, pp. 523–534.

[Lju98] L. Ljung, "System identification," in *Signal Analysis and Prediction*. Springer, 1998, pp. 163–173.

[LMT01] F.-L. Lian, J. Moyne, and D. Tilbury, "Performance evaluation of control networks: Ethernet, ControlNet, and DeviceNet," *IEEE Control Systems Magazine*, vol. 21, no. 1, pp. 66–83, 2001.

[Löf04] J. Löfberg, "Yalmip : A toolbox for modeling and optimization in MATLAB," in *In Proceedings of the CACSD Conference*, Taipei, Taiwan, 2004, pp. 284–289.

[LSKJ21] Y. Lian, J. Shi, M. P. Koch, and C. N. Jones, "Adaptive robust data-driven building control via bi-level reformulation: An experimental result," *arXiv preprint arXiv:2106.05740*, 2021.

[LVLN92] D. Leonard, N. Van Long, and V. L. Ngo, *Optimal control theory and static optimization in economics*. Cambridge, UK: Cambridge University Press, 1992.

[LWJ21] Y. Lian, R. Wang, and C. N. Jones, "Koopman based data-driven predictive control," *arXiv preprint arXiv:2102.05122*, 2021.

[MARA+16] A. Milias-Argeitis, M. Rullan, S. K. Aoki, P. Buchmann, and M. Khammash, "Automated optogenetic feedback control for precise and robust regulation of gene expression and cell growth," *Nature Communications*, vol. 7, no. 1, pp. 1–11, 2016.

[MASSO+11] A. Milias-Argeitis, S. Summers, J. Stewart-Ornstein, I. Zuleta, D. Pincus, H. El-Samad, M. Khammash, and J. Lygeros, "In silico feedback for in vivo regulation of a gene expression circuit," *Nature Biotechnology*, vol. 29, no. 12, pp. 1114–1116, 2011.

[MC76] R. D. Middlebrook and S. Cuk, "A general unified approach to modelling switching-converter power stages," in *IEEE Power Electronics Specialists Conference*, Cleveland, OH, USA, 1976, pp. 18–34.

[MDMVV89] M. Moonen, B. De Moor, L. Vandenberghe, and J. Vandewalle, "On-and off-line identification of linear state-space models," *International Journal of Control*, vol. 49, no. 1, pp. 219–232, 1989.

[ME10] A. R. Metke and R. L. Ekl, "Security technology for smart grid networks," *IEEE Transactions on Smart Grid*, vol. 1, no. 1, pp. 99–107, 2010.

[MH73] J. S. Meditch and G. H. Hostetter, "Observers for systems with unknown and inaccessible inputs," in *IEEE Conference on Decision and Control including the 12th Symposium on Adaptive Processes.* San Diego, CA, USA: IEEE, 1973, pp. 120–124.

[MK19] S. S. Madani and A. Karimi, "Data-driven distributed reactive power sharing in microgrids," in *2019 IEEE 58th Conference on Decision and Control (CDC).* Nice, France: IEEE, 2019, pp. 7512–7517.

[MKB+12] Y. Mo, T. H.-J. Kim, K. Brancik, D. Dickinson, H. Lee, A. Perrig, and B. Sinopoli, "Cyber–physical security of a smart grid infrastructure," *Proceedings of the IEEE*, vol. 100, no. 1, pp. 195–209, 2012.

[MKBG07] L. Mišković, A. Karimi, D. Bonvin, and M. Gevers, "Correlation-based tuning of decoupling multivariable controllers," *Automatica*, vol. 43, no. 9, pp. 1481–1494, 2007.

[MKK20] S. S. Madani, C. Kammer, and A. Karimi, "Data-driven distributed combined primary and secondary control in microgrids," *IEEE Transactions on Control Systems Technology*, vol. 29, no. 3, pp. 1340–1347, 2020.

[MKS+15] V. Mnih, K. Kavukcuoglu, D. Silver, A. A. Rusu, J. Veness, M. G. Bellemare, A. Graves, M. Riedmiller, A. K. Fidjeland, G. Ostrovski *et al.*, "Human-level control through deep reinforcement learning," *Nature*, vol. 518, no. 7540, pp. 529–533, 2015.

[MM09] P. McDaniel and S. McLaughlin, "Security and privacy challenges in the smart grid," *IEEE Security & Privacy*, vol. 7, no. 3, pp. 75–77, 2009.

[MMG20] V. K. Mishra, I. Markovsky, and B. Grossmann, "Data-driven tests for controllability," *IEEE Control Systems Letters*, vol. 5, no. 2, pp. 517–522, 2020.

[MMWJ20] E. T. Maddalena, C. d. S. Moraes, G. Waltrich, and C. N. Jones, "A neural network architecture to learn explicit MPC controllers from data," *IFAC-PapersOnLine*, vol. 53, no. 2, pp. 11 362–11 367, 2020.

[MNF18] A. Martinelli, P. Nahata, and G. Ferrari-Trecate, "Voltage stabilization in MVDC microgrids using passivity-based nonlinear control," in *2018*

IEEE 57th Conference on Decision and Control (CDC), Miami Beach, FL, USA, 2018, pp. 7022–7027.

[MOS20] MOSEK ApS, *The MOSEK optimization toolbox for MATLAB manual. Version 9.2.29*, 2020.

[MPG+16] S. F. Muldoon, F. Pasqualetti, S. Gu, M. Cieslak, S. T. Grafton, J. M. Vettel, and D. S. Bassett, "Stimulation-based control of dynamic brain networks," *PLoS Computational Biology*, vol. 12, no. 9, pp. 1–23, 2016.

[MPRT19] N. Matni, A. Proutiere, A. Rantzer, and S. Tu, "From self-tuning regulators to reinforcement learning and back again," in *Proceedings of the 58th IEEE Conference on Decision and Control*, Nice, France, 2019, pp. 3724–3740.

[MR08] I. Markovsky and P. Rapisarda, "Data-driven simulation and control," *International Journal of Control*, vol. 81, no. 12, pp. 1946–1959, 2008.

[MS77] R. D. Middlebrook and A. Solobdan, "A general unified approach to modelling switching-converter power stages," *International Journal of Electronics*, vol. 42, no. 6, pp. 521–550, 1977.

[MS16] A. Mitra and S. Sundaram, "Secure distributed observers for a class of linear time invariant systems in the presence of byzantine adversaries," in *55th IEEE Conference on Decision and Control (CDC)*. Las Vegas, NV, USA: IEEE, 2016, pp. 2709–2714.

[MSFT+17] L. Meng, Q. Shafiee, G. Ferrari-Trecate, H. Karimi, D. Fulwani, X. Lu, and J. M. Guerrero, "Review on control of DC microgrids and multiple microgrid clusters," *IEEE Journal of Emerging and Selected Topics in Power Electronics*, vol. 5, no. 3, pp. 928–948, 2017.

[MvD21] S. Mastellone and A. van Delft, "The impact of control research on industrial innovation: What would it take to make it happen?" *Control Engineering Practice*, vol. 111, pp. 1–9, 2021.

[MWS15] Y. Mo, S. Weerakkody, and B. Sinopoli, "Physical authentication of control systems: Designing watermarked control inputs to detect counterfeit sensor outputs," *IEEE Control Systems Magazine*, vol. 35, no. 1, pp. 93–109, 2015.

[MWVHDM06] I. Markovsky, J. C. Willems, S. Van Huffel, and B. De Moor, *Exact and approximate modeling of linear systems: A behavioral approach*. Philadelphia, PA, USA: SIAM, 2006.

[MZ10] C. Ma and J. Zhang, "Necessary and sufficient conditions for consensusability of linear multi-agent systems," *IEEE Transactions on Automatic Control*, vol. 55, no. 5, pp. 1263–1268, 2010.

[NFM13] C. Novara, L. Fagiano, and M. Milanese, "Direct feedback control design for nonlinear systems," *Automatica*, vol. 49, no. 4, pp. 849–860, 2013.

[NI14] H. Nishino and H. Ishii, "Distributed detection of cyber attacks and faults for power systems," *IFAC Proceedings Volumes*, vol. 47, no. 3, pp. 11 932–11 937, 2014.

[NKCdW+20] M. U. B. Niazi, A. Kibangou, C. Canudas-de Wit, D. Nikitin, L. Tumash, and P.-A. Bliman, "Modeling and control of COVID-19 epidemic through testing policies," *arXiv preprint arXiv:2010.15438*, 2020.

[NMDL15] V. Nasirian, S. Moayedi, A. Davoudi, and F. L. Lewis, "Distributed cooperative control of DC microgrids," *IEEE Transactions on Power Electronics*, vol. 30, no. 4, pp. 2288–2303, April 2015.

[NST+20] P. Nahata, R. Soloperto, M. Tucci, A. Martinelli, and G. Ferrari-Trecate, "A passivity-based approach to voltage stabilization in DC microgrids with ZIP loads," *Automatica*, vol. 113, pp. 1–10, 2020.

[NTFT20] P. Nahata, M. S. Turan, and G. Ferrari-Trecate, "Consensus-based current sharing and voltage balancing in DC microgrids with exponential loads," *arXiv preprint arXiv:2007.10134*, 2020.

[OPA15] K.-K. Oh, M.-C. Park, and H.-S. Ahn, "A survey of multi-agent formation control," *Automatica*, vol. 53, pp. 424–440, 2015.

[OPNSR13] R. Ortega, J. A. L. Perez, P. J. Nicklasson, and H. Sira-Ramirez, *Passivity-based control of Euler-Lagrange systems: Mechanical, electrical and electromechanical applications.* Berlin, Germany: Springer Science & Business Media, 2013.

[OSFM07] R. Olfati-Saber, A. Fax, and R. Murray, "Consensus and cooperation in networked multi-agent systems," *Proceedings of the IEEE*, vol. 95, no. 1, pp. 215–233, 2007.

[OSM04] R. Olfati-Saber and R. M. Murray, "Consensus problems in networks of agents with switching topology and time-delays," *IEEE Transactions on Automatic Control*, vol. 49, no. 9, pp. 1520–1533, 2004.

[PBB12] F. Pasqualetti, A. Bicchi, and F. Bullo, "Consensus computation in unreliable networks: A system theoretic approach," *IEEE Transactions on Automatic Control*, vol. 57, no. 1, pp. 90–104, 2012.

[PDB13] F. Pasqualetti, F. Dörfler, and F. Bullo, "Attack detection and identification in cyber-physical systems," *IEEE Transactions on Automatic Control*, vol. 58, no. 11, pp. 2715–2729, 2013.

[PDB15a] F. Pasqualetti, F. Dorfler, and F. Bullo, "Control-theoretic methods for cyberphysical security: Geometric principles for optimal cross-layer resilient control systems," *IEEE Control Systems Magazine*, vol. 35, no. 1, pp. 110–127, 2015.

[PDB15b] F. Pasqualetti, F. Dörfler, and F. Bullo, "A divide-and-conquer approach to distributed attack identification," in *2015 IEEE 54th Annual Conference on Decision and Control*, Osaka, Japan, 2015, pp. 5801–5807.

[PLMM06] J. Peças Lopes, C. L. Moreira, and A. Madureira, "Defining control strategies for microgrids islanded operation," *IEEE Transactions on Power Systems*, vol. 21, no. 2, pp. 916–924, 2006.

[POM+18] K. Paridari, N. O'Mahony, A. E.-D. Mady, R. Chabukswar, M. Boubekeur, and H. Sandberg, "A framework for attack-resilient industrial control systems: Attack detection and controller reconfiguration," *Proceedings of the IEEE*, vol. 106, no. 1, pp. 113–128, 2018.

[PSCVMV15] R. Pastor-Satorras, C. Castellano, P. Van Mieghem, and A. Vespignani, "Epidemic processes in complex networks," *Reviews of Modern Physics*, vol. 87, no. 3, p. 925, 2015.

[PT07] I. Pólik and T. Terlaky, "A survey of the S-lemma," *SIAM review*, vol. 49, no. 3, pp. 371–418, 2007.

[PZ95] T. Parisini and R. Zoppoli, "A receding-horizon regulator for nonlinear systems and a neural approximation," *Automatica*, vol. 31, no. 10, pp. 1443–1451, 1995.

[RB08] W. Ren and R. W. Beard, *Distributed consensus in multi-vehicle cooperative control*. Berlin, Germany: Springer, 2008.

[RBFTP16] S. Riverso, F. Boem, G. Ferrari-Trecate, and T. Parisini, "Plug-and-play fault detection and control-reconfiguration for a class of nonlinear large-scale constrained systems," *IEEE Transactions on Automatic Control*, vol. 61, no. 12, pp. 3963–3978, 2016.

[RBKA19] A. Romer, J. Berberich, J. Köhler, and F. Allgöwer, "One-shot verification of dissipativity properties from input–output data," *IEEE Control Systems Letters*, vol. 3, no. 3, pp. 709–714, 2019.

[RCN14] M. Rubenstein, A. Cornejo, and R. Nagpal, "Programmable self-assembly in a thousand-robot swarm," *Science*, vol. 345, no. 6198, pp. 795–799, 2014.

[RCVS07] M. Rosas-Casals, S. Valverde, and R. V. Solé, "Topological vulnerability of the European power grid under errors and attacks," *International Journal of Bifurcation and Chaos*, vol. 17, no. 7, pp. 2465–2475, 2007.

[Rec19] B. Recht, "A tour of reinforcement learning: The view from continuous control," *Annual Review of Control, Robotics, and Autonomous Systems*, vol. 2, pp. 253–279, 2019.

[RGM09] C. G. Rieger, D. I. Gertman, and M. A. McQueen, "Resilient control systems: Next generation design research," in *2009 2nd Conference on Human System Interactions*. Catania, Italy: IEEE, 2009, pp. 632–636.

[RL05] M. Rotkowitz and S. Lall, "A characterization of convex problems in decentralized control," *IEEE Transactions on Automatic Control*, vol. 50, no. 12, pp. 1984–1996, 2005.

[Rom02] I. Romero, "Dynamic load models for power systems - estimation of time-varying parameters during normal operation," Thesis, Lund Institute of Technology, 2002.

[SAJ15] H. Sandberg, S. Amin, and K. H. Johansson, "Cyberphysical security in networked control systems: An introduction to the issue," *IEEE Control Systems Magazine*, vol. 35, no. 1, pp. 20–23, 2015.

[SB18] R. S. Sutton and A. G. Barto, *Reinforcement learning: An introduction*. Cambridge, MA, USA: MIT Press, 2018.

[SCGGV14] M. Soshinskaya, W. Crijns-Graus, J. Guerrero, and J. Vasquez, "Microgrids: Experiences, barriers and success factors," *Renewable and Sustainable Energy Reviews*, vol. 40, pp. 659–672, 2014.

[SDA+14] Q. Shafiee, T. Dragičević, F. Andrade, J. C. Vasquez, and J. M. Guerrero, "Distributed consensus-based control of multiple DC microgrids clusters," in *40th Annual Conference of the IEEE Industrial Electronics Society (IECON)*. Dallas, TX, USA: IEEE, 2014, pp. 2056–2062.

[SDB19] S. Sahoo, T. Dragičević, and F. Blaabjerg, "Cyber security in control of grid-tied power electronic converters – challenges and vulnerabilities," *IEEE Journal of Emerging and Selected Topics in Power Electronics*, pp. 1–15, 2019, doi: JESTPE.2019.2953480.

[SGV14] Q. Shafiee, J. M. Guerrero, and J. C. Vasquez, "Distributed secondary control for islanded microgrids: A novel approach," *IEEE Transactions on Power Electronics*, vol. 29, no. 2, pp. 1018–1031, 2014.

[Shi98] S. M. Shinners, *Modern control system theory and design*. New York, NY, USA: John Wiley & Sons, 1998.

[Sil11] D. D. Siljak, *Decentralized control of complex systems*. Courier Corporation, 2011.

[SLA+15] J. Schulman, S. Levine, P. Abbeel, M. Jordan, and P. Moritz, "Trust region policy optimization," in *International Conference on Machine Learning*. Lille, France: PMLR, 2015, pp. 1889–1897.

[SM07] J. Slay and M. Miller, "Lessons learned from the maroochy water breach," in *International Conference on Critical Infrastructure Protection*, Hanover, NH, USA, 2007, pp. 73–82.

[Smi15] R. S. Smith, "Covert misappropriation of networked control systems: Presenting a feedback structure," *IEEE Control Systems Magazine*, vol. 35, no. 1, pp. 82–92, 2015.

[SMPD18] S. Sahoo, S. Mishra, J. C.-H. Peng, and T. Dragičević, "A stealth cyber-attack detection strategy for DC microgrids," *IEEE Transactions on Power Electronics*, vol. 34, no. 8, pp. 8162–8174, 2018.

[Söd07] T. Söderström, "Errors-in-variables methods in system identification," *Automatica*, vol. 43, no. 6, pp. 939–958, 2007.

[SPDB16] J. W. Simpson-Porco, F. Dörfler, and F. Bullo, "Voltage collapse in complex power grids," *Nature Communications*, vol. 7, no. 1, pp. 1–8, 2016.

[SPM+20] F. Strehle, M. Pfeifer, A. J. Malan, S. Krebs, and S. Hohmann, "A scalable port-hamiltonian approach to plug-and-play voltage stabilization in DC microgrids," in *2020 IEEE Conference on Control Technology and Applications (CCTA)*. Montréal, Canada: IEEE, 2020, pp. 787–794.

[SRE+19] H. Sánchez, D. Rotondo, T. Escobet, V. Puig, and J. Quevedo, "Bibliographical review on cyber attacks from a control oriented perspective," *Annual Reviews in Control*, vol. 48, pp. 103–128, 2019.

[SS89] T. Söderström and P. Stoica, *System Identification*. Hoboken, NJ, US: Prentice-Hall International, 1989.

[SSF+07] L. Schenato, B. Sinopoli, M. Franceschetti, K. Poolla, and S. S. Sastry, "Foundations of control and estimation over lossy networks," *Proceedings of the IEEE*, vol. 95, no. 1, pp. 163–187, 2007.

[SSK17] M. S. Sadabadi, Q. Shafiee, and A. Karimi, "Plug-and-play robust voltage control of DC microgrids," *IEEE Transactions on Smart Grid*, vol. 9, no. 6, pp. 6886–6896, 2017.

[SSS+03] B. Sinopoli, C. Sharp, L. Schenato, S. Schaffert, and S. Sastry, "Distributed control applications within sensor networks," *Proceedings of the IEEE*, vol. 91, no. 8, pp. 1235–1246, 2003.

[Str93] G. Strang, *Introduction to linear algebra.* Wellesley, MA: Wellesley-Cambridge Press, 1993, vol. 3.

[STSJ11] I. Shames, A. M. Teixeira, H. Sandberg, and K. H. Johansson, "Distributed fault detection for interconnected second-order systems," *Automatica*, vol. 47, no. 12, pp. 2757–2764, 2011.

[SVR+10] B. Stewart, A. Venkat, J. Rawlings, S. Wright, and G. Pannocchia, "Cooperative distributed model predictive control," *Systems & Control Letters*, vol. 59, no. 8, pp. 460–469, 2010.

[SWD+17] J. Schulman, F. Wolski, P. Dhariwal, A. Radford, and O. Klimov, "Proximal policy optimization algorithms," *arXiv preprint arXiv:1707.06347*, 2017.

[TCCS19] S. Trip, M. Cucuzzella, X. Cheng, and J. Scherpen, "Distributed averaging control for voltage regulation and current sharing in DC microgrids," *IEEE Control Systems Letters*, vol. 3, no. 1, pp. 174–179, Jan 2019.

[TFNM17] M. Tanaskovic, L. Fagiano, C. Novara, and M. Morari, "Data-driven control of nonlinear systems: An on-line direct approach," *Automatica*, vol. 75, pp. 1–10, 2017.

[TFT20] M. Tucci and G. Ferrari-Trecate, "A scalable, line-independent control design algorithm for voltage and frequency stabilization in AC islanded microgrids," *Automatica*, vol. 111, pp. 1–7, 2020.

[TFT22] M. S. Turan and G. Ferrari-Trecate, "Data-driven unknown-input observers and state estimation," *IEEE Control Systems Letters*, vol. 6, pp. 1424–1429, 2022.

[TGX+20] S. Tan, J. M. Guerrero, P. Xie, R. Han, and J. C. Vasquez, "Brief survey on attack detection methods for cyber-physical systems," *IEEE Systems Journal*, vol. 14, no. 4, pp. 5329–5339, 2020.

[TMGFT16] M. Tucci, L. Meng, J. M. Guerrero, and G. Ferrari-Trecate, "A consensus-based secondary control layer for stable current sharing and voltage balancing in DC microgrids," *arXiv preprint arXiv:1603.03624*, 2016.

[TMGFT18] ——, "Stable current sharing and voltage balancing in DC microgrids: A consensus-based secondary control layer," *Automatica*, vol. 95, pp. 1–13, 2018.

[TMP20] A. Tsiamis, N. Matni, and G. Pappas, "Sample complexity of Kalman filtering for unknown systems," in *2nd Annual Learning for Dynamics and Control (L4DC) Conference.* Cambridge, MA, USA: PMLR, 2020, pp. 435–444.

[TPSJ12] A. Teixeira, D. Pérez, H. Sandberg, and K. H. Johansson, "Attack models and scenarios for networked control systems," in *1st International Conference on High Confidence Networked Systems*. Beijing, China: ACM, 2012, pp. 55–64.

[TRFT18] M. Tucci, S. Riverso, and G. Ferrari-Trecate, "Line-independent plug-and-play controllers for voltage stabilization in DC microgrids," *IEEE Transactions on Control Systems Technology*, vol. 26, no. 3, pp. 1115–1123, 2018.

[TSSJ14] A. Teixeira, I. Shames, H. Sandberg, and K. H. Johansson, "Distributed fault detection and isolation resilient to network model uncertainties," *IEEE Transactions on Cybernetics*, vol. 44, no. 11, pp. 2024–2037, 2014.

[TSSJ15a] ——, "A secure control framework for resource-limited adversaries," *Automatica*, vol. 51, pp. 135–148, 2015.

[TSSJ15b] A. Teixeira, K. C. Sou, H. Sandberg, and K. H. Johansson, "Secure control systems: A quantitative risk management approach," *IEEE Control Systems Magazine*, vol. 35, no. 1, pp. 24–45, 2015.

[Tu19] S. L. Tu, "Sample complexity bounds for the linear quadratic regulator," Thesis, UC Berkeley, 2019.

[TvWC20] H. L. Trentelman, H. J. van Waarde, and M. K. Camlibel, "An informativity approach to data-driven tracking and regulation," *arXiv preprint arXiv:2009.01552*, 2020.

[TXFT20] M. S. Turan, L. Xu, and G. Ferrari-Trecate, "Consensusability of linear interconnected multi-agent systems," *IFAC-PapersOnLine*, vol. 53, no. 2, pp. 2915–2920, 2020, 21th IFAC World Congress.

[TXFT21] ——, "On consensusability of linear interconnected multi-agent systems and simultaneous stabilization," *IEEE Transactions on Control of Network Systems*, 2021, doi: 10.1109/TCNS.2021.3106446.

[UGC+16] D. I. Urbina, J. Giraldo, A. A. Cardenas, J. Valente, M. Faisal, N. O. Tippenhauer, J. Ruths, R. Candell, and H. Sandberg, *Survey and New Directions for Physics-Based Attack Detection in Control Systems*. US Department of Commerce, National Institute of Standards and Technology, 2016.

[Val99] M. E. Valcher, "State observers for discrete-time linear systems with unknown inputs," *IEEE Transactions on Automatic Control*, vol. 44, no. 2, pp. 397–401, 1999.

[VHKB11] K. Van Heusden, A. Karimi, and D. Bonvin, "Data-driven model reference control with asymptotically guaranteed stability," *International Journal of Adaptive Control and Signal Processing*, vol. 25, no. 4, pp. 331–351, 2011.

[VL10] K. G. Vamvoudakis and F. L. Lewis, "Online actor-critic algorithm to solve the continuous-time infinite horizon optimal control problem," *Automatica*, vol. 46, no. 5, pp. 878–888, 2010.

[VODM12] P. Van Overschee and B. L. De Moor, *Subspace identification for linear systems: Theory—Implementation—Applications.* Berlin, Germany: Springer Science & Business Media, 2012.

[VV82] M. Vidyasagar and N. Viswanadham, "Algebraic design techniques for reliable stabilization," *IEEE Transactions on Automatic Control*, vol. 27, no. 5, pp. 1085–1095, 1982.

[vWCM20] H. J. van Waarde, M. K. Camlibel, and M. Mesbahi, "From noisy data to feedback controllers: Non-conservative design via a matrix S-lemma," *IEEE Transactions on Automatic Control*, pp. 1–14, 2020, doi: 10.1109/TAC.2020.3047577.

[vWDPCT20] H. J. van Waarde, C. De Persis, M. K. Camlibel, and P. Tesi, "Willems' fundamental lemma for state-space systems and its extension to multiple datasets," *IEEE Control Systems Letters*, vol. 4, no. 3, pp. 602–607, 2020.

[vWETC20] H. J. van Waarde, J. Eising, H. L. Trentelman, and M. K. Camlibel, "Data informativity: A new perspective on data-driven analysis and control," *IEEE Transactions on Automatic Control*, vol. 65, no. 11, pp. 4753–4768, 2020.

[vWM20] H. J. van Waarde and M. Mesbahi, "Data-driven parameterizations of suboptimal LQR and H2 controllers," *arXiv preprint arXiv:1912.07671*, 2020.

[WCWK16] Z. Wang, B. Chen, J. Wang, and J. Kim, "Decentralized energy management system for networked microgrids in grid-connected and islanded modes," *IEEE Transactions on Smart Grid*, vol. 7, no. 2, pp. 1097–1105, 2016.

[Web10] C. Weber, "Adequate intraday market design to enable the integration of wind energy into the European power systems," *Energy Policy*, vol. 38, no. 7, pp. 3155–3163, 2010.

[WH94] D. Wang and A. Haldar, "Element-level system identification with unknown input," *Journal of Engineering Mechanics*, vol. 120, no. 1, pp. 159–176, 1994.

[WL14] M. Wu and D. Lu, "Active stabilization methods of electric power systems with constant power loads: A review," *Journal of Modern Power Systems and Clean Energy*, vol. 2, no. 3, pp. 233–243, 2014.

[WP97] J. C. Willems and J. W. Polderman, *Introduction to mathematical systems theory: A behavioral approach.* New York, NY, USA: Springer Science & Business Media, 1997, vol. 26.

[WRMDM05] J. C. Willems, P. Rapisarda, I. Markovsky, and B. L. De Moor, "A note on persistency of excitation," *Systems & Control Letters*, vol. 54, no. 4, pp. 325–329, 2005.

[WWHL15] W. Wang, C. Wen, J. Huang, and Z. Li, "Hierarchical decomposition based consensus tracking for uncertain interconnected systems via distributed adaptive output feedback control," *IEEE Transactions on Automatic Control*, vol. 61, no. 7, pp. 1938–1945, 2015.

[WZF19] X. Wang, J. Zhu, and J.-E. Feng, "A new characteristic of switching topology and synchronization of linear multi-agent systems," *IEEE Transactions on Automatic Control*, vol. 64, no. 7, pp. 2697–2711, 2019.

[XM21] A. Xue and N. Matni, "Data-driven system level synthesis," in *3rd Annual Learning for Dynamics and Control (L4DC) Conference.* Zurich, Switzerland: PMLR, 2021, pp. 189–200.

[XMX20] L. Xu, Y. Mo, and L. Xie, "Distributed consensus over markovian packet loss channels," *IEEE Transactions on Automatic Control*, vol. 65, no. 1, pp. 279–286, 2020.

[XTGFT21a] L. Xu, M. S. Turan, B. Guo, and G. Ferrari-Trecate, "A data-driven convex programming approach to worst-case robust tracking controller design," *arXiv preprint arXiv:2102.11918*, 2021.

[XTGFT21b] ——, "Non-conservative design of robust tracking controllers based on input-output data," in *3rd Annual Learning for Dynamics and Control (L4DC) Conference.* Zurich, Switzerland: PMLR, 2021, pp. 138–149.

[XZX19] J. Xu, H. Zhang, and L. Xie, "Consensusability of multiagent systems with delay and packet dropout under predictor-like protocols," *IEEE Transactions on Automatic Control*, vol. 64, no. 8, pp. 3506–3513, 2019.

[XZXX18] L. Xu, J. Zheng, N. Xiao, and L. Xie, "Mean square consensus of multi-agent systems over fading networks with directed graphs," *Automatica*, vol. 95, pp. 503–510, 2018.

[YIS20] M. Yin, A. Iannelli, and R. S. Smith, "Maximum likelihood estimation in data-driven modeling and control," *arXiv preprint arXiv:2011.00925*, 2020.

[YS20] M. Yin and R. S. Smith, "On low-rank hankel matrix denoising," *arXiv preprint arXiv:2012.07433*, 2020.

[YV16] C. Yu and M. Verhaegen, "Blind multivariable ARMA subspace identification," *Automatica*, vol. 66, pp. 3–14, 2016.

[YX11] K. You and L. Xie, "Network topology and communication data rate for consensusability of discrete-time multi-agent systems," *IEEE Transactions on Automatic Control*, vol. 56, no. 10, pp. 2262–2275, 2011.

[ZBP01] W. Zhang, M. Branicky, and S. Phillips, "Stability of networked control systems," *IEEE Control Systems Magazine*, vol. 21, no. 1, pp. 84–99, 2001.

[ZD15] J. Zhao and F. Dörfler, "Distributed control and optimization in DC microgrids," *Automatica*, vol. 61, pp. 18–26, 2015.

[ZLW+19] Y. Zhao, Y. Liu, G. Wen, W. Ren, and G. Chen, "Designing distributed specified-time consensus protocols for linear multiagent systems over directed graphs," *IEEE Transactions on Automatic Control*, vol. 64, no. 7, pp. 2945–2952, 2019.

[ZN42] J. G. Ziegler and N. B. Nichols, "Optimum settings for automatic controllers," *Transactions of ASME*, vol. 64, no. 11, pp. 759–765, 1942.

[ZTHK16] W. Zhang, Y. Tang, T. Huang, and J. Kurths, "Sampled-data consensus of linear multi-agent systems with packet losses," *IEEE Transactions on Neural Networks and Learning Systems*, vol. 28, no. 11, pp. 2516–2527, 2016.

[ZXXY19] J. Zheng, L. Xu, L. Xie, and K. You, "Consensusability of discrete-time multiagent systems with communication delay and packet dropouts," *IEEE Transactions on Automatic Control*, vol. 64, no. 3, pp. 1185–1192, 2019.

[ZYBV15] X. Zhong, L. Yu, R. Brooks, and G. K. Venayagamoorthy, "Cyber security in smart DC microgrid operations," in *1st IEEE International Conference on DC Microgrids (ICDCM)*, Atlanta, GA, USA, 2015, pp. 86–91.

[ZZS+17] H. Zhang, J. Zhou, Q. Sun, J. M. Guerrero, and D. Ma, "Data-driven control for interlinked AC/DC microgrids via model-free adaptive control and dual-droop control," *IEEE Transactions on Smart Grid*, vol. 8, no. 2, pp. 557–571, 2017.

Mustafa Sahin **Turan**

@ mustafasahinturan@gmail.com

Education

2021 – 2017 | **PhD in Mechanical Engineering**
Swiss Federal Institute of Technology Lausanne (EPFL), Lausanne, Switzerland

2017 – 2015 | **MSc in Electrical and Electronics Engineering**
Bilkent University, Ankara, Turkey
Thesis : Fall Detection and classification using wearable sensors

2015 – 2010 | **BSc in Mechatronics Engineering**
Sabanci University, Istanbul, Turkey
Thesis : Manipulator design, manufacturing, and control for hydrodynamic cavitation surgery

Experience

June 2015 – Feb 2013 | **Teaching Coordinator**
Academic Support Program, Sabanci University — Istanbul, Turkey
Coordinated peer study sessions on physics and mathematics.

Sept 2014 – Jun 2014 | **Powertrain Calibration Trainee**
AVL Turkey — Istanbul, Turkey
Contributed to real-life testing and calibration of diesel powertrains.

Aug 2013 – June 2013 | **Visiting Student**
Vehicle Dynamics & Control Research Laboratory, Hacettepe University — Ankara, Turkey
Designed a torque vectoring controller on Simulink.

Feb 2013 – Feb 2011 | **Teaching Assistant**
Academic Support Program, Sabanci University — Istanbul, Turkey
Taught freshman year physics to peer students.

Skills

Control Theory : Distributed consensus, multi-agent systems, cyber-attack detection, data-driven control and state estimation, microgrid control.
Software and programming : Matlab/Simulink, Python, PSCAD.